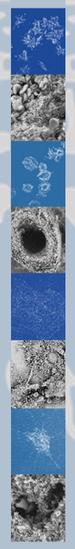

Studies on the role of cytoskeletal-regulatory and -crosslinking proteins in platelet function

***

Studien zur Rolle von Zytoskelett-regulierenden und -vernetzenden Proteinen in der Thrombozytenfunktion

Doctoral thesis for a doctoral degree

at the Graduate School of Life Sciences,

Julius-Maximilians-Universität Würzburg,

Institute of Experimental Biomedicine I

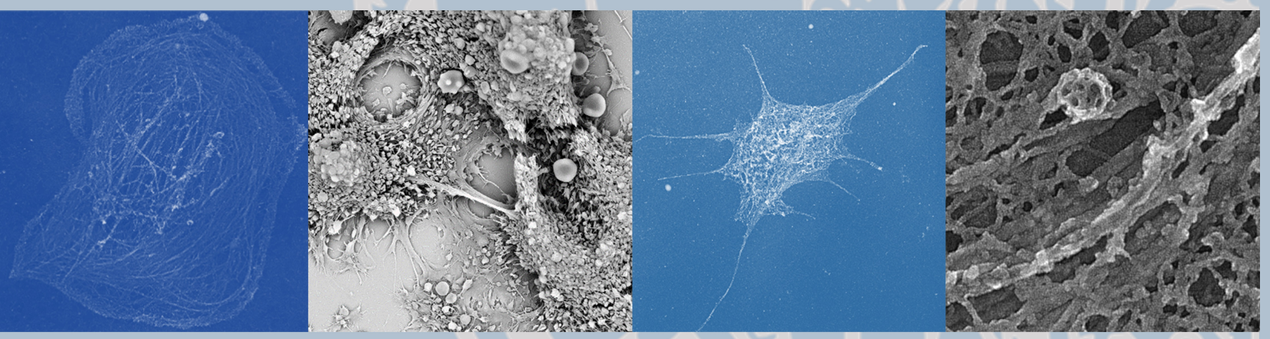

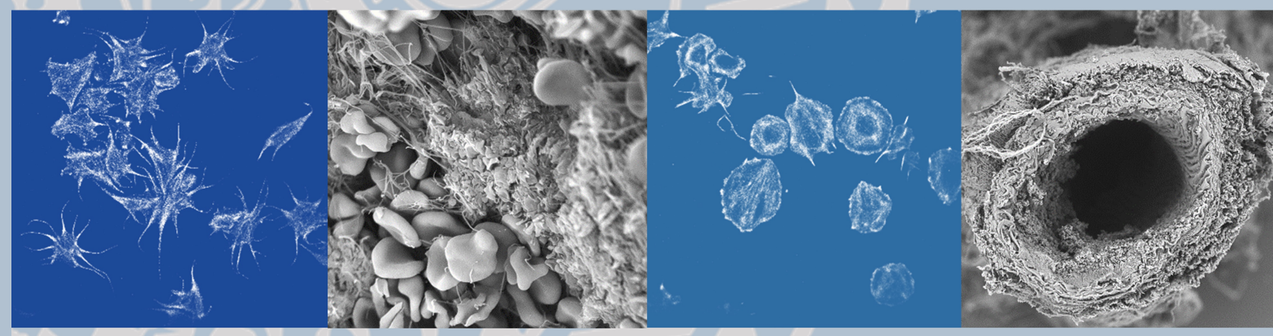

submitted by

Yvonne Schurr

from Stuttgart, Germany

- Würzburg, 2020 -

Yvonne Schurr

Studies on the role of cytoskeletal-regulatory and -crosslinking proteins in platelet function

***

Studien zur Rolle von Zytoskelett-regulierenden und -vernetzenden Proteinen in der Thrombozytenfunktion

Doctoral thesis for a doctoral degree
at the Graduate School of Life Sciences,
Julius-Maximilians-Universität Würzburg,
Institute of Experimental Biomedicine I

submitted by

Yvonne Schurr

from Stuttgart, Germany

- Würzburg, 2020 -

Submitted on:

_____

Office stamp

Members of the *Promotionskomitee*:

Chairperson: _____

Primary Supervisor: _____

Supervisor (Second): _____

Supervisor (Third): _____

Supervisor (Fourth): _____

(If applicable)

Date of Public Defense: _____

Date of Receipt of Certificates: _____

"Um die Welt in einem Sandkorn zu sehn

und den Himmel in einer wilden Blume,

halte die Unendlichkeit auf deiner flachen Hand

und die Stunde rückt in die Ewigkeit."

“To see a World in a Grain of Sand

And a Heaven in a Wild Flower,

Hold Infinity in the palm of your hand

And Eternity in an hour.”

William Blake (1757 - 1827), Auguries of Innocence

SUMMARY

Cytoskeletal reorganization in platelets is highly regulated and important for proper platelet function during activation and aggregation at sites of vascular injury. In this thesis, the role of three different cytoskeletal-regulatory and -crosslinking proteins was studied in platelet physiology using megakaryocyte- and platelet-specific knockout mice. The generation of branched actin filaments is regulated by nucleation promoting factors (NPF) and the Arp2/3 complex.

(1.) The WAVE complex is a NPF, which upregulates the Arp2/3 complex activity at the plasma membrane. As shown in this thesis, the loss of the WAVE complex subunit Cyfip1 in mice did not alter platelet production and had only a minor impact on platelet activation. However, Cyfip1 played an essential role for branching of actin filaments and consequently for lamellipodia formation *in vitro*. The importance of lamellipodia for thrombus formation and stability has been controversially discussed. Cyfip1-deficient platelets were able to form a stable thrombus *ex vivo* and *in vivo* and a hemostatic plug comparable to controls. Moreover, Cyfip1-deficient mice maintained vascular integrity at the site of inflammation. These data show that platelet lamellipodia formation is not required for hemostatic function and pathophysiological thrombus formation.

(2.) The WASH complex is another NPF, which mediates actin filament polymerization on endosomal vesicles via the Arp2/3 complex. Loss of the WASH complex subunit Strumpellin led to a decreased protein abundance of the WASH protein and to a 20% reduction in integrin αIIbβ3 surface expression on platelets and megakaryocytes, whereas the expression of other surface receptors as well as the platelet count, size, *ex vivo* thrombus formation and bleeding time remained unaltered. These data point to a distinct role of Strumpellin in maintaining integrin αIIbβ3 expression and provide new insights into regulatory mechanisms of platelet integrins.

(3.) MACF1 has been described as a cytoskeletal crosslinker of microtubules and F-actin. However, MACF1-deficient mice displayed no alterations in platelet production, activation, thrombus formation and hemostatic function. Further, no compensatory up- or downregulation of other proteins could be found that contain an F-actin- and a microtubule-binding domain. These data indicate that MACF1 is dispensable for platelet biogenesis, activation and thrombus formation. Nevertheless, functional redundancy among different proteins mediating the cytoskeletal crosstalk may exist.

ZUSAMMENFASSUNG

Sowohl bei der Thrombozytenproduktion als auch bei der Thrombozytenaktivierung nach einer Gefäßverletzung findet eine schnelle Umstrukturierung des Zytoskeletts statt, bei der Zytoskelett-regulierenden Proteine eine wichtige Rolle spielen. In dieser Dissertation wurde die Rolle von drei verschiedenen Zytoskelett-regulierenden und vernetzenden Proteinen in der Thrombozytenphysiologie mittels Megakaryozyten- und Thrombozyten-spezifischen knockout Mäusen untersucht. Die Bildung von verzweigten Aktinfilamenten wird durch *Nucleation promoting factors* (NPF) und den Arp2/3-Komplex gesteuert.

(1.) Der WAVE-Komplex ist ein NPF der die Aktivität des Arp2/3-Komplexes an der Plasmamembran reguliert. Wie in dieser Arbeit gezeigt, hatte die Defizienz der WAVE-Komplex-Untereinheit Cyfip1 keinen Einfluss auf die Thrombozytenproduktion und nur einen geringen Einfluss auf die Thrombozytenaktivierung. Cyfip1 spielte jedoch eine wesentliche Rolle für die Verzweigung von Aktinfilamenten und folglich für die *in vitro* Bildung von Lamellipodien. Die Bedeutung der Lamellipodienausbildung in Thrombozyten für die Thrombusbildung und –stabilität wurde bisher kontrovers diskutiert. Thrombozyten von Cyfip1-defizienten Mäusen bildeten *ex vivo* und *in vivo* einen stabilen Thrombus und einen hämostatischen Blutpfropfen, vergleichbar zu Thrombozyten von Kontrollmäusen. Darüber hinaus konnten Cyfip1-defiziente Mäuse die Gefäßintegrität am Ort der Entzündung aufrechterhalten. Diese Daten zeigen, dass die Ausbildung von Lamellipodien sowohl für die hämostatische Funktion als auch für die pathologische Thrombusbildung nicht erforderlich ist.

(2.) Der WASH-Komplex ist ein weiterer NPF, der die Polymerisation von Aktinfilamenten an endosomalen Vesikeln über den Arp2/3-Komplex vermittelt. Die Defizienz der WASH-Komplexuntereinheit Strumpellin führte zu einer verringerten WASH- Proteinkonzentration und resultierte in einer Abnahme der Oberflächenexpression des αIIbβ3-Integrins um 20 %, wohingegen die Expression anderer Oberflächenrezeptoren sowie die Thrombozytenzahl, -größe, *ex vivo* Thrombusbildung und die Blutungszeit unverändert blieb. Diese Daten weisen auf eine wichtige Rolle von Strumpellin bei der Aufrechterhaltung der αIIbβ3-Integrin Expression hin und liefern neue Erkenntnisse über Regulationsmechanismen von Integrinen in Thrombozyten.

(3.) MACF1 wurde aufgrund seiner Interaktion mit Mikrotubuli- und Aktinfilamenten als Zytoskelett-vernetzendes Protein beschrieben. Bei MACF1-defizienten Mäusen wurden jedoch keine Veränderungen bei der Thrombozytenproduktion, Aktivierung, Thrombusbildung und der hämostatischen Funktion festgestellt. Des Weiteren wurde keine kompensatorische Hoch- oder Herunterregulation anderer Proteine gefunden, welche ebenfalls eine F-Aktin- und eine Mikrotubuli-Bindungsdomäne besitzen. Diese Daten deuten darauf hin, dass MACF1 keine essentiellen Funktionen in Thrombozyten übernimmt. Nichtsdestotrotz besteht möglicherweise eine funktionelle Redundanz zwischen verschiedenen Proteinen, die Zytoskelett-vernetzende Interaktionen vermitteln.

CONTENTS

1 INTRODUCTION

1.1 Platelet biogenesis

Mammalian blood platelets are small cells that lack a nucleus due to their unique way of biogenesis by megakaryocytes. Megakaryocytes extend long protrusions, so-called proplatelets, into sinusoidal blood vessels where platelets are finally shed into the bloodstream by shear forces.[1–3] In all other animal species like birds and fish, cells involved in hemostasis and blood coagulation are nucleated (reviewed in Chapter I.1. in [4]).

The differentiation of stem cells to megakaryocytes is tightly regulated by transcription factors, signaling pathways, cytokines and adhesion molecules (Figure 1.1.1). Two major players, which promote the growth and development of megakaryocytes from hematopoietic stem cells, is the cellular myeloproliferative leukemia protein receptor (c-Mpl) and its ligand thrombopoietin (TPO), a glycoprotein hormone produced by the liver and kidney.[5] c-Mpl deficient mice show an 85 % decrease in platelet as well as in megakaryocyte number, whereas the amount of other hematopoietic cells is unaltered. In addition, the mean platelet volume of the remaining platelets in the c-Mpl and TPO knockout mouse lines is significantly increased.[6]

During maturation, megakaryocytes become polyploid (up to 128n) due to the process of endomitosis (repeated incomplete cell cycles lacking karyokinesis and cytokinesis),[7] and develop the demarcation membrane system (DMS), which forms the plasma membrane for future platelets.[8] The bone marrow is the main site of platelet production. In addition, megakaryocytes can also be localized in the spleen of adult mice as well as in the yolk sac and the fetal liver during early murine development.[8–10] A recent publication suggests that the lung also hosts some megakaryocytes.[11]

The force necessary for internal DMS invagination relies on the assembly of filamentous actin (F-actin) via Wiskott–Aldrich Syndrome protein (WASP)- and actin-related protein 2/3 (Arp2/3) complex-dependent mechanisms activated through phosphatidylinositol-4,5-bisphosphate (PIP_2) and Rho-like GTPases.[12] Further, cell division cycle 42 (Cdc42) protein-dependent F-actin dynamics were found to drive the structuration of the DMS to polarize membranes and nuclei territories.[13]

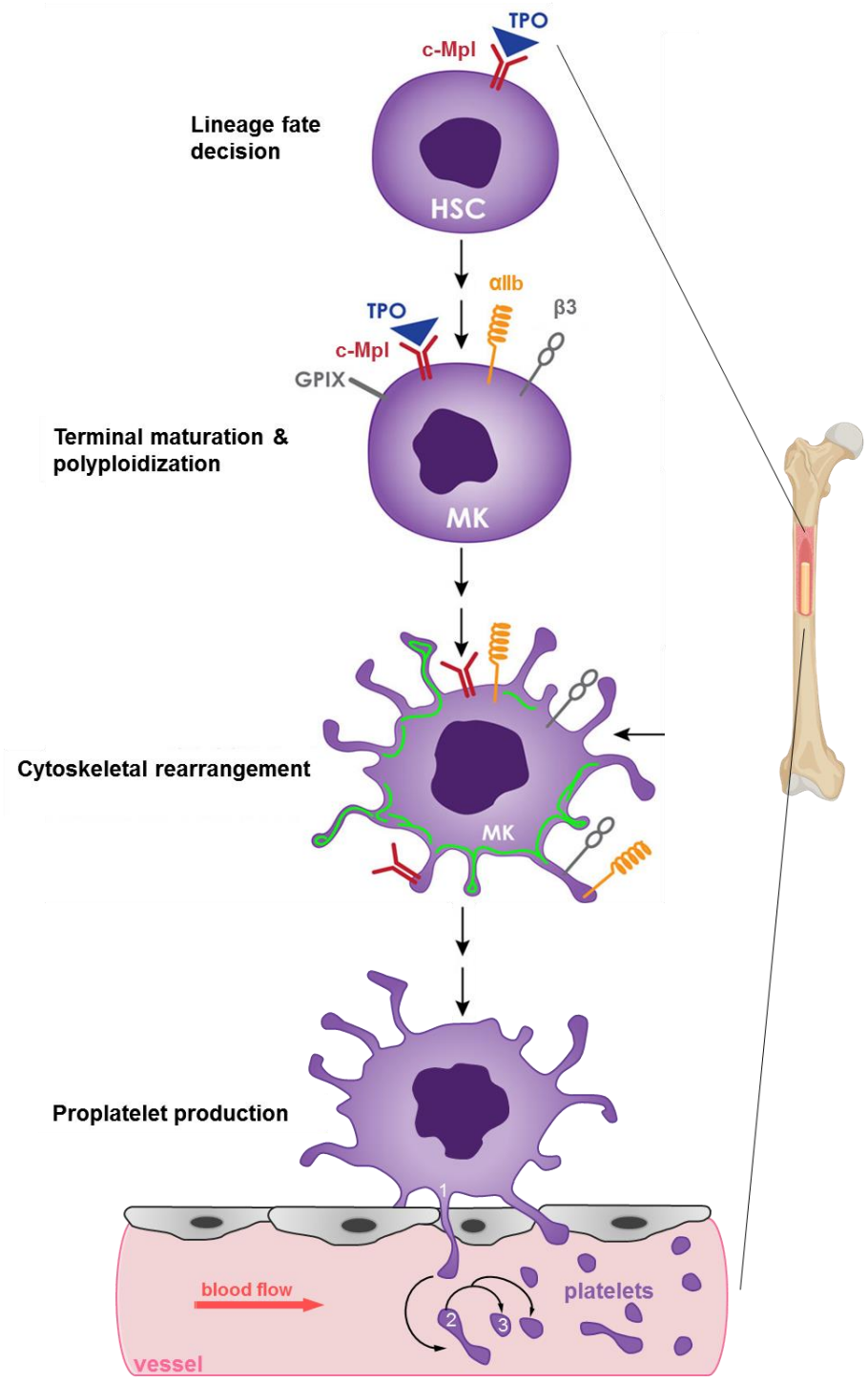

Figure 1.1.1: Megakaryocyte differentiation and platelet biogenesis. Start of megakaryopoiesis with signaling of the cytokine TPO via its receptor c-Mpl which is already expressed on the surface of hematopoietic stem cells (HSC). During multiple steps of lineage face decision, the upregulation of transcription factors leads to the expression of specific surface receptors like αIIb, β3 or GPIX. Further, terminal maturation processes like polyploidization, cytoskeletal rearrangement (e.g. in green; expression of β1-tubullin) and the extension of (1) proplatelets through the endothelium into a blood vessel take place. (2) Release of barbell-shaped proplatelets and final platelet sizing (3) occurs in the blood stream in a shear-dependent manner. Adapted from [14]

Recently, a pivotal role of Phosphoinositide-dependent protein kinase-1 (PDK1) in regulating megakaryocyte cytoskeletal dynamics, polarization, proplatelet formation and thrombopoiesis was reported. Pdk1-deficient mice showed an impaired spreading due to alterations in the actin cytoskeleton and displayed a significant macrothrombocytopenia despite a dramatically increased number of megakaryocytes in the bone marrow.[15] Also in other mouse models, like the double deficient ADF and n-cofilin animals, the loss of actin regulating proteins resulted in a defective proplatelet formation and thrombocytopenia.[16] *In vitro* observations revealed that platelet production starts with the extension of large pseudopodia that use cortical bundles of microtubules to elongate and form thin proplatelets with bulbous ends.[8] (Figure 1.1.1 and Figure 1.1.2) β1-tubulin is an essential cytoskeletal protein that dimerizes with α-tubulin and polymerizes into long microtubules that are arranged into bundles in the megakaryocyte cortex when proplatelet extension starts.[3,17] The microtubule bundles run throughout the length of proplatelet shafts and tips and provide the primary force for proplatelet elongation via dynein-dependent microtubule sliding.[18] The final production and sizing of platelets take place in a shear-dependent manner in the bloodstream. Released barbell-shaped proplatelets reversibly convert into so-called preplatelets and undergo successive rounds of fission along their midbody and at their ends.[14] (Figure 1.1.1) This process is driven by twisting microtubule-based forces until they are fragmented into individual platelets with a usual size of about 1-3 µm in diameter.[18]

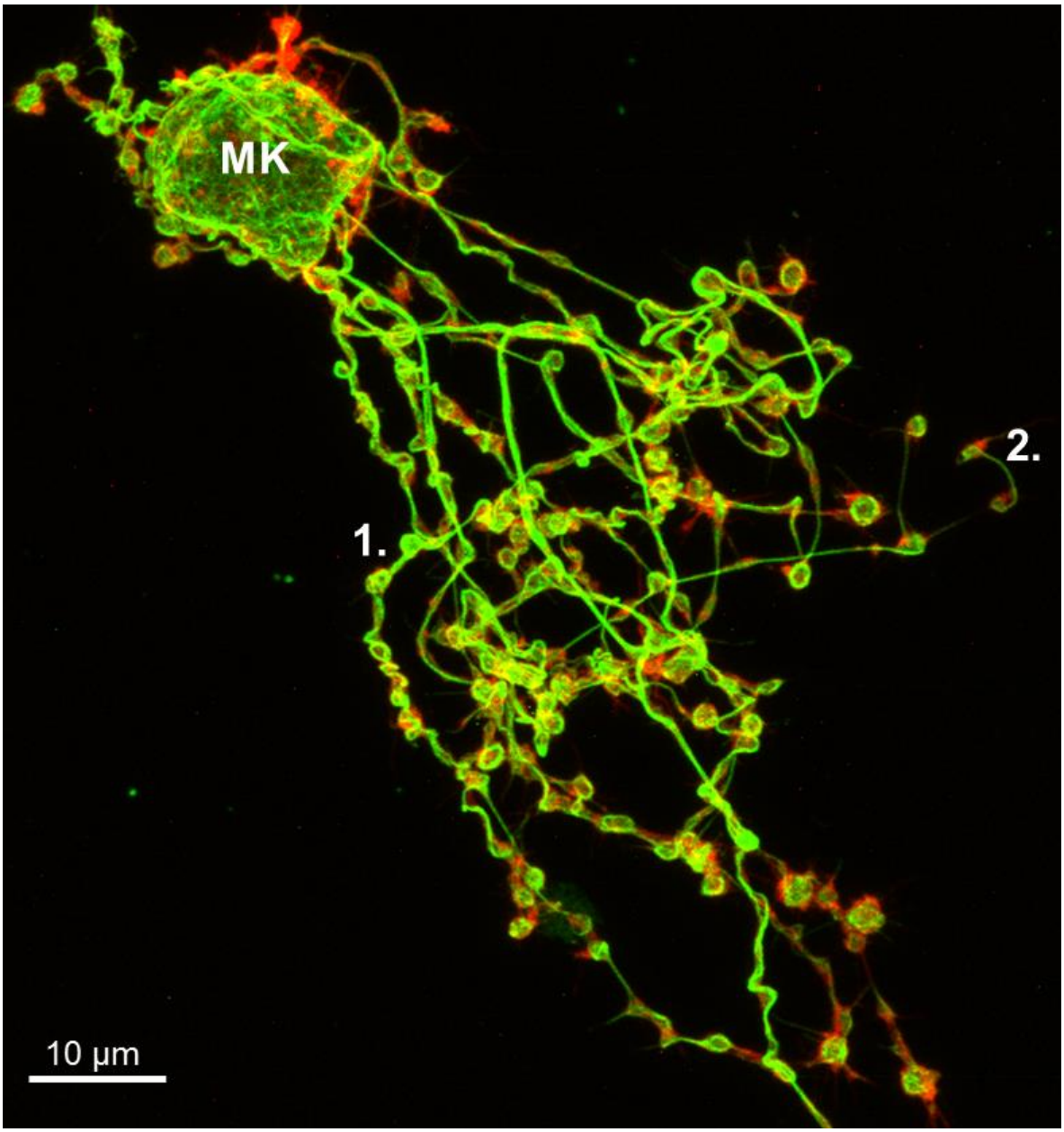

Figure 1.1.2: *In vitro* proplatelet forming megakaryocyte. Fetal liver cell-derived megakaryocytes were cultured *in vitro*. Elongated (1.) proplatelets and (2.) released barbell-shaped proplatelets were present after 5 days of culture. α-tubulin (green) and F-actin (red) were stained and visualized via confocal microscopy. Picture kindly provided by Dr. Markus Spindler.

1.2 Platelet activation and thrombus formation

Circulating platelets are essential players in hemostasis and thrombosis. A constant platelet production is required to compensate for the clearing of aged platelets by macrophages in the liver and the spleen. Thereby the platelet concentration is kept at a level of 150 000 to 450 000 platelets per microliter blood in humans and approximately 1 000 000 platelets per microliter blood in mice.[19,20] Whereas human platelets have a lifespan of 7-10 days and a diameter of 1-2 µm, murine platelets with

a diameter of 0.5 µm circulate in the blood for about 5 days.[19,20] Both human and murine platelets contain three major types of granules, which are released upon activation:[21,22] (1.) In α-granules over 300 proteins, which facilitate platelet adhesion, clot stabilization and fibrinolysis, wound repair and inflammation, are stored, including the membrane receptors P-selectin and αIIbβ3 integrin and soluble cargos like platelet factor 4 (Pf4), fibrinogen and von Willebrand factor (VWF). (2.) Dense- (δ) granules contain amines like serotonin and histamine, ADP and high concentration of cations, such as calcium, which amplify platelet activation, blood vessel constriction and wound repair. (3.) Lysosomes (or λ-granules) store proteolytic enzymes that contribute to thrombus remodeling. Disorders like the Hermansky-Pudlak syndrome with impaired formation or secretion of granules result in excessive bleeding.[21,22]

Endothelial cells keep circulating platelets in a resting and non-adherent state via the release of platelet inhibitory substances like prostaglandin I_2 and nitric oxide. In addition, endothelial cells metabolize platelet agonists like adenosine diphosphate (ADP) and thromboxane A2 into inactive products to prevent platelet activation.[23] Upon vascular injury, platelets rapidly adhere to exposed extracellular matrix proteins and form a hemostatic plug that limits excessive blood loss but also represents a major pathomechanism of ischemic cardio- and cerebrovascular diseases.[24] Thrombus formation is a multi-step process (Figure 1.2.1) that can be divided into separate phases: (1.) initial (un)stable adhesion and platelet activation, (2.) recruitment of additional platelets and aggregation, (3.) thrombin generation, (4.) stable clot formation and contraction.

At first, platelet tethering is mediated by the interaction of glycoprotein Ib-V-IX complex with immobilized VWF on exposed subendothelial collagen. This interaction enables the binding of the glycoprotein VI (GPVI) to collagen, which in turn initiates cellular activation. Subsequent inside-out upregulation of integrin affinity, granule release, and coagulant activity contribute to firm platelet adhesion and thrombus growth.[25] In parallel, the secondary hemostatic response is initiated through the extrinsic pathway of coagulation, via interaction of coagulation factor VIIa and exposed tissue factor, and the intrinsic pathway via factor IX and Prothrombin (also known as factor II), finally leading to the generation of thrombin (also known as factor IIa). These processes as well as the release of ADP and thromboxane A2 further stimulate G protein-coupled receptors (GPCR) and reinforce the activation response. Activated integrins mediate firm platelet adhesion to the vessel wall and to other platelets via binding of integrin

αIIbβ3 (also known as glycoprotein IIb/IIIa) to fibrinogen, leading to thrombus growth. Thrombin converts fibrinogen to fibrin for the formation of a stable clot. The intracellular Ca^{2+} concentration and the procoagulant activity of activated platelets, which leads to the exposure of phosphatidylserine on the platelet surface, increase during these steps finally leading to an amplification of platelet activation, clot stabilization, blood vessel constriction and inflammation.[25,26]

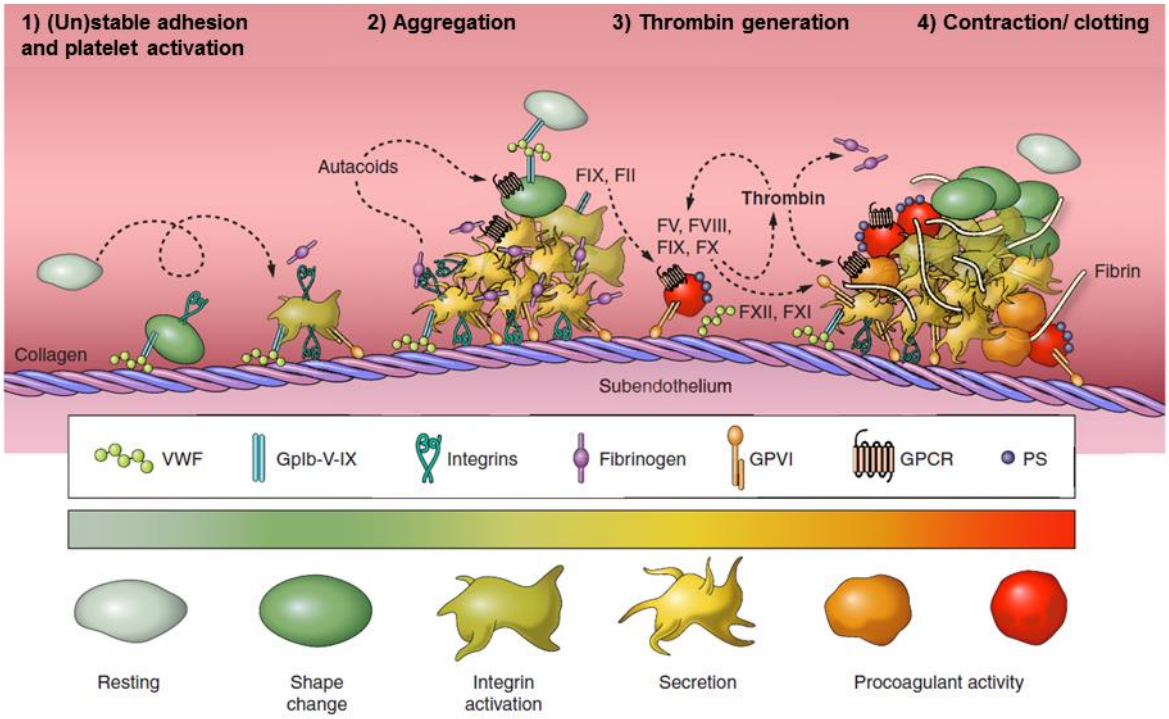

Figure 1.2.1: Platelet activation and thrombus formation. Resting platelets express many surface receptors that respond to ligands that are exposed upon injury and/or inflammation of the vessel wall. In a first step, tethering of platelets at the site of injury is mediated. Platelet binding to collagen induces the cellular activation, resulting in platelet shape change, granule release and the conformational activation of integrins. Activation of additional platelets leads to thrombus growth. In parallel, the secondary hemostatic response is initiated through the extrinsic pathway of coagulation. These processes further stimulate GPCR receptors and the activation response. Activated integrins mediate firm platelet adhesion to the vessel wall and to other platelets. Fibrin production leads to the formation of a stable clot. The heat map indicates the increase in intracellular Ca^{2+} concentration (green = low Ca^{2+} to red = high Ca^{2+} signal) during all steps and depicts the procoagulant activity of activated platelets, which leads to the exposure of phosphatidylserine (PS) on the platelet surface. Taken from [26].

During vascular injury and thrombus growth platelets become activated by various agonists. However, these agonists vary in their origin, potency and mobility. Collagen fibers are immobile and only found at the bottom of a thrombus, whereas ADP and

thromboxane A2 are freely diffusible. In contrast, thrombin is mainly present within the thrombus core and its distribution is limited by interactions with other proteins and inhibitors.[27] Using a fluorescein coupled albumin biosensor and a thrombin activity sensor, a low transport region (Figure 1.2.2 A) was found to match to the region with the greatest platelet packing density, lowest porosity therefore a decreased plasma molecule penetration but high thrombin activity.[27] Slower molecular transport in the core region supports the storage of soluble agonists, which in turn contributes to full platelet activation, α-granule release as well as P-selectin exposure. Faster molecule and protein transport rates and greater thrombus instability is found within the thrombus shell. (Figure 1.2.2 A-C) This architecture supports a limited platelet activation and thrombus size.[27] However, regional differences within hemostatic thrombi are not only limited by the extend of platelet activation but also by surrounding physical differences.[28]

In the central part of a vessel the velocity reaches its maximum, which gradually diminishes as the blood approaches the vessel wall.[29] Further, rotating erythrocytes, which constitute 40 % of the blood volume, increase the concentration of platelets near the vessel wall.[30] Depending on the vessel diameter different shear flow rates can be found. High shear rates are found in small (100-150 µm diameter) capillaries and arterioles (1000-1800 s^{-1}), whereas low shear rates are found in the aorta, arteries and venules (150-400 µm diameter and a shear rate of 100-300 s^{-1}).[31] An increasing shear rate also increases the platelet deposition to the surface, activation, adhesion and cohesion.[29] To mimic *in vivo* thrombus formation, whole blood can be perfused at different shear rates over a collagen-coated surface. (Figure 1.2.2 D) Microscopic investigations of the platelet shape and especially the cytoskeletal organization of platelets in an *in vivo* formed thrombus are important to understand the architecture of a thrombus, however this has only been poorly studied. Therefore, *ex vivo* thrombus formation might be a useful technique to investigate the cytoskeletal organization of platelets in different thrombus layers. Which cytoskeletal structures are important for thrombus formation is only poorly studied and if the generation of F-actin dependent platelet lamellipodia plays an essential role during these processes is discussed controversially.[32–36]

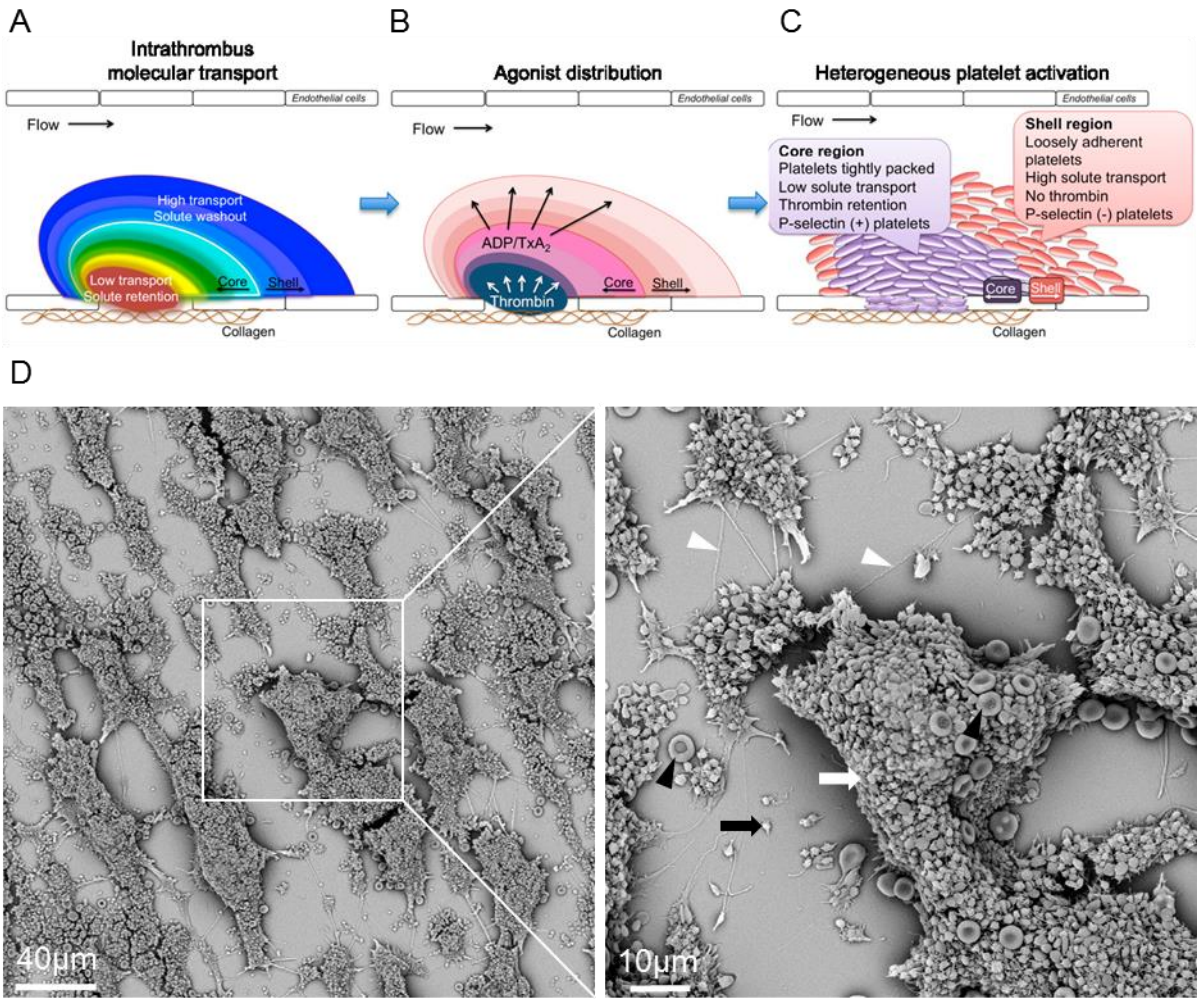

Figure 1.2.2: Thrombus architecture and *ex vivo* thrombus formation. During thrombus growth platelets become activated, change their shape, retract and tightly pack together. (A) This leads to the formation of low transport solute retention and high transport solute washout region. (B) The agonist distribution differs within the thrombus core and shell region. (C) Platelets within a thrombus have a heterogeneous activation status. A-C taken from [27]. (D) *Ex vivo* thrombus formation. Murine whole blood was perfused at a shear rate of 1000 s^{-1} over a collagen-coated surface and further analyzed by scanning electron microscopy. Erythrocytes (black arrowhead), collagen fibers (white arrowhead), single platelets (black arrow) and platelet aggregates (white arrow) are indicated.

1.3 The actin cytoskeleton

Actin is an evolutionarily highly conserved protein. Structurally and functionally related actin molecules can be found in bacteria, archaea and eukaryotes.[37] Many eukaryotes, including budding yeast or the green alga *Chlamydomonas*, are equipped with a single actin gene to generate all required cytoskeletal structures. In contrast, humans have three actin coding genes, α-actin for muscles, β-actin for nonmuscle cells and γ-actin for smooth muscles and nonmuscle cells.[38] Mutations in α-actin cause myopathy- and

angiopathy-associated defects, mutations of the β-actin and γ-actin isoforms lead to a diverse spectrum of diseases including deafness, cancer and developmental disorders.[39]

In many cells, actin (e.g. *ACTB* gene coding for 375 amino acids and 42kDa weight) is one of the most abundant proteins, often accounting for more than 10 % of total protein content. The actin filament has a diameter of about 8 to 10 nm.[40] Actin participates in a large variety of cellular processes such as phago- and endocytosis, cell polarization, migration and cytokinesis. These processes depend on the dynamic behavior of actin to polymerize to filaments and the following depolymerization of these filaments back into globular (G-) actin, the actin monomer.[40]

Generally, actin filament polymerization occurs in three phases: (1.) nucleation; (2.) elongation and a (3.) steady state phase. In the nucleation phase, actin monomers assemble to form polarized actin filaments that consist of a (10 times) faster-growing (+) barbed end and a slower-growing (-) pointed end. Spontaneous actin polymerization strongly depends on the concentration of free actin monomers. Actin dimers and trimers are very unstable, whereas the addition of a fourth and more subunit is more stable. Due to the energetically unfavorable situation, the formation of a polymerization-competent nuclei is the rate-limiting step, whereas F-actin elongation proceeds rapidly.[41]

Actin contains an adenosine triphosphate (ATP) nucleotide-binding cleft and forms a right-handed F-actin helix when polymerized. ATP-bound G-actin monomers start to polymerize spontaneously *in vitro* in the presence of K^+ or Mg^{2+}. Over time ATP, bound to the polymerized subunits is hydrolyzed randomly ($t_{1/2}$ = 2 s) to ADP and phosphate (P_i).[42] The dissociation of phosphate from F-actin is slow ($t_{1/2}$ = 6 min) and occurs first before ADP-bound G-actin is released from the pointed end into the soluble pool of actin monomers. Many actin-binding proteins that either play a role in the different dynamic phases of actin filament polymerization or the molecular and spatial F-actin organization have been identified (Figure 1.3.1).

The dynamic regulation of F-actin polymerization and depolymerization plays an essential role in the function of platelets and megakaryocytes. Platelets contain about two million actin molecules of which approximately 40-50 % of the total actin monomer concentration is implemented in 2000-5000 actin filaments in resting platelets.[17,43] Upon activation of platelets with thrombin the amount of F-actin quickly increases to

70 %.[44,45] Although there are several causes (e.g. autoimmune reactions) that lead to a low platelet count, many inherited thrombocytopenias in humans are associated with defects in platelet biogenesis and are caused by mutations in genes coding for direct or indirect F-actin interacting proteins. One example is the Arp2/3 complex, which initiates the formation of branched actin filaments at membranes throughout the cell (Figure 1.3.1 B and Chapter 1.3.1).[46] A homozygous frameshift mutation in the human *ARPC1B* gene leads to a loss of ARPC1B protein expression and also reduces the expression of the whole Arp2/3 complex. This loss causes a microthrombocytopenia and is associated with inflammatory disease.[47] Another example is Filamin A, which tethers platelet receptors like glycoprotein Ibα and integrin αIIbβ3 to the cytoskeleton and crosslinks actin fibers (Figure 1.3.1 H). Mutations in the X-linked *FILAMIN A* gene are associated with thrombocytopenia, an abnormal differentiation of *in vitro* cultured megakaryocytes,[48] altered GPVI signaling pathway dependent platelet responses and thrombus formation. Further, Filamin A-negative platelets showed an enhanced spreading, suggesting that Filamin A has a negative effect on cytoskeletal reorganization.[49]

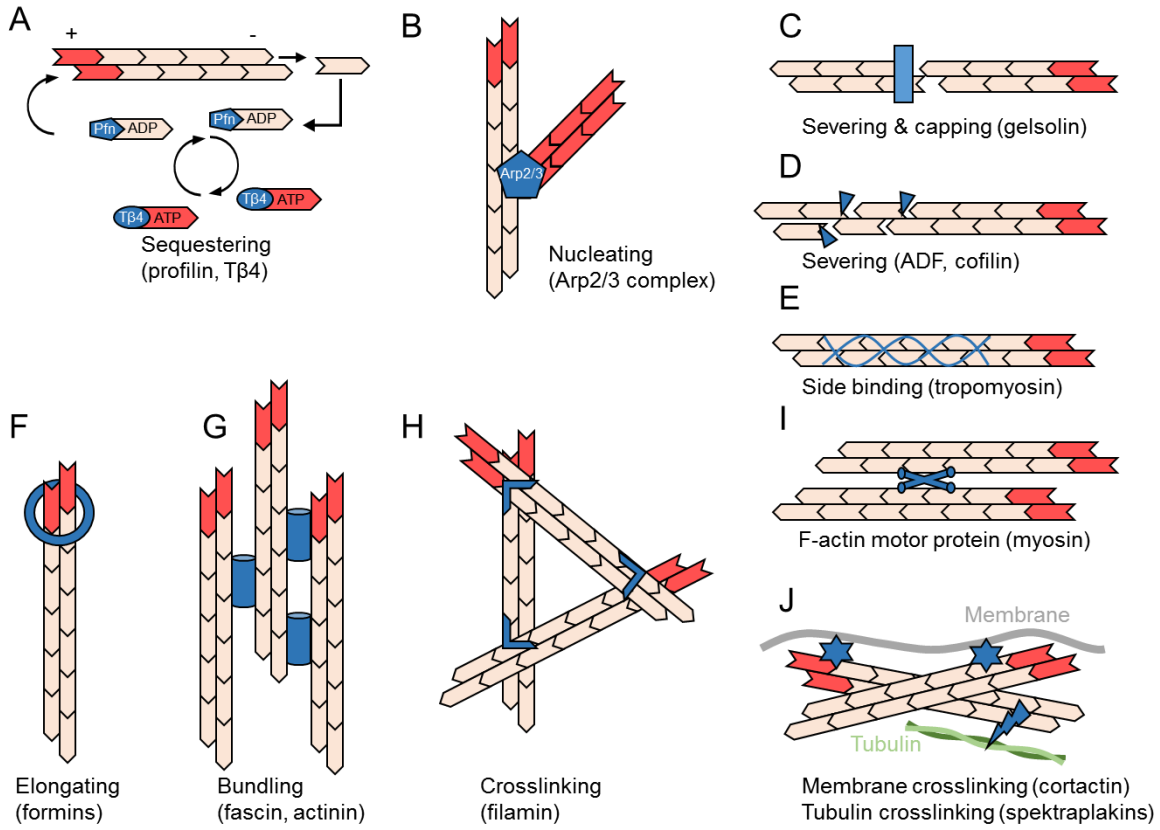

Figure 1.3.1: Exemplary actin-binding and regulating proteins. (A) G-actin can be sequestered by profilin or thymosin beta-4 (Tβ4). (B) The Arp2/3 complex is stabilizing actin nuclei and initiating the formation of 70° branched actin filaments at the side of pre-existing mother filaments. (C) Gelsolin is an F-actin severing and capping protein. (D) Cofilin and Actin depolymerizing factor (ADF) severs and depolymerizes ADP-G-actin from actin filaments. (E) Tropomyosins stabilize existing actin filaments via lateral binding along both strands. (F) Formins stabilize actin dimers and support the actin nucleation and elongation process. (G) Fascin and actinin organize F-actin filaments in straight bundles. (H) Filamin organizes actin filaments into cross-linked actin webs. (I) Myosins are a large family of ATP-dependent motor proteins that are responsible for actin-based motility and contractility. (J) Cortactin crosslinks F-actin to cell membranes. Spectraplakins build a connection between F-actin and microtubules. Adapted from [41].

1.3.1 Regulation of the Arp2/3 complex

The Arp2/3 complex is an assembly of seven subunits (ARPC1, ARPC2, Arp2, ARPC3, Arp3, ARPC4, ARPC5), that is intrinsically inactive because the Arp2 and Arp3 subunits are held apart by the other subunits.[50] The Arp2/3 complex is activated by multiple nucleation-promoting factors (Figure 1.3.1) including five subfamilies: (1.) WASP and neuronal-WASP (N-WASP; also known as WASL), (2.) the three WASP family verprolin homolog isoforms (WAVE1–WAVE3), (3.) WASP homolog associated with actin, membranes and microtubules (WHAMM), (4.) WASP and SCAR homolog

(WASH), and (5.) junction-mediating regulatory protein (JMY).[51] Upon activation, the Arp2/3 complex binds to an actin filament, whereby the Arp2 and Arp3 subunits move closer together and form the basis for the growth of a branch. The free barbed end of the daughter filament elongates, whereas the Arp2/3 complex anchors the pointed end of the filament rigidly to the side of the mother filament.[46]

The mammalian WASP family proteins possess a carboxy-terminal homologous sequence, the WCA region, consisting of WASP homology 2 (WH2) domain (also known as verprolin homology domain), the connecting domain (also known as cofilin homology domain), and the acidic region, by which they bind to and activate the Arp2/3 complex.[52] In addition to the WCA domain the WASP family proteins also contain unique domains that regulate their assembly into macromolecular complexes, their subcellular localization and their interaction with proteins that regulate their activity. Thereby, the spatial and temporal activity of the Arp2/3 complex can be regulated, and thus the formation of branched F-actin at membranes throughout the cell (Figure 1.3.1).

N-WASP is ubiquitously distributed, whereas WASP is restricted to hematopoietic cells.[53] Upon interaction with Cdc42, the autoinhibited conformation of (N-) WASP is relieved and the protein can proceed with actin nucleation by activation of Arp2/3 via the WCA domain.[54] (N-) WASP is involved in F-actin dependent and Arp2/3 mediated processes like endocytosis, phagocytosis, host-pathogen interactions and invadopodia formation (Figure 1.3.3 A). Patients with function-disrupting mutations in the *WASp* gene suffer from the Wiskott–Aldrich syndrome (WAS) and display several immune cells related phenotypes, microthrombocytopenia and excessive bleeding.[55] Megakaryocytes of WASp-deficient mice are unable to form podosomes and prematurely form proplatelets into the bone marrow.[56,57] Similarly, during early spreading, platelets from WASp-deficient mice and WAS patients are unable to form actin nodules, which are integrin-dependent actin-rich structures that are enriched in the adhesion-related proteins talin and vinculin.[58]

Polyubiquitylation of the intrinsically inactive macromolecular pentameric WASH regulatory complex (SHRC) is regulated by the TRIM27-containing ubiquitin ligase complex, which causes a conformational change of the WASH subunit that results in exposure of its WCA domain.[59] The WASH complex is involved in receptor trafficking, maintenance of the endolysosomal structure and endosomal F-actin nucleation and

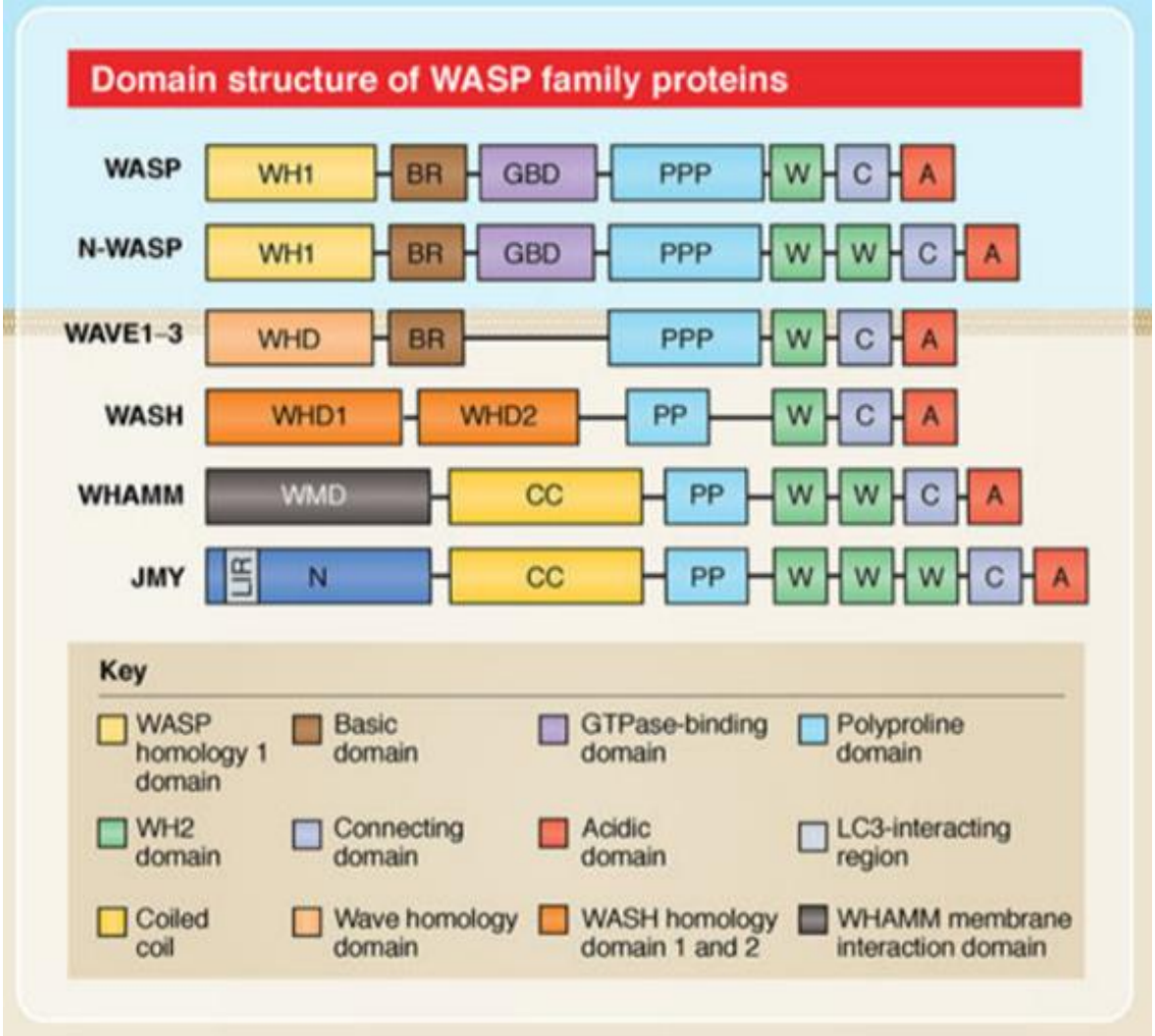

Figure 1.3.2: Domain structure of mammalian WASP family proteins. The mammalian WASP family proteins possess a WCA region domain by which they bind to and activate the Arp2/3 complex. The WH1 domain is required to stabilize N-/WASP. Direct binding of GTP-bound Cdc42 to the GTPase binding domain (GBD) domain relieves the autoinhibitory fold of WASP. Phosphatidyl-inositol (4,5)-bisphosphate binding to N-WASP basic domain promotes F-actin nucleation. Binding of G-actin bound profilin to the polyproline domain provides a pool of monomeric actin for F-actin generation. WAVE possesses an N-terminal Wave homology domain and promotes lamellipodia formation. WASH contains an N-terminal WASH homology domain 1 (WHD1) as well as a tubulin-binding WHD2 domain and was found to localize to endosomes. Upon Rab1 binding to the N-terminal WHAMM membrane interaction domain (WMD), WHAMM mediates actin assembly and membrane recruitment is inhibited. Further, WHAMM carries a coiled-coil (CC) microtubule-binding domain and has been found to localize to the endoplasmatic reticulum. JMY can promote Arp2/3 dependent branched actin filaments and also generates unbranched filaments via the tandem WH2 domains. JMY can be found at the leading edge of a cell but also in the nucleus upon DNA damage. Adapted from [51].

vesicle scission (Figure 1.3.3 A). The subunits of the WASH regulatory complex are expressed in human and mouse platelets.[60,61] However, its role in platelets has not been studied so far.

The pentameric WAVE regulatory complex (Figure 1.3.3 B) is structurally related to the WASH regulatory complex. Upon interaction of the Ras-related C3 botulinum toxin substrate 1 (Rac1) with the WAVE complex subunit Cyfip1/2 the WCA domain is exposed and induces Arp2/3 mediated branched F-actin formation.[62] The WAVE complex is involved in lamellipodia formation, cell migration and invasion.

WHAMM (Figure 1.3.3 C) possesses an actin nucleation activity and is localized to the endoplasmatic reticulum (ER)-Golgi intermediate compartment (ERGIC), induces membrane tubulation and regulates vesicle transport between Golgi and ER.[63]

Originally, JMY (Figure 1.3.3 C) was identified as a transcriptional co-factor in the protein 53-response to deoxyribonucleic acid (DNA) damage.[64] In addition, JMY was found to localize at the leading edge of the cell and to activate the Arp2/3 complex, thereby producing branched actin filaments.

Further, JMY can generate unbranched actin filaments via its tandem WH2 domains and is involved in vesicle trafficking from the trans-Golgi network.[64,65] According to proteomic analyses, JMY is expressed at low levels in murine but not in human platelets.[60,61]

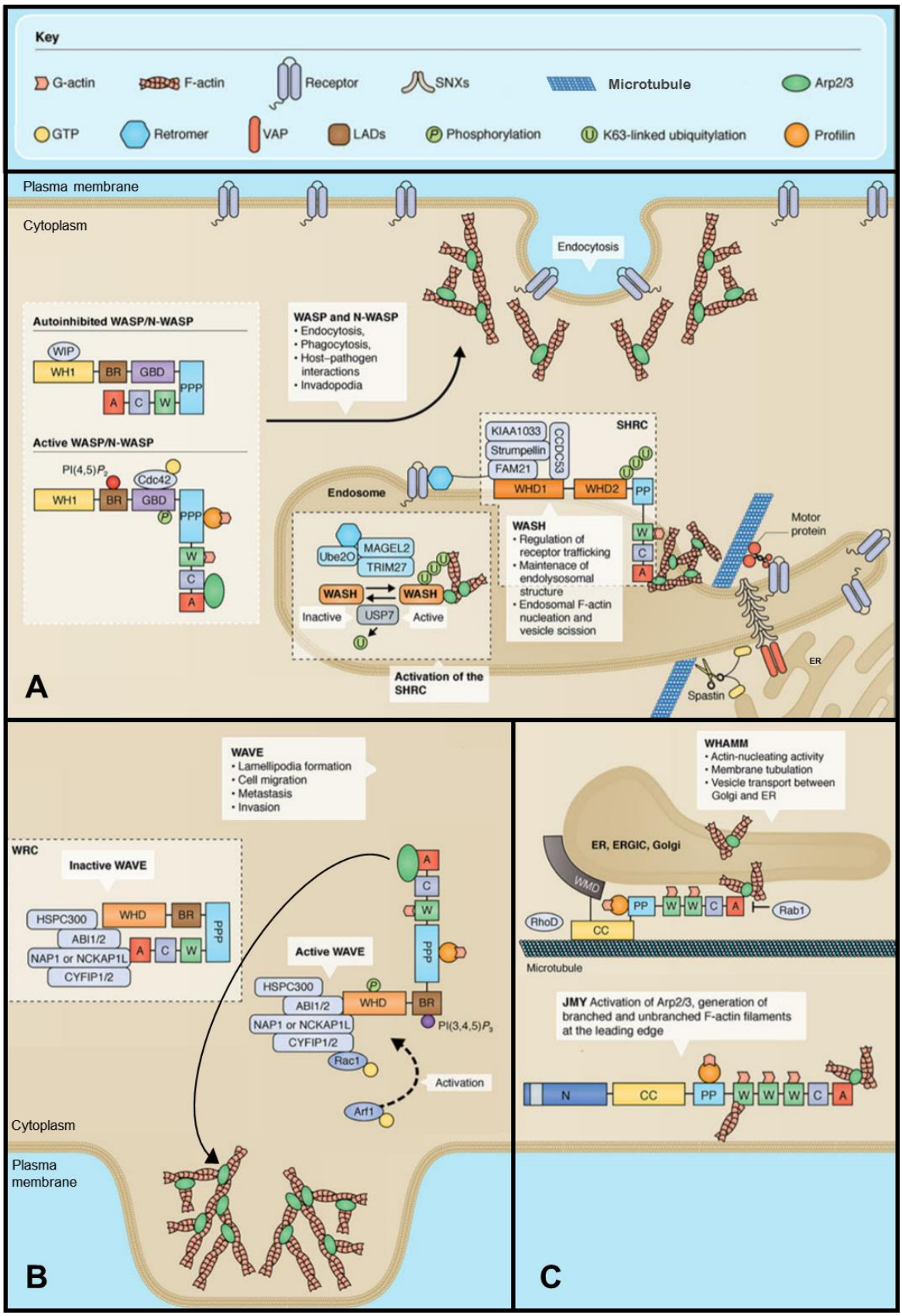

Figure 1.3.3: Role of WASP family proteins as nucleation-promoting factors of the Arp2/3 complex. (A) Cdc42 activates (N-) WASP which can proceed with actin nucleation by activation of the Arp2/3 complex via interaction with the WCA domain. (N-) WASP is involved in F-actin dependent and Arp2/3 mediated processes like endocytosis,

phagocytosis, host-pathogen interactions and invadopodia formation. Polyubiquitylation of pentameric WASH regulatory complex (SHRC) causes a conformational change and the exposure of the WCA domain. The WASH complex is involved in receptor trafficking, maintenance of the endolysosomal structure and endosomal F-actin nucleation and vesicle scission. (B) Upon interaction of Rac1 with the WAVE complex subunits Cyfip1/2 the WCA domain is exposed and induces Arp2/3 complex mediated branched F-actin formation at the plasma membrane. Thus, the WAVE complex is involved in lamellipodia formation, cell migration and invasion. (C) WHAMM possesses an actin nucleation activity and is localized to the endoplasmatic reticulum (ER)-Golgi intermediate compartment (ERGIC), induces membrane tubulation and regulates vesicle transport between Golgi and ER. JMY is localized at the leading edge of the cell, activates the Arp2/3 complex and thus produces branched F-actin filaments, further JMY has the ability to generate unbranched actin filaments via its tandem WH2 domains. Adapted from [51].

1.3.2 Cyfip1 and the WAVE complex

The human Cytoplasmic FMRP (Fragile X mental retardation protein)-interacting Protein 1, abbreviated CYFIP1 (also known as P140SRA-1 or SRA-1) is an evolutionary highly conserved protein with 1253 amino acids (140 kDa), that shares 88 % amino acid sequence identity with its homolog CYFIP2.[66] In 2001, human CYFIP1 and CYFIP2 were described as members of a highly conserved protein family of FMRP- interacting proteins, which share 99 % amino acid sequence identity with their mouse orthologues.[66] Further, CYFIP proteins have been linked to the fragile X mental retardation syndrome,[67] the Angelman syndrome,[68] autism and other neurological disabilities in humans.[69,70] Recently, it was shown that Cyfip1 haploinsufficient rats show myelin thinning, abnormal oligodendrocytes and behavioral inflexibility.[71] In mice, haploinsufficiency of Cyfip1 produces fragile X-like phenotypes, whereas knockout embryos with disruption of both copies of *Cyfip1* cannot be found even in early embryonic (E) stages.[72] This indicates that Cyfip1 is essential for early embryonic development. Cyfip1 and Cyfip2 have different patterns of expression during murine brain development. While in mice, Cyfip1 is expressed at all ages with a peak in the third postnatal (P3) week, Cyfip2 is moderately expressed at P3 and gradually increases after P7.[73]

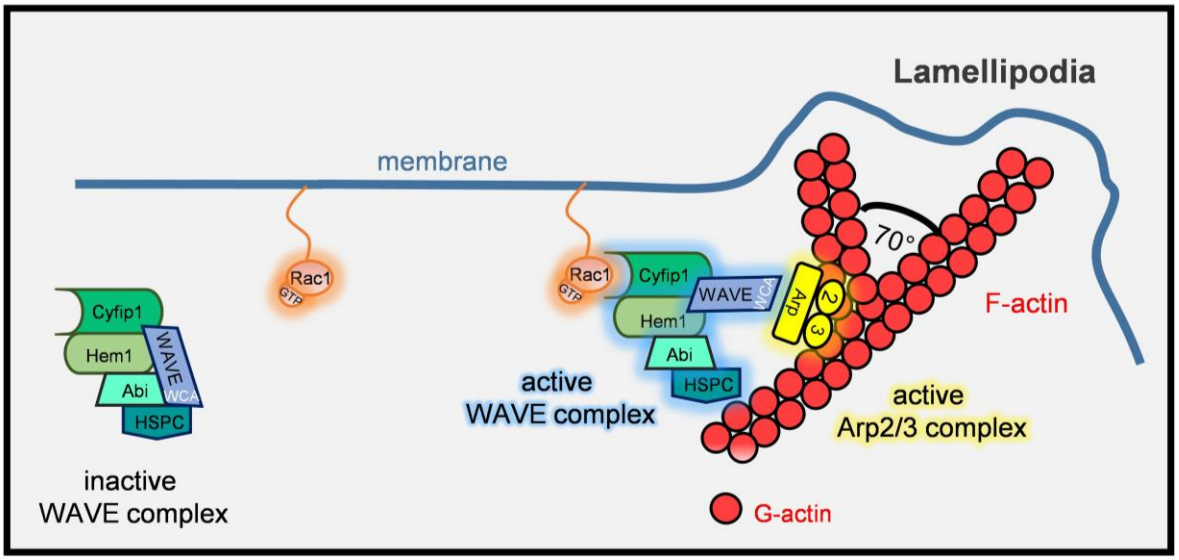

Figure 1.3.4: Illustration of WAVE complex-mediated lamellipodia formation. The WCA domain of the WAVE protein is masked in the inactive WAVE complex. Upon interaction of the subunit Cyfip1/2 and Rac1-GTP, the WCA domain of the WAVE protein is exposed and interacts with Arp2/3, forming branched actin filaments. Adapted from [74].

In 1997, Cyfip1 has been described as specifically Rac1-associated protein (SRA-1) that also interacts with the actin cytoskeleton. The N-terminal domain (amino acid 1-407) of Cyfip1 was found to be responsible for the interaction with Rac1.[75] Further, Cyfip1 was identified as a subunit of the WASp family verprolin-homologous protein (WAVE) regulatory complex, a five-subunit protein complex (Figure 1.3.4), which includes the proteins WAVE-1/-2/-3, Abelson interactor 1/2 (ABI1/2), NCK associated protein1 (NCKAP1) or Hematopoietic protein 1 (HEM1; also known as NCKAP1L), Hematopoietic Stem/Progenitor Cell Protein 300 (HSPC300; also known as BRICK1) and Cyfip1/2.[51] The combination of different paralogous subunits creates a diverse repertoire of 36 different pentameric mammalian WAVE complexes and this diversity of complexes most likely regulates the activity of the three WAVE proteins within the complex.[74] The WAVE proteins were shown to be actin nucleation-promotion factors (NPFs) of the Arp2/3 complex. The molecular mechanism of WAVE protein activation was studied in HEK293 cells that stably expressed FLAG-tagged subunits of the WAVE complex. Considering the diverse repertoire of WAVE complexes, Derivery *et al.* focused on the major WAVE complex expressed by Hela cells consisting of Cyfip1, NCKAP1, WAVE2, ABI1 and HSPC300.[76] They found that the WCA domain of the WAVE protein is masked in the native WAVE complex and due to this, it is *per se* inactive. However, upon interaction of the subunit Cyfip1/2 and Rac1 bound to

guanose-5´-intriphosphate (GTP), the WCA domain of the WAVE protein is exposed and interacts with Arp2/3, forming branched actin filaments (Figure 1.3.4).[74] Lack of any subunit of the WAVE complex leads to proteasomal degradation of all components.[77,78]

Table 1.3.1 Platelet proteomic studies. Copy numbers of subunits of the WAVE complex, of Rac1, Arpc2 and actin determined by quantitative mass spectrometry. Adapted from [60,61].

Platelet protein	*Human* [60] *[Protein copy number]*	*Murine* [61] *[Protein copy number]*
Cyfip1	6000	6021
Cyfip2	2600	308
Wave1 (also known as Wasf1)	1400	Not listed
Wave2 (also known as Wasf2)	3100	6178
Wave 3 (also known as Wasf3)	1000	Not listed
Hem1(also known as Nap1 or NCKAP1L)	4400	5411
Abi1/2 (splice variants)	7500/3800	3194
HSP300 (also known as Brick1)	8600	8391
Rac1	32900	16000
Arpc2	17400	49677
Actin	795000	882635

Proteomics studies (Table 1.3.1) and western blot analysis identified all three WAVE isoforms to be expressed in human platelets.[60,61,79] In murine platelets only WAVE2 was detected by proteomic[61] analysis whereas further publications also confirmed the expression of the WAVE1 isoform via western blot[80] analysis. Homozygous disruption of the *Wave1* gene in mice resulted in postnatal lethality with an average lifespan of 23.6 days.[81] Analysis of platelets of young mutant mice (age of 14-20 days) revealed that WAVE1 plays an important role downstream of GPVI.[80] WAVE2-null mice died at embryonic day 12.5 and their *in vitro* differentiated megakaryocytes exhibited spreading defects.[82] The Cyfip1 protein is mainly in a complex with the WAVE2 isoform,[76,83,84] its role for platelet function has not been studied so far. *In vitro* studies have shown that after getting in contact with immobilized adhesive proteins such as fibrinogen, platelets start to spread and form finger-like protrusions at first, so-called filopodia. These filopodia are then remodeled into lamellipodia, which are flat, undulating cellular protrusions with orthogonally arrayed short actin filaments. A fully

spread platelet displays a circumferential zone of orthogonally arrayed short filaments within lamellipodia.[44] The formation of platelet lamellipodia was shown to be an Arp2/3 dependent mechanism since platelets with a 95 % decreased expression of the Arp2/3 complex subunit Arpc2 were unable to form lamellipodia.[36] Further, a role for the small GTPase Rac1 in platelet lamellipodia formation was demonstrated using mice with deletion of Rac1 in the hematopoietic system (Mx1-Cre).[32,33] Whether the WAVE complex and especially the Cyfip1 subunit, is also an important regulator of the Arp2/3 complex and thereby essential for the formation of lamellipodia in platelets has not been studied so far.

1.3.3 Strumpellin and the WASH complex

Strumpellin is an 1159-residue (134 kDa) protein, encoded by the *SPG8* (also known as *KIAA0196*) gene. The only known domain in Strumpellin is, compared to proteins of the spectrin family that carry long spectrin domains, a short central spectrin repeat.[85] In humans, several unique mutations in the *SPG8* gene have been associated with hereditary spastic paraplegia (HSP, also known as Strumpell-Lorrain disease), a group of inherited neurodegenerative diseases, whose main feature is a progressive gait disorder.[86,87] The symptoms depend on the type of HSP. So far more than 70 spastic paraplegia gene loci (SPG), including the *SPG8* gene, have been reported with a worldwide prevalence of 1-18 in 100 000.[88,89] Immunoblot analyses demonstrated the presence of Strumpellin in various human tissues with increased expression in the lung and the brain.[90]

Strumpellin is a component of the Wiskott-Aldrich syndrome protein and Scar homologue (WASH, or SHRC) complex, a 500 kDa core complex containing the subunits Wiskott–Aldrich Syndrome protein (WASH), Strumpellin, Family with sequence similarity 21 (FAM21), Strumpellin and WASH-interacting protein (SWIP) and Coiled-coil domain-containing protein 53 (CCDC53).

The generation of constitutive WASH knockout mice results in embryonic lethal animals before embryonic stage E7.5.[94] Heterozygous Strumpellin-deficient animals were shown to be viable and fertile, whereas matings of heterozygous mice did not result in homozygous Strumpellin-deficient offsprings. Further analyses of embryonic stage E13.5 also showed no presence of homozygous embryos in dissected uteri, indicating that Strumpellin is essential for survival of very early embryonic stages.[95]

The Arp2/3 complex is regulated by several NPFs (Figure 1.3.3) and especially the WASH and the WAVE complex share several similarities. Four of the five WASH complex subunits show a distant amino acid sequence identity and a significant structural protein homology to the subunits of the WAVE regulatory complex (see Chapter 1.3.1 and 1.3.2). Strumpellin and NCKAP1 show a significant similarity across their lengths with 13 % amino acid sequence identity and SWIP shares a 14 % amino acid sequence identity with Cyfip1. The N-termini of WASH and WAVE as well as CCDC53 and HSPC300 are predicted to form similar structural coiled-coils. Only the WASH subunit FAM21 shares no sequence or structural similarity to the WAVE subunit ABI1/2.[93] This indicates that the WASH and the WAVE complex have a similar structural and probably functional organization (Figure 1.3.3 A-B). However, in contrast to the WAVE complex, the WASH complex localizes at the membrane of endosomal subdomains, where it regulates F-actin dependent Arp2/3 activity. At these subdomains also other components like the retromer complex, the Arp2/3 complex and F-actin and are found.[94]

The retromer complex is part of the endosomal protein sorting machinery by recognizing specific proteins like the Mannose-6-phosphate receptor (M6PR) at endosomal membranes.[95] In Hela cells, the WASH complex subunit FAM21 was shown to interact with the retromer complex through multiple binding sites. Upon knockdown of the retromer complex, the WASH complex is localized in the cytosol instead of endosomal membranes.[96] The recruitment of the WASH complex to endosomes via the retromer complex enables the activation of the Arp2/3 complex via the WCA domain of the WASH protein subunit. Exposure of this domain was shown to be regulated by polyubiquitination of the WASH protein subunit, a process catalyzed by the E3 ubiquitin ligase TRIM27.[59] The generation of branched actin networks at the endosomal surface, leads to the elongation of specific endosomal regions and the formation of so called endosomal tubules in tight coordination with microtubule motors.[97]

Cells communicate and interact with their environment via cell surface receptors that receive extracellular signals from e.g. matrix proteins or other cells. The regulation of these interactions does not only occur at the basis of ligand-receptor binding but can also crucially depend on the number of receptors present on the cell surface. Besides transcriptional- and translational-dependent mechanisms that initially determine the number of cell surface receptors, endocytic trafficking pathways which shuttle

receptors and receptor-ligand complexes away from and back to the plasma membrane are important regulatory mechanisms.[98,99] The actin cytoskeleton contributes to endocytic trafficking as a molecular scaffold, providing the mechanical forces to deform membranes or to facilitate vesicle abscission.[100,101] For example, N-WASP supports the generation of branched actin networks on clathrin-coated vesicles. Together with BAR domain proteins and dynamin, actin is described to form a cage around the newly formed neck of a nascent vesicle.[102,103] Dynamin accomplishes the scission of the vesicle via its GTPase-powered compression mechanism. After final vesicle cropping, the clathrin coat disassembles and actin polymerizes at one vesicle pole to promote its further trafficking within the cytoplasm. It was shown that the WASH complex, which colocalizes with F-actin and the Arp2/3 complex, is present on Early endosome antigen 1 (EEA1) positive endosomal vesicles.[104] Thus, once a vesicle has become an early endosome it is rather associated with the WASH complex than N-WASP. However, it is not clear when and how this exchange between N-WASP and the WASH complex is accomplished. Knockout of the WASH subunit in fibroblasts results in enlarged and collapsed endosomes as well as a loss in lysosomal compartment integrity that in turn results in impaired trafficking of the epidermal growth factor receptor and the transferrin receptor.[91] In ovarian cancer cells, WASH was shown to colocalize to the early endosomal markers: EEA1, Ras-related protein Rab-4 and 5 (Rab4 and Rab5). In addition, WASH was associated with late endosomal vesicles markers CD63 and Rab7 and partially overlapped with the lysosomal sialic acid transporter sialin and with marker proteins of the Golgi complex.[105] Integrin recycling was shown to be crucial for cancer cell invasiveness, since depletion of the WASH protein in A2780 cancer cells impaired the α5β1 integrin-mediated invasive migration.[105] The invasive defect in WASH knockout cells was rescued upon expression of endogenous WASH protein via transfection of pEGFP-C1-mWASH vector, and WASH overexpression increased α5β1-integrin surface expression and invasion.

The sorting, fission and fusion processes that are required for vesicle trafficking are based on the machinery of Rab GTPases and tethering proteins like EEA1, that initiate the initial vesicle and organelle membrane interaction.[96] The excessive endosomal tubulation along microtubules, in WASH-deficient fibroblasts, appears on all organelles of the endosomal/lysosomal system with enrichment in early and late endosomes.[94,106] The precise organelles were identified by costaining with respective Rab GTPases or

other endosomal markers like EEA1. Like WASH-deficiency, the inhibition of dynamin leads to the formation of long vesicular tubules. In this dynamin inhibited cells the WASH complex is localized at the base of this tubules.[106] This highlights the role of the WASH complex in integrin receptor trafficking, the maintenance of endolysosomal structures and invasive migration processes. However, if the WASH complex and especially the Strumpellin subunit are important for platelet biology is unknown.

1.4 The microtubule cytoskeleton

As the largest filamentous components of the eukaryotic cytoskeleton, microtubules are vital as they direct cell division, motility, shape and differentiation. Microtubules are polarized structures consisting of α- and β-tubulin heterodimer subunits assembled into linear protofilaments. In mammals, 13 protofilaments build a 24 nm wide, polar, cylindric and hollow microtubule.[107] The αβ heterodimers are oriented with their β-tubulin monomer pointing towards the faster-growing (+) end and their α-tubulin monomer exposed to the slower-growing (-) end. The (+) end usually has a GTP-bound cap of one tubulin layer that stabilizes the microtubule structure. Upon loss of this GTP cap the microtubule filament rapidly depolymerizes.[107] A third tubulin isoform, γ-tubulin, functions as template for the correct assembly of eukaryotic microtubules. Other tubulin isoforms (δ, ε, ζ, η) are found in cilia or flagella of specific organisms.[108] Despite the fact that microtubules are assembled from evolutionarily highly conserved heterodimers of α- and β-tubulin, these filaments can adapt to a huge variety of functions. The functional specialization of microtubules is regulated via: 1. the expression of five different α- and eight different β-tubulin isotypes; 2. posttranslational modifications of tubulin; and 3. by the interaction of tubulin with diverse microtubule-associated proteins (MAPs).[109]

In mammals, β1-tubulin is exclusively expressed in megakaryocytes and platelets and represents the predominant isoform in those cells.[110] Besides β1-tubulin, α-tubulin and smaller fractions of β2- and β5-tubulin were shown to be also present in murine platelets. Homozygous β1-tubulin-deficient mice fully develop and appear at an expected Mendelian ratio. However, the loss of β1-tubulin leads to a defect in platelet biogenesis that results in a 50 % reduced platelet count and increased bleeding compared to wild-type (WT) animals.[110]

Posttranslational modifications like (poly) glutamylation, (poly) glycylation, acetylation, methylation, phosphorylation and de-/tyrosination are generated on the microtubule

polymer. Most tubulin posttranslational modifications are found within the C-terminal tails which are exposed to the outer surface of assembled microtubules and serve as key interaction sites for MAPs. In addition to the expression of different tubulin isoforms, posttranslational modifications develop the so-called tubulin code, a regulatory mechanism that controls the specialization of the microtubule cytoskeleton.[109] Defects in tubulin acetylation caused by a histone deacetylase inhibitor or genetic knockdown, impairs the maturation of megakaryocytes and platelet formation.[111,112] Acetylated microtubules that are organized in the marginal band, maintain the discoid shape of resting platelets. Upon platelet activation, microtubules are reorganized and the control of acetylation and deacetylation is important during platelet spreading.[113]

MAPs which regulate the assembly of microtubules can be categorized according to their function as stabilizers, destabilizers, severing proteins, capping proteins, bundling and cross-linking proteins. Two major classes of ATP dependent motor proteins, namely kinesins and dyneins, use microtubules as tracks for intracellular transport. Further, dynein-based sliding of overlapping, antiparallel microtubules past each other was shown to drive proplatelet elongation.[18]

Cytoplasmic linker proteins (CLIPs) anchor organelles to microtubules to promote cell organization. In addition, some proteins involved in signal transduction, translation and metabolism bind to microtubules.

1.5 Cytoskeletal crosstalk

The cell shape, mechanics, dynamics and resistance to mechanical forces are determined by the architecture and the interplay of cytoskeletal structures. Besides actin and microtubule filaments, intermediate filaments are the third polymer type of the cytoskeleton. In contrast to actin and microtubule filaments, which consist of conserved globular proteins with a nucleotide-binding and a hydrolytic activity, intermediate filaments with a diameter of about 10 nm are assembled of filamentous proteins that share conserved structures but have no enzymatic activity.[114] In humans about 67 genes are coding for intermediate-filament proteins (e.g. vimentin, desmin, peripherin, nestin or lamin), which are divided into five distinct types depending on their sequence identity and tissue distribution.[115,116] Although intermediate filaments have been found to be associated with actin filaments in human platelets,[117] the role of intermediate filaments as proteins that mediate cytoskeletal crosstalk has only been

poorly investigated in platelets and megakaryocytes. Due to the complexity of the three cytoskeletal components, they have rather been studied as separate components. Although many cytoskeletal regulated processes seem to proceed separately from each other, the presence of proteins that directly (e.g. spectraplakins) interact with different cytoskeletal components or indirectly mediate interactions via signaling mechanisms (e.g. Rho GTPases [114]) suggests that the cytoskeleton should no longer be considered as a collection of individual proteins but rather as a system in which the components work with and coregulate each other to exert their cellular function.[118] For example, studies on formin proteins in megakaryocytes and platelets indicate that they play an important role in regulating the actin and the tubulin cytoskeleton.[119] Inhibition of the FH2 domain of formin proteins blocks actin dependent platelet spreading and impairs the posttranslational acetylation of microtubules.[120]

1.5.1 Macf1 as cytoskeletal crosslinking protein

Spectraplakins are evolutionarily conserved proteins with an enormous size (300-800 kDa) and unusual in their capacity to simultaneously bind and regulate microtubules and F-actin.[121] The spectraplakin family only consists of two mammalian members, the Microtubule-actin cross-linking factor 1 (MACF1; also known as ACF7; actin cross-linking factor 7) and Dystonin (Dst, also known as bullous pemphigoid antigen 1, Bpag1).[122]

Spectraplakins (Figure 1.5.1) carry two calponin-homology domains that facilitate the interaction with F-actin, a plakin domain, a spectrin-repeat domain, an EF-hand motive for direct calcium-sensing or binding, and a glycine/arginine-rich (GAR) domain, which is responsible for binding to microtubules.[123] The spectrin repeats are besides a spacer region between the N and C termini thought to equip these proteins with flexibility and to enable them to respond elastically to applied extensions and mechanical forces.[122] Instead of a large number of different genes, the members of the spectraplakin family generate a high diversity through differential promoter usage and splicing resulting in a diversity of different isoforms, each with the ability to interact with different cytoskeletal or membrane components. Full-length MACF1 is ubiquitously expressed, whereas Dystonin is mainly present in the brain.[122,124] Constitutive MACF-deficient mice die at the gastrulation stage and display developmental retardation at embryonic stage 7.5, with defects in the formation of the primitive streak, node and mesoderm.[125] Heterozygous MACF1-deficient mice are fertile and display no overt phenotype. In

contrast to constitutive MACF1-deficient mice, constitutive Dystonin-deficient mice survive until weaning and suffer primarily from sensory neuron degeneration.[125] Although both spectraplakin members are closely related and have similar domains, the expression of Dystonin, already detectable at E7.5, cannot compensate for the loss of MACF1 in these animals, suggesting that MACF1 and Dystonin are not completely functionally redundant and probably play distinct roles *in vivo.*[125]

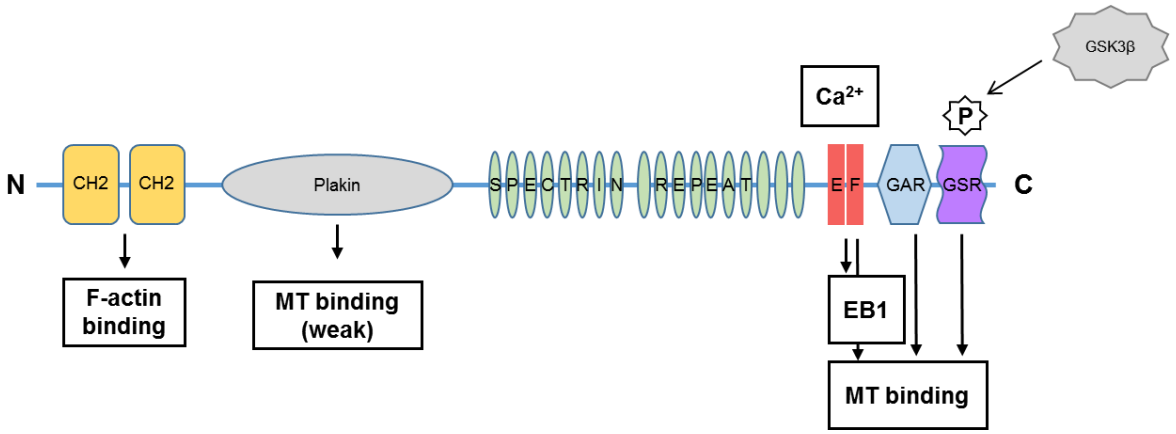

Figure 1.5.1 Mammalian full-length spectraplakin isoform MACF1a1. Different types of functional domains can be found in this family of proteins: a calponin-type actin-binding domain composed of CH1 and CH2 regions, a plakin domain, an α-helical spectrin repeat domain, an EF-hand, a glycine/arginine-rich (GAR) motive and a glycine-serine-arginine rich domain (GSR)-domain, responsible for microtubule-associated protein RP/EB family member 1 (EB1) and microtubule (MT) binding. The GSR-domain is phosphorylated by the Glycogen synthase kinase 3 beta (GSK3β). Adapted from [122].

Conditional targeting of MACF1 in primary mouse keratinocytes results in defective wound healing when cells are subjected to an *in vitro* scratch-wound assay.[126] The defects in cell migration on fibronectin-coated surfaces are based on aberrantly robust focal adhesions (Figure 1.5.2). Focal adhesions are complex plasma membrane-associated macromolecular assemblies that engage with the surrounding extracellular matrix via integrin receptors and physically connect with the actin cytoskeleton through the recruitment of numerous focal adhesion-associated proteins. Of note, by reduction of the amount of the coated fibronectin, the differences in velocities displayed by control and MACF1-deficient cells were largely equalized. This suggests that the aberrant migration was caused by defective adhesion of the MACF1-deficient keratinocytes to the underlying matrix substrate.[126] Focal adhesions are more stable in the absence of MACF1, indicating that it regulates cell migration by promoting the dynamics of focal adhesions. In endodermal cells, MACF1 was described as an essential integrator of actin-dependent microtubule dynamics.[127] Further, MACF1

knockdown in neuronal culture systems demonstrated that MACF1 is essential for axon extension and the organization of neuronal microtubules, a function dependent on both the microtubule and F-actin-binding domains.[128] These data demonstrate that the crosstalk between cytoskeletal components is essential for the orchestration of basic cellular functions. However, this cytoskeletal crosstalk has only been poorly studied in platelet biology, and the role of MACF1 in megakaryocytes and platelets is still unknown.

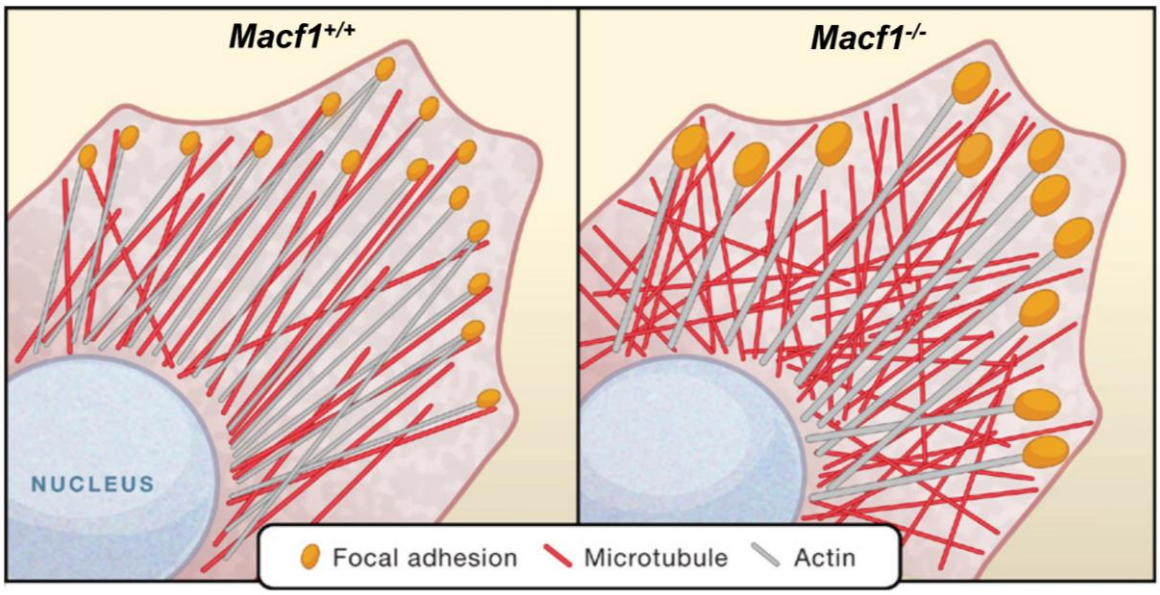

Figure 1.5.2: MACF1 coordinates actin and microtubules in cytoskeleton-focal adhesion dynamics. The spectraplakin MACF1 directly binds both microtubules and actin filaments and has an actin-dependent ATPase activity. In *Macf1*$^{+/+}$ cells (left), MACF1 coordinates the targeting of microtubules to focal adhesions, where they direct disassembly of the adhesion contacts and promote cell movement. MACF1-deficient cells (right) show altered microtubule organization accompanied by a loss of microtubule targeting to focal adhesions, which become stabilized and enlarged. Taken from [129].

2 AIM OF THE STUDY

To maintain hemostasis and several other platelet-related functions, the human body produces 100 billion platelets daily.[130] Many direct and indirect cytoskeletal regulating, interacting or crosslinking proteins have been shown to be involved in platelet production and function. Mouse models particularly for actin binding and regulatory proteins, such as gelsolin, profilin 1, Arp2/3 and twinfilin, provided evidence for a role of the cytoskeleton in platelet morphology, shape change and activation. The aim of the study was to investigate the role of three different cytoskeletal regulating and crosslinking proteins in platelet physiology.

Cyfip1

During platelet spreading, the actin cytoskeleton undergoes rapid rearrangement, forming filopodia and lamellipodia. Cyfip1 is a subunit of the WAVE regulatory complex which has been shown to drive lamellipodia formation by enhancing actin nucleation via the Arp2/3 complex in other cell types. Previous data suggest that the WAVE regulatory complex might function as an important regulator of Arp2/3-dependent lamellipodia formation in platelets.[131] Controversial data have been published on the role of lamellipodia in thrombus formation and stability.[32–36] If Cyfip1 is an essential player in these processes is unknown. Accordingly, the aim of this study was to investigate the impact of Cyfip1 deficiency on platelet physiology. Therefore, conditional megakaryocyte- and platelet-specific *Cyfip1*$^{fl/fl\ PF4\text{-}Cre}$ mice were analyzed.

Strumpellin

Endocytosis in megakaryocytes and platelets, such as the uptake of fibrinogen from plasma by αIIbβ3 integrin, is crucial for the loading of granules and thus for platelet effector function. The underlying mechanisms of cargo sorting and receptor trafficking are poorly understood, and key regulatory proteins remain to be identified. Strumpellin is a component of the WASH complex which is the major endosomal actin polymerization-promoting complex. In other cell types, the WASH complex is recruited to subdomains of early endosomes and generates an actin network, thereby coordinating endosomal protein sorting. The function of the WASH complex in megakaryocytes and platelets nonetheless remains unknown. Accordingly, the aim of this study was to investigate the role of Strumpellin in platelet biogenesis, function and reactivity. Therefore, conditional megakaryocyte- and platelet-specific *Strumpellin*$^{fl/fl\ PF4\text{-}Cre}$ mice were analyzed.

Macf1

The cytoskeleton is no longer considered as a collection of individual proteins but rather as a system in which the components work with and coregulate each other to exert their cellular function. Spectraplakins, including the protein MACF1, are evolutionarily conserved proteins and unusual in their capacity to simultaneously bind and regulate microtubules and F-actin. The interaction of cytoskeletal components is essential for the orchestration of basic cellular functions. This crosstalk has only been poorly studied in platelet biology, and the role of MACF1 in megakaryocytes and platelets is still unknown. Therefore, megakaryocyte- and platelet-specific knockout mice were used to investigate the function of MACF1 in platelet formation, *in vitro* platelet activation as well as aggregation.

3 MATERIAL

3.1 Animals

All animal studies were approved by the district government of Lower Franconia and performed in accordance with relevant guidelines and regulations. Male and female mice were analyzed between 6 and 20 weeks of age if not stated differently.

Macf1$^{fl/fl}$ mice were intercrossed with mice carrying the Cre-recombinase under the platelet factor 4 (*Pf4*) promoter [132] to generate platelet- and megakaryocyte-specific Macf1-knockout (further referred to as *Macf1$^{-/-}$*) mice. *Macf1$^{fl/fl}$* mice were obtained from the Jackson Laboratory and initially generated and described by Elaine Fuchs.[126]

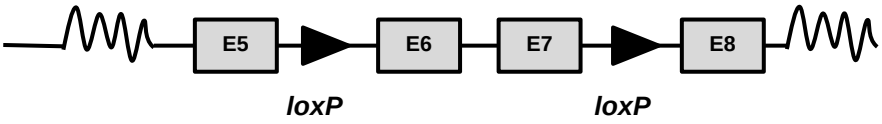

Figure 3.1.1: Position of *loxP* sites in *Macf1* gene.
The loxP sites are localized after exon 5 and after exon 7.

Cyfip1$^{fl/fl}$ mice were intercrossed with mice carrying the Cre-recombinase under the *Pf4* promoter[132] to generate platelet- and megakaryocyte-specific Cyfip1-knockout (further referred to as *Cyfip1$^{-/-}$*) mice. *Cyfip1$^{fl/fl}$* mice were obtained from Laura Machesky and generated by Sheila Bryson (Beatson Institute, Glasgow, UK). They were created from an embryonic stem (ES) cell clone (DEPD00521_7_E11) obtained from the NCRR-NIH supported KOMP Repository (www.komp.org) and generated by the CSD consortium for the NIH funded Knockout Mouse Project (KOMP). Following importation, the ES cells were cultured on a MEF feeder layer. Correct targeting of *Cyfip1* was confirmed on DNA extracted from the ES cell clone by PCR on the 5' side (CATTCTAACGTTCAAGATCGCAGACCAG and CACAACGGGTTCTTCTGTTAG TCC; 7.5kb) and on the 3' side (CATGTCTGGATCCGGGGGTACC GCGTCGAG and GATCTCCTGGTGCGGCATGCAAGC; 7.1kb). The presence of the isolated 3' loxP site was also confirmed by PCR (AAGCAGTCCGTGCTGAGATG and GAACCAAGCTCCCAGATTCC; 262bp). Following confirmation of the genotyping of the targeted clone, mouse lines were derived by injection of ES cells into C57BL/6J blastocysts. After breeding of chimeras, germline offspring were identified by coat color

and the presence of the modified allele was confirmed with the 3' loxP primers described above. Mice were subsequently crossed with a mouse line expressing Flpe (Tg(ACTFLPe)9205Dym) to delete the selectable marker by recombination at the FRT sites. Correct removal of the lacZ gene and Neo cassette was confirmed by PCR across the remaining FRT site (CTCTTCTTGTGGACCGCATC and CACGGTAGCCTGACAAGAGG; 562bp).[133]

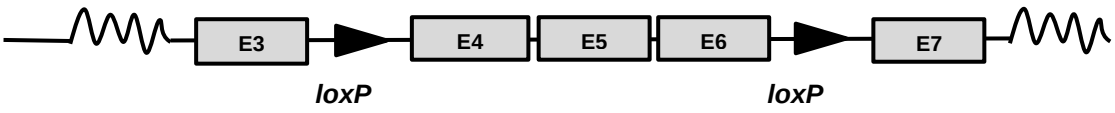

Figure 3.1.2: Position of *loxP* sites in *Cyfip1* gene.
The loxP sites are localized after exon 3 and after exon 6.

***Strumpellin*$^{fl/fl}$** mice were intercrossed with mice carrying the Cre-recombinase under the *Pf4* promoter[132] to generate platelet- and megakaryocyte-specific Strumpellin-knockout (further referred to as *Strumpellin*$^{-/-}$) mice. *Strumpellin*$^{flox/flox}$ mice were obtained from Laura Machesky and generated by Sheila Bryson (Beatson Institute, Glasgow, UK). An ES cell clone (HEPD0534-7-C01) for the conditional knockout of the *Strumpellin* gene (E430025E21Riktm1a (EUCOMM) Hmgu) was obtained from the IKMC repository.[134] Cells were cultured using standard protocols on DR4 irradiated MEF monolayers cells.[135] Appropriate targeting of the *Strumpellin* gene in the ES cell clone was confirmed by screening the 5' (GCTAGTGTCAGCGACAGAGTGCGCG CTC and CACAACGGGTTCTTCTGTTAGTCC) and 3' sides (TCTATAGTCGCA GTAGGCGG and CAGGTTC ACTGGCAGGTCGTGCTGTTAG AC) by PCR using Expand Long Template PCR (Roche) with the oligos indicated according to manufacturer's instructions. The presence of the isolated loxP site was also confirmed by PCR (TCATTCCCAGCACCTGTGTC and TGAACTGATGGCGAGCTCAG). Following confirmation of correct targeting, mouse lines were derived by injection of ES cells into C57BL/6J blastocysts according to standard protocols.[136] Resultant chimeric mice were identified by their agouti coat color. After breeding of chimeras, germline transmitting chimeras were identified by the coat color of their offspring and the presence of the modified allele was confirmed by genotyping with the 3' loxP primers described above. Heterozygous mice were subsequently crossed with a mouse line expressing Flpe (Tg(ACTFLPe)9205Dym) to delete the selectable marker

by recombination at the FRT sites.[133] Correct removal of the lacZ gene and selectable marker cassette was validated by PCR across the remaining FRT site (CCAGAGGTGTGGCTCATAGG and TGACTGTTGGACAGGACACG). Following removal of the cassette exon, the modified allele has two loxP sites remaining flanking exon 12 (Ensembl ID: ENSMUSE00000222520 in mouse genome assembly GRCm38.p4) of the *Strumpellin* gene. Following Cre recombination exon 12 is deleted resulting in premature termination of messenger ribonucleic acid (mRNA) translation.

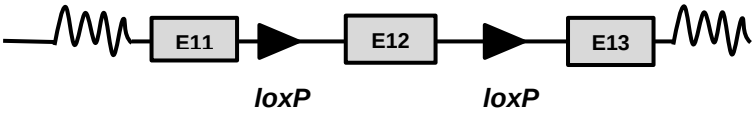

Figure 3.1.3: Position of *loxP* sites in *Strumpellin* gene.
The loxP sites are localized after exon 11 and after exon 12.

3.2 Antibodies

Commercial purchased antibodies

Antibody	Host	Manufacturer	Reference/ Catalogue Nr.
Anti-Macf1	mouse	Santa Cruz	#sc-377532
Anti-Macf1	rabbit	Bethyl	#A304-564A
Anti-ACF7	rabbit	Elaine Fuchs	Provided by E.F.
Anti-Dystonin	mouse	Abcam	#55654
Anti-Strumpellin	rabbit	Abcam	#101222
Anti-Cyfip1/Sra1	rabbit	Millipore	#2703674
Anti-GAPDH	rabbit	Sigma	#99545
Anti-Gas2L1	rabbit	Thermo Fisher	#PA5-21729
Anti-Filamin A	rabbit	Cell Signaling	#4762
Anti-DAMM1	mouse	Santa Cruz	#sc-100942
Anti-mDia1	rabbit	Abcam	#ab129167
Anti-WASP	rabbit	Cell Signaling	#4860
Anti-acetylated-tubulin	mouse	Santa Cruz	#sc-23950
Anti-α-tubulin	mouse	Sigma	#T6074
Anti-actin	rabbit	Sigma	#A2066
Anti-Rac1	mouse	BD Biosciences	#610650
Anti-Profilin1	rabbit	Sigma	#P7749
Anti-Arpc2	rabbit	Millipore	#07-227
Anti-WAVE2	rabbit	Cell Signaling	#3659
Anti-WAVE1	rabbit	Invitrogen	#PA5-78273

Antibody with conjugate	Conjugate	Manufacturer	Clone/ Catalogue Nr.
Anti-CD105 (endoglin)	Alexa Fluor 647	eBioscience	MJ7/18
Anti-CD105 (endoglin)	Alexa Fluor 594	eBioscience	MJ7/18
Anti-α-tubulin	Alexa Fluor 488	Abcam	B-5-1-2
Donkey anti-mouse IgG	Cy3	Jackson Immuno	#715-166-152
Donkey-anti-rabbit IgG	Cy3	Jackson Immuno	#711-165-153
Donkey-anti-mouse IgG	Dylight 405	Jackson Immuno	#715-475-150
Goat-anti-rabbit IgG	Alexa Fluor 488	Invitrogen	#A11008
Anti-rabbit-IgG	HRP	Dako	#P0448
Anti-mouse-IgG	HRP	Dako	#P0447
Anti-rat-IgG	HRP	Dako	#P0450

Homemade monoclonal antibodies

Homemade monoclonal antibodies were generated and modified in the Nieswandt laboratory. Labelling with fluorescein isothiocyanate (FITC) or phycoerythrin (PE) was performed using commercial kits according to the manufacturer's instruction. Annexin-A5 was purified in the Nieswandt laboratory and conjugated to DyLight 488.

Antigen	Antibody	Clone	Isotype	Reference
GPIbα	p0p/B	57E12	IgG2b	Massberg, JEM 2003
GPIbα	p0p4	15E2	IgG2b	Bergmeier, Blood 2000
GPIX	p0p6	56F8	IgG2b	Nieswandt, Blood 2000
GPV	DOM2	89H11	IgG2a	Nieswandt, Blood 2000
CD9	ULF1	96H10	IgG2a	unpublished
GPVI	JAQ1	98A3	IgG2a	Nieswandt, JBC 2000
αIIbβ3	JON1	6C10	IgG2b	Nieswandt, Blood 2000
αIIbβ3	JON2	45A9	IgG2a	Nieswandt, Blood 2000
αIIbβ3	JON3	3F3	IgG1	Nieswandt, Blood 2000
αIIbβ3	JON6	14A3	IgG2b	unpublished
αIIbβ3	JON/A	4H5	IgG2b	Bergmeier, Cytometry 2002
αIIbβ3	MWReg30	5D7	IgG1	Nieswandt, Blood 1999
α2β1	LEN1	12C6	IgG2b	Nieswandt, JBC 2000
CLEC-2	INU1	11E9	IgG1	May, Blood 2009
P-selectin	WUG 1.9	5C8	IgG1	unpublished
β3	EDL-1	57B10	IgG2a	Nieswandt, Blood 2000
α5	BAR-1	25B11	IgG1	Grüner, Blood 2003

3.3 Chemicals

Reagent	Manufacturer
Acetone	Roth (Karlsruhe, Germany)
Adenosine diphosphate (ADP)	Sigma-Aldrich (Schnelldorf, Germany)
Agarose	Roth (Karlsruhe, Germany)
Ammonium peroxidsulfate (APS)	Roth (Karlsruhe, Germany)
Annexin V-FITC	provided by Jonathan F. Tait (Medical Center Washington, USA)
Apyrase (grade III)	Sigma-Aldrich (Schnelldorf, Germany)
Benzyl alcohol	Sigma-Aldrich (Schnelldorf, Germany)
Benzyl benzoate	Sigma-Aldrich (Schnelldorf, Germany)
Bovine serum albumin (BSA)	AppliChem (Darmstadt, Germany)
Collagen related peptide (CRP)	CRB Cambridge Research Biochemicals (Billingham, UK)
Collagen type I (human placenta)	Sigma-Aldrich (Schnelldorf, Germany)
Collagen type IV (human placenta)	Sigma-Aldrich (Schnelldorf, Germany)
Convulxin (CVX)	Axxora (Lörrach, Germany)
dNTP	Fermentas (St. Leon-Rot, Germany)
Dream Taq Polymerase	Fermentas (St. Leon-Rot, Germany)
Dream Taq Polymerase 10x buffer	Fermentas (St. Leon-Rot, Germany)
Eosin	Roth (Karlsruhe, Germany)
Ethanol	Roth (Karlsruhe, Germany)
Ethylene glycol-bis(2-aminoethylether)-N,N,N',N'-tetraacetic acid (EGTA)	Sigma-Aldrich (Schnelldorf, Germany)
Ethylenediaminetetraacetic acid (EDTA)	AppliChem (Darmstadt, Germany)
Eukitt	Sigma-Aldrich (Schnelldorf, Germany)
Fibrinogen	Sigma-Aldrich (Schnelldorf, Germany)
Fibronectin	Sigma-Aldrich (Schnelldorf, Germany)
Fluoroshield mounting medium with DAPI	Sigma-Aldrich (Schnelldorf, Germany)
GeneRuler 100 bp DNA Ladder	Fermentas (St. Leon-Rot, Germany)
Glutaraldehyde	Merck (Darmstadt, Germany)
Hematoxylin	Sigma-Aldrich (Schnelldorf, Germany)
Heparin sodium	Ratiopharm (Ulm, Germany)
Hirudin	CoaChrom Diagnostica GmbH (Maria Enzersdorf, Austria)
Horm collagen	Takeda (Linz, Austria)
IGEPAL CA-630	Roth (Karlsruhe, Germany)
Isofluran CP	cp-pharma (Burgdorf, Germany)
Isopropanol	Roth (Karlsruhe, Germany)
Lipopolysaccharide	Sigma-Aldrich (Schnelldorf, Germany)
Midori Green DNA stain	Nippon Genetics (Düren, Germany)
Neuraminidase	Sigma-Aldrich (Schnelldorf, Germany)
Osmium tetraoxide	Merck (Darmstadt, Germany)
PageRuler prestained protein ladder	Fermentas (St. Leon-Rot, Germany)
Paraffine	Roth (Karlsruhe, Germany)
Paraformaldehyde (PFA)	Sigma-Aldrich (Schnelldorf, Germany)

Phalloidin-Alexa647N	Sigma-Aldrich (Schnelldorf, Germany)
Phalloidin-FITC	Enzo Life Sciences (New York, USA)
Phenol/Chloroform	Roth (Karlsruhe, Germany)
Poly-L-lysine	Sigma-Aldrich (Schnelldorf, Germany)
Prostacyclin (PGI_2)	Sigma-Aldrich (Schnelldorf, Germany)
Protease inhibitor cocktail	Sigma-Aldrich (Schnelldorf, Germany)
Proteinase K	Fermentas (St. Leon-Rot, Germany)
Rat serum	Sigma-Aldrich (Schnelldorf, Germany)
Rhodocytin	J. Eble (University Hospital Frankfurt, Germany).
Roti Lumin plus ECL solution	Roth (Karlsruhe, Germany)
Rotiphorese gel 30 acrylamide	Roth (Karlsruhe, Germany)
Sodium orthovanadate	Sigma-Aldrich (Schnelldorf, Germany)
Stem cell factor (SCF)	BioLegend (San Diego, USA)
Streptomycin	PAN (Aidenbach, Germany)
Sucrose	Roth (Karlsruhe, Germany)
Super cryo embedding medium (SCEM)	Section lab (Hiroshima, Japan)
Tannic acid	Merck (Darmstadt, Germany)
Tetramethylethylenediamine (TEMED)	Roth (Karlsruhe, Germany)
Thrombin from human plasma	Roche Diagnostics (Mannheim, Germany)
TPO (conditioned medium)	Nieswandt laboratory (Würzburg, Germany)
Triton X-100	AppliChem (Darmstadt, Germany)
Tween 20	Roth (Karlsruhe, Germany)
U46619	Enzo Lifesciences (Lörrach, Germany)
Uranyl acetate	EMS (Hatfield, USA)
Xylol	Roth (Karlsruhe, Germany)

3.4 Buffer

Buffers were prepared using deionized water obtained from a MilliQ Water Purification System (Millipore, Schwalbach Germany). NaOH or HCl was used to adjust the pH.

- **Blocking solution for immunoblotting**

TBS-T	-
BSA	5 %

- **CATCH buffer**

PBS	-
HEPES	25 mM
EDTA	3 mM
BSA	3.5 %

- **Cacodylate buffer, pH 7.2**

Sodium cacodylate	0.1 M

- **ELISA carbonate coating buffer, pH 9.0**

$NaHCO_3$	0.1 M

- **ELISA wash buffer**

NaCl	300 mM
Tween 20	0.05 %
in PBS	1 x

- **Lysis buffer for DNA isolation, pH 7.2**

TRIS base	100 mM
EDTA	5 mM
NaCl	200 mM
SDS	0.2 %
Proteinase K	100 µg/ml

- **Hepes-Tyrode-buffer without Ca^{2+}**

NaCl	137 mM
KCl	2.7 mM
$NaHCO_3$	12 mM
NaH_2PO_4	0.43 mM
$MgCl_2$	1 mM
HEPES	5 mM
BSA	0.35 %
Glucose	1 %

- **Hepes-Tyrode-buffer with Ca^{2+}**

NaCl	137 mM
KCl	2.7 mM
$NaHCO_3$	12 mM
NaH_2PO_4	0.43 mM
$CaCl_2$	2 mM
$MgCl_2$	1 mM
HEPES	5 mM
BSA	0.35 %
Glucose	1 %

- **IP-buffer**

NaCl	155 mM
EDTA	1 mM
NaN_3	0.005 %
Tris HCl	15 mM

- **Phosphate buffered saline, pH 7.14**

NaCl	137 mM
KCl	2.7 mM
KH_2PO_4	1.5 mM
Na_2HPO_4	8.0 mM

- **Protein lysis buffer, 2x, pH 7.4**

HEPES	15 mM
NaCl	150 mM
EGTA	10 mM
Triton X-100	2 %
(Protease inhibitor cocktail)	1:100

- **PHEM buffer, pH 7.2**

PIPES	60 mM
HEPES	25 mM
EGTA	10 mM
$MgSO_4$	2 mM

- **Separation gel buffer, pH 8.8**

Tris-HCl	1.5 M

- **Stacking gel buffer, pH 6.8**

Tris-HCl	0.5 M

- **SDS sample buffer, 4x reducing**

Tris-HCl	200 mM
Glycerol	40 %
SDS	8 %
Bromophenol blue	0.04 %
β-Mercaptoethanol	20 %

- **SDS PAGE Laemmli buffer**

TRIS	40 mM
Glycine	0.95 mM
SDS	0.5 %

- **TAE buffer, 50x, pH 8.0**

TRIS	200 mM
Acetic acid	5.7 %
EDTA	50 mM

- **TE-buffer (DNA), pH 8.0**

TRIS base	10 mM
EDTA	1 mM

- **Tris-buffered saline (TBS), pH 7.3**

NaCl	137 mM
TRIS/HCl	20 mM

- **TBS-T washing buffer**

TBS (1x)	-
Tween20	0.1 %

- **Transfer buffer for immunoblotting**

$NaHCO_3$	10 mM
Na_2CO_3	3 mM

3.5 Devices

Device	Company
Cryotom CM1900	Leica (Wetzlar, Germany)
Eppendorf centrifuge 5415C	Eppendorf AG (Hamburg, Germany)
Eppendorf centrifuge 5427R	Eppendorf AG (Hamburg, Germany)
FACS Calibur	BD Biosciences (Heidelberg, Germany)
Gene Touch Thermal Cycler	Biozym Scientific GmbH (Oldenburg, Germany)
Herolab	Herolab GmbH (Wiesloch, Germany)
Leica EM ACE600	Leica (Wetzlar, Germany)
Leica EM CPD300	Leica (Wetzlar, Germany)
MultiImage II FC Light Cabinet	Alpha Innotech corporation (San Leandro, USA)
Nikon ECLIPSE TS 100	Nikon GmbH (Düsseldorf, Germany)
Nanodrop 2000c	Thermo Fisher Scientific (Carlsbad, USA)
Phenom Pro	Thermo Fisher Scientific (Carlsbad, USA)
Hemavet 950	Drew Scientific Group (Miami Lakes, USA)
Sysmex KX 21N	Sysmex GmbH (Norderstedt, Germany)
TCS SP5 CLSM	Leica (Wetzlar, Germany)
TCS SP8 CLSM	Leica (Wetzlar, Germany)
JEM-2100 Electron microscope	JEOL GmbH (Freising, Germany)
VWR MEGA STAR 1.6R	VWR part of avantor (Darmstadt, Germany)
Zeiss EM 900	Carl Zeiss (Oberkochen, Germany)

4 METHODS

4.1 Genotyping of mice

Isolation of genomic DNA from mouse tissue

A 5 mm² piece of mouse ear was incubated overnight at 56°C and 900 rpm or for 3 h at 56°C and 1400 rpm in 500 µl of lysis buffer. Cellular proteins and lipids were removed by the addition of 500 µl of phenol/chloroform/isoamyl alcohol (25:24:1). Samples were mixed and centrifuged for 10 min at 10000 rpm in an Eppendorf 5417R tabletop centrifuge at room temperature (RT). After centrifugation, the aqueous nucleic acid-containing upper phase was transferred into a new tube containing 500 µl isopropanol to precipitate the DNA/mRNA. Subsequently, the nucleic acids were spun down by centrifugation for 15 min at 14000 rpm and 4°C. The pellet was washed and dehydrated by the addition of 500 µl 70 % ethanol with subsequent centrifugation for 15 min at 14000 rpm. Before dissolving the pellet in 50 µl TE buffer, the pellet was allowed to dry for 30 min at 37°C.

Genotyping of *Macf1*$^{-/-}$ mice

Macf1$^{fl/fl}$ mice were genotyped by polymerase chain reaction (PCR) with 5'AAAGAAACGGAAATACTGGCC3' and 5'GCAGCTTAATTCTGCCAAATTC3' primers for floxed *Macf1* and with 5'CTCTGACAGATGCCAGGACAQ3' and 5'TCTCTGCCCAGAGTCATCCT3' primer (biomers.net, Ulm Germany) for Pf4-Cre.

Expected results *Macf1*: Wild type allele = 660 bp Mutant allele= 700 bp

Macf1 flox PCR:		
Reagent	**Stock conc.**	**Volume**
Buffer	10 x	2.5 µl
$MgCl_2$		2.5 µl
dNTP mix	10 mM	1 µl
Forward primer	0.01µg/µl	1 µl
Reverse primer	0.01µg/µl	1 µl
H_2O		15.75 µl
Taq Pol.	20 u	0.25 µl
DNA		1 µl
		25 µl

PCR program:		
Cycles	**Temperature**	**Duration**
1	94°C	3:00 min
2	94°C	0:30 min
3 x 35	60°C	0:30 min
4	72°C	0:60 min
5	72°C	2:00 min
6	4°C	∞

PF4-Cre PCR (Biomers.net):		
Reagent	**Stock conc.**	**Volume**
Buffer	10 x	2.5 µl
dNTP mix	10 mM	1 µl
Forward primer	0.01µg/µl	1 µl
Reverse primer	0.01µg/µl	1 µl
H_2O		17.25 µl
DreamTaq Pol.	20 u	0.25 µl
DNA		2 µl
		25 µl

PCR program:		
Cycles	**Temperature**	**Duration**
1	94°C	3:00 min
2	94°C	0:30 min
3 x 35	54°C	0:30 min
4	72°C	0:45 min
5	72°C	3:00 min
6	4°C	∞

Genotyping of *Cyfip1*$^{-/-}$ mice

Cyfip1$^{fl/fl}$ mice were genotyped by PCR with 5'ACCTAT GGGATTTTACCCTTCTTAC3' and 5'ACTACCTATAATGCAGACCTGAAGC3' primers for floxed *Cyfip1* and with 5'CCCATACAGCACTTTTG3' and 5'TGCACAGTCAGCAGGTT3' primer (Invitrogen Thermo Fisher Scientific, Carlsbad, USA) for Pf4-Cre.

Expected results *Cyfip1*: Wild type allele = 295 bp Mutant allele= 490 bp

Cyfip1 flox PCR:		
Reagent	**Stock conc.**	**Volume**
Buffer	10 x	2.5 µl
dNTP mix	10 mM	1 µl
Forward primer	0.01µg/µl	1 µl
Reverse primer	0.01µg/µl	1 µl
H_2O		17.25 µl
DreamTaq Pol.	20 u	0.25 µl
DNA		2 µl
		25 µl

PCR program:		
Cycles	**Temperature**	**Duration**
1	94°C	3:00 min
2	94°C	0:30 min
3 x 35	60°C	0:30 min
4	72°C	0:45 min
5	72°C	3:00 min
6	4°C	∞

PF4-Cre PCR (Invitrogen):		
Reagent	**Stock conc.**	**Volume**
Buffer	10 x	2.5 µl
dNTP mix	10 mM	1 µl
Forward primer	0.01µg/µl	1 µl
Reverse primer	0.01µg/µl	1 µl
H_2O		17.25 µl
DreamTaq Pol.	20 u	0.25 µl
DNA		2 µl
		25 µl

PCR program:		
Cycles	**Temperature**	**Duration**
1	94°C	3:00 min
2	94°C	0:30 min
3 x 35	54°C	0:30 min
4	72°C	0:45 min
5	72°C	3:00 min
6	4°C	∞

Genotyping of *Strumpellin1*$^{-/-}$ mice

Strumpellin$^{fl/fl}$ mice were genotyped by PCR with 5'GGGTA AGTGCTGGTCTCAAGTCAC3' and 5'GCAAATCTA AGTGCTCAGGTGCTC3' primers for floxed *Strumpellin* and with 5'CCCATACAGCACTTTTG3' and 5'TGCACAGTCAGCAGGTT3' primer (Invitrogen Thermo Fisher Scientific, Carlsbad, USA) for Pf4-Cre.

Expected results *Strumpellin*: Wild type allele = 481 bp Mutant allele= 618 bp

Strumpellin flox PCR:		
Reagent	**Stock conc.**	**Volume**
Buffer	10 x	2.5 µl
dNTP mix	10 mM	1 µl
Forward primer	0.01µg/µl	1 µl
Reverse primer	0.01µg/µl	1 µl
H_2O		17.25 µl
DreamTaq Pol.	20 u	0.25 µl
DNA		2 µl
		25 µl

PCR program:		
Cycles	**Temperature**	**Duration**
1	94°C	3:00 min
2	94°C	0:30 min
3 x 35	60°C	0:30 min
4	72°C	0:45 min
5	72°C	3:00 min
6	4°C	∞

PF4-Cre PCR (Invitrogen):		
Reagent	**Stock conc.**	**Volume**
Buffer	10 x	2.5 µl
dNTP mix	10 mM	1 µl
Forward primer	0.01µg/µl	1 µl
Reverse primer	0.01µg/µl	1 µl
H_2O		17.25 µl
DreamTaq Pol.	20 u	0.25 µl
DNA		2 µl
		25 µl

PCR program:		
Cycles	**Temperature**	**Duration**
1	94°C	3:00 min
2	94°C	0:30 min
3 x 35	54°C	0:30 min
4	72°C	0:45 min
5	72°C	3:00 min
6	4°C	∞

4.2 Reverse transcriptase PCR

Washed platelets (see Chapter 4.3 Platelet preparation) or mechanically mashed tissue samples were lysed in in 200 µl IP buffer and transferred to 1 ml TRIZOL. Samples were vortexed for 10 min at room temperature before 250 µl chloroform was added and samples were vortexed for another 10 min at room temperature. After centrifugation for 10 min at 10000 rpm at 4°C, the RNA containing upper phase was transferred into a new tube containing 1 ml ice cold isopropanol and incubated over night at -20°C. After centrifugation for 10 min at 14000 rpm at 4°C the RNA pellet was

washed twice with 1 ml 70 % ethanol and another two times of centrifugation. Finally the supernatant was discarded, and the RNA-pellet was dried at room temperature for 30 min. RNA from platelet samples was solved in 20 µl RNAse free water tissue samples were solved in 200 µl RNAse free water supplemented with (1:500) RNAsin. The RNA concentration was determined using a Nanodrop device.

cDNA synthesis: 1 µg RNA, 2 µl of random primer mix was adjusted with H_2O to 20 µl and incubated at 70°C for 10 min. Further, 4 µl first strand buffer, 2 µl dithiothreitol (DTT), 1 µl dNTPs, 0.1 µl RNAsin and 1 µl RT super script reverse transcriptase was added to the denatured RNA mix and incubated at 42°C for 2 h. The reaction was inactivated by incubation at 70°C for 10 min. Further, 1 µg of synthesized cDNA was further used to determine the expression of different Dystonin isoforms in control and MACF1-deficient platelets and tissue samples.

cDNA- PCR mix		
Reagent	**Stock conc.**	**Volume**
Taq Buffer	10 x	2.5 µl
dNTP mix	10 mM	0.5 µl
Forward Primer	0.01µg/µl	0.5 µl
Reverse Primer	0.01µg/µl	0.5 µl
H_2O		17.2 µl
Taq Pol.	5 U/µl	0.3 µl
$MgCl_2$	25 mM	2.5 µl
cDNA	1 µg/µl	1 µl
		25 µl

PCR program:			
Cycles		**Temperature**	**Duration**
1		96°C	3:00 min
2		96°C	0:30 min
3	x 40	56°C	0:30 min
4		72°C	0:40 min
5		72°C	5:00 min
6		4°C	∞

	Gene	**Primer sequence**
RT-forward	common- Bpag1a/b	5′ATTCAAGAGTTCATGGACCTACGGACAC3′
RT-reverse	Bpag1a	5′TAATTAGGCGGTTTTCAGTCTGGGTGAG3´
RT-reverse	Bpag1b	5′CAATAAGGCCTCTTAAAACTGCCTGAAA3′
RT-forward	GAPDH	5´GGGTTCCTATAAATACGGACTGC3´
RT-reverse	GAPDH	5´CCAATACGGCCAAATCCGTTC3´

4.3 Platelet preparation

Mouse blood (>700 µl) was collected in a reaction tube containing 20 U/ml heparin in TBS, pH 7.3 (300 µl). Blood-heparin mixture was centrifuged at 800 rpm (~300 *g*,

Eppendorf centrifuge 5415C) for 5 min. Supernatant (platelet rich plasma, PRP) was transferred into new reaction tubes containing 300 µl heparin 20 U/ml in TBS. After centrifugation at 800 rpm for 5 min the PRP-containing supernatant was transferred into a new reaction tube and supplemented with prostaglandin (PGI_2; 50 nM) and apyrase (0.02 U/ml). To wash the platelets, samples were centrifuged at 2800 rpm (~800 *g*, Eppendorf centrifuge 5427R) for 5 min and platelet pellet was resuspended in 1 ml Tyrode`s buffer without Ca^{2+}, containing 50 nM PGI_2 and 0.02 U/ml apyrase. This washing step was repeated, and platelet count was adjusted by measuring the platelet concentration with a hematological analyzer (Sysmex KX 21N). Desired platelet concentration was adjusted by centrifugation at 2800 rpm (~800 *g*, Eppendorf centrifuge 5427R) for 5 min and subsequent resuspension of the pellet in calculated volume with Tyrode`s buffer with or without Ca^{2+} (depending on the experiment) and with 0.02 U/ml apyrase. The washed platelets were incubated for 30 min at 37°C before they were used for experiments.[19]

4.4 Immunoblotting

Proteins of lysed platelets were separated by sodium dodecyl sulfate-polyacrylamide gel electrophoresis and blotted onto polyvinylidene difluoride membranes. After blocking, membranes were incubated with the indicated antibody overnight. Horseradish peroxidase-conjugated secondary antibodies and enhanced chemiluminescence solution (MoBiTec) were used for visualization. Immunoblots were recorded directly using an Amersham Imager 600 (GE Healthcare) or with an Amersham Hyperfilm (GE Healthcare) and subsequent developing by a Cawomat 2000 IR apparatus (CAWO Solutions).

4.5 P-Selectin enzyme-linked immunosorbent assay

The concentration of P-selectin in control and *Strumpellin*$^{-/-}$ platelet lysates was determined using the commercial RayBio® Mouse P-Selectin enzyme-linked immunosorbent assay kit (accession number #Q01102; Peachtree Corners, USA). Different lysate dilutions (1:1200-1:4800) were added on a 96-well plate coated with an antibody specific for mouse P-Selectin. Immobilized P-Selectin present in the platelet lysates was then detected using a biotinylated anti-mouse P-Selectin antibody, HRP-conjugated streptavidin and TMB substrate solution. Platelet lysates from one P-

selectin-deficient mouse was used as a negative control. All steps were performed according to the manufacturer's protocol.

4.6 Flow cytometry

All samples were measured on a FACSCalibur (BD Biosciences, Heidelberg, Germany).

Glycoprotein expression: Heparinized whole blood was diluted 1:20 in Tyrode's-HEPES buffer, incubated with saturating amounts of fluorophore-conjugated antibodies for 15 min at RT and finally analyzed.

For activation studies, blood samples were washed twice with Tyrode-HEPES buffer, incubated with agonists and fluorophore-labeled antibodies for 15 min at RT, and then analyzed.

Determination of actin polymerization: Washed platelets were incubated with a Dylight-649 labeled anti-GPIX antibody derivative (20 µg/mL) and either left unstimulated or were treated with the indicated agonists for 2 min. Platelets were fixed with 10 % PFA, permeabilized with 1 % Triton X-100, stained with 10 µM phalloidin-fluorescein isothiocyanate for 30 min to label actin fibers.

To measure the fibrinogen binding capacity, washed platelets were pelleted by centrifugation for 5 minutes at 2800 rpm and resuspended in Tyrode's buffer containing 2 mM $CaCl_2$ (18000 platelets/µl). The platelets were kept resting or were activated with indicated agonists. Further, platelets were incubated with Alexa488-conjugated fibrinogen from human plasma (50 µg/ml, Invitrogen #F13191) for 5 min at 37°C and diluted with 500 µl PBS before measurement.

Uptake of fibrinogen: Washed platelets were pelleted by centrifugation for 5 minutes at 2800 rpm and resuspended in Tyrode's buffer (18,000 platelets/µl). To analyse the uptake of fibrinogen platelets were incubated with Alexa488-conjugated fibrinogen from human plasma (150 µg/ml, Invitrogen #F13191) for 0, 5, 15 or 30 min at 37°C. After fixation with 2 % PFA in PBS buffer overnight at 4°C, the signal of the extracellular bound Alexa488-conjugated fibrinogen was quenched with 0.1 % trypan blue was added to the platelets, incubated for 10 min and diluted with 500 µl PBS before measurement.

4.7 Aggregometry

Washed platelets (160 µl with $0.5x10^6$ platelets/µl) were analyzed in the presence (CRP, U46619, collagen and rhodocytin) or absence (thrombin) of 70 µg/ml human fibrinogen (Sigma). PRP was used for ADP-induced aggregation. Light transmission was recorded on a four-channel aggregometer (Fibrintimer, APACT, Hamburg, Germany) for 10 min and expressed in arbitrary units, with buffer or platelet-poor plasma representing a light transmission of 100 %.

4.8 Clot retraction

PRP ($3x10^5$ platelets/µl) was incubated with bovine thrombin (Sigma 4 U/ml) and $CaCl_2$ (20 mmol/l) for 60- 80 min. Clot retraction was recorded with a digital camera.

4.9 Platelet spreading

For spreading, coverslips (or 8-well ibid polymer chamber slides, ibidi GmbH Gräfelfing, Germany) were coated with either 100 µl human fibrinogen (100 µg/ml in PBS) fibronectin (100 µg/ml in PBS), CRP (100 µg/ml in PBS) or laminin (50 µg/ml in PBS) overnight at 4°C and blocked with 1 % BSA in PBS at 37°C for 1 h.

For spreading on Horm collagen, coverslips (or 8-well ibid polymer chamber slides) were coated with 80 µl Horm collagen (200 µg/ml in SKF solution) at 37°C overnight, washed with PBS and blocked with 1 % BSA in PBS for 1 h at 37°C.

Further, all slides were rinsed with 1 ml Tyrode's buffer before 20 µl washed platelets (150000 - 300000 /µl) in 70 µl Tyrode's buffer, activated with 0.01 U/ml thrombin (Roche), were spread on coated coverslips. Platelets were fixed with 4 % PFA in PBS at different time points. Spread platelets were visualized with a Zeiss Axiovert 200 inverted microscope (100x/1.4 oil objective). Digital images were recorded using a CoolSNAP-EZ camera (Visitron) and analyzed using ImageJ software.

4.10 Immunofluorescence

All samples were mounted with Fluoroshield™ and visualized with either a Leica TCS SP5 or SP8 confocal microscope.

Washed resting platelets were fixed and permeabilized with 2 % PFA and 0.1 % IGEPAL CA-630 in PBS and immobilized on poly-L-lysine coated surface. Preparation of spread platelets was performed as described before (Chapter 4.9). F-actin was

stained using phalloidin-Atto647N (0.075 pg/µl, Sigma-Aldrich) and α-tubulin using Alexa488-conjugated anti-α-tubulin antibodies (1 µg/ml, Thermo Fisher). Samples were further stained using specific primary antibodies as indicated and the respective secondary fluorescence-conjugated IgG.

Cold-induced microtubule disassembly in platelets: Microtubules were depolymerized by incubation of washed platelets at 4°C for 3.5 h; reassembly was allowed by subsequent rewarming of the sample at 37°C for 30 min. Samples maintained at 4°C and 37°C, as well as rewarmed platelets were fixed and permeabilized in PBS supplemented with 1.5 % PFA and 0.075 % IGEPAL CA-630 and allowed to adhere to a poly-L-lysine-coated coverslip. The samples were then blocked with 5 % BSA in PBS buffer and stained using Alexa488-conjugated anti-α-tubulin antibodies (1 µg/ml, clone B-5-1-2, Thermo Fisher) and Phalloidin-Dylight650 (Thermo Fisher #21838) for 1 hour at RT.

4.11 *direct* Stochastic optical reconstruction microscopy (*d*STORM)

F-actin: Spread platelets were fixed with 3 % glyoxal solution, permeabilized with 0.25 % Triton-X, quenched with 100 mM NH_4Cl/100 mM glycine, blocked in 5 % BSA and stained with Alexa Fluor 647 phalloidin. α-tubulin: Spread platelets were fixed with cytoskeleton buffer 1 and 2, which contains 0.3 % and 2 % glutaraldehyde, respectively, permeabilized with 0.25 % Triton-X, quenched with 0.1 % $NaBH_4$, blocked in 5 % BSA and stained with Alexa Fluor 647 coupled anti-α-tubulin antibody. One-color *d*STORM samples were imaged on a widefield setup based on an inverted microscope (Olympus IX-71) equipped with an oil immersion objective (Olympus APON 60xO TIRF, NA 1.49). The dye was excited with a semiconductor laser at 639 nm at an irradiation intensity of ~ 7 kW/cm^2 (Genesis MX639-1000, Coherent). The excitation light was spectrally filtered from the emitted fluorescence using an emission filter Brightline HC 679/41 (Semrock). Imaging was performed with an EMCCD camera (iXon Ultra 897, Andor) at a frame rate of 67 Hz for 30000 frames in photoswitching buffer containing 100 mM β-mercaptoethylamin pH 7.4.[137] *d*STORM images were reconstructed using the open-source software rapidSTORM 3.[138] *d*Storm experiments shown in this study were performed in collaboration with Charly Kusch of the Nieswandt research group.

4.12 Transmission electron microscopy (TEM)

All samples were visualized either with a Zeiss EM900 or a JEM-2100 Electron microscope.

Visualization of the platelet ultrastructure:

Washed platelets were fixed with 2.5 % glutaraldehyde in 50 mM cacodylate buffer (pH 7.2). After embedding in epon 812, ultra-thin sections were generated and stained with 2 % uranyl acetate and lead citrate.

Visualization of the platelet cytoskeleton:

The cytoskeleton of resting platelets, spread platelets (15 min either on fibrinogen or CRP) or platelets perfused over a collagen coated surface were visualized by TEM.

To prepare samples of resting platelets, washed platelets were spun (5 min at 280 g) onto poly-L-lysine-coated coverslips in PHEM buffer supplemented with 0.75 % Triton X-100, 1 µM phalloidin, 1 µM taxol and 0.1 % glutaraldehyde. After washing with PHEM buffer containing 0.1 µM phalloidin and taxol, adherent platelets were fixed for 10 min in PHEM buffer supplemented with 1 % glutaraldehyde.

To prepare samples of spread platelets, washed platelets were spun (5 min at 280 g) onto fibrinogen (100 µg/ml) or CRP (100 µg/ml)-coated slides in Tyrodes–HEPES buffer and were either left unstimulated (CRP) or stimulated with 0.01 U/ml thrombin (fibrinogen) and incubated for 15 min. For preparation of platelet samples from blood perfused over a collagen coated surface see Chapter 4.14. To stop the reaction, coverslips were incubated for 5 min with PHEM buffer containing 0.75 % Triton X-100, 0.1 % glutaraldehyde, 1 µM phalloidin and taxol. After a quick washing step with PHEM buffer containing 0.1 µM phalloidin and taxol, adherent platelets were fixed for 10 min in PHEM buffer supplemented with 1 % glutaraldehyde.

Afterwards, samples were sequentially incubated 0.1 % tannic acid and 0.2 % uranyl acetate. Dehydration was performed by transferring samples through graded acetone. Critical point drying was done in a Leica EM CPD300. Samples were finally coated with 1.2 nm of platinum with rotation at 45°C and 3 nm of carbon at 90°C without rotation under high vacuum in a Leica EM ACE600. Replicas were floated, picked up on formvar-carbon-coated grids and examined.

4.13 Scanning electron microscopy (SEM)

Samples from resting platelets, spread platelets or platelets perfused over a collagen coated surface were visualized with a Phenom Pro scanning electron microscope.

Samples were fixed with 6.25 % glutaraldehyde in 50 mM phosphate buffer (pH 7.4) for 1 h at RT and overnight at 4°C. The samples were washed five times with 100 mM phosphate buffer (100 mM KH_2PO_4/100 mM Na_2HPO_4, volumes 12.5/87.5) and further applied to a 30-100 % acetone gradient for dehydration and stored in 100 % acetone for 16 h. Critical point drying was done in a Leica EM CPD300. Samples were finally coated with gold in an Emitech sc7320 sputter coater and visualized.

4.14 Platelet adhesion and thrombus formation under flow conditions

Coverslips were coated with 200 µg/m Horm collagen at 37°C overnight, washed with PBS and blocked with 1 % BSA in PBS for 1 h at 37°C. Blood was collected in heparin (20 U/ml) and further diluted (2:1) in Tyrode's buffer supplemented with Ca^{2+}, incubated with Dylight-488-conjugated anti-GPIX derivative (0.2 µg/ml) at 37°C for 5 min. Transparent flow chambers with a slit depth of 50 µm, equipped with the coated coverslips, were connected to the blood-filled syringe. Perfusion was performed at shear stress equivalent to a wall shear rate of 150, 1000 or 1700 s^{-1}. Blood was perfused for 4 min over the collagen-coated surface and washed with Tyrode's buffer for 4 min.

For analyses of phosphatidylserine (PS) exposing platelets under flow conditions, heparinized whole blood was supplemented with additional 5 U/ml heparin, Dylight-649-conjugated anti-GPIX derivative (0.2 µg/ml) and Dylight-488-conjugated Annexin A5 (0.25 µg/ml) and perfused over the collagen coated surface for 4 min. Afterwards, the flow chamber was rinsed for 4 min with Tyrode's buffer supplemented with 5 U/ml heparin and Dylight-488-conjugated Annexin A5 (0.25 µg/ml). Procoagulant activity was defined as the ratio of surface coverage of Annexin A5 positive/PS-exposing platelets to the total surface covered by platelets. Image analysis was performed using ImageJ software.

4.15 Bleeding time

Mice were anesthetized by intraperitoneal injection of a combination of midazolam, medetomidine and fentanyl (5, 0.5 and 0.05 mg/kg body weight) and placed on a

heating map to prevent hypothermia. After 5 min paw reflexes were tested to assure proper anesthesia. Further, a 2 mm segment of the tail tip was removed with a scalpel. Tail bleeding was monitored by gently absorbing blood with a filter paper in 20 s intervals without making contact with the wound site. Once no more blood was observed on the paper, it was determined that bleeding had ceased. Otherwise, experiments were stopped after 20 min.

4.16 $FeCl_3$-induced thrombus formation in mesenteric arterioles

Four- to five-week-old mice were anesthetized, and the mesentery was exteriorized through a midline abdominal incision. Arterioles were visualized with a Zeiss Axiovert 200 inverted microscope (10×/0.3 NA objective) equipped with a 100-W HBO fluorescent lamp source, and a CoolSNAP-EZ camera (Visitron). Digital images were recorded and analyzed offline with MetaVue software. The injury was induced by topical application of a 3 mm^2 filter paper saturated with $FeCl_3$ (20 %). Adhesion and aggregation of fluorescently labeled platelets (DyLight-488-conjugated anti-GPIX IgG-derivative) in arterioles were monitored for 40 min or until complete occlusion occurred (blood flow stopped for longer than 1 min). $FeCl_3$- injury experiments shown in this study were performed in collaboration with Sarah Beck of the Nieswandt research group.

4.17 Mechanically-induced thrombus formation in the abdominal aorta

The abdominal cavity of anesthetized mice was longitudinally opened, and the abdominal aorta was prepared. An ultrasonic flow probe (Transonic Flowprobe 0.5 PSB 274; Altron, Medical Electronics, Fürstenfeldbruck) was placed around the aorta, and thrombosis was induced by one firm compression with a forceps for 20 s. Blood flow was monitored until complete occlusion occurred, otherwise, experiments were stopped manually after 30 min. Aorta occlusion experiments shown in this study were performed in collaboration with Sarah Beck of the Nieswandt research group.

4.18 Reverse passive Arthus reaction

Mice were anesthetized and shaved using a Contura HS61 hair cutter (Wella, Schwalbach, Germany). The reverse passive Arthus (rpA) reaction was elicited by intradermal injection of anti-BSA antibody (5 µg/µl) using a 30-G needle followed by intravenous injection of BSA (in PBS 75 µg protein/g mouse). After 4 h mice were killed

and skinned. Pictures of the skins were taken and analyzed. For quantification of the hemoglobin concentration, punch biopsies of inflamed skin areas were homogenized in 500 µl PBS. The homogenate was cleared by centrifugation at 15000 g for 10 min and the supernatant was used for analysis. The optical density at 405 nm was measured to quantify the hemoglobin content. Platelet depleted animals were used as control for severe bleeding. Platelet depletion was induced using the GPIbα antibody (emfret analytics). rpA experiments shown in this study were performed in collaboration with Julia Volz of the Nieswandt research group.[139]

4.19 Lipopolysaccharide-induced inflammation of the lung

Mice were anesthetized and inoculated intranasally with 10 µg Lipopolysaccharide (LPS; Sigma #L8643). After 4 h bronchoalveolar lavage (BAL) was performed by cannulation of the trachea. The lungs were flushed out with 1 ml PBS and the hemoglobin concentration in the BAL fluid was quantified at the optical density of 405 nm. Platelet depleted animals were used as control for severe bleeding. Platelet depletion was induced using the GPIbα antibody (emfret analytics). LPS-induced inflammation experiments shown in this study were performed in collaboration with Julia Volz of the Nieswandt research group.[139]

4.20 Cryo sectioning and staining

Femora of mice were isolated, fixed with 4 % PFA and 5 mM sucrose for 1 h under agitation, transferred into 10 % sucrose in PBS and dehydrated using a graded sucrose series (each 24 h in 10 %, 20 % and 30 % sucrose in PBS). Subsequently, the samples were embedded in Cryo-Gel and frozen at -20°C. Organs were sliced into 10 µm sections on Kawamoto[140] adhesive films with a cryotom (Leica CM1900) and fixed on superfrost glass slides. Samples were probed rehydrated with PBS and blocked with 5 % BSA before staining. Alexa488-conjugated anti-GPIX antibodies (1.33 µg/ml; clone 56F8) were used to specifically label platelets and megakaryocytes, and Alexa647-conjugated anti-CD105 antibodies (3.33 µg/ml, MJ7/18) to stain the endothelium. Nuclei were stained using Fluoroshield with DAPI (Sigma-Aldrich). Samples were visualized with a Leica TCS SP5 or SP8 confocal microscope (Leica Microsystems).

4.21 Preparation of paraffin sections and Hematoxylin/Eosin staining

Five-micrometer-thick sections of formalin-fixed paraffin-embedded spleens of male and female mice were prepared, deparaffinized and stained with hematoxylin and eosin. The number of megakaryocytes was analyzed with an inverted Leica DMI 4000 B microscope.

4.22 Determination of megakaryocyte ploidy

For determination of ploidy levels from bone marrow-derived megakaryocytes, mice were sacrificed and femoral bone marrows were flushed out in 2 ml CATCH buffer. Single cell suspension was obtained by pipetting the bone marrow suspension up and down using a syringe and needles with different gauge (18 G, 22 G, finally 26 G). The suspension was passed through a cell strainer (100 µm) into a 50 ml canonical tube to remove bone and other solid tissue parts. For bone marrow cell-derived megakaryocytes in culture, cells were centrifuged for 5 min at 200 g at RT and washed once with 1 ml PBS. 200 µl of this suspension were used to obtain one sample per condition. The samples were centrifuged at 1200 rpm for 5 min at RT and the cell pellet was resuspended in 400 µl 1:1 mixture CATCH/PBS + 5 % FCS. All samples were incubated for 15 min on ice with anti-CD16/CD32 antibodies (0.02 µg/µl; clone 2.4G2). All samples except control samples (pooled samples from each genotype without MK staining) were incubated for 20 min on ice with FITC-labeled anti-αIIbβ3 antibodies (clone 5D7) to stain the MK population. After adding 1 ml 1:1 mixture CATCH/PBS + 5 % FCS per sample and centrifugation at 1200 rpm for 5 min at RT, the cell pellet was resuspended in 250 µl PBS with 0.1 % EDTA and fixed with 250 µl 1 % PFA in PBS per sample for 10 min on ice. To remove the fixative, cell suspension was washed with 3 ml PBS per sample and after centrifugation at 1200 rpm for 10 min the cell pellet was resuspended in 500 µl PBS/0.1 % Tween for 10 min on ice to permeabilize the cells. The washing step with 3 ml PBS was repeated and the DNA was stained using propidium iodide (PI; final concentration: 25 µg/ml) in H_2O supplemented with ribonuclease (RNase; final concentration: 100 µg/ml) over night at 4°C in the dark. Analysis was performed on a FACS Calibur (BD Bioscience).

4.23 Culture of fetal liver cell derived megakaryocytes

Pregnant mice were sacrificed and embryos (Day: E13.5 - E14.5) were isolated. The fetal liver was removed and placed in DMEM medium containing 10 % FCS, 1 %

streptomycin/penicillin. To obtain a single-cell suspension, fetal liver cells were isolated by pipetting up and down with syringes and needles of different gauge (18 G, 22 G, and finally 26G). Next, cell suspension was passed through a cell strainer (70 µm) to remove connective tissue. Cell suspension was centrifuged at 200 g for 5 min at RT and cell pellet was resuspended in DMEM medium containing 10 % FCS, 1 % streptomycin/penicillin and thrombopoietin (1:1000, TPO conditioned medium). The cells were cultured for 3 days at 37°C and 5 % CO_2. On day 3, the megakaryocytes were isolated via a BSA gradient. Therefore, cell suspension was added on top of the pre-warmed BSA gradient (3 % BSA in PBS overlaid with 1.5 % BSA in PBS) and incubated for 30 min at RT. After removing the BSA, the megakaryocyte pellet was resuspended in DMEM medium containing 10 % FCS, 1 % streptomycin/penicillin and TPO (1:1000 of TPO conditioned).

Analysis of proplatelet forming megakaryocytes was performed on day 4 of culture (one day after BSA gradient) in 6-well culture plates. 5 visual fields per fetal liver with a megakaryocyte density of about 10 megakaryocytes per visual field were analyzed. Proplatelet forming megakaryocytes were defined as megakaryocytes with at least one (proplatelet-sized) protrusion with a clearly visible tip.

4.24 Data analysis

The presented results are mean ± standard deviation from at least two to three independent experiments per group, if not stated otherwise. Differences between control and knockout mice were statistically analyzed using the Mann-Whitney-U test. *P*-values <0.05 were considered as statistically significant: **P*<0.05; ***P*<0.01, ****P*<0.001. Results with a *P*-value > 0.05 were considered as not significant.

5 RESULTS

5.1 Crucial role for Cyfip1 in F-actin branching and lamellipodia formation in platelets

5.1.1 *Cyfip1*$^{-/-}$ mice display normal platelet counts and only moderately impaired platelet activation

To study the function of Cyfip1 in platelets, mice carrying the *Cyfip1* gene flanked by loxP sites were crossed with transgenic mice expressing the Cre recombinase under the control of the megakaryocyte- and platelet-specific platelet factor (Pf) 4 promoter (*Cyfip1*$^{fl/fl\ Pf4\text{-}Cre}$ further referred to as *Cyfip1*$^{-/-}$, *Cyfip1*$^{fl/fl}$ further referred to as *Cyfip1*$^{+/+}$ which served as controls). The lack of the Cyfip1 protein in platelet lysates of *Cyfip1*$^{-/-}$ mice was confirmed by Western blot analysis, whereas Cyfip1 was detected at a size of 145 kDa in in lysates of control and heterozygous *Cyfip1*$^{+/-}$ mice (Figure 5.1.1 A). *Cyfip1*$^{-/-}$ mice displayed normal blood cell count parameters (Table 5.1.1), including platelet count, and only a slight but significant reduction in platelet volume (Figure 5.1.1 B and Table 5.1.1). Analysis of transmission electron micrographs (data not shown, see doctoral thesis of Andreas Sperr, which is in preparation) revealed a comparable platelet ultrastructure as well as numbers of α-granules, dense granules and vacuoles in platelets of *Cyfip1*$^{+/+}$ and *Cyfip1*$^{-/-}$ mice (Figure 5.1.1 C). The expression of prominent glycoproteins on the platelet surface (Table 5.1.2) was comparable between *Cyfip1*$^{+/+}$ and *Cyfip1*$^{-/-}$ mice.

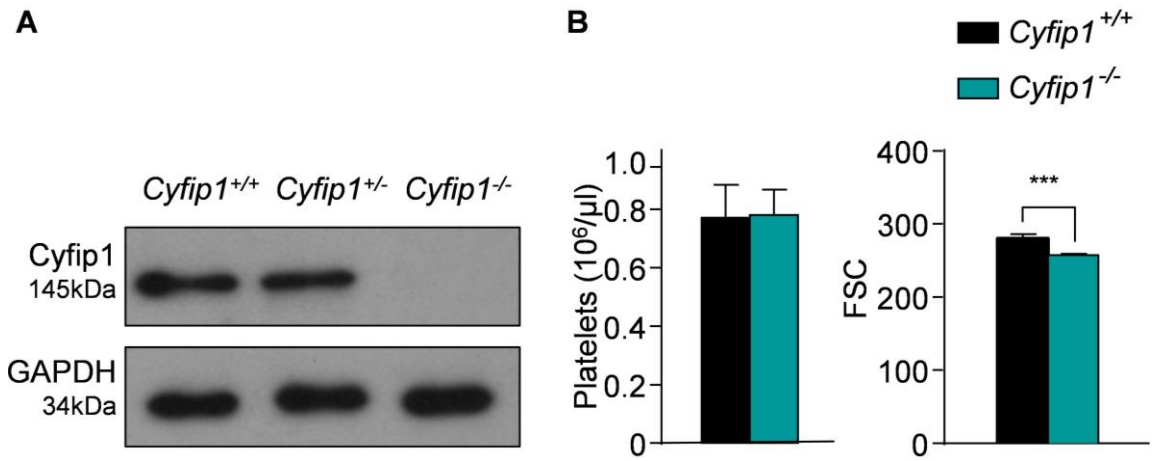

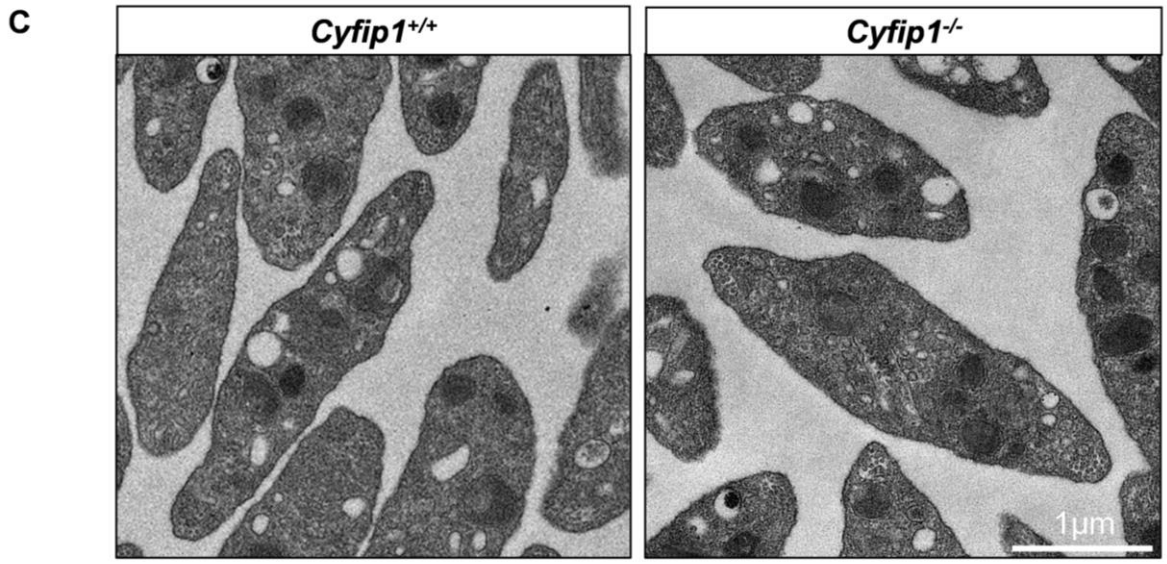

Figure 5.1.1: Normal count and decreased size of *Cyfip1*$^{-/-}$ platelets. (A) The expression of Cyfip1 protein in platelets was assessed by Western blot analysis. Glyceraldehyde 3-phosphate dehydrogenase (GAPDH) served as loading control (n=1). (B) Platelet count per µl and platelet size given as forward scatter (FSC) was determined via flow cytometry (n=4, representative for four independent experiments). Values are mean ± s.d. ***P<0.001. (C) Ultrastructure of resting platelets. Scale bar: 1 µm (n=4).

Table 5.1.1: Unaltered blood count parameters in Cyfip1-deficient mice. Blood count parameters as measured in a Hemavet hematology analyzer (n=6, representative for two independent experiments).

	***Cyfip1*$^{+/+}$**	***Cyfip1*$^{-/-}$**	***p***
Platelet Count [10^3/µl]	729.11 ± 40.80	729.33 ± 131.53	0.99
Mean Platelet Volume [fl]	5.11 ± 0.16	4.83 ± 0.07	0.001***
White Blood Cells [10^3/µl]	9.64 ± 3.27	8.65 ± 2.68	0.56
Neutrophils [10^3/µl]	1.33 ± 0.41	1.87 ± 1.88	0.55
Lymphocytes [10^3/µl]	7.93 ± 2.99	6.43 ± 2.96	0.39
Monocytes [10^3/µl]	0.37 ± 0.28	0.34 ± 0.19	0.80
Eosinophils [10^3/µl]	0.01 ± 0.01	0.02 ± 0.01	0.39
Red Blood Cells [10^6/µl]	10.43 ± 0.85	10.79 ± 0.48	0.35
Hemoglobin [g/dl]	14.22 ± 1.33	14.77 ± 0.90	0.39
Hematocrit [%]	42.99 ± 3.48	43.93 ± 2.11	0.55
Mean Corpuscular Volume [fl]	41.21 ± 0.97	40.73 ± 0.45	0.25
Mean Corpuscular Hemoglobin [pg]	13.62 ± 0.44	13.70 ± 0.53	0.79
Mean Corpuscular Hemoglobin Concentration [g/dl]	33.04 ± 1.01	33.62 ± 0.97	0.33
Red Blood Cell Distribution Width [%]	17.43 ± 0.44	17.43 ± 0.36	1

	Cyfip1$^{+/+}$	*Cyfip1*$^{-/-}$	*p*
GPIb	387 ± 7	374 ± 10	0.43
GPIX	359 ± 8	346 ± 5	0.37
GPV	201 ± 3	197 ± 3	0.47
CD9	797 ± 6	785 ± 13	0.62
GPVI	39 ± 1	39 ± 1	0.82
αIIbβ3	456 ± 6	429 ± 16	0.26
α2	44 ± 2	43 ± 1	0.82
β1	149 ± 10	144 ± 5	0.82
CLEC-2	114 ± 1	112 ± 2	0.36

Table 5.1.2: Unaltered platelet glycoprotein expression in Cyfip1-deficient mice. Platelet glycoprotein expression was determined via flow cytometry (n=4, representative for five independent experiments). Values are mean ± s.d.

Cyfip1 is a subunit of the 400 kDa, hetero-pentameric WAVE complex which is composed of the proteins WAVE-1/-2/-3, ABI1/2, NAP1 (also known as NCKAP1 or NCKAP1L), Cytoplasmic FMR1-interacting protein (Cyfip) 1/2 and HSPC300.[51] The WAVE complex is inactive towards the Arp2/3 complex but can be stimulated by the Rac1 GTPase.[62] The impact of Cyfip1-deficency in platelets on other subunits of the WAVE complex was analyzed in a Western blot approach. In contrast to the weak but unaltered expression of the WAVE1 protein, the expression of the WAVE2 protein was reduced in Cyfip1-deficent platelets, indicating instability of the complex in the absence of Cyfip1 (Figure 5.1.2). These results are in line with a study on megakaryocytes, where a WAVE2-deficiency alters the expression of Abi1 but not of WAVE1.[82] In platelets, this indicates a minor relevance of the WAVE1 protein as a subunit of the WAVE complex and vice versa a minor impact on WAVE1 when other WAVE complex subunits are lost. Furthermore, the expression of Rac1 and Arpc2 remained unaltered upon Cyfip1 deficiency (Figure 5.1.2).

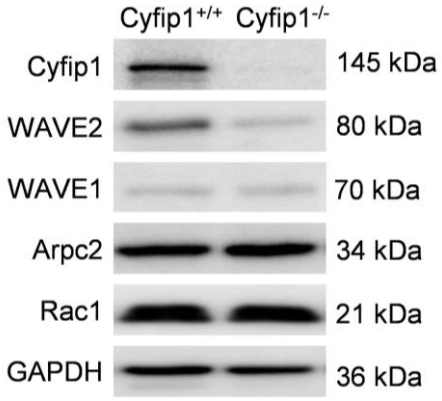

Figure 5.1.2: Cyfip1 deficiency leads to decreased abundance of the WAVE2 protein. Expression of indicated proteins in control and mutant platelets was assessed by Western blot analysis. GAPDH served as loading control (n=3).

The WAVE regulatory complex is activated by Rac1 interaction with the WAVE complex subunit Cyfip1.[74] Interestingly, Rac1-deficient platelets show a strong activation defect in response to GPVI-dependent or CLEC-2-dependent agonists like collagen, CRP or rhodocytin, respectively.[33] However, activation of Cyfip1-deficient platelets was only moderately reduced in response to all tested agonists as measured by αIIbβ3 integrin activation and P-Selectin surface exposure (Figure 5.1.3).

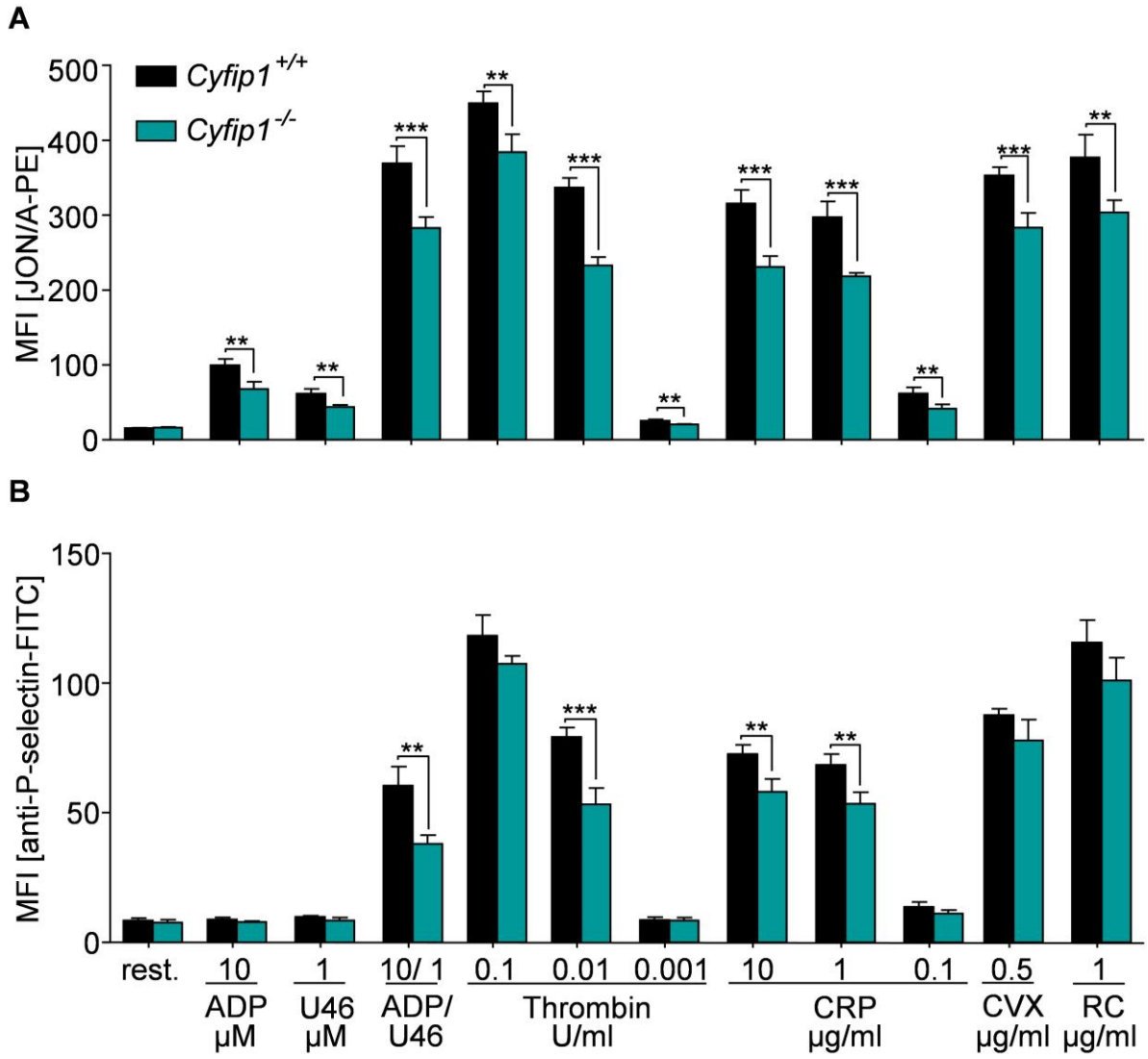

Figure 5.1.3: Moderately reduced activation of *Cyfip1*$^{-/-}$ platelets. Flow cytometric determination of the mean fluorescence intensity (MFI) of (A) inside-out activation of the αIIbβ3 integrin (JON/A-PE antibody) and (B) degranulation-dependent P-selectin exposure (FITC-labelled anti-P-selectin antibody) in response to the agonists ADP, U46619 (thromboxane analogue), thrombin (Thr), collagen related peptide (CRP), convulxin (CVX) and rhodocytin (RC) on control and Cyfip1-deficient platelets. (n=5, representative for four independent experiments); values are mean ± s.d. **P<0.01, ***P<0.001.

The Arp2/3 complex is activated by the WAVE regulatory complex downstream of Rac1. To investigate how platelet activation is affected by the actin cytoskeleton and to compare this to the involvement of the Arp2/3 complex, activation studies with control platelets in the presence of the Arp2/3 inhibitor, CK-666, and the fungal toxin, cytochalasin D, a potent actin polymerization inhibitor, were performed. Control platelets incubated with CK-666 (inhibition of Arp2/3-induced actin filament branching) displayed reduced activation similar to the reduction seen with *Cyfip1*$^{-/-}$ platelets. Preincubation of platelets with cytochalasin D had a stronger effect on agonist-induced

activation as compared to Cyfip1-deficient platelets (data not shown, see doctoral thesis of Andreas Sperr, which is in preparation). These data suggest that the moderately reduced activation of *Cyfip1*$^{-/-}$ platelets is rather caused by an Arp2/3-related defect than an upstream signaling defect.

To test the functional consequences of this moderate activation defect, *in vitro* aggregation studies were performed. *Cyfip1*$^{-/-}$ platelets aggregated normally to the G protein-coupled agonist thrombin and the GPVI-specific agonist collagen-related peptide (CRP), even at very low concentrations (Figure 5.1.4). Consistently a delay in the onset of aggregation in response to low concentrations of collagen was observed. However, the amplitude as a measure for maximum platelet aggregation was comparable between control and mutant platelets. In comparison, Rac1-deficient platelets were shown to display a strong aggregation defect, when washed platelets were preincubated with apyrase (2 U/ml) and indomethacin (10 µM) to prevent the effect of second wave mediators, and then activated with high concentrations of collagen.[33] *Cyfip1*$^{-/-}$ platelets aggregated normally at high collagen concentrations under these conditions (10 and 20 µg/ml collagen, Figure 5.1.4), excluding a selective GPVI signaling defect in *Cyfip1*$^{-/-}$ platelets as observed for Rac1-deficient platelets.[33]

In addition, changes in protein tyrosine phosphorylation upon stimulation with CRP were assessed and a comparable total tyrosine phosphorylation pattern in *Cyfip1*$^{-/-}$ platelets compared to *Cyfip1*$^{+/+}$ was detected by Western blot (data not shown, see doctoral thesis of Andreas Sperr, which is in preparation). Taken together, lack of Cyfip1 only moderately and non-selectively impairs platelet activation, which has no major effect on platelet-platelet interaction.

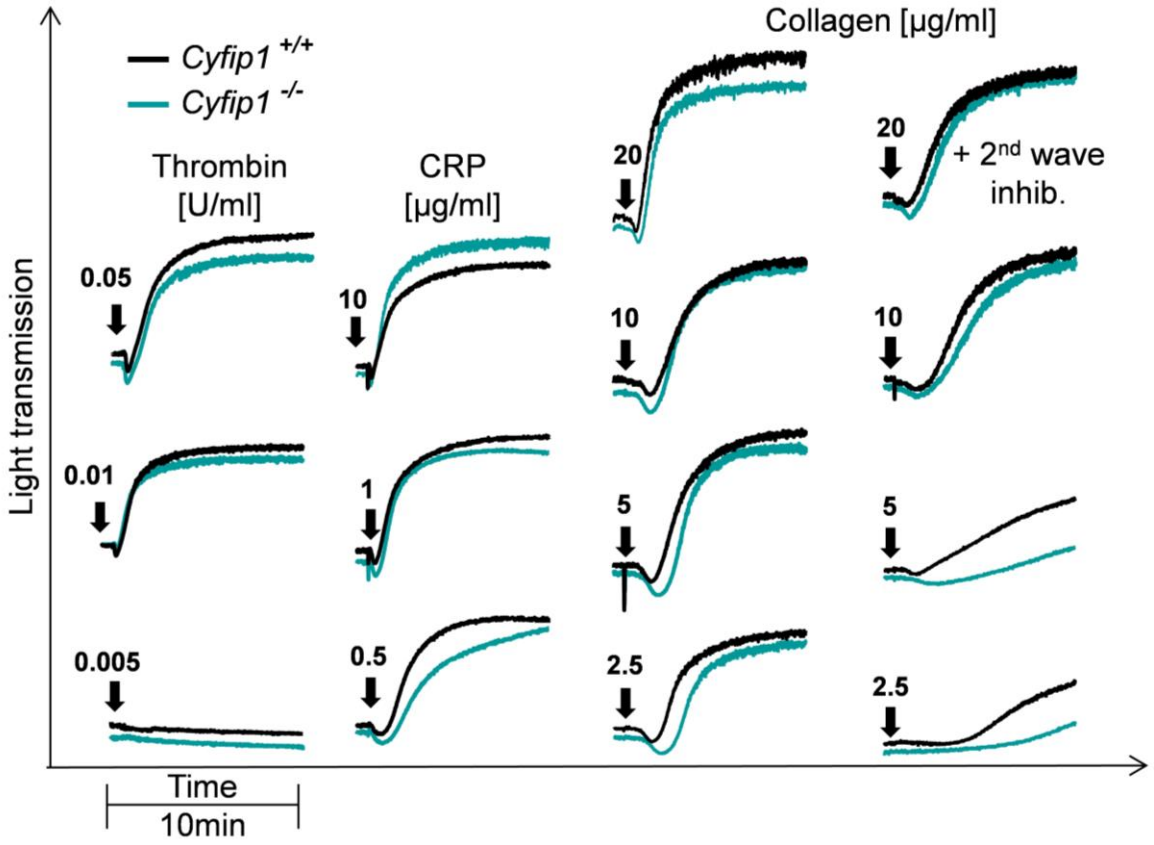

Figure 5.1.4: Cyfip1-deficient platelets display a mild aggregation delay in response to low dose collagen and second wave inhibition. Washed platelets from *Cyfip1*$^{+/+}$ and *Cyfip1*$^{-/-}$ mice were activated with the indicated agonists. 2nd wave inhibitors: Indomethacin 10 µM, EDTA 5 mM, Apyrase 2 U/ml (representative curve of at least six independent samples).

5.1.2 Absent lamellipodia formation of *Cyfip1*$^{-/-}$ platelets on different matrices in static spreading assays

It has been shown that the WAVE regulatory complex drives lamellipodia formation in other cell types by enhancing actin nucleation via the Arp2/3 complex.[62,141,142] Therefore, the role of the WAVE complex subunit Cyfip1 in platelet lamellipodia formation was studied with a static platelet spreading assay. During the process of platelet spreading four consecutive phases can be observed: (I) adhesion of resting platelets, (II) formation of filopodia, (III) a combination of filopodia and lamellipodia, and (IV) only lamellipodia.[44] *Cyfip1*$^{-/-}$ platelets adhered to fibrinogen under static conditions and formed filopodia, but strikingly, lamellipodia formation (phases III and IV) was completely abolished (Figure 5.1.5 A-B).

However, the transition from resting platelet to filopodia-forming platelet was unaltered between both groups, as revealed by live-imaging of platelet spreading. Shown in representative videos of thrombin activated *Cyfip1*$^{+/+}$ (Supplemental Video 1) and *Cyfip1*$^{-/-}$ (Supplemental Video 2) platelets spread on fibrinogen for 20 minutes. Cyfip1-deficient platelets, which reached the spreading phase II, formed more filopodia with increased length compared to *Cyfip1*$^{+/+}$ platelets in phase II (Figure 5.1.5 A and Figure 5.1.6, statistical analysis see doctoral thesis of Andreas Sperr, which is in preparation).

To assess this in more detail, the cytoskeletal organization of spread platelets was analyzed by platinum replica electron[143] (Figure 5.1.6) and super-resolution microscopy by *d*STORM (Figure 5.1.7 A).[144] Orthogonally arrayed short actin filaments were formed in the circumferential zone of spread control platelets. In contrast, Cyfip1-deficient platelets showed filopodia consisting of parallel bundles of actin filaments (Figure 5.1.6).

In agreement, *Cyfip1*$^{-/-}$ platelets were principally able to assemble filamentous actin as determined by the F-actin content in resting platelets and in platelets after activation with CRP or thrombin by flow cytometry. Only a slightly decreased content was observed in CRP-activated platelets but not resting or thrombin-activated platelets (Figure 5.1.7 B). However, the F-actin ratio of activated platelets over resting platelets revealed no significant differences, demonstrating that mutant platelets can assemble F-actin after activation similar to controls (Figure 5.1.7 C).

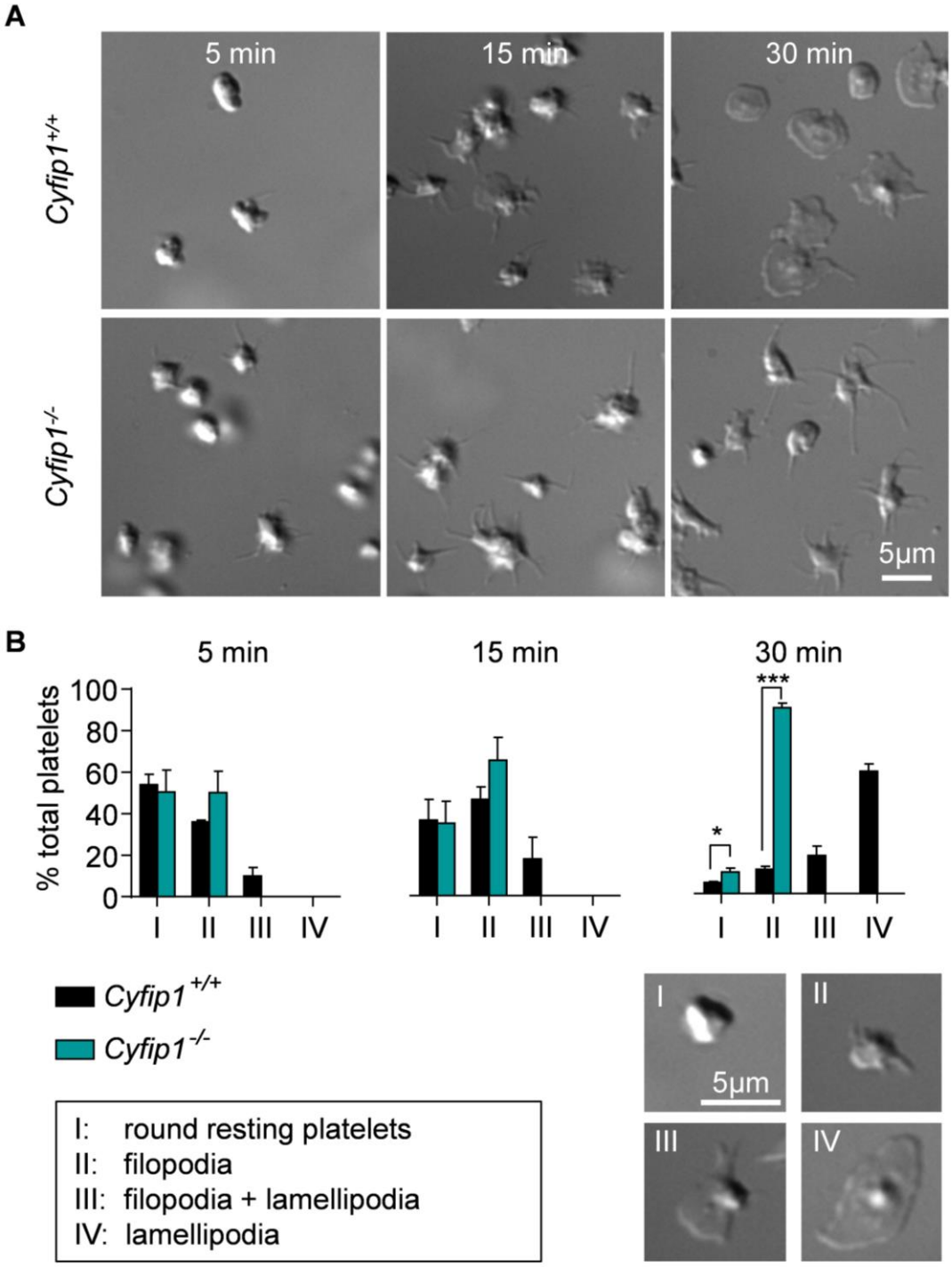

Figure 5.1.5: Cyfip1-deficient platelets are unable to form lamellipodia on a fibrinogen-coated surface. (A) Washed platelets were allowed to spread on fibrinogen, following fixation at the indicated time points. (n=3, representative for three independent experiments). Scale bar: 5 µm. (B) Quantification of the different spreading phases of fixed platelets after 5, 15 and 30 minutes from differential interference contrast images. Phase I: round and resting platelets; Phase II: platelets with filopodia; Phase III: platelets with filopodia and lamellipodia; Phase IV: "fried-egg-like" shape, fully spread platelets with only lamellipodia. Values are mean ± s.d. ***P<0.001

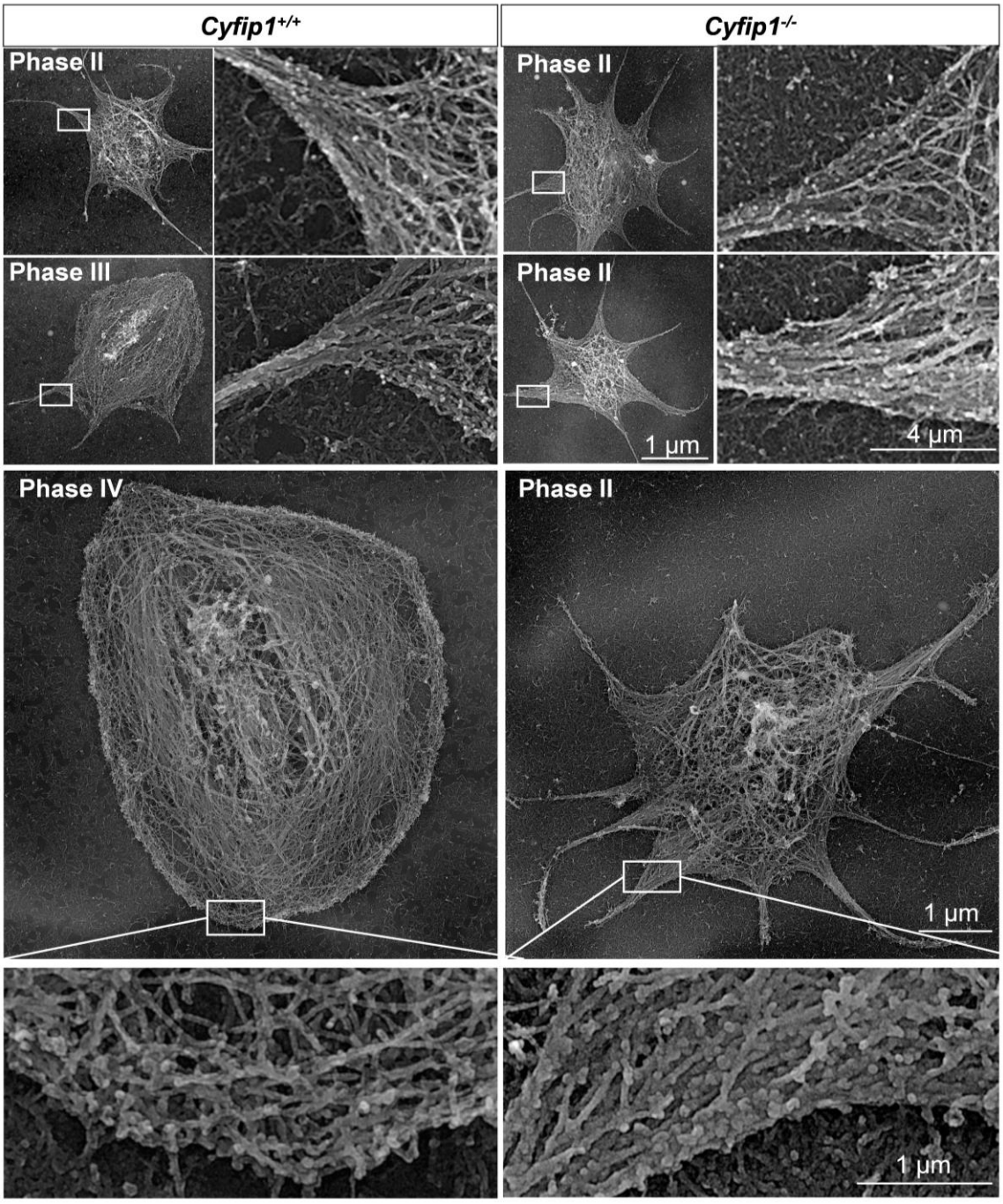

Figure 5.1.6: Cyfip1-deficient platelets cannot form branched actin filaments. Platinum replica electron microscopic images of the cytoskeleton ultrastructure of control and Cyfip1-deficient platelets spread on fibrinogen after 15 min. (n=2)

The localization of Arp2/3 in platelets spread on fibrinogen was analyzed and Arp2/3 was found to be strongly present at the circumferential zone of fully spread (lamellipodia; white arrowhead) control platelets (Figure 5.1.8). *Cyfip1*$^{-/-}$ platelets showed a stronger dot-like staining at the peripheral zone compared to control platelets in spreading phase II were the staining appeared more distributed along the

membrane. However, despite slightly differences in the intensity of the Arp2/3 staining in *Cyfip1*$^{-/-}$ platelets in the peripheral zone, Arp2/3 was found to be localized to filopodia in control and in mutant platelets. This indicates that not altered localization, but impaired Cyfip1-mediated Arp2/3 activation is causative for abolished lamellipodia formation.

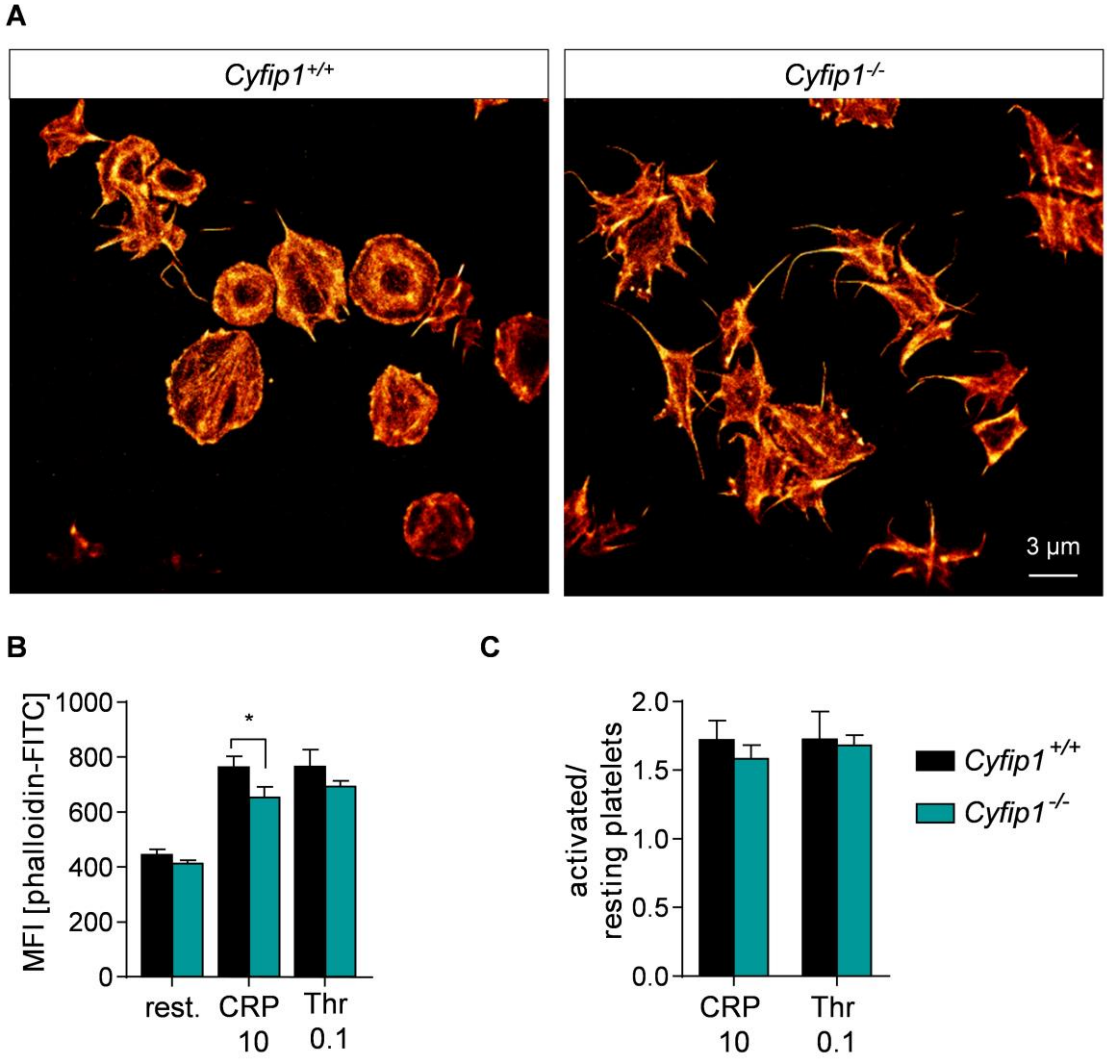

Figure 5.1.7: Lack of lamellipodia formation but normal agonist induced F-actin assembly in *Cyfip1*$^{-/-}$ platelets. (A) *d*STORM images of the platelet actin cytoskeleton on fibrinogen after 30 min. (n=2, representative for two independent experiments). (B) F-actin content under resting conditions and upon stimulation with CRP (10 µg/ml) or thrombin (Thr 0.1 U/ml) was assessed by measuring the mean fluorescence intensity of bound FITC labeled phalloidin in flow cytometry. (C) The ratio of mean fluorescent intensity of activated vs. resting samples reflecting F-actin polymerization rates. (n=4, representative for three independent experiments); values are mean ± s.d. **P*<0.05.

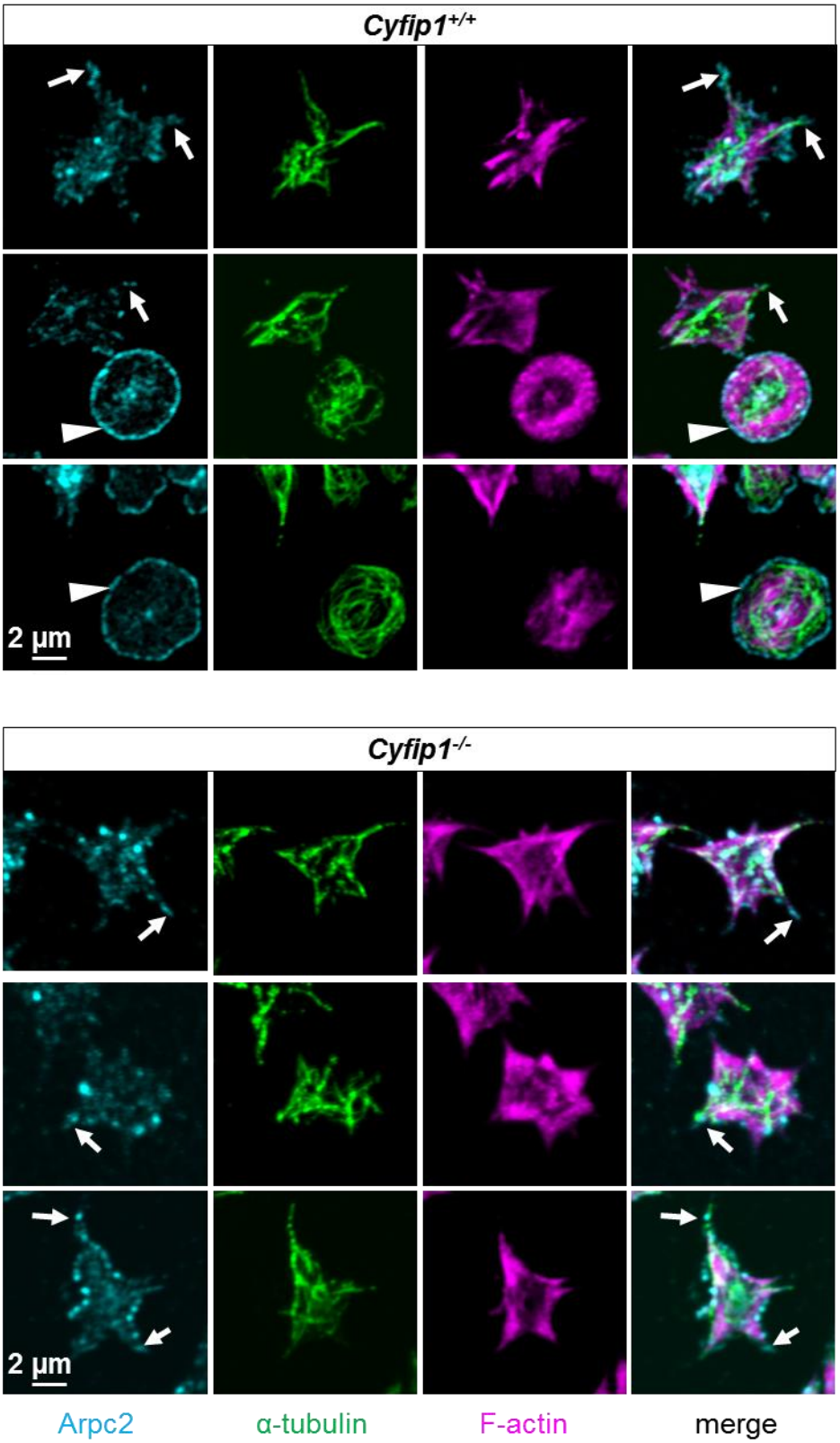

Figure 5.1.8: Arp2/3 localization in platelets spread on fibrinogen. Platelets were spread on a fibrinogen coated surface for 30 min and stained for Arp2/3 (cyan), α-tubulin (green) and F-actin (purple). Filopodia (white arrow) and lamellipodia (white arrowhead) are indicated. (n=3).

Next, Cyfip1-deficient platelets were spread on different matrices to analyze the formation of lamellipodia on other surfaces. Likewise, mutant platelets could not form lamellipodia on collagen IV, laminin and CRP and were unable to reorganize actin filaments into short, branched filaments (Figure 5.1.9 A-B). Images of the Cyfip1-deficient platelet cytoskeleton ultrastructure on CRP after 15 min only revealed filopodia structures (Figure 5.1.9 B) compared to *Cyfip1*$^{+/+}$ platelets, which showed partially branched F-actin at the cell rim. Further it appears that the coated substrate already influences the shape of spread control platelets.

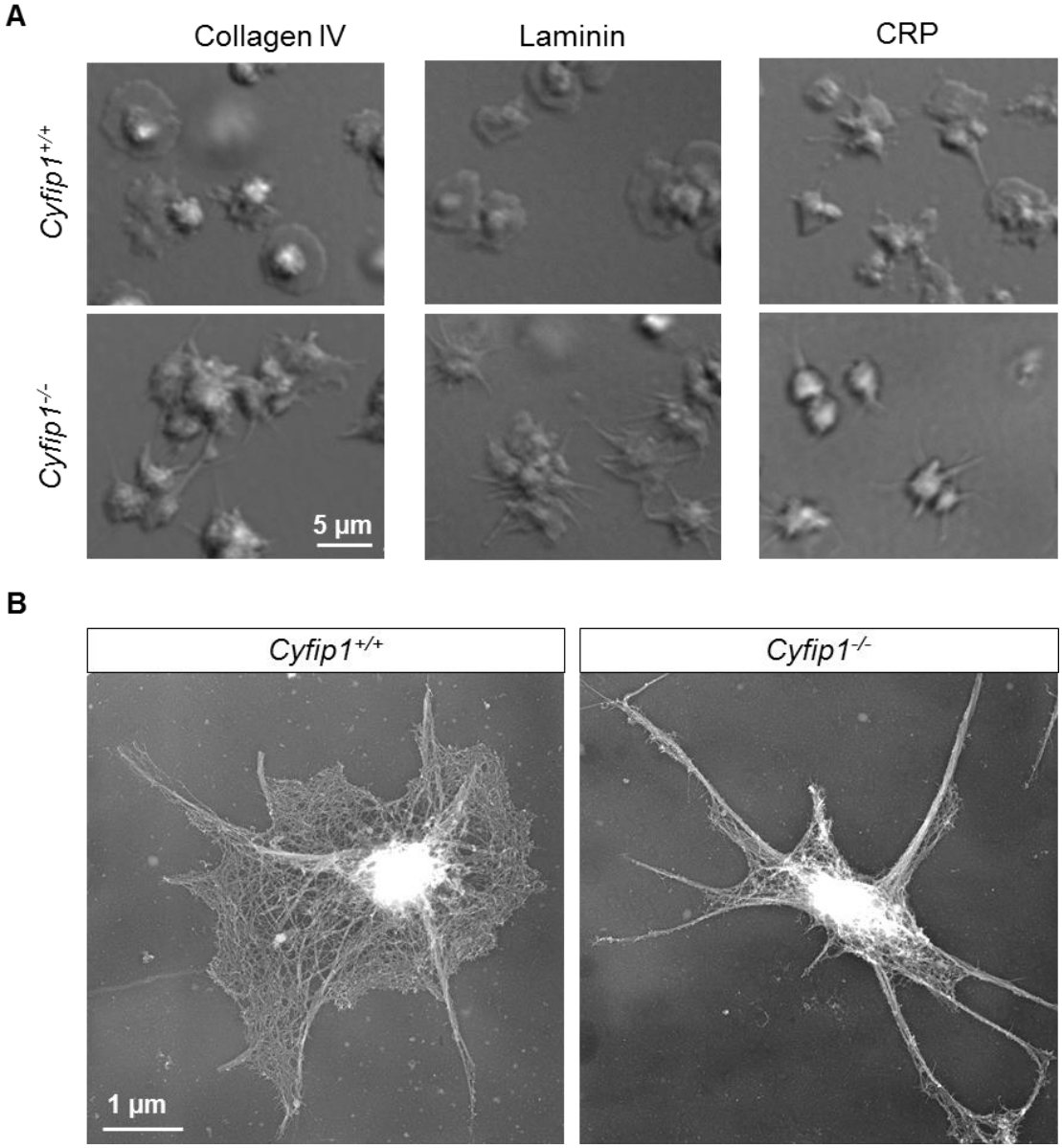

Figure 5.1.9: Abolished lamellipodia formation of mutant platelets on different matrices. (A) Washed platelets were allowed to spread on collagen IV, laminin or CRP for 30 min. (n=3) Scale bars: 5 µm. (B) Images of the platelet cytoskeleton ultrastructure on CRP after 15 min. (n=5)

In addition the localization of Arp2/3 in platelets spread on differently coated surfaces like Horm collagen (mostly collagen I), CRP and fibronectin (Figure 5.1.10 A-C) was analyzed via confocal microscopy. Control platelets spread on Horm collagen or CRP rather form filopodia than lamellipodia. Comparable to the Arp2/3 localization of platelets spread in phase II on a fibrinogen coated surface, *Cyfip1*$^{-/-}$ platelets spread on Horm collagen, CRP or fibronectin also showed a stronger dot-like staining at the peripheral zone compared to control platelets. As already shown for platelets spread on fibrinogen (Figure 5.1.8), despite slightly differences in the intensity of the Arp2/3 staining in *Cyfip1*$^{-/-}$ platelets in the peripheral zone, Arp2/3 was found to be localized to filopodia in control and in mutant platelets. This indicates that not altered localization, but impaired Cyfip1-mediated Arp2/3 activation is causative for abolished lamellipodia formation. Further, these results support previous findings (Figure 5.1.9) that Cyfip1-deficient platelets cannot form Arp2/3-dependent branched actin filaments under any condition, independent of the coated surface, which are necessary for lamellipodia formation.

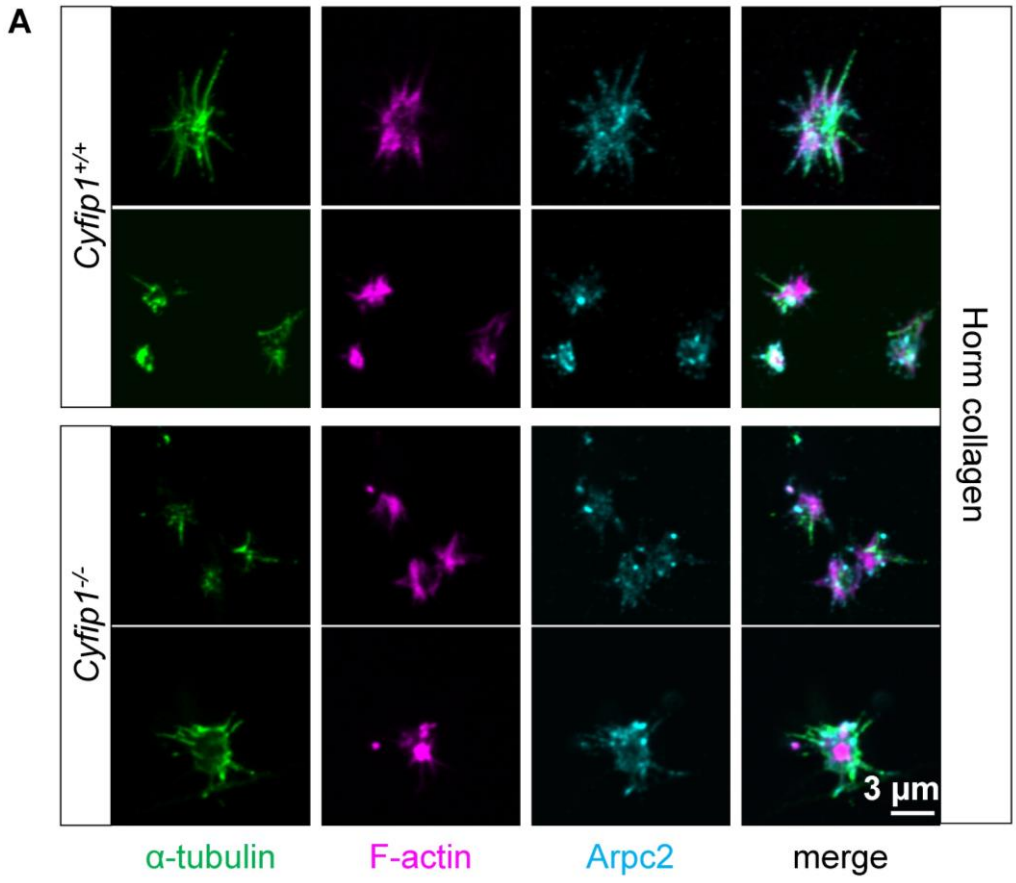

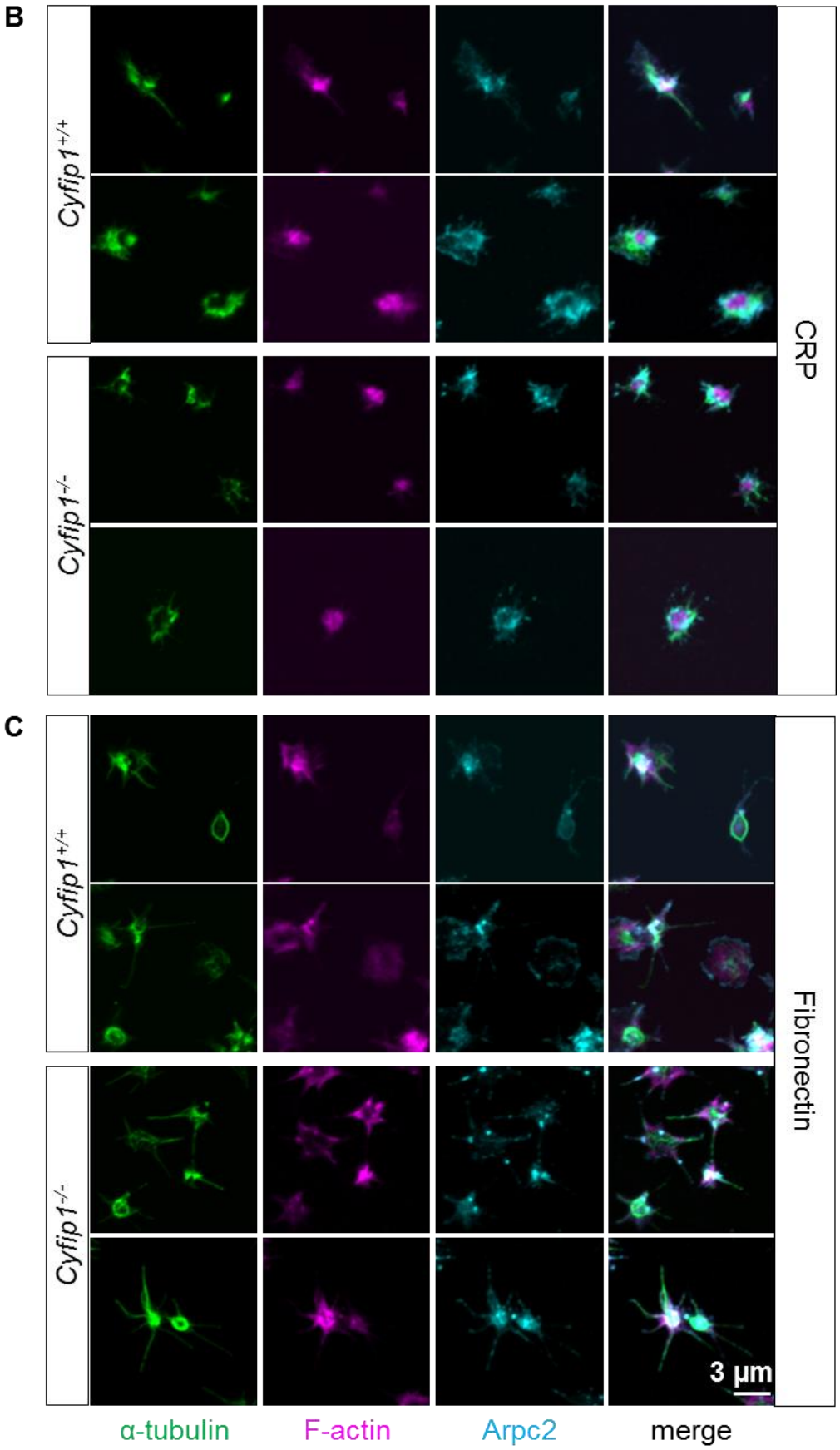

Figure 5.1.10: Arp2/3 localization in platelets spread on different matrices. Platelets were spread on a (A) Horm collagen (mostly collagen I), (B) CRP or (C) fibronectin coated surface for 30 min and stained for α-tubulin (green), F-actin (purple) Arpc2 (cyan). (n=3).

5.1.3 Lack of Cyfip1 does not affect microtubule de- and repolymerization

It has been shown, that an altered F-actin regulation can also affect the arrangement and dynamics of microtubules.[145] The cytoskeletal organization of resting *Cyfip1*$^{-/-}$ platelets was analyzed. Images of the platelet cytoskeleton ultrastructure on poly-L-lysine revealed a normal actin scaffold and the characteristic ring structure organized by microtubules, designated as the marginal band (Figure 5.1.11 A).

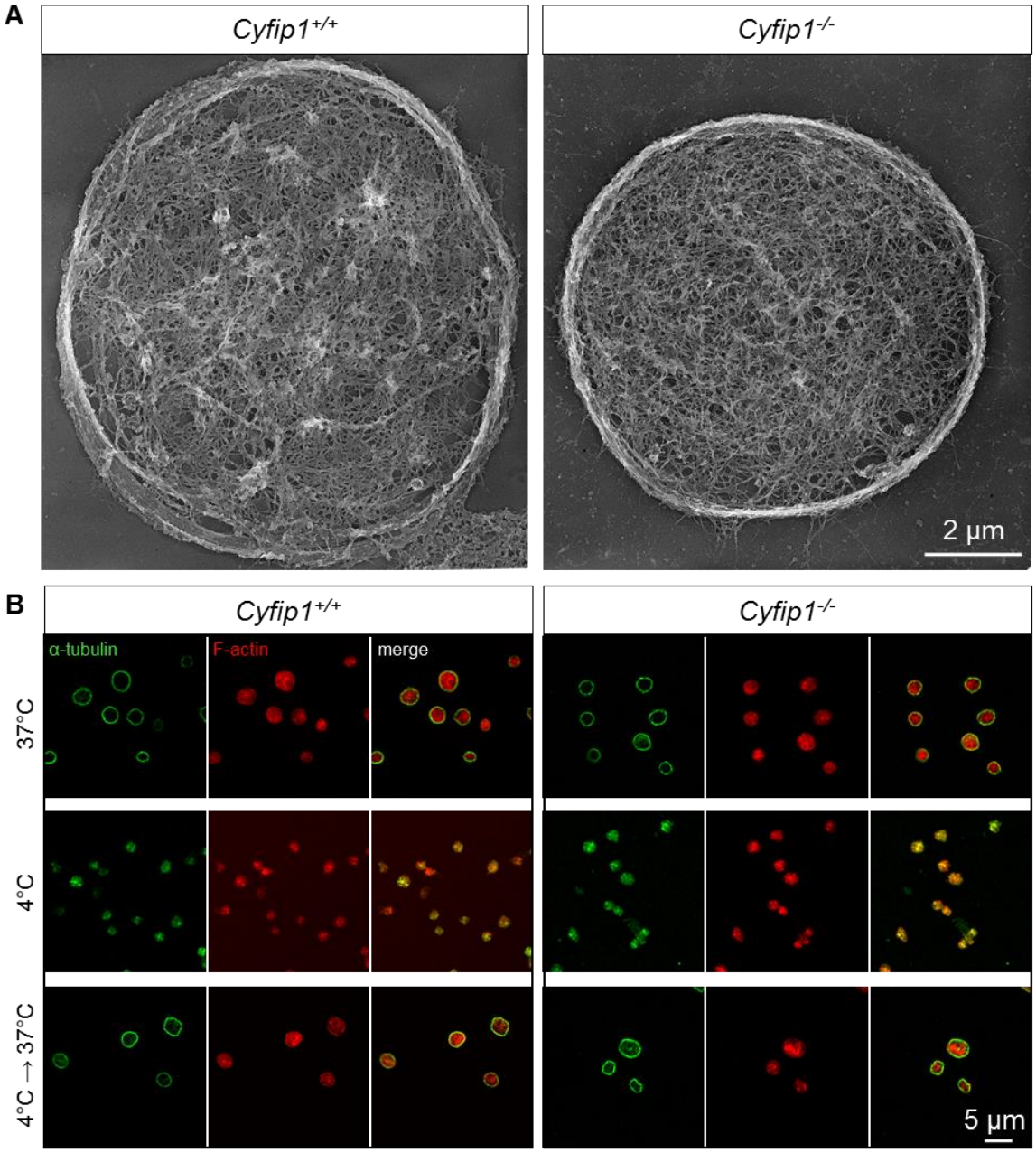

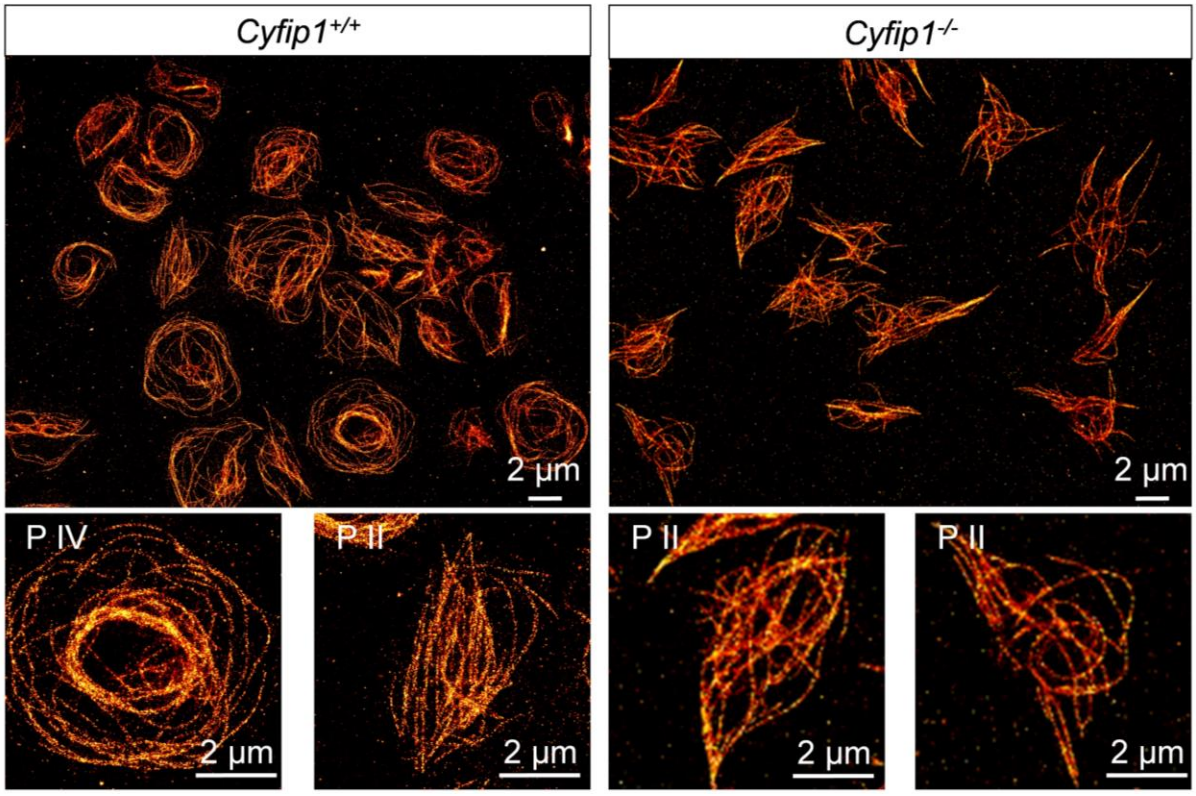

Figure 5.1.11: Lack of Cyfip1 does not affect microtubule de- and repolymerization. (A) Images of the platelet cytoskeleton ultrastructure on poly-L-lysine (n = 2). (B) Representative confocal microscopy images of immunostained resting platelets on poly-L-lysine (PLL). Washed platelets were fixed either after 3.5 h at 37°C (resting), after 3.5 h at 4°C (disassembly) or after 3.5 h at 4°C followed by 30 min at 37°C (reassembly). *Cyfip1*$^{+/+}$ and *Cyfip1*$^{-/-}$ platelets were stained for F-actin (red) and α-tubulin (green). (C) *d*STORM images of the platelet tubulin cytoskeleton on fibrinogen after 30 min. (n=2) Zoom-in of control platelets in spreading phase II and IV and of mutant platelets in phase II. Scale bar: 2 µm (n = 3, representative for three independent experiments).

Next, the number of microtubule coils per platelet was quantified. Cyfip1-deficient platelets had a decreased number of microtubules compared to controls (microtubule number: *Cyfip1*$^{+/+}$ 10.51 ± 2.5 and *Cyfip1*$^{-/-}$ 8.94 ± 2.4, **P<.004; n>36; TEM pictures not shown, see doctoral thesis of Andreas Sperr, which is in preparation). The cold resistance of microtubules was analyzed by incubating platelets at different temperatures to induce dis- or reassembly of microtubules. Fixation and staining for α-tubulin of the platelets revealed comparable dis- and reassembly of microtubules (Figure 5.1.11 B). The microtubule organization assessed by *d*STORM (Figure 5.1.11 C) of *Cyfip1*$^{-/-}$ platelets spread on fibrinogen for 30 min was as would have been expected for control platelets in phase II.

5.1.4 Lamellipodia are not required for *ex vivo* thrombus formation

Platelets from mice lacking Rac1 or Arp2/3 are unable to restructure their shape into lamellipodia in spreading experiments on fibrinogen.[33,36] However, Rac1 was shown to be essential for activation of PLCγ2,[33] a key effector enzyme in the GPVI signaling cascade in platelets, limiting the utility of this mouse model to study the function of lamellipodia during thrombus formation. Similarly, *Arpc2*$^{fl/fl,Pf4\text{-}Cre}$ mice exhibited a marked reduction in the peripheral platelet count and the protein was largely but not completely lost in those platelets.[36]

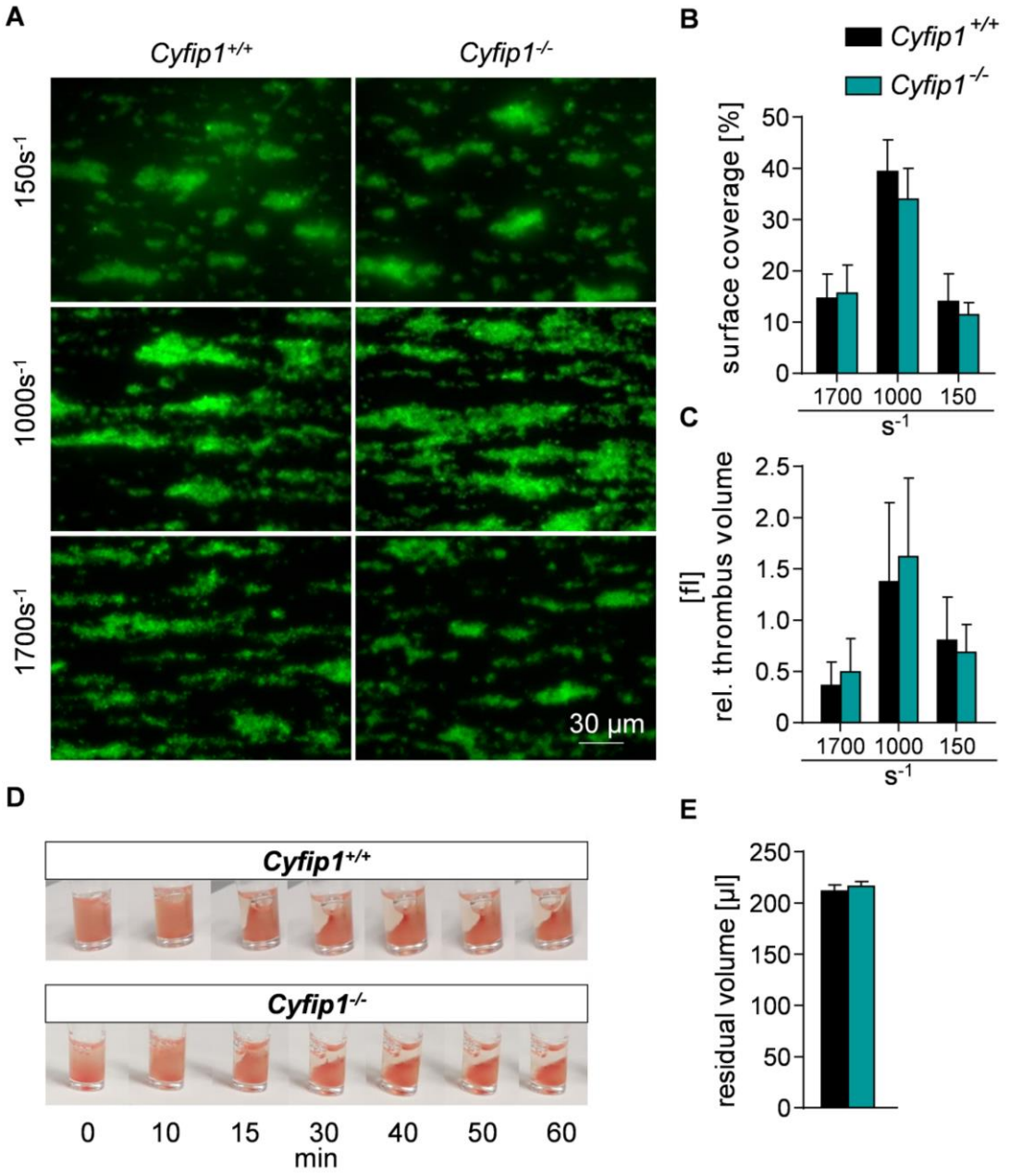

Figure 5.1.12: Normal *ex vivo* thrombus formation and clot retraction of Cyfip1-deficient platelets. (A) Thrombus formation was assessed on collagen at different shear rates. Shown are representative fluorescence pictures of platelets stained with a Dylight-488

anti-GPIX antibody. (n=5, representative for three independent experiments) Scale bar: 30 µm. (B) Surface coverage and (C) relative thrombus volume given as fluorescence intensity (fl) were quantified. (D) Clot formation was observed over time and (E) residual serum volume was measured after 60 min (n=3, representative for two independent experiments).

Cyfip1$^{-/-}$ mice are the first animal model displaying an isolated defect in lamellipodia formation but no major defects in any other platelet function. Thus, *Cyfip1*$^{-/-}$ mice represent a unique system to address the role of lamellipodia in thrombus formation. To induce thrombus formation in an *in vitro* system, whole blood was perfused over a Horm collagen-coated surface in a flow chamber at different shear rates (150 s^{-1}, 1000 s^{-1}, 1700 s^{-1}). Interestingly, surface coverage (Figure 5.1.12 A-B) and thrombus volume (Figure 5.1.12 A, C) were comparable between samples from *Cyfip1*$^{+/+}$ (Supplemental Video 3) and *Cyfip1*$^{-/-}$ (Supplemental Video 4) mice. Kinetics of single platelet adhesion and embolization of smaller platelet aggregates appeared normal. Similarly, *Cyfip1*$^{-/-}$ platelets showed effective thrombus compaction under flow (Supplemental Video 4) and clot retraction *in vitro* (Figure 5.1.12 D-E).

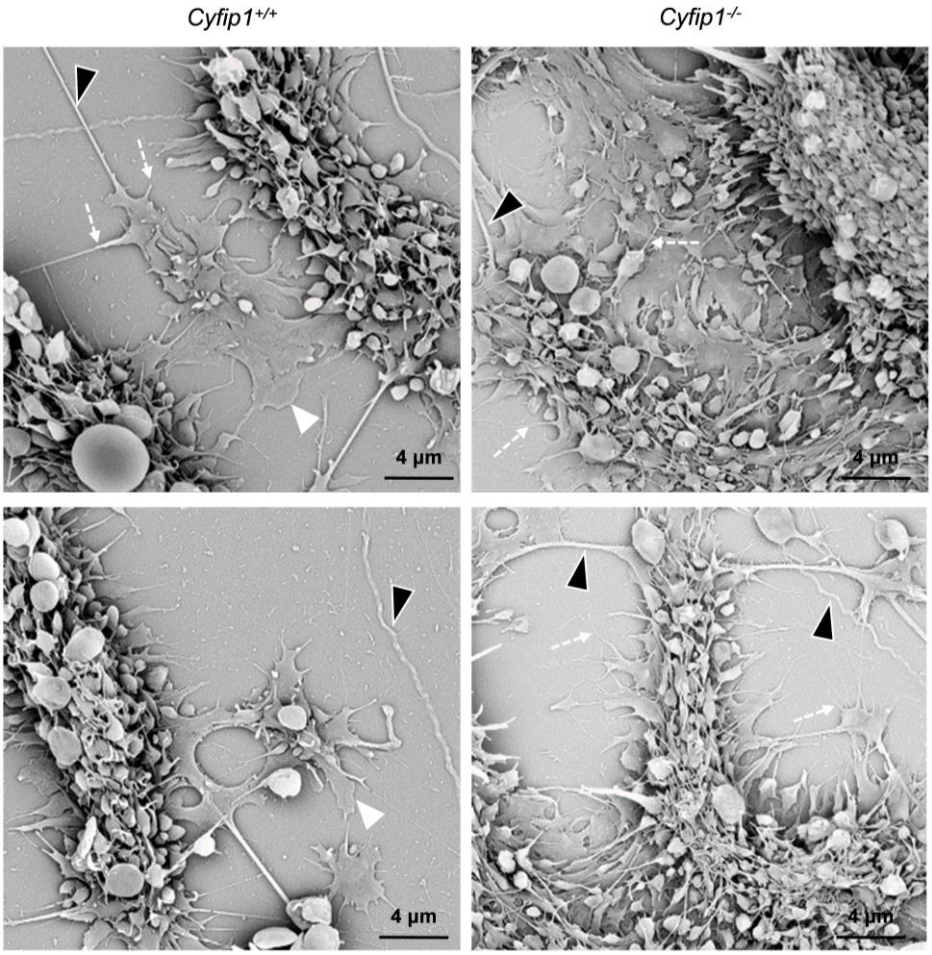

Figure 5.1.13: Flattened platelets with filopodia-like structures at the bottom of the thrombus. Scanning electron microscopic image of platelets after experimentally-induced

ex vivo thrombus formation on collagen. White arrow indicates a filopodium, black arrowhead indicates collagen fiber and white arrowhead indicates lamellipodia-like structures. (n=4)

Video analyses of whole blood from *Cyfip1*$^{+/+}$ mice perfused over collagen at a shear rate of 150 s^{-1} for 4 minutes revealed that single platelets at times formed filopodia to grab collagen fibers before they became fully activated and initiated thrombus formation (Supplemental Video 5). Surprisingly, fully spread control platelets (equivalent to phase IV platelets in the static spreading assay) with circumferential lamellipodia were never observed under these conditions. These findings were corroborated when the flow chamber was removed from the glass coverslip after the experiment and prepared the sample for scanning (Figure 5.1.13) and platinum replica (Figure 5.1.14) electron microscopic analyses. Investigation of control and *Cyfip1*$^{-/-}$ platelet morphology showed that in general, platelets form filopodia in the thrombus shell (Figure 5.1.13) and are flattened with filopodia structures and parallel actin bundles when in direct contact to collagen fibers at the bottom of the thrombus (Figure 5.1.13 and Figure 5.1.14 A), contrary to the abundant fully spread platelets with circumferential lamellipodia observed in a static spreading assay (Figure 5.1.5 A and Figure 5.1.6). Some unspread platelets at collagen fibers were found in control and mutant samples and only in a few control platelets small parts of branched actin filaments could be identified at the cell boundary (Figure 5.1.14 B and Table 5.1.3)
Taken together, these results demonstrate that lamellipodia formation is not required for stable thrombus formation *ex vivo* and that morphological changes of platelets differ between a static spreading assay and thrombus formation under flow.

Table 5.1.3: Quantification of F-actin organization of platelets after experimentally-induced *ex vivo* thrombus formation on collagen. Quantitative analysis of the distribution of platelet spreading stages under flow conditions based on the cytoskeletal organization. n ≥ 52 platelets per genotype were counted.

	(1) Unspread	(2) spread, parallel actin filaments	(3) Spread, partially branched actin filaments	fully spread, circumferential zone with branched actin filaments (equivalent to phase IV in the static spreading assay)
Cyfip1$^{+/+}$	17 %	64 %	19 %	0/58
Cyfip1$^{-/-}$	19 %	81 %	0 %	0/52 (Number of platelets/total platelets)

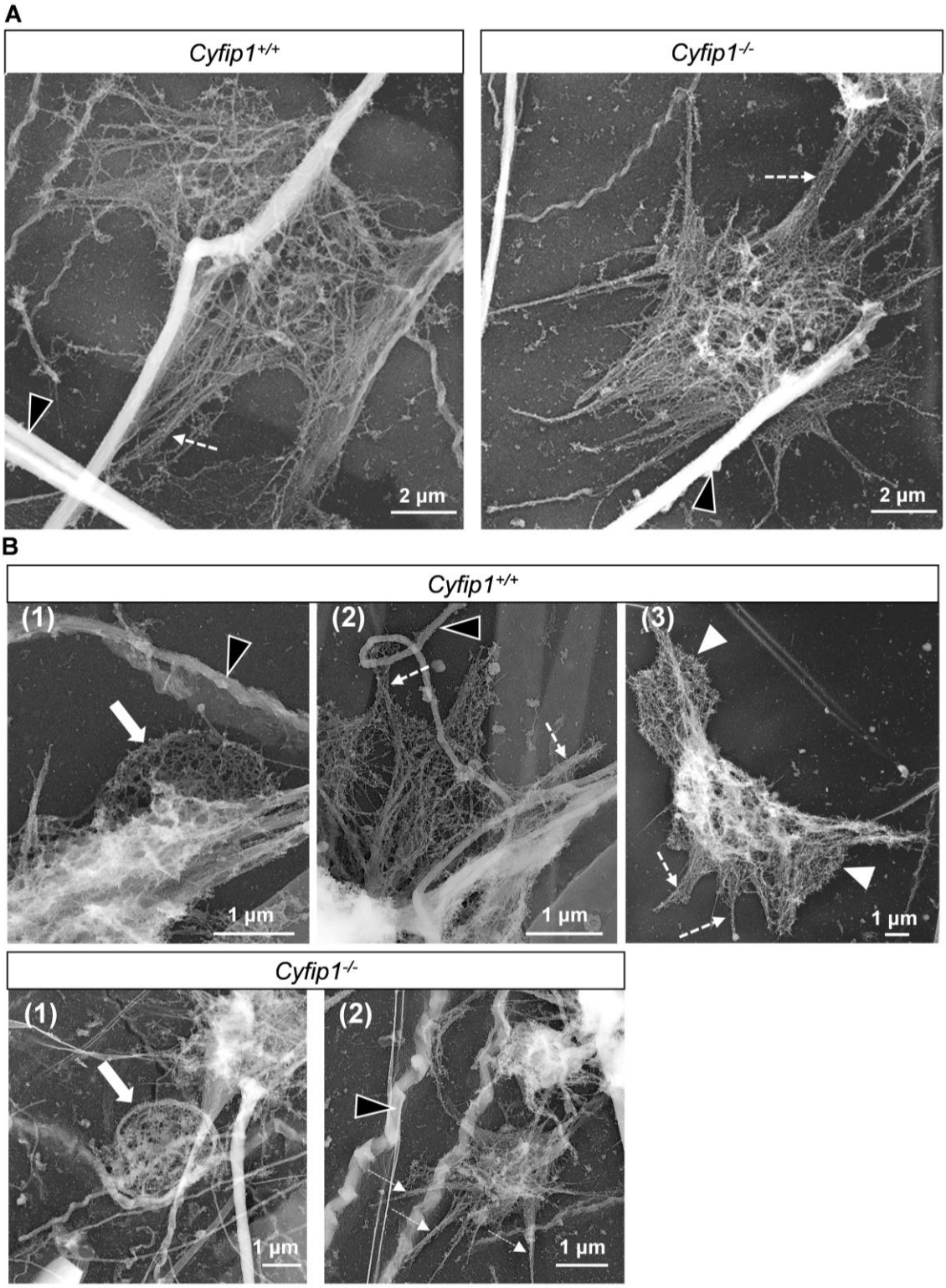

Figure 5.1.14: Platinum replica electron microscopy of platelets after experimentally-induced *ex vivo* thrombus formation on collagen. (A-B) Representative images of the platelet cytoskeleton after experimentally induced *ex vivo* thrombus formation on collagen. Different spreading phases of adherent platelets to collagen fibers are shown. (B) White arrow indicates unspread platelet; dashed white arrow indicates a filopodium with parallel actin filaments; white arrowhead indicates branched actin filaments; black arrowhead indicates collagen fibers. Scale bars: 1 µm. (1) = unspread, (2) = spread, parallel actin filaments, and (3) = spread, partially branched actin filaments.

5.1.5 *Cyfip1*$^{-/-}$ platelets can expose phosphatidylserine on the surface

A distinct population of highly activated platelets has been described residing close to collagen fibers and as patches around a thrombus *in vitro* and *in vivo*.[146,147] These platelets are characterized by surface-exposed phosphatidylserine (PS), which supports coagulation factor complex assembly, and hence is a key regulatory event in murine arterial thrombus formation.[146,147] To test whether *Cyfip1*$^{-/-}$ platelets can regulate coagulant activity, washed platelets were stimulated with ionomycin, a combination of CRP and thrombin or alone, and PS exposure was determined by Annexin V binding (Figure 5.1.15 A-B).

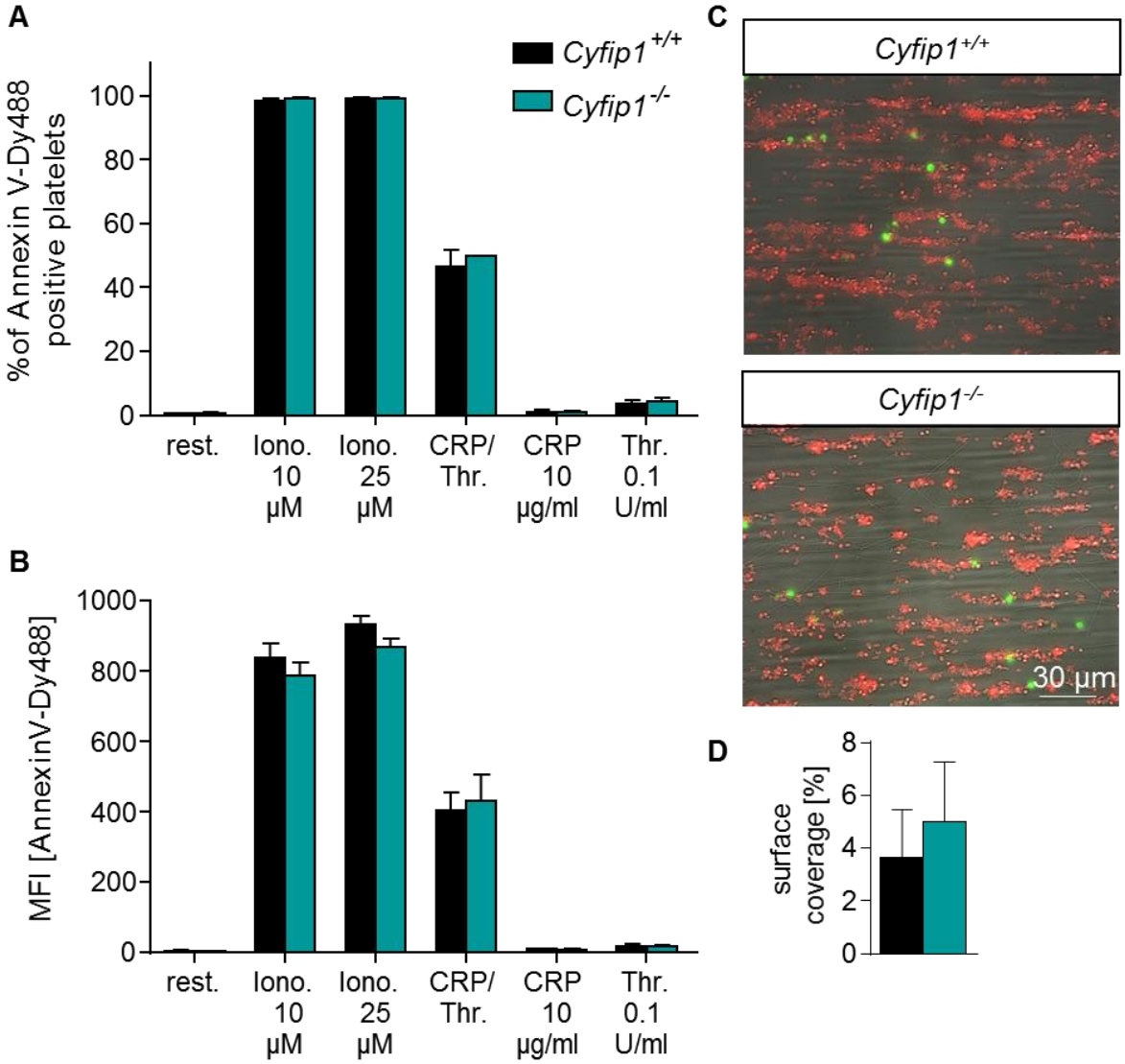

Figure 5.1.15: Cyfip1 knockout platelets have comparable procoagulant characteristics. Flow cytometric measurement of phosphatidylserine (PS) exposure by Annexin V binding. (A) Percentage of Annexin V-positive platelets and (B) respective mean

fluorescent intensity of Annexin V-positive platelets (n=5, representative for three independent experiments). (C) Representative images of *ex vivo* thrombus formation under high dose heparin at a shear rate of 1000 s^{-1}; All platelets were stained with the p0p6 anti-GPIX Alexa 647-conjugated antibody (red), PS-positive platelets (green) were stained with DyLight 488-conjugated Annexin V. (D) Determination of surface coverage of PS-positive platelets normalized to all adherent platelets (n=3, representative for three independent experiments).

While ionomycin efficiently induced PS exposure, platelets stimulated with CRP or thrombin alone could hardly bind Annexin V. The combination of CRP and thrombin induced PS exposure on more than 40 % of control and mutant platelets. Next, whole blood was perfused over immobilized collagen and the number and surface coverage of PS-positive collagen-adherent platelets were analyzed. The surface coverage of PS-positive platelets was comparable between control and mutant samples (Figure 5.1.15 C-D). These data show that platelets can regulate coagulant activity without the necessity to form lamellipodia.

5.1.6 Normal bleeding times, arterial thrombus formation and maintenance of vascular integrity in *Cyfip1*$^{-/-}$ mice

The relevance of lamellipodia structures for *in vivo* platelet function was analyzed in different hemostatic and thrombotic mouse models. Bleeding times after tail tip amputation were comparable between control and *Cyfip1*$^{-/-}$ mice (Figure 5.1.16 A). The application of 20 % ferric chloride ($FeCl_3$) on the exteriorized mesenteric arterioles of *Cyfip1*$^{-/-}$ mice resulted in comparable platelet adhesion, the appearance of first thrombi (Figure 5.1.16 B-C) and time to the formation of occlusive thrombi (Figure 5.1.16 D, Supplemental Videos 6 and 7).

Similarly, thrombus growth was studied in a second model of arterial thrombosis, in which the abdominal aorta is mechanically injured and blood flow is monitored by an ultrasonic perivascular Doppler flowmeter. In this model, thrombus formation and occlusion of the vessel in *Cyfip1*$^{-/-}$ mice occurred with similar kinetics as in controls (Figure 5.1.17 A-B).

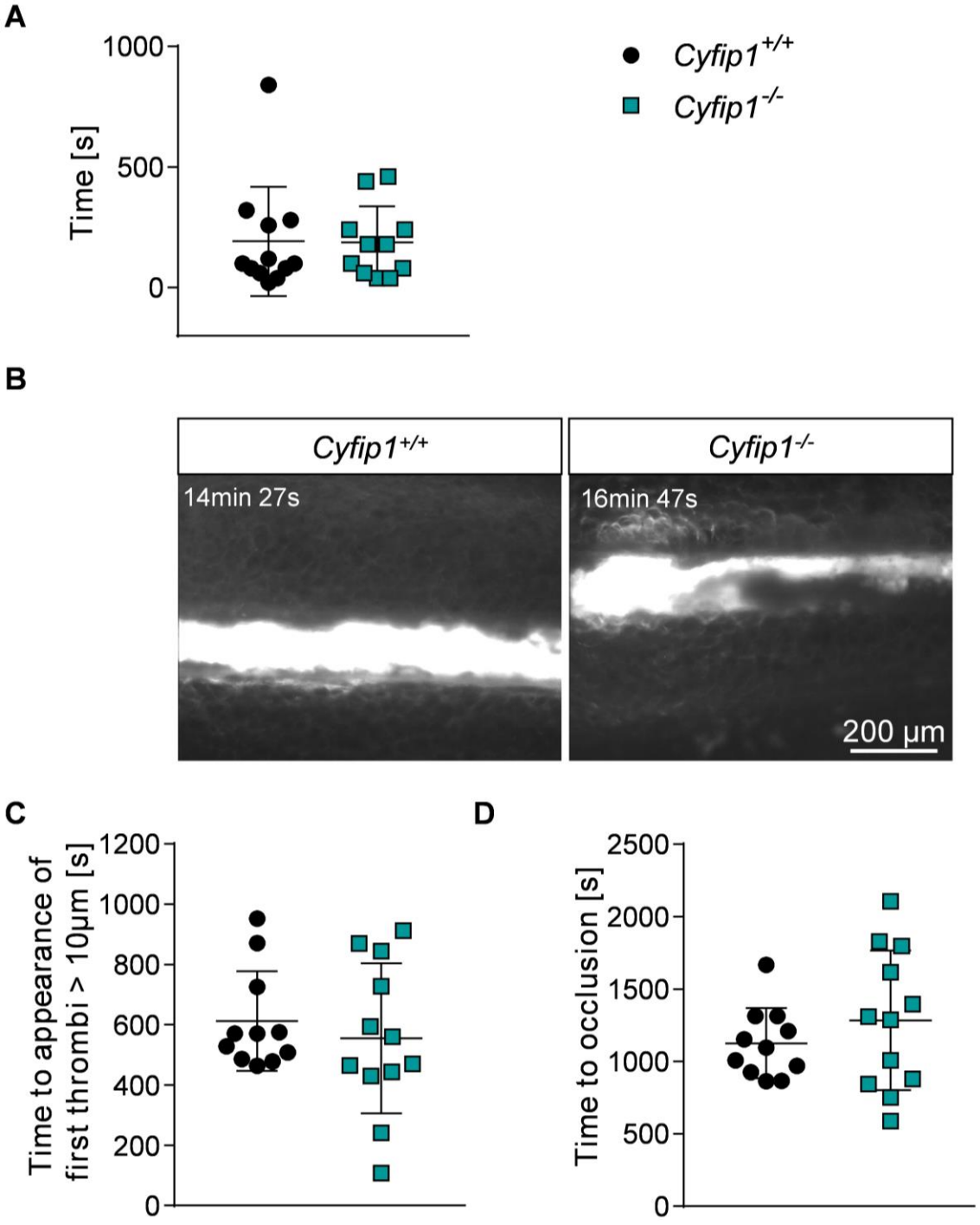

Figure 5.1.16: Lamellipodia formation is not required for hemostatic function and arterial thrombus formation. (A) A 2-mm segment of the tail tip was cut, and bleeding was determined to have ceased when no blood drop was observed on the filter paper. Each symbol represents one individual. (B) Mesenteric arterioles were treated with 20 % $FeCl_3$, and adhesion and thrombus formation of DyLight 488 anti-GPIX (p0p6) antibody labeled platelets were monitored by *in vivo* fluorescence microscopy. Representative images are shown. (C) Statistical evaluation of the time to appearance of a first thrombus and (D) time to occlusion.

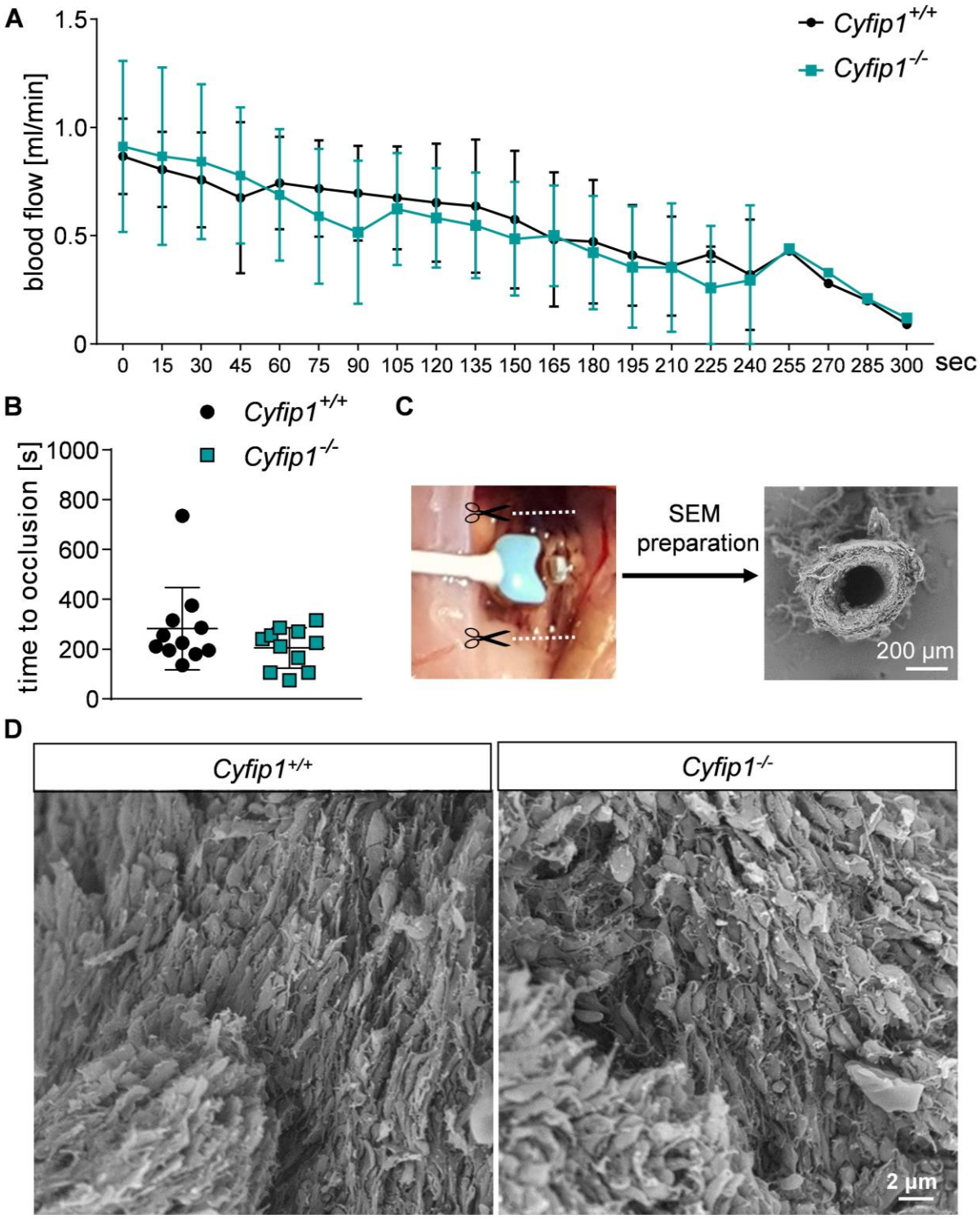

Figure 5.1.17: Occlusive thrombus formation in mice. The abdominal aorta was mechanically injured using forceps (compression for 15 s), and blood flow was monitored. (A) Representative curve values and mean +/- s.d are shown. (B) Time to occlusion after mechanical injury. Each symbol represents one individual; Mean +/- s.d. (C) Isolation of aorta and preparation for scanning electron microscopy (SEM) is shown. (D) SEM of an *in vivo* formed thrombus. (n=4)

Finally, the aorta was isolated and the shape of single platelets in the experimentally-induced *in vivo* thrombus was analyzed (Figure 5.1.17 C-D). Again, platelets with lamellipodia could not be observed, instead, platelets which formed filopodia were found. This shows that lamellipodia structures are not required for the classical formation of a hemostatic plug or a pathological thrombus *in vivo*.

It has been reported that inflammation represents an unconventional hemostatic situation in which individual platelets are sufficient to prevent bleeding.[148] To test whether platelet lamellipodia structures play a role in this process, mice were challenged in two different models, namely the reverse passive Arthus reaction (intravenous injection of antigen, followed by intradermal injection of antibody) and LPS-induced lung inflammation. As expected, when platelets were depleted in mice by injection of an anti-GPIbα antibody, severe inflammatory bleeding in the skin (Figure 5.1.18 A-B) and into the lung (Figure 5.1.18 C-D) was observed, demonstrating the importance of platelets to maintain vascular integrity as reported previously.[149] Finally, control and *Cyfip1*$^{-/-}$ mice were subjected to the reverse passive Arthus reaction of the skin and LPS-induced lung inflammation. *Cyfip1*$^{-/-}$ mice did not show signs of bleeding in these experimental settings, suggesting that platelet lamellipodia formation is dispensable for maintaining vascular integrity at sites of acute inflammation (Figure 5.1.18 A-D).

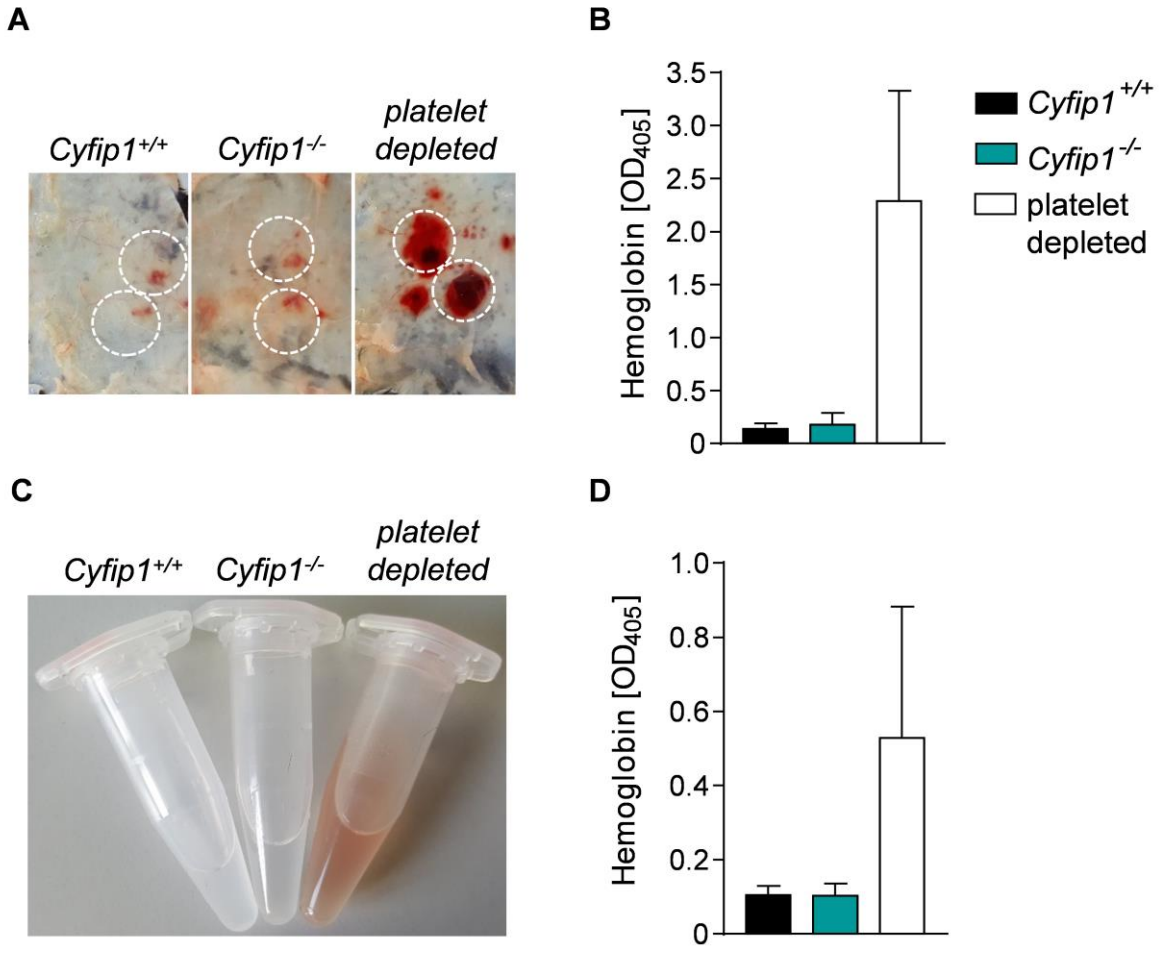

Figure 5.1.18: Maintenance of vascular integrity in *Cyfip1*$^{-/-}$ mice. (A) Mice were subjected to the reverse passive Arthus reaction to induce local skin inflammation and representative images are shown. (B) Hemoglobin content in tissue punch biopsies from inflammatory spots was quantified (n=4, representative for three independent experiments). (C) Representative images of bronchoalveolar lavage liquid at 4 hours after LPS application. (D) Quantification of the hemoglobin content in bronchoalveolar lavage liquid. Platelet depleted animals served as a positive control of inflammatory bleeding in both models (n=5, representative for three independent experiments).

5.2 WASH complex subunit Strumpellin regulates αIIbβ3 surface expression

5.2.1 Strumpellin-deficiency decreases the protein abundance of the WASH protein in platelets

It was shown in mice, that the WASH subunit Strumpellin is necessary for the survival of very early embryonic stages and for the attachment of blastocyst to the epithelial lining of the maternal uterus.[92] Due to this, megakaryocyte- and platelet-specific Strumpellin-deficient mice (*Strumpellin*$^{fl/fl,\ Pf4\text{-}Cre}$ further referred to as *Strumpellin*$^{-/-}$) and the respective littermate controls (*Strumpellin*$^{fl/fl}$ further referred to as *Strumpellin*$^{+/+}$) were studied.

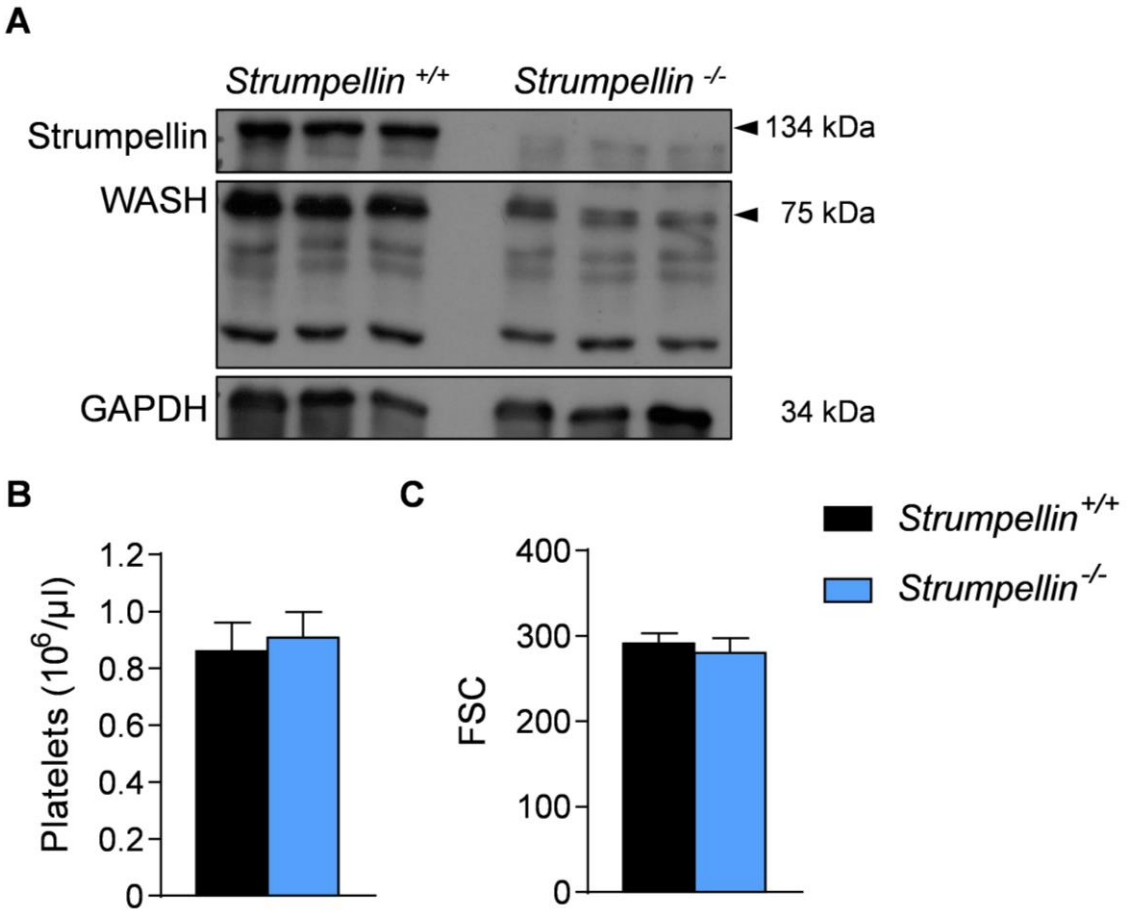

Figure 5.2.1: Strumpellin deficiency affects the protein abundance of the WASH protein in resting platelets (A) Expression of Strumpellin and WASH protein in platelets was assessed by Western blot analysis. GAPDH served as a loading control (n=3). (B) Platelet count per µl and (C) platelet size, given as forward scatter (FSC), was determined via flow cytometry (n=6, representative for four independent experiments). Values are mean ± s.d.

Strumpellin$^{-/-}$ mice were viable, fertile, and born at normal Mendelian ratio (data not shown). The absence of Strumpellin in mutant platelets was confirmed by Western blot analysis (Figure 5.2.1 A). The WASH complex comprises five proteins: KIAA1033 (also known as SWIP), Strumpellin, FAM21, WASH1, and CCDC53.[93,150] In line with previous data in mammalian cells, in which RNA interference (RNAi)-mediated silencing of individual WASH complex subunits resulted in instability and degradation of other WASH complex components,[93,94,106] a decreased expression of the WASH protein (75 kDa) in Strumpellin-deficient platelets (Figure 5.2.1 A) was found. The anti-WASH antibody also detected several unspecific bands below 75 kDa which remained unaltered between control and Strumpellin-deficient platelet samples. Count and size of platelets and other blood cells was comparable between *Strumpellin*$^{+/+}$ and *Strumpellin*$^{-/-}$ mice as determined by flow cytometry and a hematology analyzer (Figure 5.2.1 B-C and Table 5.2.1)

Table 5.2.1: Unaltered blood count parameters in Strumpellin-deficient mice. Blood count parameters as measured in a Hemavet hematology analyzer (n=6, representative for three independent experiments).

	***Strumpellin*$^{+/+}$**	***Strumpellin*$^{-/-}$**	**Sign.**
Platelet Count [10^3/µl]	701 ± 40	702 ± 72	n.s.
Mean Platelet Volume [fl]	4.9 ± 0.10	4.9 ± 0.15	n.s.
White Blood Cells [10^3/µl]	5.8 ± 1.4	7.9 ± 1.3	n.s.
Neutrophils [10^3/µl]	0.71 ± 0.07	0.93 ± 0.25	n.s.
Lymphocytes [10^3/µl]	4.8 ± 1.27	6.6 ± 1.3	n.s.
Monocytes [10^3/µl]	0.34 ± 0.06	0.37 ± 0.14	n.s.
Eosinophils [10^3/µl]	0.0 ± 0.0	0.0 ± 0.0	n.s.
Red Blood Cells [10^6/µl]	10.6 ± 0.48	10.4 ± 0.18	n.s.
Hemoglobin [g/dl]	14.3 ± 0.40	14.0 ± 0.42	n.s.
Hematocrit [%]	42.9 ± 1.25	42.5 ± 1.28	n.s.
Mean Corpuscular Volume [fl]	40.3 ± 1.18	40.7 ± 0.58	n.s.
Mean Corpuscular Hemoglobin [pg]	13.4 ± 0.23	13.4 ± 0.21	n.s.
Mean Corpuscular Hemoglobin Concentration [g/dl]	33.4 ± 0.80	33.0 ± 0.10	n.s.
Red Blood Cell Distribution Width [%]	17.43 ± 0.06	17.47 ± 0.46	n.s.

5.2.2 Decreased αIIbβ3 integrin expression in Strumpellin-deficient platelets and megakaryocytes

The surface expression of major glycoproteins present on platelets was determined by flow cytometry assay employing specific FITC-labeled antibodies. Strumpellin-deficient platelets displayed a prominent 20 % decreased integrin αIIbβ3 surface expression and a slightly increased GPVI, β1 and CLEC-2 surface expression in resting conditions (Table 5.2.2).

	***Strumpellin*$^{+/+}$**	***Strumpellin*$^{-/-}$**	**Sign.**
GPIb	326±13.4	314±5.2	n.s.
GPIX	381±16.7	394±8.4	n.s.
GPV	426±40.5	401±13.3	n.s.
CD9	818±37.1	822±32.8	n.s.
GPVI	37±2.0	45±1.1	**
αIIbβ3 (JON6)	483±27.2	405±17.3	***
α2	45±2.2	45±1.8	n.s.
β1	171±4.3	179±5.1	*
CLEC-2	112±2.9	118±2.4	**

Table 5.2.2 Decreased αIIbβ3 surface expression in *Strumpellin*$^{-/-}$ platelets. Diluted whole blood was incubated with FITC-labelled antibodies and measured as mean fluorescence intensity (MFI) by flow cytometry; (n = 6, representative for three independent experiments); **P*<0.05, ***P*<0.01, ****P*<0.001.

The decrease in αIIbβ3 surface expression was further confirmed by various anti-αIIbβ3 antibodies and one anti-β3 antibody (Figure 5.2.2 A). The histogram of the αIIbβ3 flow cytometric assay was further analyzed to figure out whether the whole platelet population displays a decreased αIIbβ3 expression or only a platelet subpopulation showed a severely decreased αIIbβ3 expression. The whole histogram of the Strumpellin-deficient platelet population (Figure 5.2.2 B-C) was shifted to the left, suggesting that the αIIbβ3 expression on every single platelet is 20 % decreased.

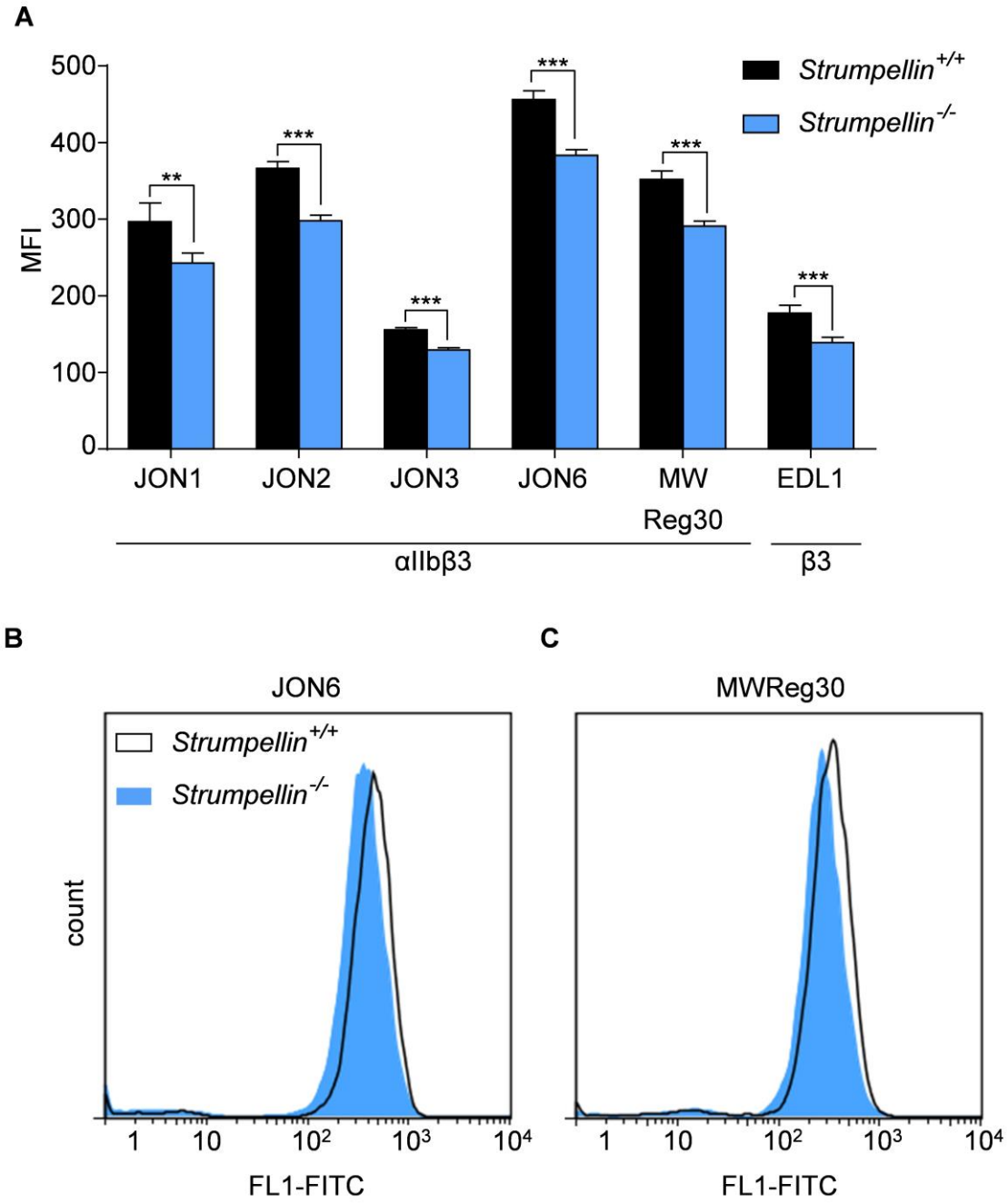

Figure 5.2.2: Decreased αIIbβ3 surface expression on *Strumpellin*$^{-/-}$ platelets. (A) Diluted whole blood was incubated with various anti-αIIbβ3 FITC-labelled antibodies and one anti-β3 antibody and mean fluorescence intensity (MFI) was determined by flow cytometry (n = 5). (B-C) Histogram of platelet population of the respective flow cytometric measurement performed in A, depicted for two different anti-αIIbβ3 FITC-labelled antibodies (B) JON6 and (C) MWReg30. ***P*<0.01, ****P*<0.001.

Further, megakaryocytes in the bone marrow of Strumpellin-deficient mice were investigated. Localization, number (pictures and statistical analysis, see doctoral thesis of Lucy Reil, which is in preparation) as well as ploidy of bone marrow megakaryocytes

was unaltered (Figure 5.2.3 A). The structure and size of the spleen appeared normal, and the number of megakaryocytes was comparable between control and mutant mice (pictures and statistical analysis, see doctoral thesis of Lucy Reil, which is in preparation). Additionally, the bone marrow derived megakaryocytes of mutant mice also displayed a 20 % decreased αIIbβ3 surface expression, which is in line with the results of the surface expression of αIIbβ3 in Strumpellin-deficient platelets (Figure 5.2.3 B).

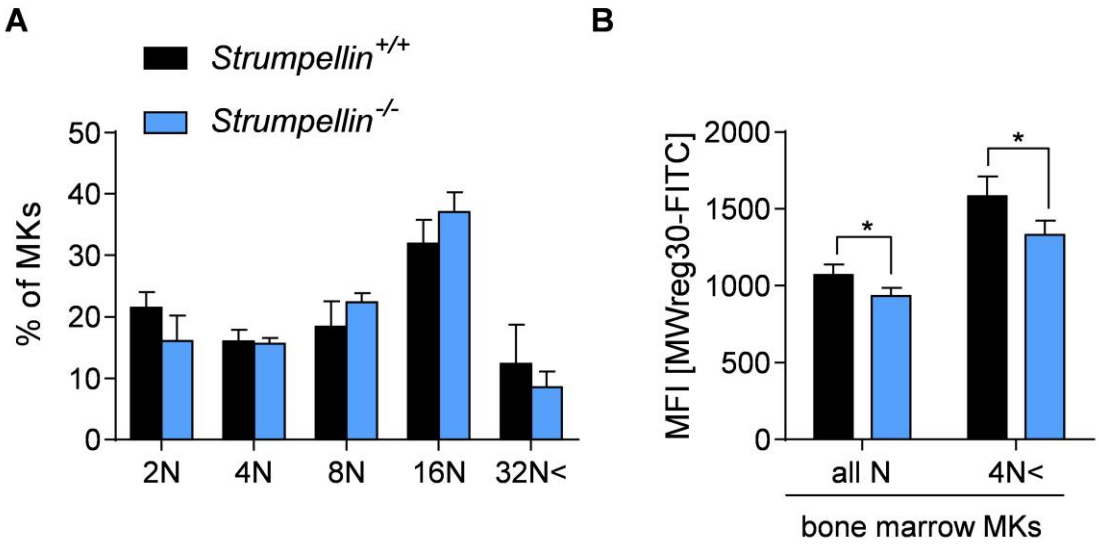

Figure 5.2.3: Ploidy and αIIbβ3 surface expression of Strumpellin-deficient megakaryocytes. The membrane of freshly isolated bone marrow megakaryocytes was stained with an anti-αIIbβ3 antibody (MWReg30) and after fixation and permeabilization the DNA was stained with propidium iodide. (A) Ploidy and (B) αIIbβ3-surface expression was assessed by flow cytometry (n = 3, representative for three independent experiments); **P*<0.05.

5.2.3 Decreased αIIbβ3 integrin activation of Strumpellin-deficient platelets after stimulation with different agonists

Endocytosis in megakaryocytes and platelets, such as the uptake of fibrinogen from plasma by αIIbβ3 integrin, is crucial for the loading of granules and thus for platelet effector function. Strumpellin-deficient platelets showed, in addition to the already decreased αIIbβ3 surface expression under resting conditions, decreased αIIbβ3 integrin activation after stimulation with different agonists (Figure 5.2.4). The active form of αIIbβ3 was measured by a specific PE-coupled anti-αIIbβ3 antibody (Figure 5.2.4), whereas the general αIIbβ3 expression that includes active and inactive αIIbβ3 was measured by FITC-labelled anti-αIIbβ3 antibody after platelet activation with different agonists (Figure 5.2.5 A-B). After platelet activation, the additional exposure of the internal pool of αIIbβ3 was not sufficient to compensate for the decreased surface exposure in resting platelets (Figure 5.2.5 A-B). These results were confirmed by the permeabilization of resting platelets and subsequent αIIbβ3 staining (Figure 5.2.5 C).

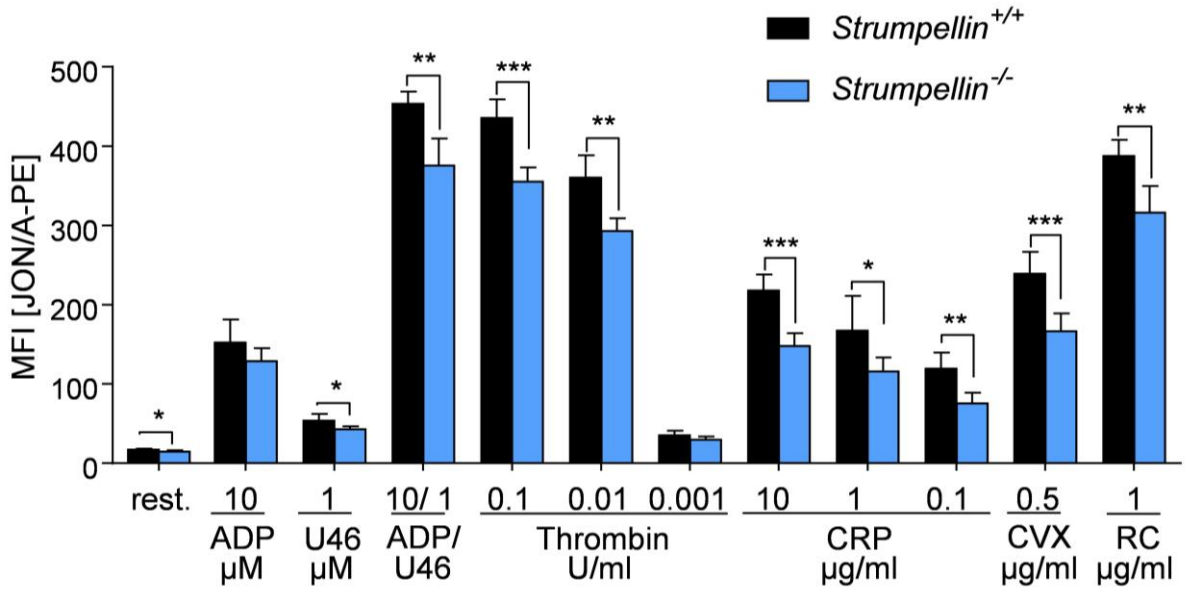

Figure 5.2.4 Reduced αIIbβ3 integrin activation of *Strumpellin*$^{-/-}$ platelets: Flow cytometric determination of inside-out activation of the αIIbβ3 integrin (JON/A-PE antibody) in response to the agonists ADP, U46619 (thromboxane A2 analogue), thrombin (Thr), collagen related peptide (CRP), convulxin (CVX) and rhodocytin (RC). (n=5, representative for three independent experiments); values are mean ± s.d. ***P*<0.01, ****P*<0.001.

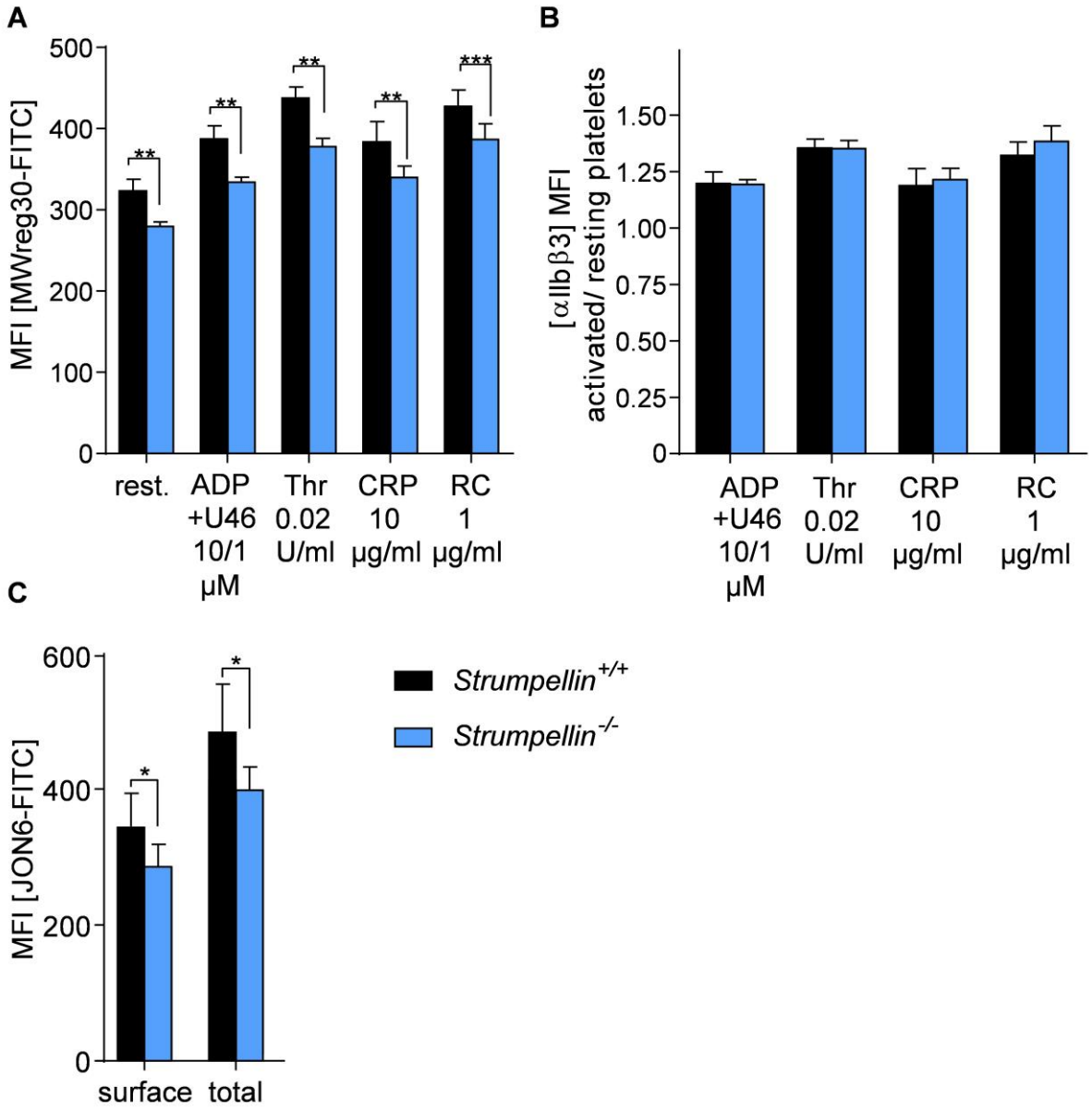

Figure 5.2.5: The total pool of αIIbβ3 in *Strumpellin*$^{-/-}$ platelets is 20 % decreased. (A) Flow cytometric determination of overall (active and inactive) αIIbβ3 surface expression after platelet activation (JON6-FITC antibody) with the agonists ADP and U46, thrombin (Thr), collagen related peptide (CRP) and rhodocytin (RC). (B) The ratio of αIIbβ3 surface expression in activated to resting platelets (n=5). (C) αIIbβ3 surface expression and total abundance measured after platelet permeabilization. Values are mean ± s.d. **P*<0.05 ***P*<0.01, ****P*<0.001.

Further, the functionality of the αIIbβ3 integrin was tested in a fibrinogen binding assay (Figure 5.2.6 A). Although the fibrinogen binding to αIIbβ3 was moderately reduced, probably due to the already decreased αIIbβ3 surface exposure, the uptake of fibrinogen into resting platelets was, despite a delay within the first 5 min, comparable to control platelets after 30 min of incubation (Figure 5.2.6 B). This result was further

confirmed by western blot analysis (data not shown, see doctoral thesis of Lucy Reil, which is in preparation). In addition, normal platelet spreading (quantification see doctoral thesis of Lucy Reil) suggests unaltered functionality of the αIIbβ3 integrin (Figure 5.2.6 C).

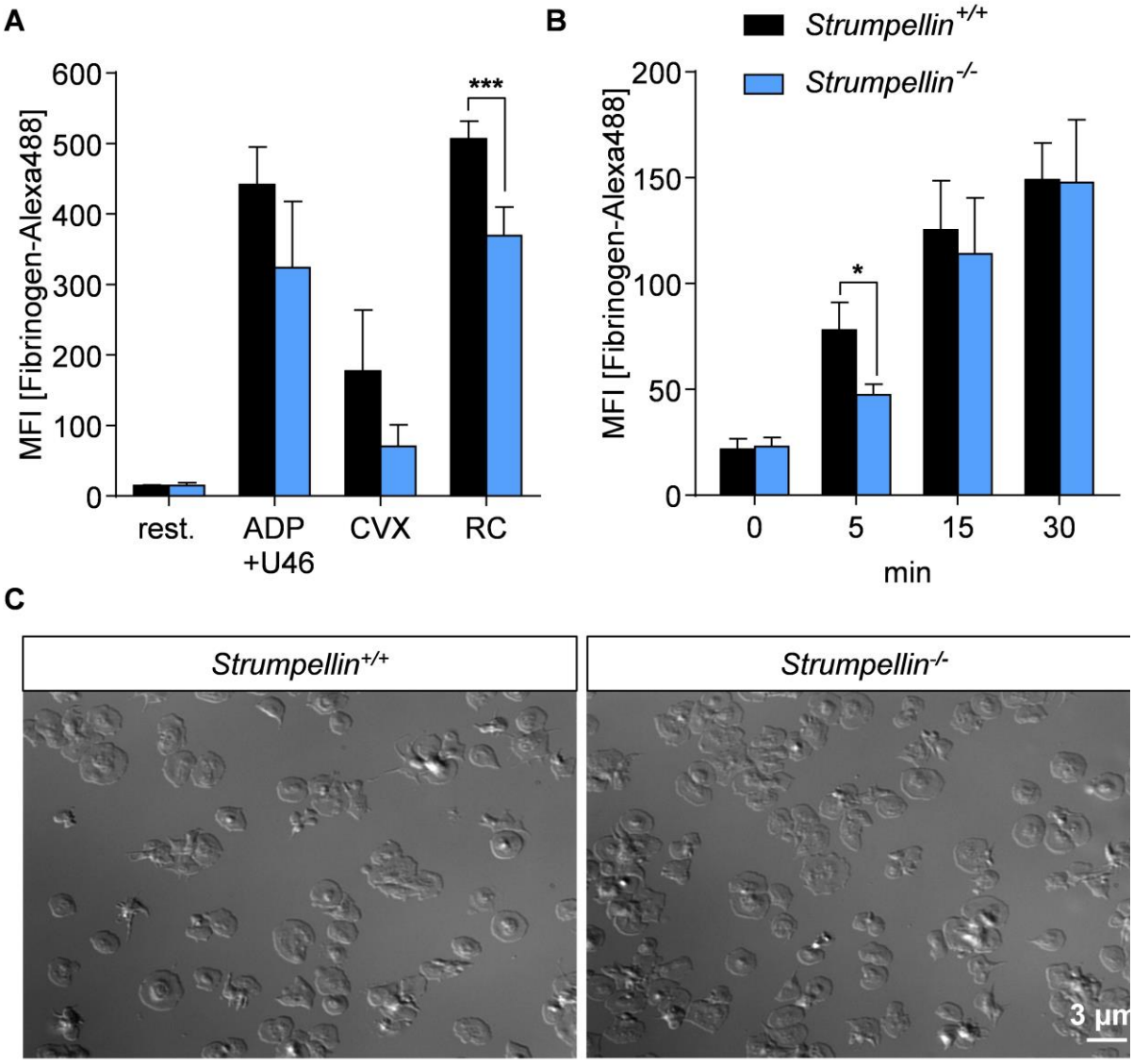

Figure 5.2.6: Fibrinogen-based αIIbβ3 integrin functionality in *Strumpellin*$^{-/-}$ platelets. (A) Fibrinogen binding to αIIbβ3 integrin was assessed by incubation of washed platelets with Alexa-488 coupled fibrinogen under resting and activated conditions using the agonists ADP (10 µM) and U46619 (U46; 1 µM; thromboxane A2 analogue), convulxin (0.5 µg/ml; CVX) and rhodocytin (1 µg/ml; RC), followed by flow cytometric analysis. (B) Washed platelets were incubated with Alexa-488 coupled fibrinogen. After respective time points, cells were fixed with 2 % PFA and extracellular bound fibrinogen signal was quenched by 5 min incubation with 0.5 % trypan blue, before flow cytometric analysis. (C) Platelets were activated with 0.01 U/ml thrombin and spread on a fibrinogen coated surface for 30 min at 37°C. Values are mean ± s.d. **P*<0.05 ***P*<0.01, ****P*<0.001.

5.2.4 Unaltered P-selectin exposure in response to various agonists in Strumpellin-deficient platelets

The WASH complex was shown to be involved in endosomal trafficking and endosomal tubulation processes.[91] Knockout of the WASH subunit in fibroblasts results in enlarged and collapsed endosomes as well as a loss in lysosomal compartment integrity, that resulted in impaired trafficking of the epidermal growth factor receptor and the transferrin receptor. While most of the membrane proteins stored in α-granules, such as CD9 and the integrin subunits αIIb, β3 and α6, are already prominently present on the platelet surface under resting conditions, P-selectin is not present before platelet activation.[21,22] This allows the use of P-selectin surface expression as a marker for platelet α-granule secretion. To investigate if Strumpellin-deficiency affects P-selectin exposure, platelets were activated with different GPCR, GPVI and C-type lectin-like receptor 2 (CLEC-2)-dependent agonists. P-selectin surface exposure after activation (Figure 5.2.7 A) and the total concentration (Figure 5.2.7 B) of P-selectin in control and Strumpellin-deficient platelets was mainly unaltered. Only after activation with rhodocytin the P-selectin exposure was slightly decreased. This suggests an overall unaltered α-granule release upon loss of Strumpellin in platelets.

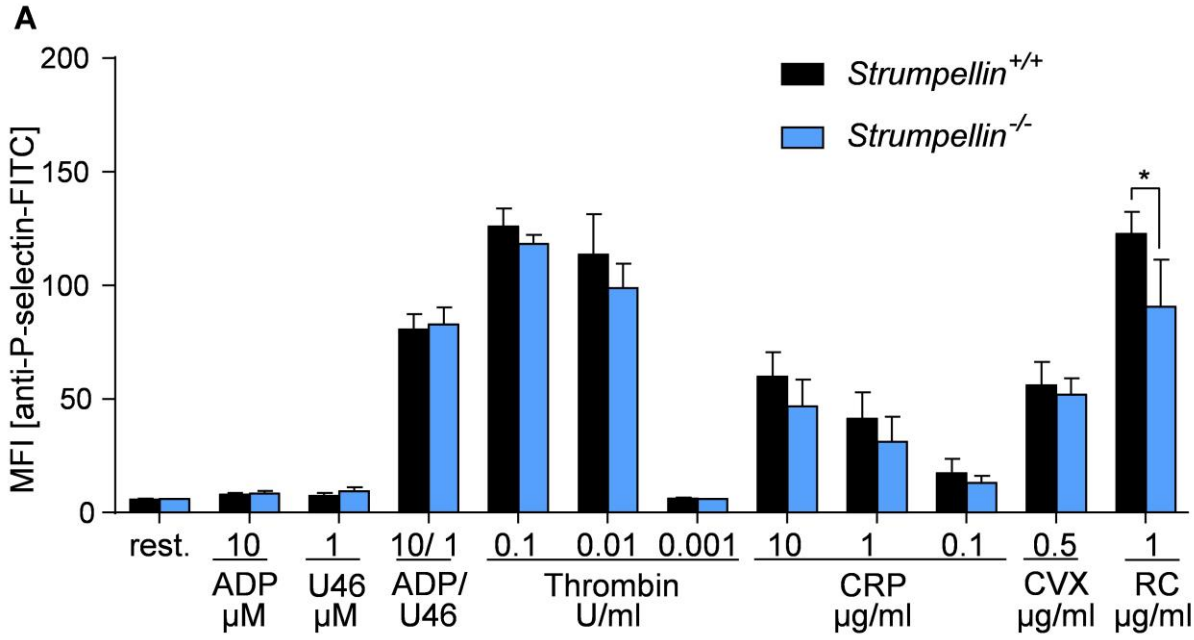

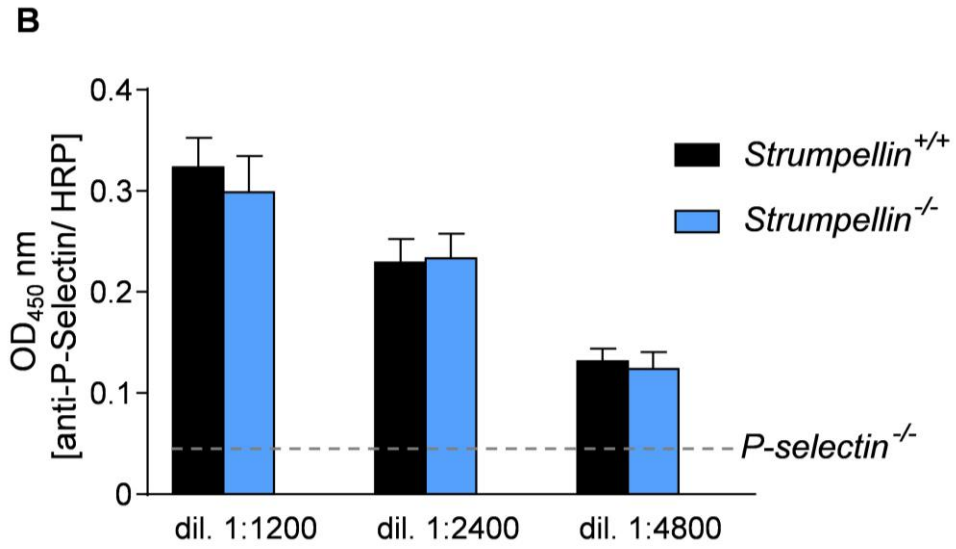

Figure 5.2.7: Unaltered P-selectin exposure of *Strumpellin*$^{-/-}$ platelets in response to GPCR, GPVI and CLEC-2-dependent agonists. (A) Degranulation dependent P-selectin exposure using a FITC-labelled anti-P-selectin antibody (n = 5, representative for three independent experiments) in response to indicated agonists ADP, U46619 (thromboxane A2 analogue), thrombin (Thr), collagen related peptide (CRP), convulxin (CVX) and rhodocytin (RC) were determined by flow cytometry. (B) Quantitative P-selectin enzyme-linked immunosorbent assay (ELISA). The concentration of P-selectin in control and *Strumpellin*$^{-/-}$ platelet lysates was determined using a commercial ELISA kit. Results for different lysate dilutions (1:1200-1:4800) were detected using a biotinylated anti-mouse P-Selectin antibody and HRP-conjugated streptavidin. Platelet lysate from one P-selectin-deficient mouse was used as a negative control (indicated as dotted line). (n = 6, representative for three independent experiments). Values are mean ± s.d. **P*<0.05 ***P*<0.01.

5.2.5 Strumpellin deficiency does not affect actin or microtubule polymerization in platelets

The WASH complex generates Arp2/3 complex dependent branched actin networks at the endosomal surface.[97] To investigate if the decrease of the Arp2/3 nucleation-promoting factor WASH and the loss of the Strumpellin-subunit affect the general assembly of actin, resting and activated platelets were stained with phalloidin-FITC and analyzed by flow cytometry. Upon platelet activation, the amount of F-actin increased in WT and *Strumpellin*$^{-/-}$ platelets to a similar extent (Figure 5.2.8 A-B). This indicates that the loss of Strumpellin does not impair F-actin assembly. The formation of WASH-dependent endosomal tubules proceeds in tight coordination with microtubules and microtubule motors.[97] The capacity of microtubules to dis- or reassemble in the absence of Strumpellin was analysed by incubation of platelets for 3 h at different temperatures and subsequent staining for F-actin and α-tubulin (Figure 5.2.8 C). At 37°C resting platelets have a well-organized marginal band with multiple

microtubules, which is depolymerized upon cold-induced incubation at 4°C. The repolymerization of the marginal band can be induced by changing the temperature of incubated platelets from 4°C back to 37°C after 3 hours of incubation. Despite the lack of Strumpellin, the dis- and reassembly of microtubules was comparable to control platelets.

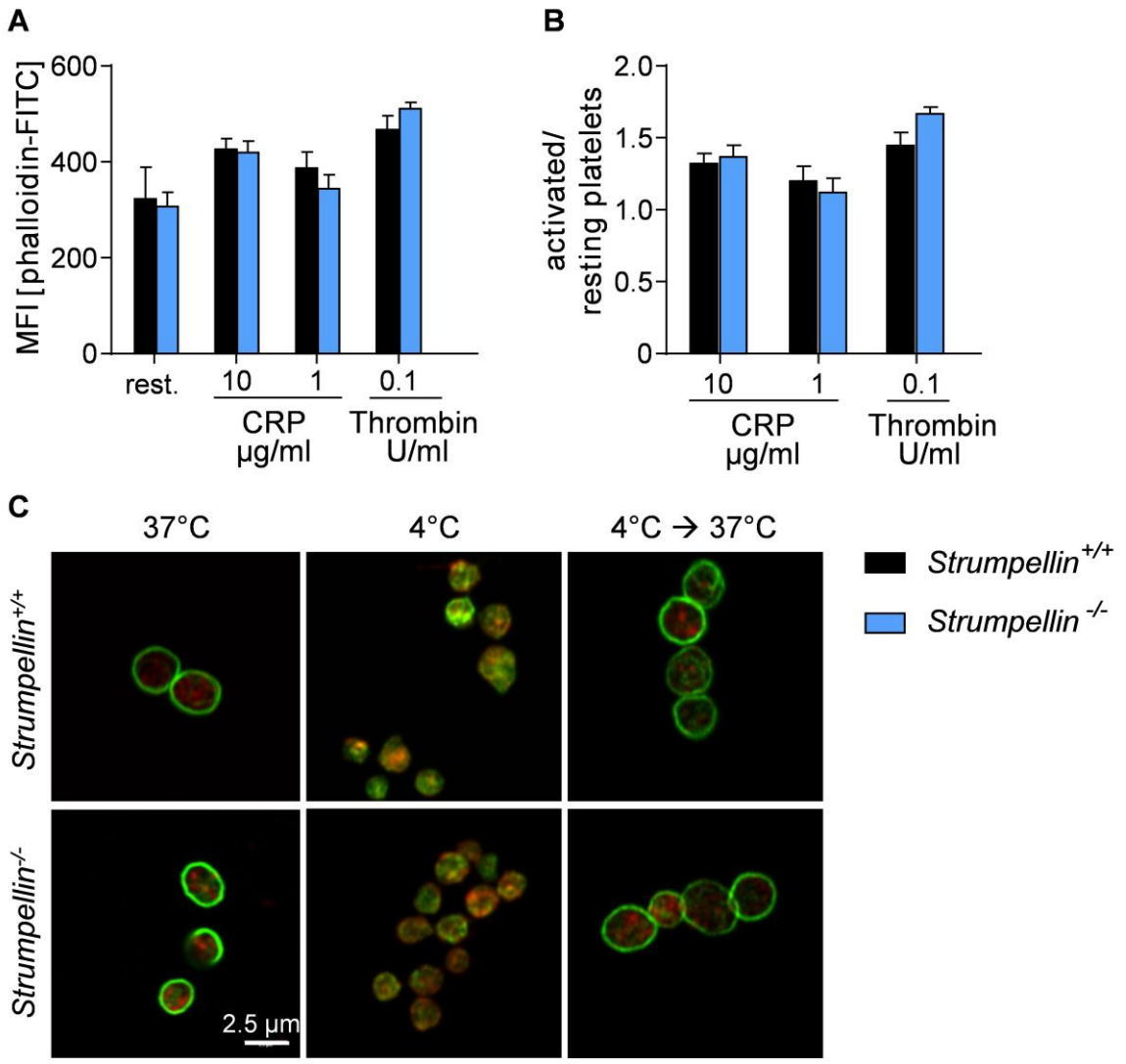

Figure 5.2.8 Lack of Strumpellin does not affect actin or microtubule dynamics. (A) Resting or either CRP- or thrombin-activated platelets were fixed, permeabilized, stained with phalloidin-FITC, and analysed by flow cytometry. (B) The ratio of polymerized actin in activated vs. resting platelets was determined (n = 3, representative for two independent experiments). (C) Representative confocal microscopy images of immunostained resting platelets on poly-L-lysine (PLL). Washed platelets were fixed either after 3.5 h at 37°C (resting), after 3.5 h at 4°C (disassembly) or after 3.5 h at 4°C followed by 30 min at 37°C (reassembly). *Strumpellin*$^{+/+}$ and *Strumpellin*$^{-/-}$ platelets were stained for F-actin (red) and α-tubulin (green). (n = 5).

5.2.6 Strumpellin deficiency does not affect thrombus formation and hemostasis

To investigate if the decreased αIIbβ3 surface expression in Strumpellin-deficient platelets impairs the thrombus formation under flow conditions, platelet adhesion on collagen in a whole-blood perfusion assay at shear rates of 1000 s^{-1} was studied. Control and mutant platelets rapidly adhered to collagen and consistently formed stable 3-dimensional thrombi (Figure 5.2.9 A). Although Strumpellin-deficient platelets display a decreased αIIbβ3 surface expression, the surface coverage and thrombus volume were comparable between blood from *Strumpellin*$^{+/+}$ and *Strumpellin*$^{-/-}$ mice (Figure 5.2.9 B). In addition, comparable bleeding times were measured for control and mutant mice, indicating that Strumpellin is not required to maintain the hemostatic function (Figure 5.2.9 C). Taken together, these data indicate that 20% decreased integrin surface expression does not impair platelet adhesion and that Strumpellin is dispensable for thrombus formation and hemostasis.

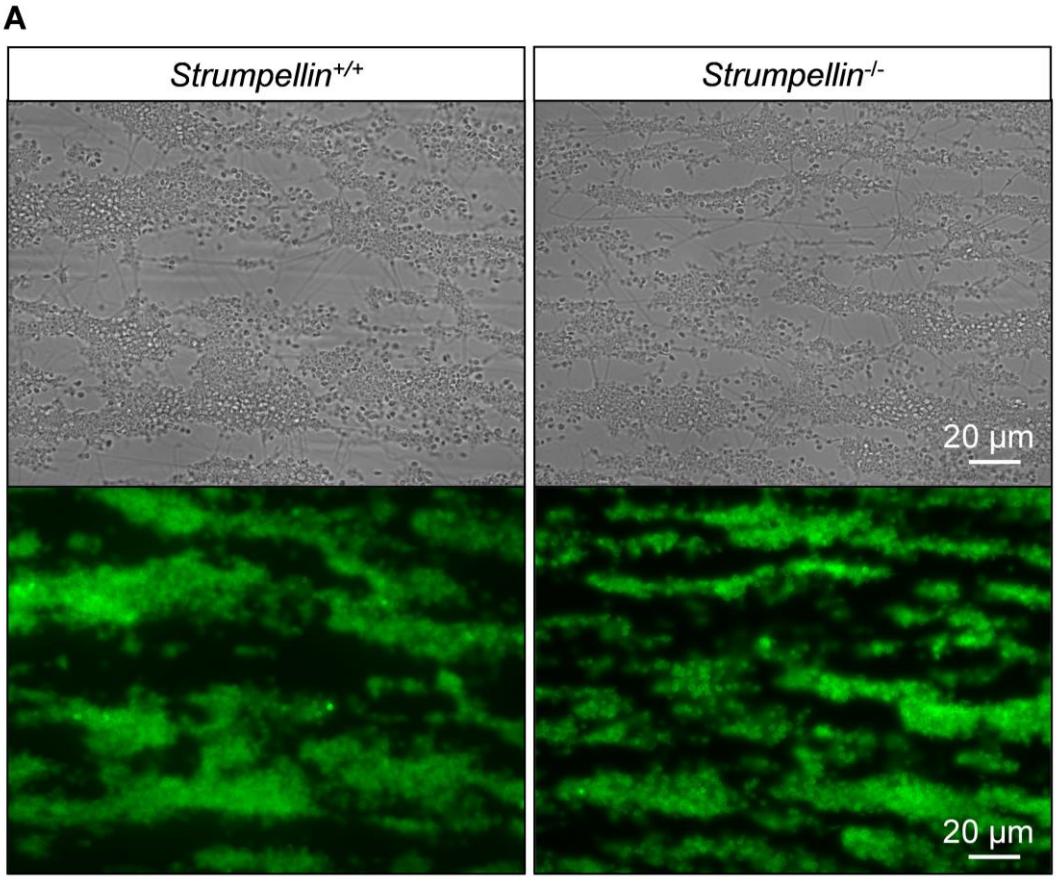

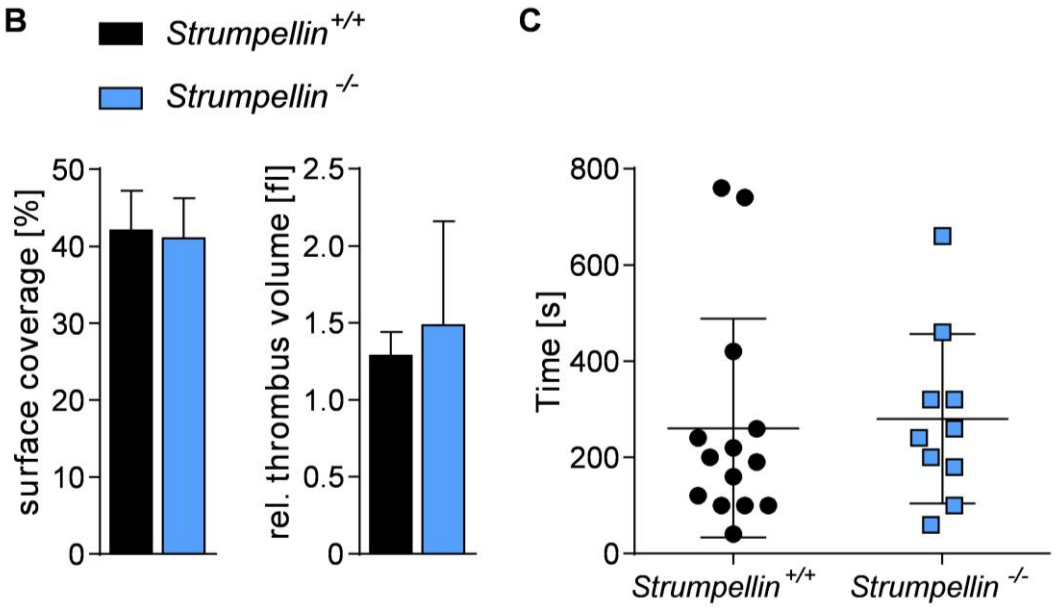

Figure 5.2.9: Strumpellin deficiency does not affect *ex vivo* thrombus formation and tail bleeding time. (A) Thrombus formation was assessed on collagen at a wall shear rate of 1000 s^{-1}. Shown are representative bright-field (upper panel) and fluorescence (lower panel) pictures of platelets stained with a Dylight-488 anti-GPIX antibody. (n = 5, representative for one independent experiment). (B) Surface coverage and relative thrombus volume were quantified according to fluorescence distribution and intensity, respectively. (C) Determination of tail bleeding time of *Strumpellin*$^{+/+}$ and *Strumpellin*$^{-/-}$ mice was performed on filter paper.

5.3 The cytoskeletal crosslinking protein MACF1 is dispensable for thrombus formation and hemostasis

5.3.1 MACF1 deficiency does not affect platelet count, size and other blood parameters

Due to embryonic lethality of constitutive MACF1-deficient mice on day 11.5 (E11.5),[125] megakaryocyte- and platelet-specific knockout mice (*Macf1*$^{fl/fl,\ Pf4\text{-}Cre}$ further referred to as *Macf1*$^{-/-}$) and the respective littermate controls (*Macf1*$^{fl/fl}$ further referred to as *Macf1*$^{+/+}$*)* were studied. *Macf1*$^{-/-}$ mice were viable, fertile and born at normal Mendelian ratio (data not shown). Absence of MACF1 in mutant megakaryocytes and platelets was confirmed by Western blot analysis with two different antibodies, whereas two specific MACF1 bands, conferring to the isoforms MACF1a1-3 (500-620 kDa) and MACF1b (800 kDa), were detectable in lysates of control samples (Figure 5.3.1 A-B).[122,151]

The localization of MACF1 in resting platelets on poly-L-lysine was investigated and immunostainings revealed a ring-shaped expression of MACF1 close to the membrane and only a weak localization in the platelet cytoplasm (Figure 5.3.1 C).[126] This result indicates that MACF1 might crosslink microtubules and F-actin at the platelet membrane. In contrast, MACF1-deficient platelets showed no MACF1 expression, confirming the results obtained by Western blot analysis (Figure 5.3.1 A-B). Further staining with an anti-rabbit-IgG antibody serving as staining control also showed no unspecific binding of the secondary Cy3-conjugated (Jackson Immuno #711-165-153) antibody.

The count of platelets and other blood cells was comparable between *Macf1*$^{+/+}$ and *Macf1*$^{-/-}$ mice as determined by flow cytometry and a hematology analyzer (Figure 5.3.2 A-B and Table 5.3.1). Platelet shape and ultrastructure were unaltered in *Macf1*$^{-/-}$ mice, as confirmed by transmission electron microscopy (Figure 5.3.2 C).

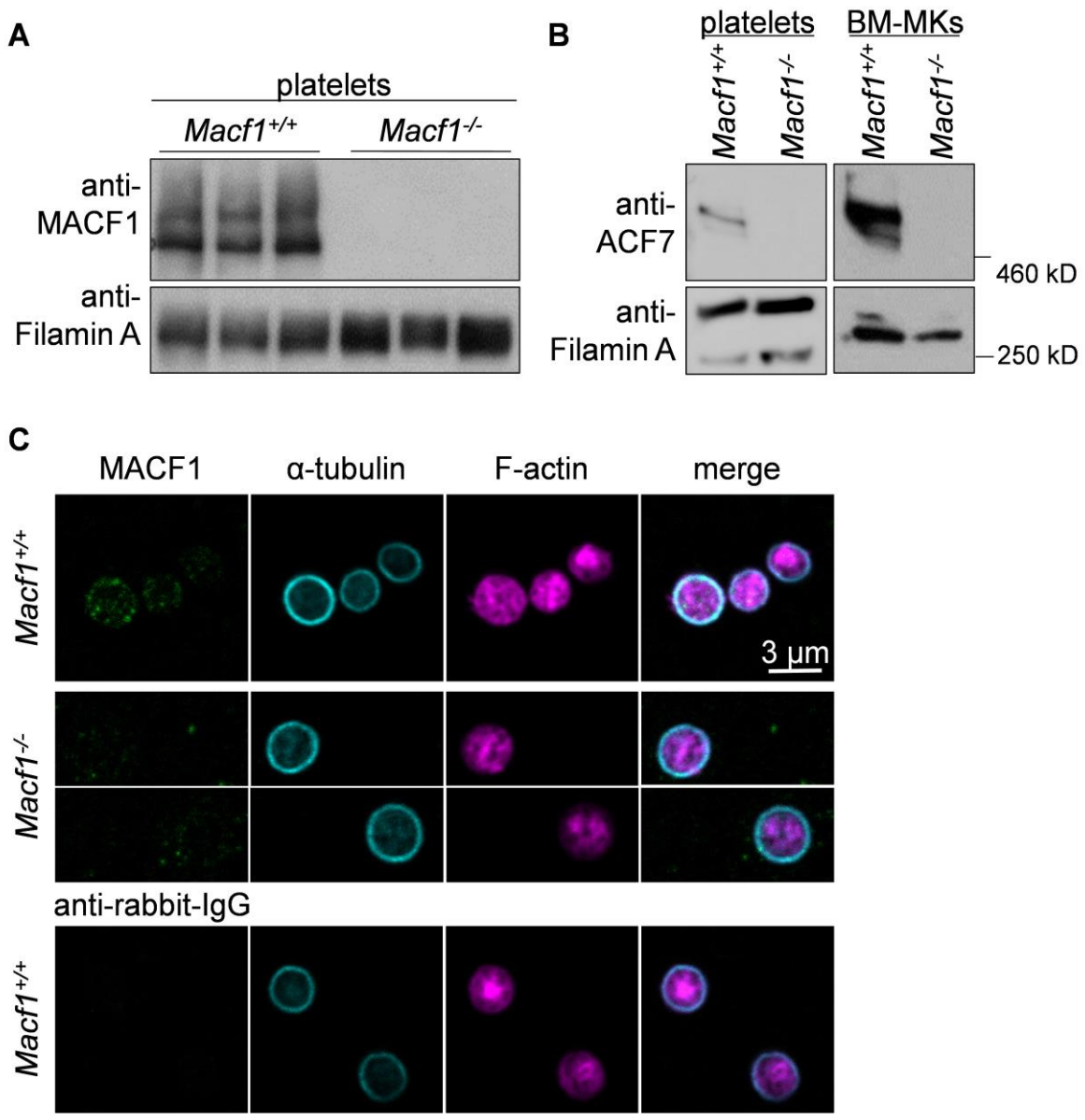

Figure 5.3.1: Verification of MACF1 deficiency in platelets and megakaryocytes. Western blot analysis of MACF1 expression in (A) platelets using the anti-MACF1 antibody (Bethyl; #A304-564A) and in (B) platelets and megakaryocytes using the MACF1/ACF7-antibody (provided by Elaine Fuchs). Loading control: Filamin A. (C) Immunostaining of resting platelets on poly-L-lysine. Green: MACF1/ACF7 (provided by Elaine Fuchs), cyan: α-tubulin, purple: F-actin. Anti-rabbit-IgG served as staining control. Scale bar: 3 µm. (A-C) Representative of at least 3 versus 3 samples.

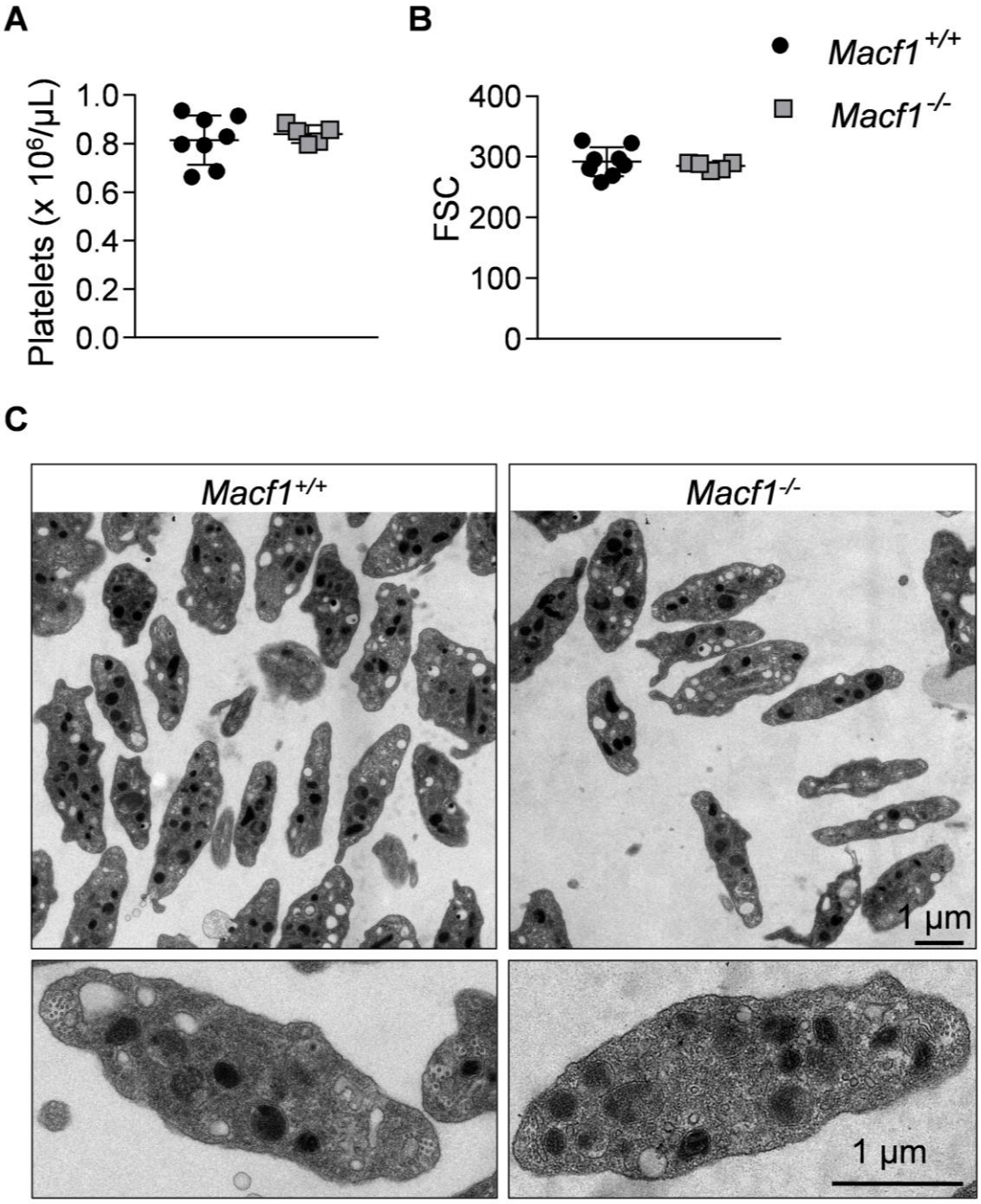

Figure 5.3.2: MACF1 deficiency has no effect on platelet count and size (A) Platelet count per µl and (B) platelet size given as mean forward scatter (FSC) were determined via flow cytometry. (C) Representative transmission electron micrographs from *Macf1*$^{+/+}$ and *Macf1*$^{-/-}$ platelets. Representative of at least 3 versus 3 samples.

Table 5.3.1: MACF1 deficiency in megakaryocytes and platelets has no effect on whole blood parameters. Whole blood parameters determined by a hematology analyzer (n = 3 versus 3, representative for two independent experiments).

	Macf1$^{+/+}$			*Macf1*$^{-/-}$			*p*
Platelets (10³/µL)	867.80	±	57.15	826.33	±	23.7	0.10
MPV (fL)	4.88	±	0.15	5.00	±	0.22	0.71
Leukocytes (10³/µL)	6.66	±	1.25	4.67	±	1.91	0.16
Neutrophils (10³/µL)	2.45	±	1.23	2.26	±	1.52	0.74
Lymphocytes (10³/µL)	3.92	±	1.23	2.17	±	1.44	0.13
Monocytes (10³/µL)	0.28	±	0.09	0.21	±	0.23	0.99
Eosinophils (10³/µL)	0.02	±	0.01	0.02	±	0.02	0.86
Erythrocytes (10³/µL)	9.55	±	0.63	10.01	±	0.47	0.82
MCV (fL)	45.42	±	1.40	44.40	±	0.33	0.79

Another member of the spectraplakin family is Dystonin. To investigate whether Dystonin is also expressed in platelets or is expressed upon the loss of MACF1, the mRNA expression of Dystonin was determined via reverse transcriptase PCR, since western blot analyses with respective Dystonin antibodies did not work. The mRNA expression of Dystonin isoform a and b was detectable in murine spleen and heart tissue control samples, whereas no expression was detected in platelet samples from *Macf1*$^{+/+}$ and *Macf1*$^{-/-}$ mice (Figure 5.3.3). Indicating that MACF1 is the only spectraplakin expressed in murine platelets, and that the loss of MACF1 is not compensated by upregulation of Dystonin.

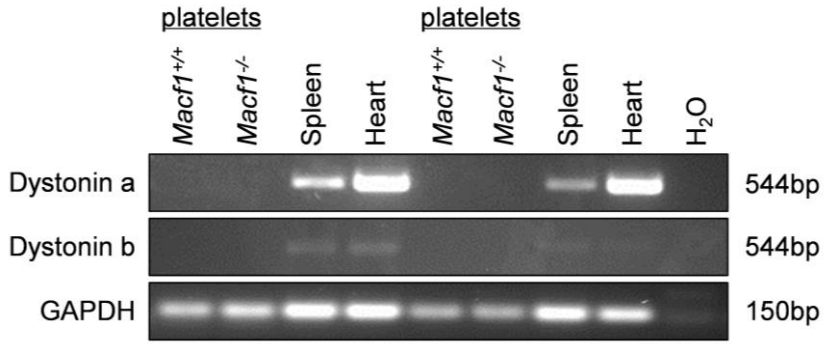

Figure 5.3.3 Dystonin expression in control and MACF1-deficient platelets. mRNA expression of Dystonin a and Dystonin b isoform was determined via reverse transcriptase PCR. mRNA extracted from the spleen and the heart served as positive control (n = 2).

5.3.2 Unaltered inside-out activation and aggregation of *Macf1*$^{-/-}$ platelets

To study the role of MACF1 in platelet function, first the surface expression of platelet glycoprotein receptors was analyzed by flow cytometry and revealed only a minor decrease in GPVI expression on mutant platelets (Table 5.3.2).

	Macf1$^{+/+}$	*Macf1*$^{-/-}$	*p*
GPIb	310 ± 15	288 ± 7	0.30
GPIX	388 ± 13	380 ± 3	0.80
GPV	217 ± 9	207 ± 3	0.40
CD9	862 ± 23	814 ± 69	0.80
GPVI	43 ± 1.7	38 ± 0.6	0.01**
αIIbβ3	478 ± 31	483 ± 6	0.95
α2	43 ± 2.7	43 ± 1.4	0.95
β1	146 ± 7	137 ± 13	0.80
CLEC-2	135 ± 4.8	134 ± 4.2	0.95

Table 5.3.2 Determination of glycoprotein expression. Diluted whole blood was incubated with FITC-labelled antibodies and glycoprotein expression on the surface of platelets was measured as mean fluorescence intensity (MFI) by flow cytometry; (n = 3); ***P*<0.01.

Further, the surface exposure of P-selectin and activation of the platelet integrin αIIbβ3 was analyzed after incubation with different agonists. Comparable results for control and *Macf1*$^{-/-}$ platelets were obtained after stimulation of G-protein coupled receptors with ADP, the thromboxane A2 analogue U46619, a combination of both, or thrombin. Similarly, MACF1-deficient platelets exhibited a comparable degree of activation upon stimulation of the GPVI-ITAM (immunoreceptor tyrosine-based activation motif) pathway with collagen-related peptide (CRP) or convulxin, and of the hemITAM receptor, CLEC-2 (C-type lectin-like receptor 2), with rhodocytin (Figure 5.3.4 A-B).

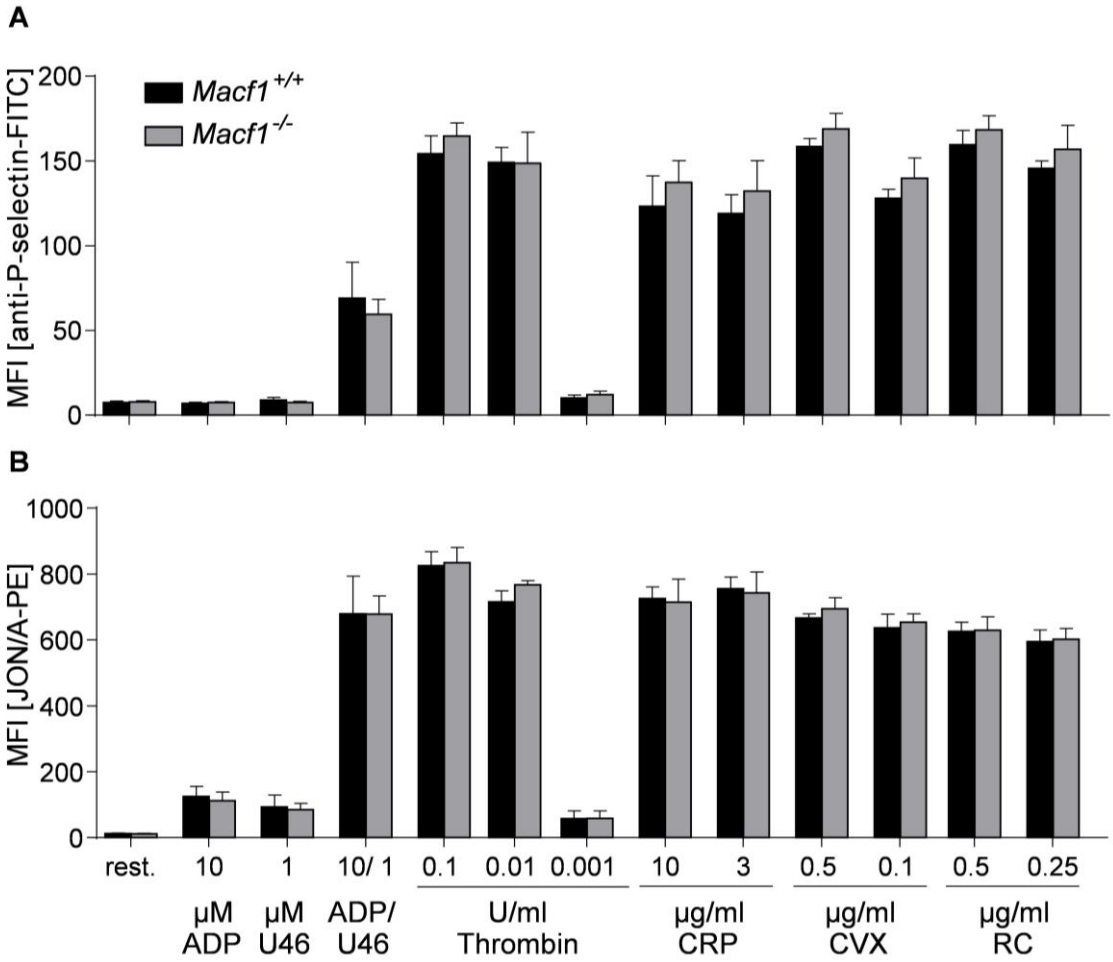

Figure 5.3.4: Unaltered P-selectin exposure and αIIbβ3 integrin activation of *Macf1*$^{-/-}$ platelets in response to GPCR, GPVI and CLEC-2-dependent agonists. (A) Degranulation dependent P-selectin exposure using a FITC-labelled anti-P-selectin antibody and (B) inside-out activation of αIIbβ3 integrin using the JON/A-PE antibody (n=6, representative for four independent experiments) in response to indicated agonists ADP, U46619 (thromboxane analogue), thrombin (Thr), collagen related peptide (CRP), convulxin (CVX) and rhodocytin (RC) were determined by flow cytometry.

To clarify the role of MACF1 for platelet shape change and aggregation, *in vitro* aggregation studies were performed. All agonists induced a comparable activation-dependent change from discoid to spherical shape of control and *Macf1*$^{-/-}$ platelets, which can be seen in aggregometry as a short decrease in light transmission following the addition of agonists. Further, *Macf1*$^{-/-}$ platelets showed a normal onset and degree of aggregation in response to the GPCR agonists ADP, U46619 and thrombin, as well as to the GPVI and CLEC-2 agonists collagen and rhodocytin, respectively (Figure 5.3.5).

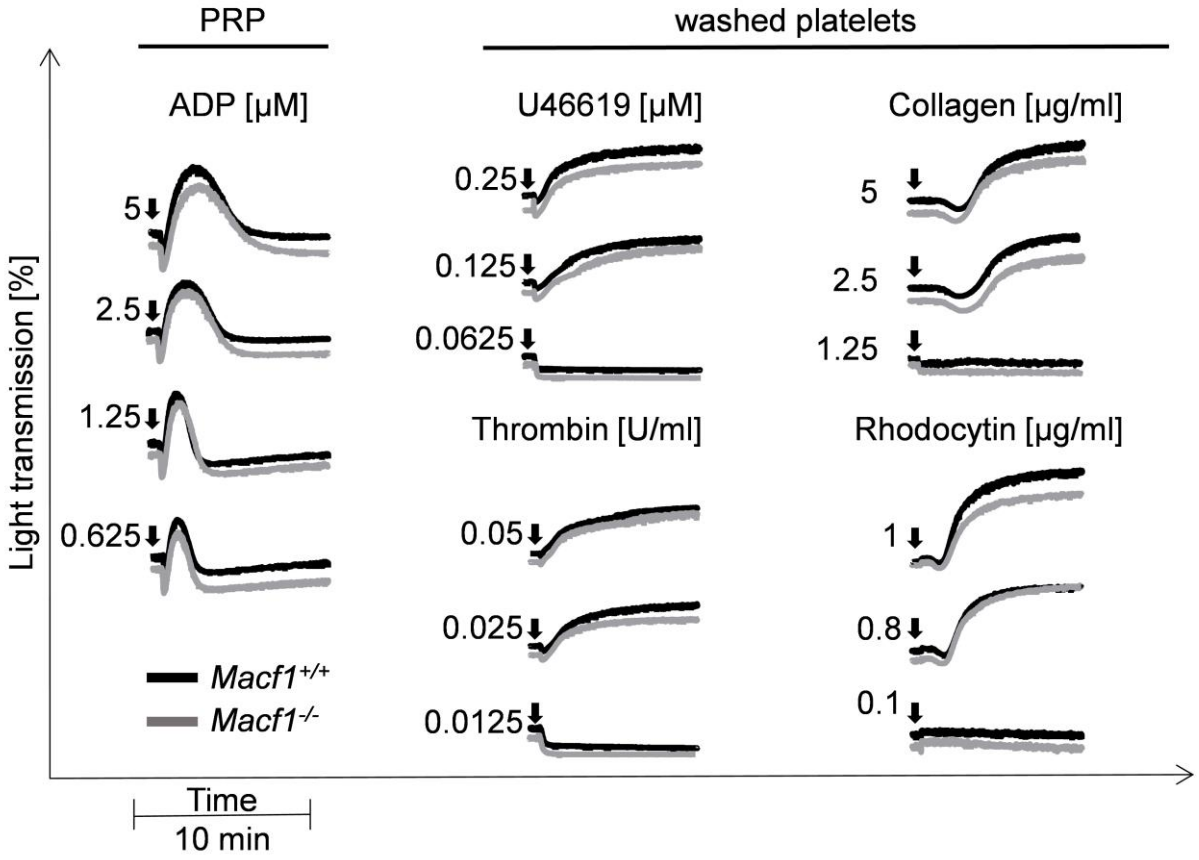

Figure 5.3.5: Unaltered aggregation responses to GPCR, GPVI and CLEC-2-dependent agonists of *Macf1*$^{-/-}$ platelets. Platelet rich plasma (PRP) or washed platelets from *Macf1*$^{+/+}$ and *Macf1*$^{-/-}$ mice were activated with the indicated concentrations of G-protein-coupled receptor (GPCR) agonists (ADP, U46619, thrombin), GPVI dependent agonist (collagen) and CLEC-2 dependent agonist (rhodocytin); (n = 3-8).

5.3.3 Lack of MACF1 has no impact on the localization and functionality of microtubules

In various cell types, MACF1 has been shown to be important for crosslinking microtubules and F-actin and thereby controlling cytoskeletal rearrangement.[122] Therefore, the role of MACF1 as a regulator of cytoskeletal dynamics in platelets was investigated. First the cytoskeletal organization of resting *Macf1*$^{-/-}$ platelets was analyzed. TEM analysis revealed a normal actin scaffold and the characteristic ring structure organized by microtubules, designated as the marginal band (Figure 5.3.6).

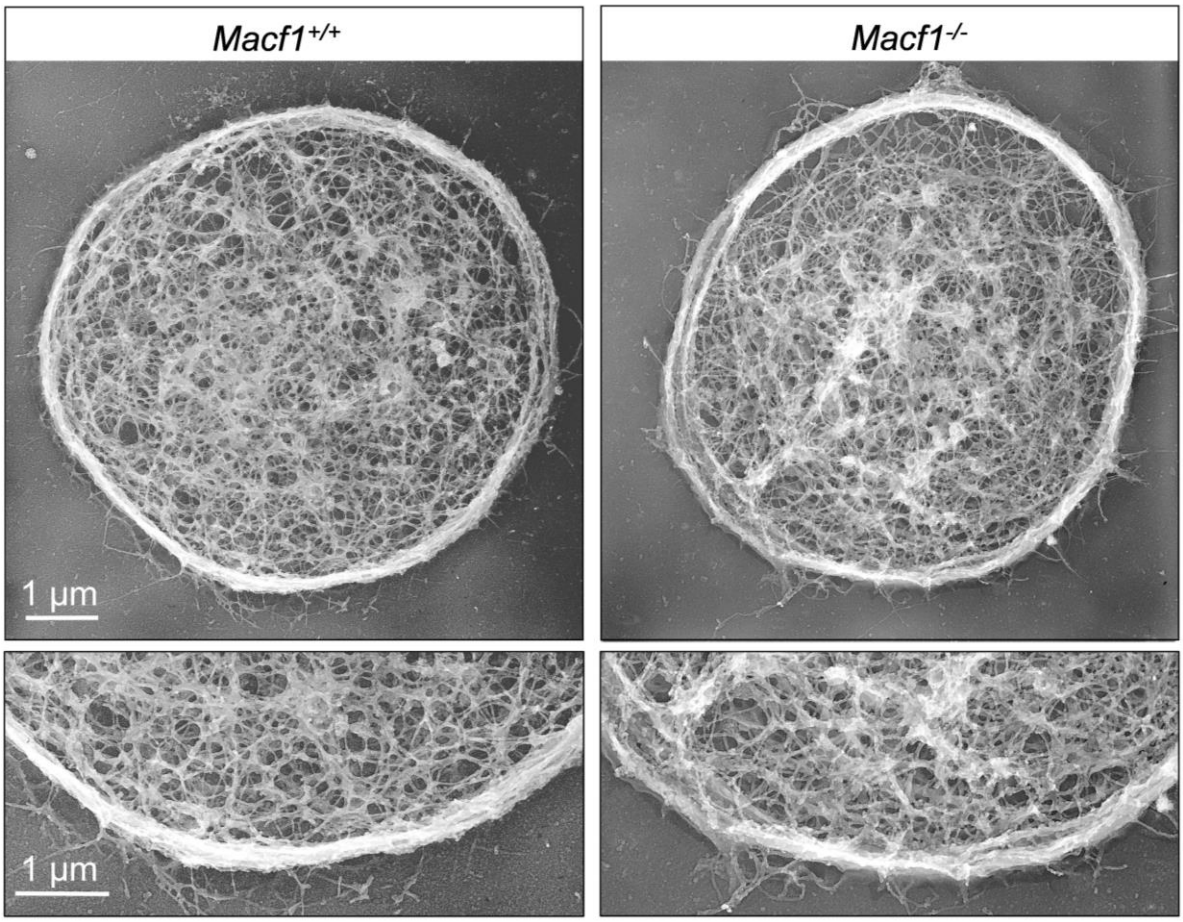

Figure 5.3.6: Lack of MACF1 does not affect microtubule and actin arrangement in resting platelets. Images of the platelet cytoskeleton ultrastructure on poly-L-lysine (n = 2).

Next, the number of microtubule coils per platelet was quantified. MACF1-deficient platelets had a similar number of microtubules compared to controls (Figure 5.3.7 A-B). The cold resistance of microtubules was analyzed by incubating platelets at different temperatures to induce dis- and reassembly of microtubules. Platelet fixation and staining for α-tubulin revealed comparable dis- and reassembly of microtubules (Figure 5.3.7 C).

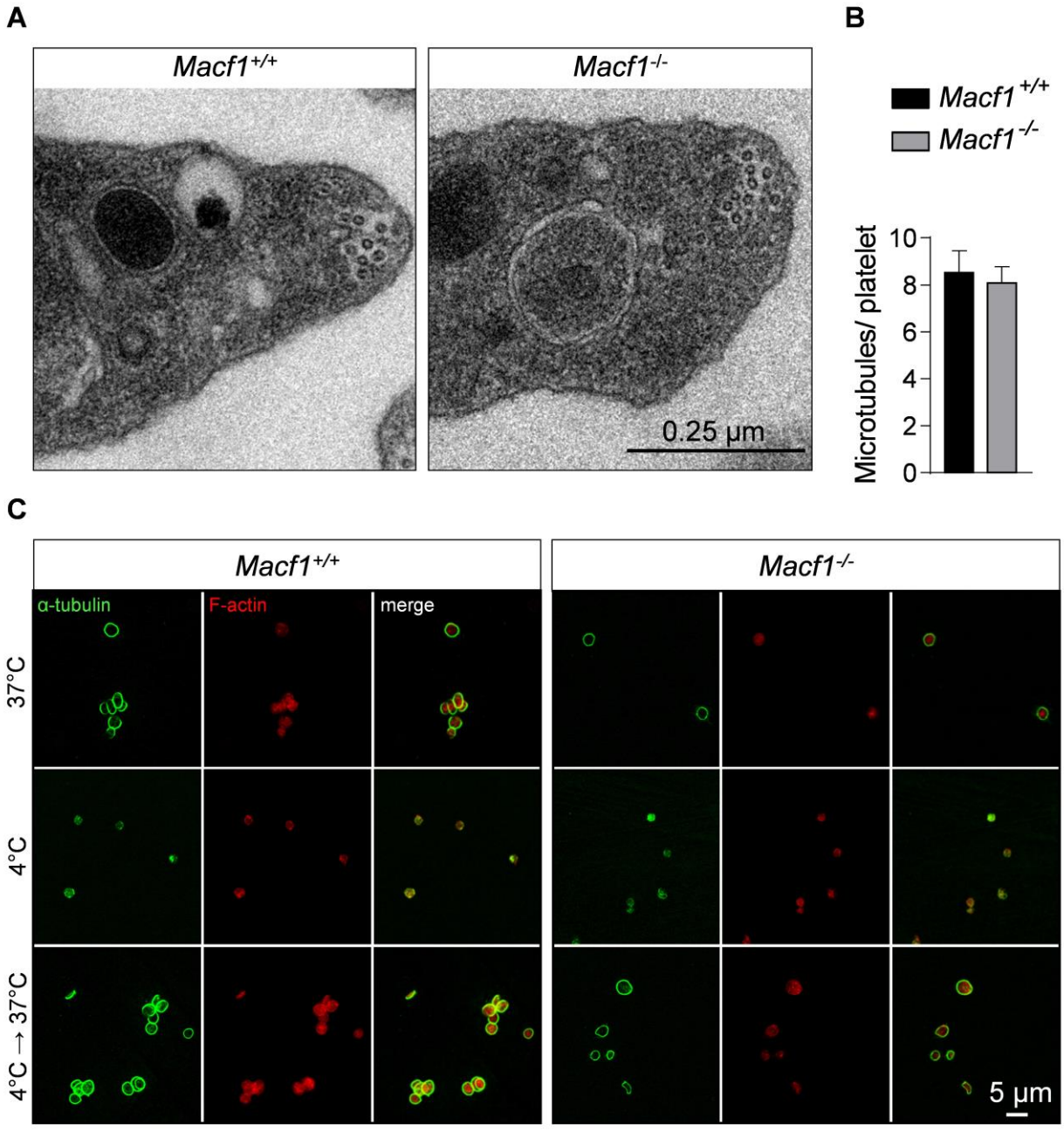

Figure 5.3.7: Lack of MACF1 does not affect microtubule number and dynamics. (A) TEM images of resting platelets (n = 4) and (B) evaluation of microtubule number. (C) Representative confocal microscopy images of immunostained resting platelets on poly-L-lysine (PLL). Washed platelets were fixed either after 3.5 h at 37°C (resting), after 3.5 h at 4°C (disassembly) or after 3.5 h at 4°C followed by 30 min at 37°C (reassembly). *Macf1*$^{+/+}$ and *Macf1*$^{-/-}$ platelets were stained for F-actin (red) and α-tubulin (green). (n = 3, representative for three independent experiments).

5.3.4 MACF1-deficiency has no impact on platelet spreading and reorganization of the actin cytoskeleton

To investigate the organization and rearrangement of the cytoskeleton in *Macf1*$^{-/-}$ platelets, spreading experiments on a fibrinogen-coated surface were performed. Mutant platelets were able to rearrange the cytoskeleton and formed filopodia and lamellipodia as revealed by differential interference contrast imaging (Figure 5.3.8 A) and by TEM analysis after removing the platelet membrane (Figure 5.3.9). A significantly delayed transition of mutant platelets forming filopodia and lamellipodia (phase III) to platelets forming lamellipodia (fully spread, phase IV) was only observed at the 15 min time point. After 30 min the number of fully spread platelets was comparable (Figure 5.3.8 B).

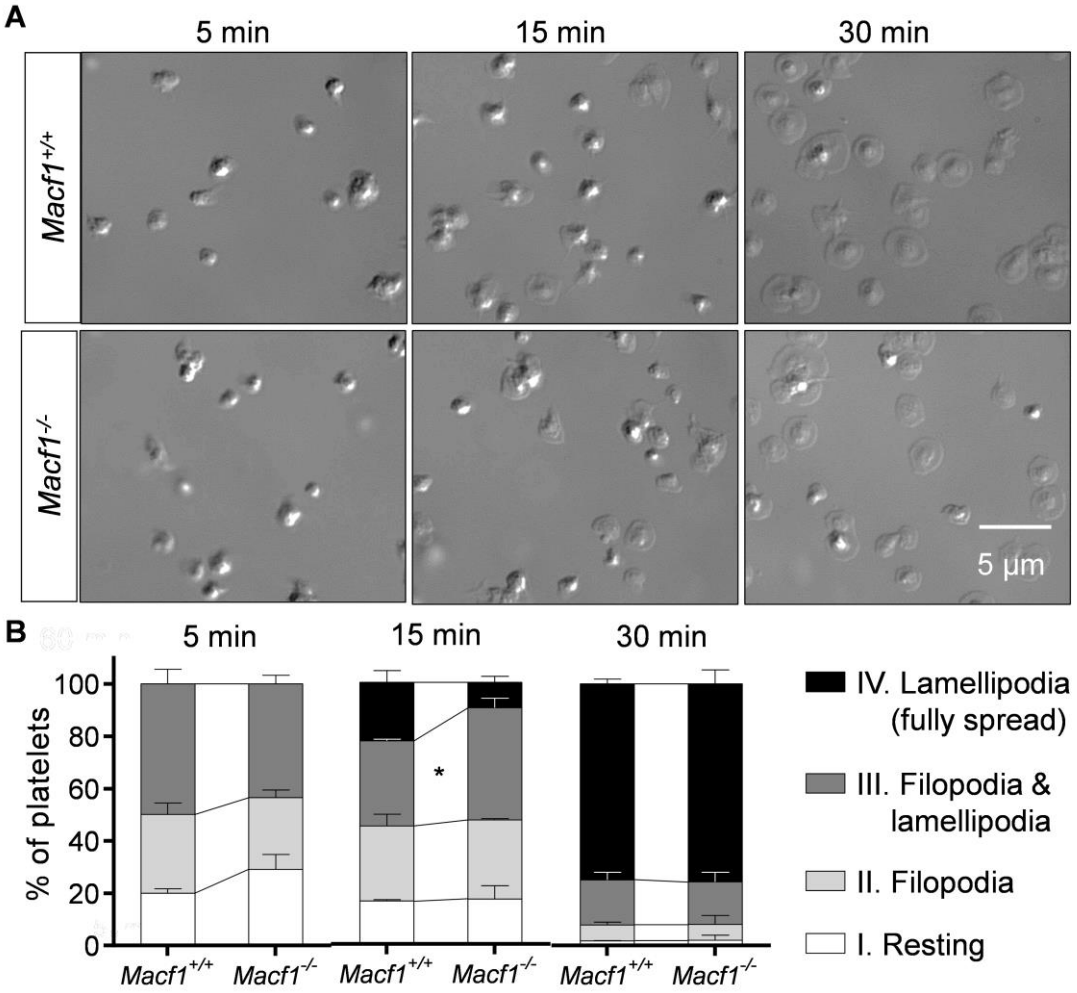

Figure 5.3.8: *Macf1*$^{-/-}$ platelets are able to adhere and spread on fibrinogen. (A) Representative images and (B) statistical analysis of *Macf1*$^{+/+}$ and *Macf1*$^{-/-}$ platelets activated with 0.01 U/ml thrombin and spread on a fibrinogen coated surface for 5, 15 and 30 min at 37°C (n = 3) **P*<0.05.

To investigate if the loss of the MACF1 affects the general assembly of actin fibers, resting or activated platelets were stained with phalloidin-FITC and analyzed by flow cytometry. Upon platelet activation, the amount of F-actin increased in *Macf1*$^{+/+}$ and *Macf1*$^{-/-}$ platelets to a similar extent (Figure 5.3.10 A-B). This indicates that the loss of MACF1 does not impair F-actin assembly.

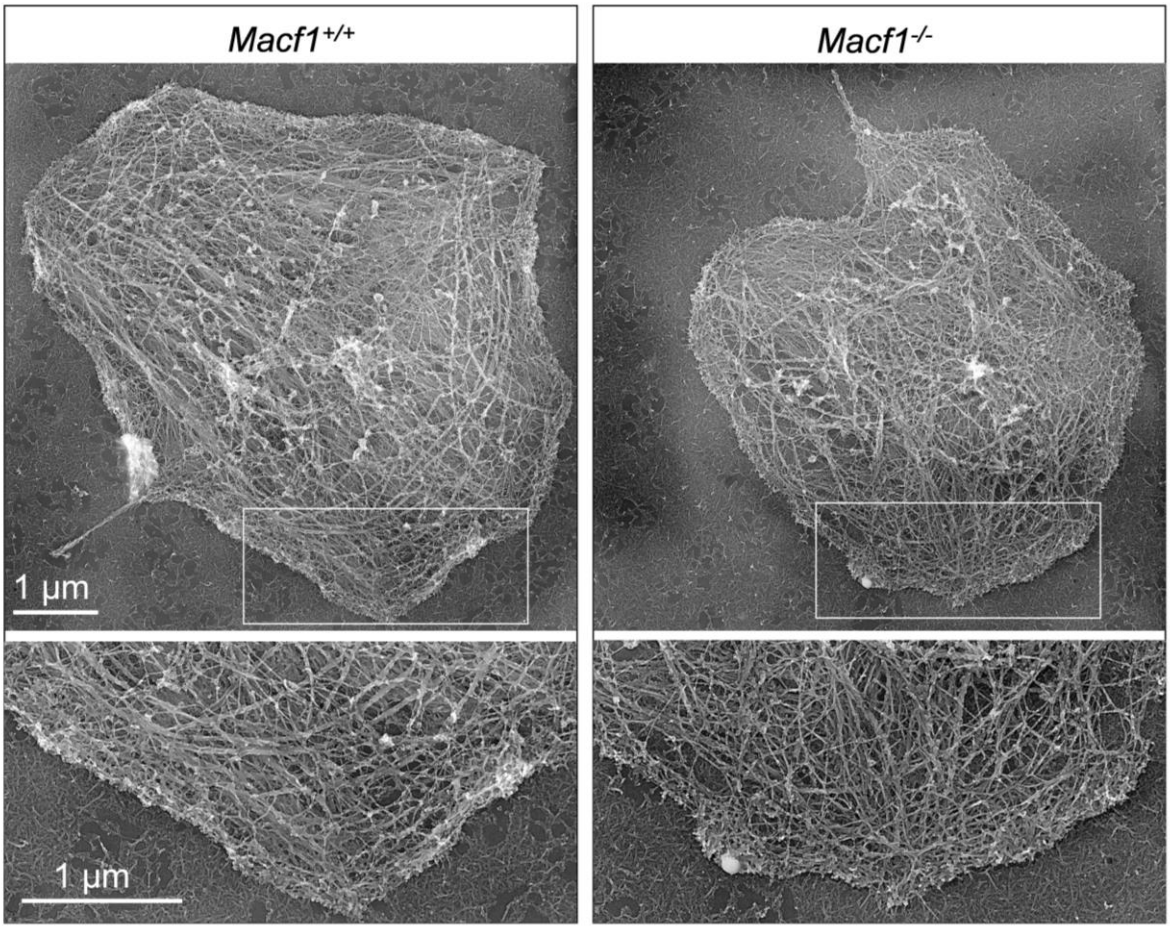

Figure 5.3.9: Cytoskeletal ultrastructure. Representative transmission electron micrographs of the cytoskeleton ultrastructure of control and and *Macf1*$^{-/-}$ platelets spread on fibrinogen for 15 min in the presence of 0.01 U/ml thrombin (n = 2).

In addition, it was assessed whether MACF1 deficiency might impair the cytoskeletal reorganization when platelets are treated with cytoskeletal-modifying toxins, such as colchicine (inhibits microtubule polymerization), latrunculin A (prevents actin polymerization) or paclitaxel (inhibits microtubule disassembly). However, in the presence of these toxins no effect of MACF1 deficiency on platelet spreading was observed (Figure 5.3.10 C).

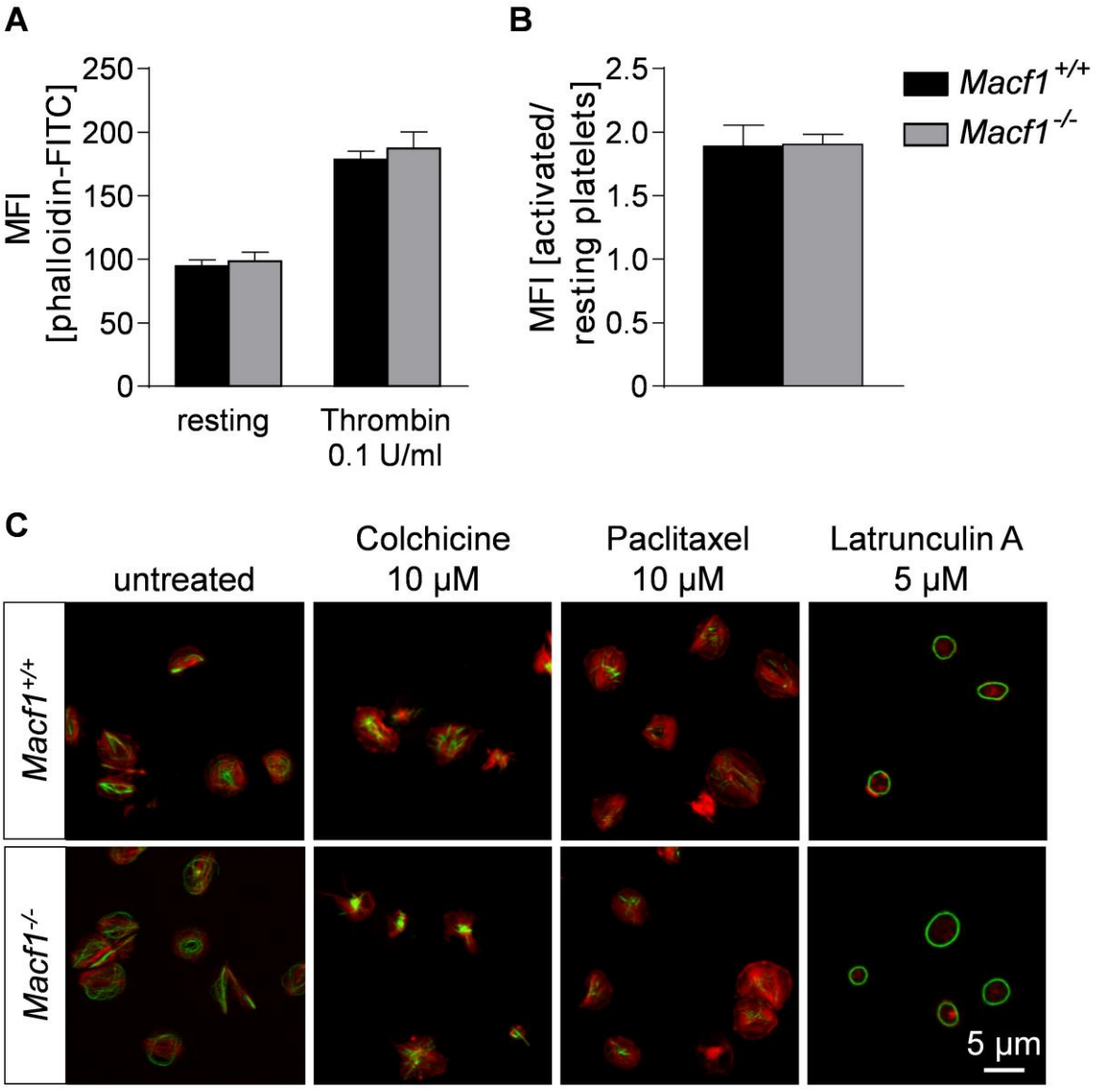

Figure 5.3.10: Lack of MACF1 does not affect actin dynamics. (A) Resting or thrombin-activated platelets were fixed, permeabilized, stained with phalloidin-FITC, and analyzed by flow cytometry. (B) The ratio of polymerized actin in activated vs. resting platelets was determined (n=3, representative for two independent experiments). (C) Platelets pre-treated with indicated cytoskeletal-modifying toxins were allowed to spread on fibrinogen for 30 min; α-tubulin (green), F-actin (red). Values are mean ± s.d. (n=3, representative for three independent experiments).

5.3.5 MACF1 is not important for thrombus formation, clot retraction and hemostasis

Upon vascular injury, platelet adhesion and aggregation occur in the peripheral bloodstream where shear forces strongly influence platelet function. To test the role of MACF1 in thrombus formation under flow, platelet adhesion to collagen in a whole-blood perfusion assay at shear rates of 1000 s^{-1} was studied. Control and mutant platelets rapidly adhered to collagen and consistently formed stable 3-dimensional thrombi (Figure 5.3.11 A). Surface coverage and thrombus volume were comparable between blood from *Macf1*$^{+/+}$ and *Macf1*$^{-/-}$ mice, indicating that MACF1 is dispensable for thrombus formation (Figure 5.3.11 B).

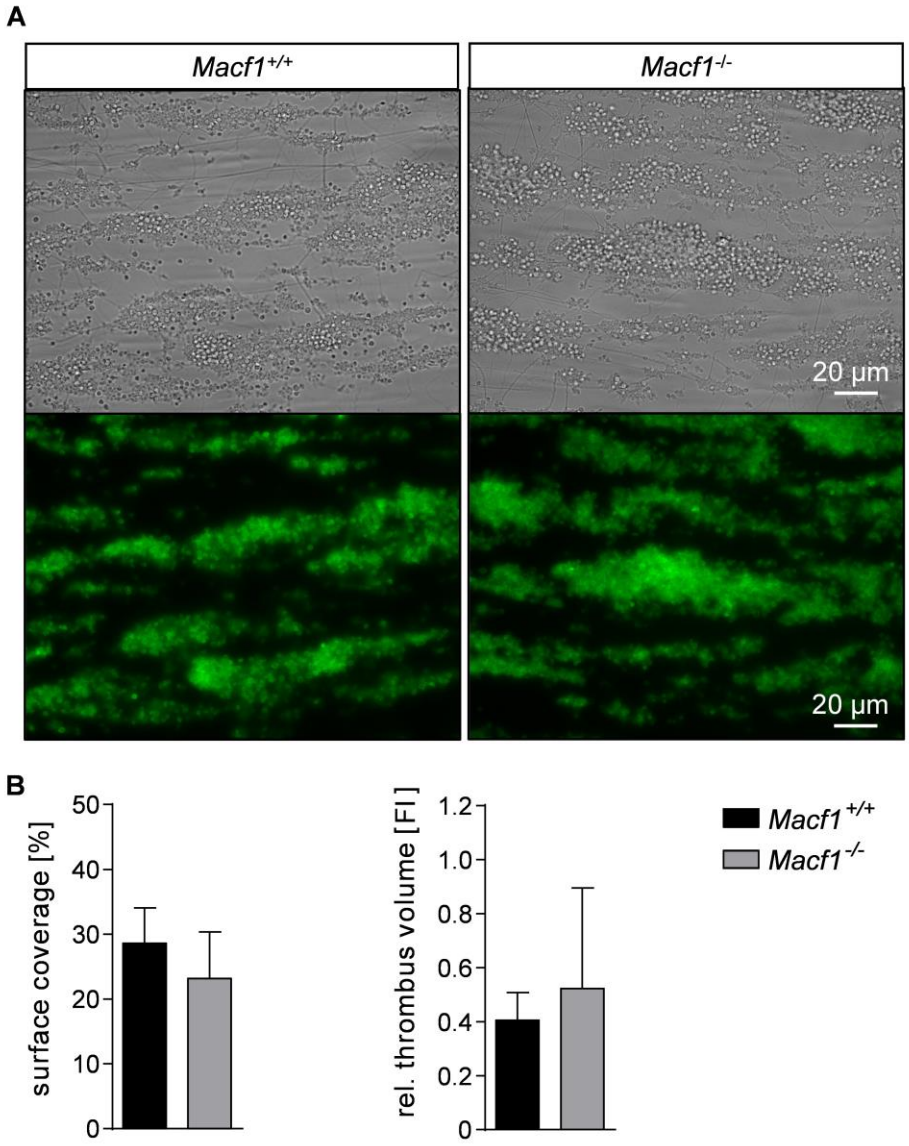

Figure 5.3.11: MACF1 is not important for thrombus formation.
(A) Thrombus formation was assessed on collagen at a wall shear rate of 1000 s^{-1}. Shown are representative bright-field (upper panel) and fluorescence (lower panel) pictures of

platelets stained with a Dylight-488 anti-GPIX antibody (n = 6, representative for two independent experiments). (B) Surface coverage and relative thrombus volume were quantified according to fluorescence distribution and fluorescence intensity, respectively.

To further assess integrin outside-in signalling, which is an important mechanism to stabilize thrombi, a clot retraction assay was performed. However, no differences were found in the kinetics of clot retraction between PRP from both mouse strains (Figure 5.3.12 A-B). In addition, comparable bleeding times were measured for control and mutant mice, indicating that MACF1 is not required to maintain the hemostatic function (Figure 5.3.12 C). Taken together, these data demonstrate that MACF1 is dispensable for thrombus formation and hemostasis.

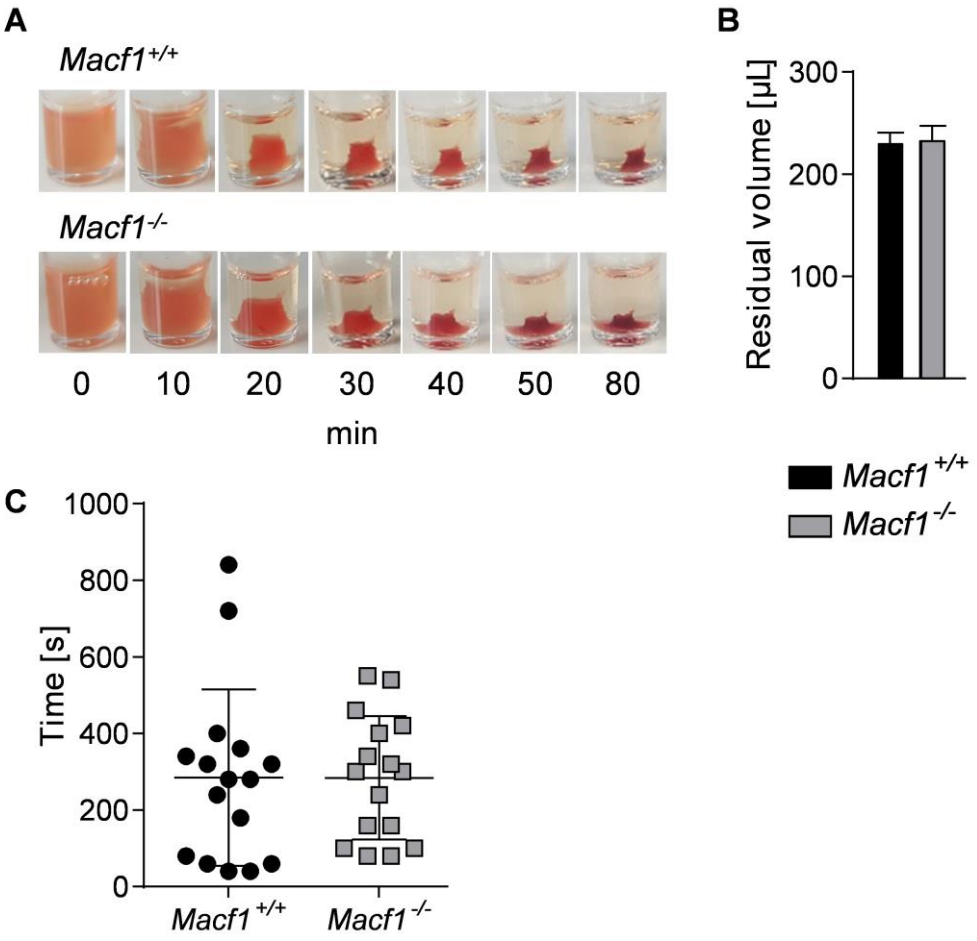

Figure 5.3.12: Normal clot retraction *in vitro* and unaltered hemostatic function in MACF1-deficient mice. (A) Clot formation was observed over time and (B) residual serum volume was measured (n = at least 3, representative for three independent experiments). (C) Determination of tail bleeding time performed on filter paper of *Macf1*$^{+/+}$ and *Macf1*$^{-/-}$ mice.

6 DISCUSSION

6.1 Platelet lamellipodia formation is not required for thrombus formation and stability

Static platelet spreading assays, particularly on fibrinogen-coated surfaces, are frequently performed as a measure of the contribution of outside-in signaling and cytoskeletal rearrangement in platelet function,[152] as well as a readout for functional properties of *in vitro* produced platelets.[153–156] *In vitro*, four stages of platelet spreading can be observed: (I) adhesion of resting platelets, (II) formation of finger-like protrusions, called filopodia, (III) a combination of filopodia and plate-like extensions, called lamellipodia, and (IV) only lamellipodia. Under dynamic conditions, platelets adhere to the exposed extracellular matrix, become activated and thereby change their shape, which is accompanied by the secretion and synthesis of several prothrombotic factors, which together contribute to the activation of more platelets and finally leads to aggregate formation.

It has been debated for years whether the stages of *in vitro* platelet spreading, particularly lamellipodia formation, also contribute to platelet adhesion and activation under dynamic conditions *in vivo*. Platelet lamellipodia have been suggested to be important for the initiation of thrombus growth when platelets are in direct contact with extracellular matrix components, most notably collagen.[32,34,35] In contrast, other publications provided indirect evidence that lamellipodia formation is not crucial for thrombus formation and hemostasis.[33,36,47] The mouse model of Arp2/3 deficiency displayed a marked microthombocytopenia due to defects in platelet production and an increased clearing rate of platelets from the circulation, and an impaired platelet spreading comparable to Cyfip1-deficent animals.[36] Despite a 95% loss of Arp2/3, these platelets only showed a mild activation defect, an intact hemostasis and no signs of inflammatory bleeding. Rac1-deficient platelets also showed an impaired spreading, but in addition a severe activation and aggregation defect in response to GPVI-dependent agonists (CRP, collagen and convulxin).[33] The impaired platelet adhesion and thrombus formation of Rac1-deficient platelets on collagen under flow conditions could be fully restored by coinfusion of ADP and thromboxane A2 analogue (U46). These data already indicated that an impaired GPVI-dependent signaling was responsible for the observed activation and aggregation defects rather than a defect in cytoskeletal dynamics. However, these additional defects in both Arp2/3 and Rac1-

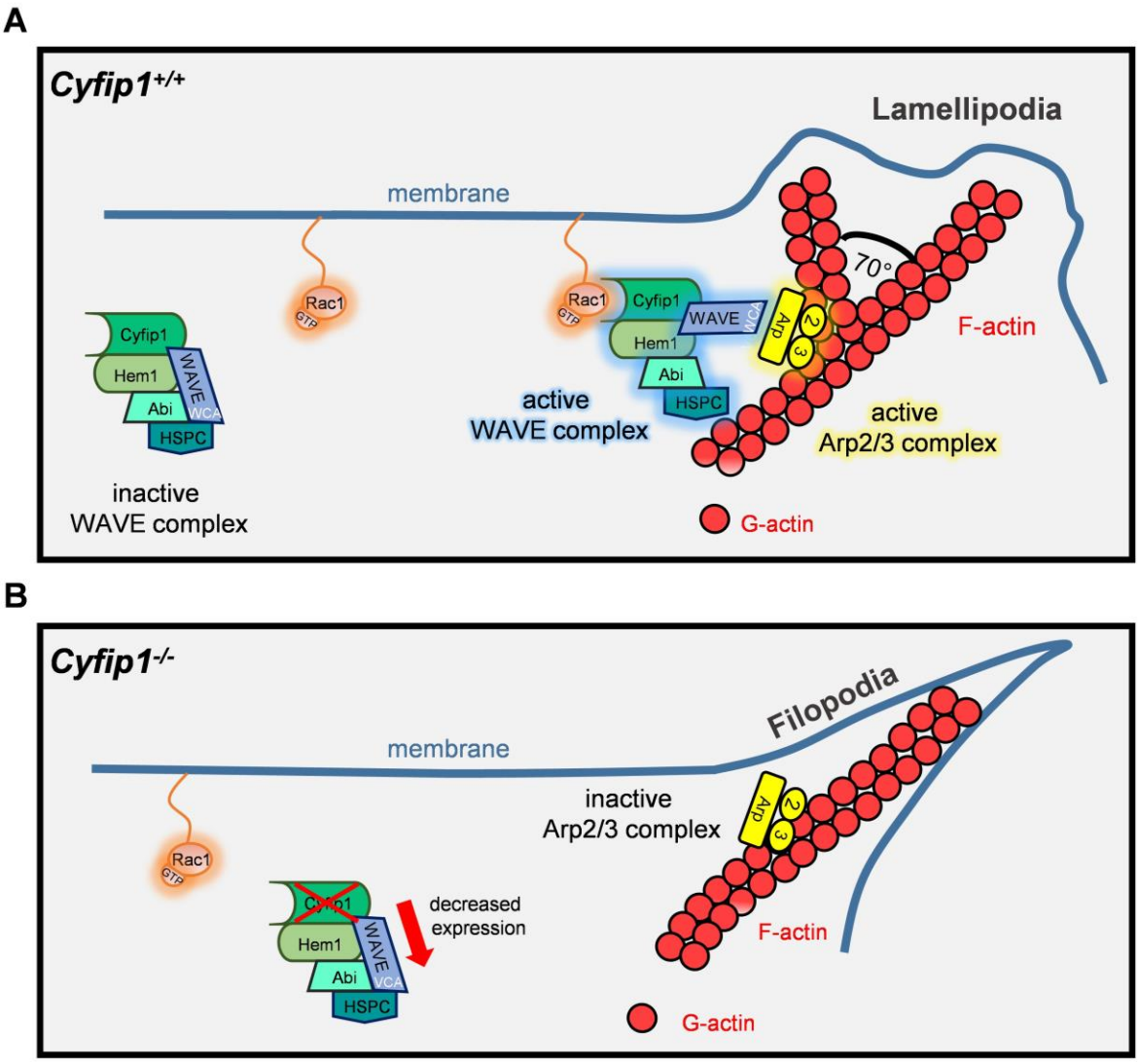

Figure 6.1.1: Cyfip1 plays a crucial role for branching of actin filaments. (A) Previously published affinity purification data from HEK 293T cell lines expressing FLAG-tagged subunits of the WAVE complex[74] revealed that the WCA domain of the WAVE protein is masked in the inactive WAVE complex. Upon interaction of the Cyfip subunit and Rac1-GTP, the WCA domain of the WAVE protein is exposed and interacts with Arp2/3, forming branched actin filaments and lamellipodia.[74] (B) Data from this thesis revealed that Cyfip1-deficiency in platelets results in a decreased expression of the WAVE2 subunit of the WAVE complex, whereas the expression of the Arpc2 subunit and Rac1 remain unaltered. In line with previous data from other cells[36,74] we suggest that the Arp2/3 complex remains inactive in *Cyfip1*$^{-/-}$ platelets, thereby these platelets only form filopodia during spreading, whereas lamellipodia structures cannot be formed.

deficient animals made it difficult to investigate the role of lamellipodia in platelet adhesion and thrombus formation. The analysis of *Cyfip1*$^{+/+}$ and *Cyfip1*$^{-/-}$ mice with abolished platelet lamellipodia (Figure 5.1.5 and Figure 5.1.6) formation, but only minimal side-effects in platelet function (Figure 5.1.1 to Figure 5.1.4), provides for the first time definitive evidence that platelet lamellipodia (Figure 6.1.1) formation is not

required for stable thrombus formation *ex vivo* (Figure 5.1.12 and Figure 6.1.2) and *in vivo* (Figure 5.1.17), hemostatic plug formation as well as for maintenance of vascular integrity in inflammatory settings (Figure 5.1.18). Moreover, it was demonstrated by direct observation that platelets display different morphological changes in a static spreading assay compared to an *ex vivo* formed thrombus under flow where platelets only formed filopodia to adhere to collagen fibers (Supplemental Video 5) and to an *in vivo* formed thrombus as visualized by scanning electron microscopy in an experimentally-induced arterial thrombus (Figure 5.1.17). Further, it was shown that control and mutant platelets in direct contact with collagen fibers at the bottom of the thrombus were flattened but formed filopodia structures with parallel actin filaments (Figure 6.1.2). Fully spread platelets with circumferential lamellipodia, as can be observed in the static spreading assay (phase IV), were absent under these flow conditions (Figure 5.1.6 and Figure 5.1.14). However, although platelet lamellipodia are not required for the formation and overall stability of thrombi, it cannot be excluded that lamellipodia formation might still be important in other thrombi-related processes, such as vessel repair.

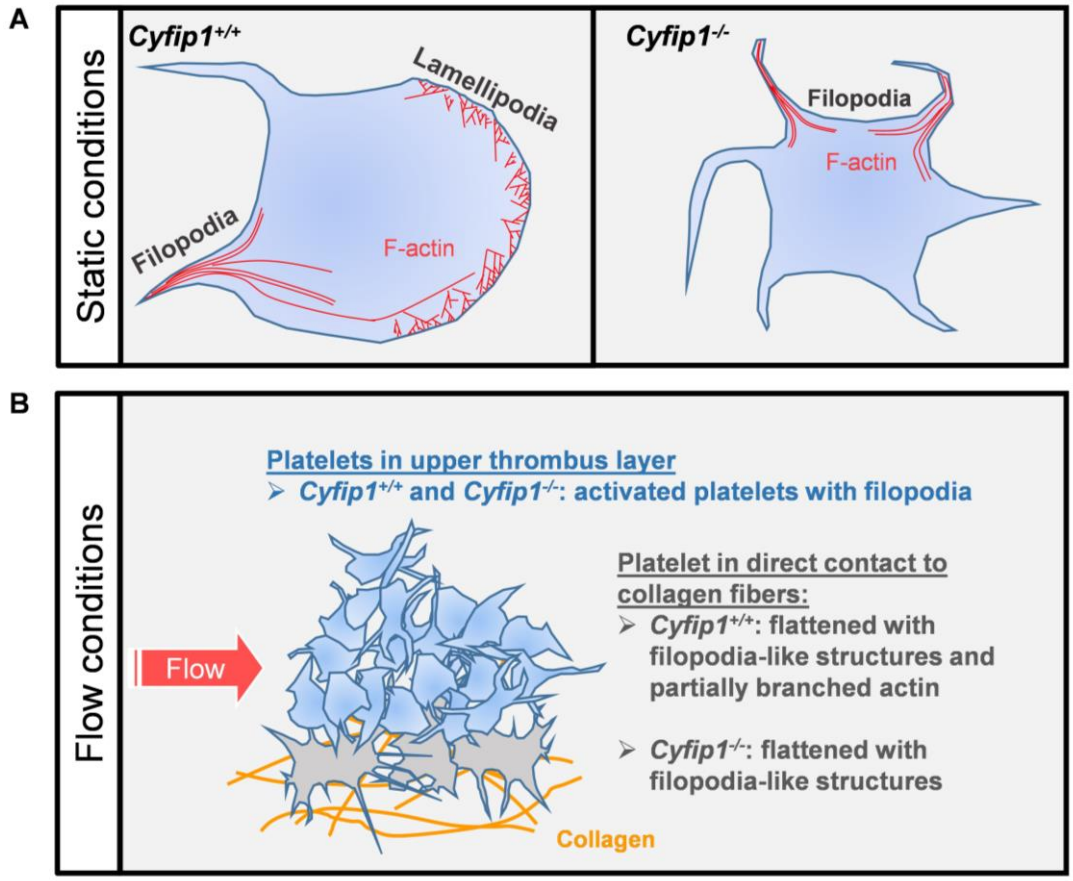

Figure 6.1.2: The role of lamellipodia formation in platelet spreading and thrombus formation. (A) Cyfip1 plays a crucial role in the branching of actin filaments and for

lamellipodia formation as seen in static spreading assays. (B) Control platelets in direct contact with collagen fibers form filopodia-like structures and partially branched actin under flow conditions, whereas platelets in the upper thrombus layer only form filopodia. Despite the defective lamellipodia formation, Cyfip1-deficient mice can form stable thrombi *ex vivo* and *in vivo*. These data suggest that lamellipodia formation is not required for the formation of a hemostatic plug or thrombus.

Interestingly, it was previously demonstrated that Arp2/3 complex activation is normal in platelets lacking WASp and hypothesized that other proteins probably WAVE2 or cortactin or both activate the Arp2/3 complex.[131] In this thesis it is shown that Cyfip1-deficient platelets have a reduced WAVE2 expression (Figure 5.1.2) and cannot form Arp2/3-dependent branched actin filaments (Figure 5.1.6). Thus, these data strongly suggest for the first time that the WAVE2 protein/complex regulates Arp2/3 activity in platelets.

It was recently shown that collagen-adherent platelets can transform into PS-exposing balloon-like structures, which was termed procoagulant spreading and likely contributes to hemostatic and thrombotic responses *in vivo* by amplifying procoagulant responses.[157] The ability of mutant platelets to expose PS on the surface after stimulation with CRP and thrombin *in vitro* and under dynamic conditions *ex vivo* was tested and comparable results were obtained for control and mutant mice (Figure 5.1.15). This indicates that platelets do not need to form lamellipodia in order to expose PS on the surface. Hence, the bridging mechanism of platelets and their coagulation response seem to be intact in Cyfip1-deficient platelets, enabling them to initiate thrombus formation.

However, one question remains unanswered: what is the role of lamellipodia in platelet function? There are several possibilities: (I) Lamellipodia structures could be an *in vitro* phenomenon during static platelet spreading. However, this is rather unlikely, since many other cells also produce this dense network of branched actin filaments contributing to important cellular functions. (II) The platelet machinery forming lamellipodia might be a relic of evolution, no longer needed for the specialized functions platelets have, and thus is dispensable. Until now, either possibility cannot be excluded. However, it is most likely that (III) platelet lamellipodia play an important role in other processes besides the initiation of thrombus formation and thrombus stability. These membrane protrusions at the leading edge of cells drive cell migration in many physiological and pathological situations.[158] Recently, it was reported that platelets

actively migrate at sites of a formed thrombus.[159] The authors concluded from their findings that platelet migration might be too slow to contribute to thrombus formation, but might play a role in thrombus reorganization and consolidation. The data of *Cyfip1*$^{-/-}$ mice show that platelet lamellipodia, which are most likely a prerequisite for platelet migration, are not important for thrombus formation, supporting the conclusion by Gaertner *et al.* of the dispensable role of platelet migration in thrombus growth. Thrombus reorganization was not directly analyzed, however, single platelets in an experimentally-induced arterial thrombus were visualized and optical analysis revealed that platelets exclusively form filopodia or filopodia-like structures (Figure 5.1.17). These data suggest that at least lamellipodia are not important in the reorganization of a thrombus. Interestingly, Gaertner and colleagues could show that platelets also migrate to sites of infection in order to help trap bacteria and clear the vascular surface.[159] The authors used platelets from *Myh9*$^{-/-}$ mice, which are unable to migrate, however, can extend lamellipodia but without stress fiber-like formation.[160] It will be interesting to investigate whether Cyfip1-deficient platelets with absent lamellipodia formation can migrate *in vitro* and *in vivo* and whether Cyfip1 is a key protein in bacteria scavenging and bundling at sites of infection.

6.2 WASH complex subunit Strumpellin selectively regulates integrin αIIbβ3 expression

The number of receptors present on the cell surface is an important mechanism to regulate cell interactions. Several endosomal receptor cargos have been analyzed for their dependence on WASH complex function. While WASH depletion does not affect the kinetics of transferrin uptake or recycling,[104] it was shown to impair integrin recycling.[105] This indicates that specific cargos depend on different WASH-dependent or –independent transport and recycling mechanisms.

Platelet adhesion, activation and aggregation in response to the exposed extracellular matrix of damaged vessels requires the coordinated interaction of several platelet surface receptors with adhesive macromolecules (e.g. collagen-bound von Willebrand factor) and adhesion receptors of the integrin family are required for firm adhesion and thrombus growth.[161] Further, endocytosis and endosomal trafficking in megakaryocytes and platelets is crucial for the loading of granules, such as the uptake of fibrinogen from plasma by αIIbβ3 integrin, and thus platelet effector function. However, the underlying mechanisms of cargo sorting and receptor trafficking are

poorly understood, and key regulatory proteins remain to be identified. The role of the WASH complex subunit Strumpellin in murine megakaryocytes and platelets was investigated. Strumpellin deficiency led to a decreased protein abundance of the WASH protein in resting platelets (Figure 5.2.1 A). Similar results were found in Strumpellin-deficient (siRNA knockdown) melanocytes that expressed other WASH complex subunits (except WAFL) at a reduced level of 20-30 %.[162] Platelet count and size as well as and general blood parameters remained unaltered upon loss of Strumpellin (Figure 5.2.1 B-C and Table 5.2.1). Flow cytometric analysis revealed a 20 % decrease in integrin αIIbβ3 surface expression on resting platelets (Table 5.2.2 and Figure 5.2.2). By contrast, the expression of other receptors (e.g. GPV, GPIb, α2 and β1 integrins) was unaltered compared to wild-type controls (Table 5.2.2). Despite a moderately reduced integrin αIIbβ3 (Figure 5.2.4) activation after platelet stimulation and the general reduced αIIbβ3 surface expression, the uptake of fibrinogen into platelets was comparable between control and Strumpellin-deficient platelets. Furthermore, a reduced number of αIIbβ3 integrins could be mobilized to the surface upon activation indicating also a decreased internal pool of αIIbβ3 in knockout platelets (Figure 5.2.5). However, these platelets showed unaltered integrin αIIbβ3-dependent spreading on fibrinogen (Figure 5.2.6 C) and unaltered bleeding times (Figure 5.2.9). Also the P-selectin content (Figure 5.2.7 B)and α-granule recruitment to the plasma membrane (Figure 5.2.7 A) was comparable between *Strumpellin*$^{+/+}$ and *Strumpellin*$^{-/-}$ platelets. These results are in line with data from heterozygous β3-integrin mutant mice that show a 50 % reduced expression of wild-type αIIbβ3 integrin, without displaying a bleeding defect.[163]

Mutant bone marrow megakaryocytes displayed normal ploidy, but integrin αIIbβ3 surface expression was reduced suggesting a megakaryocyte intrinsic defect (Figure 5.2.3). These data point to a distinct role of Strumpellin in maintaining integrin αIIbβ3 expression in megakaryocytes and platelets and provide new insights into regulatory mechanisms of platelet integrins. Several hypotheses could explain how Strumpellin affects the αIIbβ3 expression: I. Impaired/slower recycling rate of integrins; II. Higher degradation rate of integrins; III. Insufficient storage in α-granules; IV. Insufficient production (transcription/translation/folding).

Similar to the results from this dissertation, a direct requirement for the WASH complex and Arp2/3-mediated actin polymerization on endosomes was reported for α5β1 integrin recycling. In ovarian cancer cells (A2780) siRNA mediated knockdown of

WASH led to a decreased surface expression of α5β1 integrin. WASH-depletion did not alter the colocalization of α5β1 with EEA1, Rab11 or sialin, but resulted in an increased colocalization with the multivesicular body/late endosome marker CD63 and compartments involved in trafficking back to the plasma membrane.[105] This suggests that also in platelets and megakaryocytes the decreased αIIbβ3 expression might be based on an impaired or slower recycling.

In this study, a significantly increased number of α-granules (*Strumpellin*$^{+/+}$ 2.65; *Strumpellin*$^{-/-}$ 3.36 p = 0.003) and a slightly increased number of dense-granules (*Strumpellin*$^{+/+}$ 0.5; *Strumpellin*$^{-/-}$ 0.68 p = 0.05) was detected in Strumpellin-deficient platelets compared to controls (pictures and further analysis see doctoral thesis of Lucy Reil, which is in preparation). These results indicate that Strumpellin-deficiency alters the number of vesicles in platelets. However further investigations, especially regarding the colocalization of WASH, αIIbβ3 integrin and different endosomal markers, are required to elucidate the reason for the decreased αIIbβ3 integrin expression in Strumpellin-deficient platelets (Figure 6.2.1). Previous research on mammalian cell lines indicated that deletion of one individual subunit of the WASH complex leads to the destabilization of the entire complex.[91,93,106] However, a study of melanocyte-specific Strumpellin-deficient mice revealed that the WASH complex can still assemble and localize to endocytic compartments in cells in the absence of Strumpellin.[162] Further, in this publications the presence of two distinct WASH complexes, one associated with and one without Strumpellin, was shown by blue Native-PAGE.[162] Despite the lack of Strumpellin, a certain amount of surface αIIbβ3 expression can still be expressed in megakaryocytes and platelets. So far, no other protein is known to substitute Strumpellin. Since Strumpellin deficiency in platelets resulted in a decreased but not completely abolished WASH expression (Figure 5.2.1 A), this might indicate that the depletion of Strumpellin in megakaryocytes and platelets still leaves enough residual WASH complex activity to maintain αIIbβ3 expression at least partially. Compared to the high abundance of αIIbβ3 with a protein copy number (pcn) of about 100 000, the expression of β1 (pcn = 30855) and α2 (pcn = 17591) is rather low in murine platelets.[61] In A2780 ovarian carcinoma cells WASH was found to colocalize to α5β1 integrin on early and late endosomal vesicles. In those cells, the recycling of α5β1 also regulates the cell invasive motility. WASH depletion leads to an accumulation of α5β1 integrin in pre-lysosomal compartments and to an invasion defect.[105] In MDA-MB-231 cancer cells it was shown that active β1-integrins are mainly

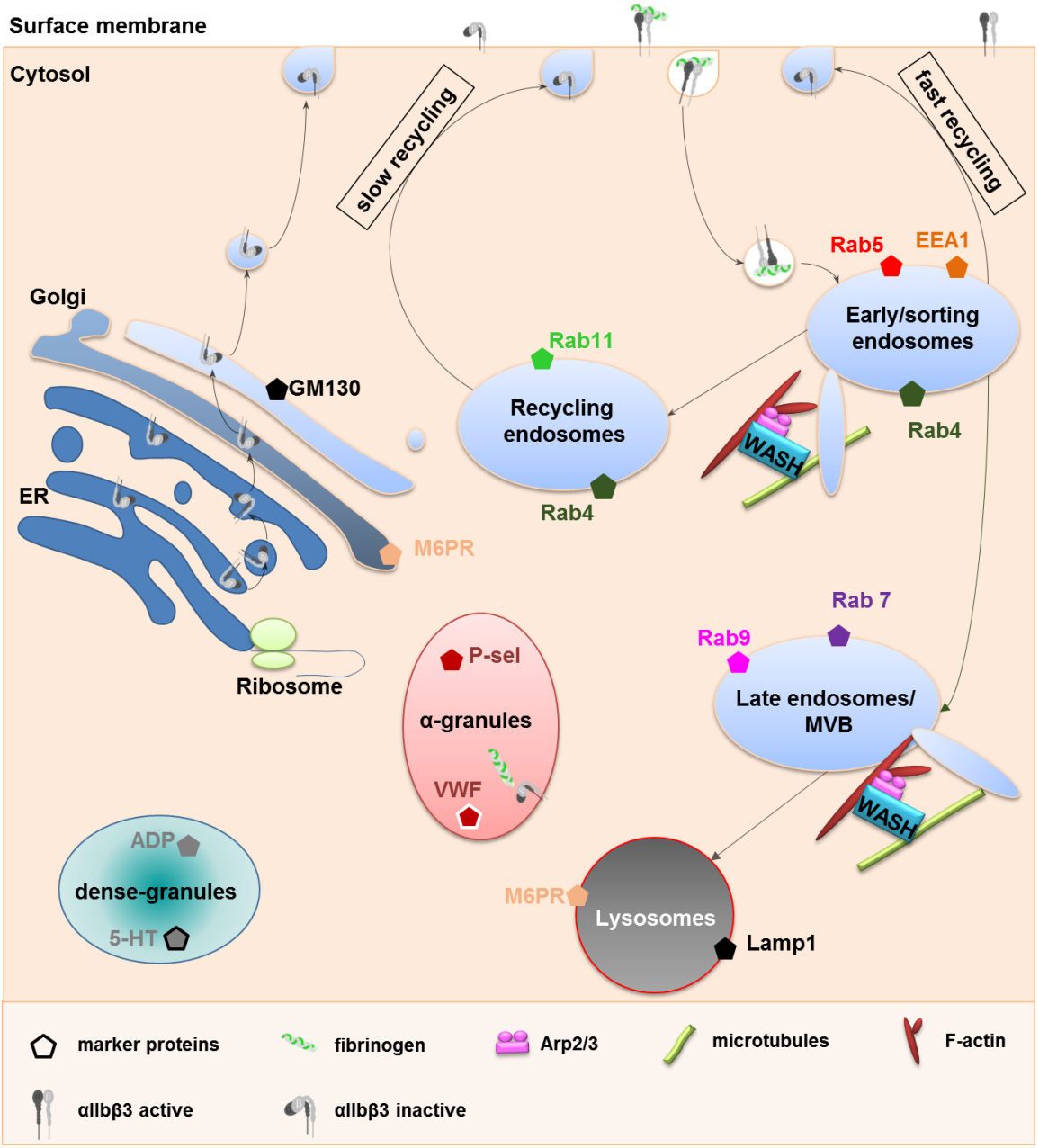

Figure 6.2.1: Putative model of integrin trafficking and colocalization of the WASH complex to various endocytic markers in platelets. According to immunofluorescence data from 3T3 cells, the WASH complex is localized to a restricted domain of endosomes where endosomal tubules are elongated with the support of F-actin networks and microtubules.[106] Fibrinogen from the blood plasma binds to αIIbβ3 integrin on platelets, gets internalized and stored in α-granules.[161] The αIIbβ3 integrin receptor can be recycled back to the surface membrane. Various endocytic markers are used to define the different compartments. Rab4 and Rab11 are localized on recycling endosomes. EEA1, Rab4 and Rab5 are markers for early/sorting endosomes. Rab7 and Rab9 are present on Late endosomes/multivesicular bodies (MVB). The Mannose-6-phosphate receptor (M6PR) and the golgin subfamily A member 2 (GM130) are localized on Golgi compartments. The Lysosomal-associated membrane protein 1 (Lamp1) and M6PR are a marker for lysosomes. Platelet α-granules store amongst others von Willebrand factor (VWF), P-selectin and fibrinogen. Platelet dense-granules store amongst others ADP and serotonin (5-HT). Adapted from [106].

localized in the cytoplasm, whereas inactive β1-integrins are rather found at the plasma membrane.[164] In these cancer cells both, active and inactive β1-integrins are endocytosed in a clathrin-dependent manner, however, the endocytosis rate of active β1-integrins is much higher. The platelet α2β1 integrin receptor binds, besides GPVI as the major signaling receptor, to collagen.[165] The collagen-binding capacity of α2β1 integrin is increased after stimulation with agonists (e.g. ADP) and induces collagen internalization. Flow cytometry analysis in human[166] platelets revealed that despite collagen internalization, the α2β1 surface expression does not significantly change upon activation. Interestingly, in Strumpellin-deficient platelets the β1-integrin surface expression was slightly increased, whereas no significant changes in the α2-integrin subunit surface expression were detected compared to controls (Table 5.2.2). This might suggest several aspects: 1) The α2β1 trafficking and recycling dynamics are much lower compared to αIIbβ3; 2) the remaining WASH complex activity in Strumpellin-deficient platelets is sufficient to maintain the surface expression of β1- and α2- integrin subunits but not for the highly expressed αIIb and β3 subunits or 3) in contrast to αIIbβ3 integrin, α2β1 integrin is not internalized during the lifetime of a non-activated platelet therefore the surface expression is not impaired in Strumpellin-deficient platelets. However, to understand the different mechanisms and recycling routes of receptor trafficking in platelets and megakaryocytes, especially microscopy-based colocalization studies are required with compartment specific markers as proposed in Figure 6.2.1.

6.3 Functional redundancy among different proteins might compensate for the loss of Macf1 in platelets

In this thesis, megakaryocyte- and platelet-specific knockout mice were used to assess the role of the cytoskeletal crosslinker protein MACF1 for platelet production and function. MACF1 has been described to be an important regulator of microtubules and F-actin in various cell types, such as endodermal cells[127], keratinocytes[126] and neurons[128]. However, alterations in platelet production, platelet activation, clot retraction, thrombus formation and hemostatic function were not detected in MACF1-deficient mice. This result is surprising because platelets undergo intensive shape change, activate integrins, release granules and transduce mechanical forces to fulfill their function, and these processes strongly depend on cytoskeletal rearrangement. Overall, only a subtle difference in spreading kinetics at the time point of 15 min was found. Thus, the experimental findings did not reveal an important role of MACF1 in

platelet physiology. However, MACF1 is expressed in wildtype mouse platelets, since two specific MACF1 protein bands were detected, conferring to the known Macf1a1-3 (500-620 kDa) and Macf1b (800 kDa) isoforms,[122] which were missing in lysates of MACF1-deficient platelets and megakaryocytes, demonstrating the loss of the protein in those cells (Figure 5.3.1). A compensatory mechanism by the other spectraplakin family member Dystonin can be excluded, since the isoforms Dystonin a and Dystonin b could not be detected by RT-PCR in control or mutant platelets (Figure 5.3.3). This finding is supported by proteomics studies on human and mouse platelets, which found MACF1 but not Dystonin expressed in platelets.[60,61]

Over the last few years, different ways of crosstalk between the actin and microtubule cytoskeleton have been discovered ranging from direct physical crosslinks to more indirect mechanisms, such as shared regulators of dynamical properties.[118] Other physical crosslinker proteins, besides spectraplakins, are the growth arrest-specific 2-like (GAS2-like) proteins. Members of the GAS2 family resemble spectraplakins as they possess both actin- and microtubule-binding regions, but lack the plakin domains.[167] Interestingly, Preciado López et al. engineered a minimal version of MACF1, the actin-binding, microtubule plus-end tracking protein, called TipAct, where the plakin domain and spectrin-repeat rod was replaced.[168] This short version was sufficient to crosslink and to enable mechanical feedback between actin and microtubule organization, implying that TipAct contains the key functional domains of spectraplakins. Thus, the GAS2 protein family might compensate for the lack of MACF1 in the knockout platelets. This family consists of the four members GAS2, GAS2-like 1 (Gas2L1), GAS2-like 2 and GAS2-like 3, of which only Gas2L1 seems to be expressed in platelets (protein copy number: 3074 copies of Gas2L1 and 1632 copies of MACF1 in mouse platelets,[61] 1600 copies of Gas2L1 and 1300 copies of MACF1 in human platelets[60]). To determine whether Gas2L1 is up- or downregulated in Macf1-deficient platelets, the protein expression was compared to lysates of control platelets by Western blot analysis. However, the Gas2L1 expression was comparable between platelet lysates from *Macf1*$^{+/+}$ *and Macf1*$^{-/-}$ mice (Figure 6.3.1). Formins are another group of cytoskeletal crosstalk regulators with DAAM1, mDia1 (DIAPH1) and FHOD1 as the major proteins expressed in platelets.[119] Studies on mDIA knockout mice revealed that the deficiency does not alter platelet activation, spreading and aggregation, presumably due to functional redundancy with other formin proteins.[119,173] However, a role of this protein in platelet formation was demonstrated by DIAPH1

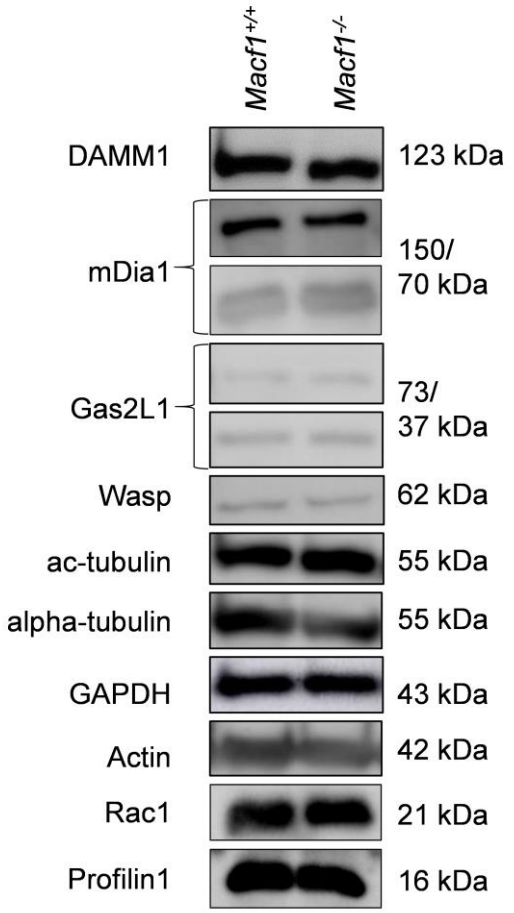

Figure 6.3.1: Normal expression of other cytoskeletal regulating proteins in MACF1-deficient platelets. Expression of different cytoskeleton regulatory proteins in *Macf1*$^{+/+}$ and *Macf1*$^{-/-}$ platelets was assessed by Western blot analysis. GAPDH served as a loading control (n = 3).

knockdown in cultured human megakaryocytes[170] and by the description of two unrelated pedigrees with a DIAPH1 R1213* variant.[171] Therefore, the expression of DAAM1, mDIA1 and the direct binding protein profilin 1, which was recently described to be an important regulator of actin and microtubule structure and dynamics in platelets, were determined. However, a compensatory up- or downregulation of these proteins in mutant platelets was not found (Figure 6.3.1). Nevertheless, it is intriguing to speculate that functional redundancy among different proteins mediating the cytoskeletal crosstalk may exist. But this requires further investigation.

7 OUTLOOK AND CONCLUDING REMARKS

Potential roles of platelet lamellipodia

In summary, the results of this dissertation show that Cyfip1-deficiency does not alter platelet biogenesis and has no major impact on platelet activation, but that Cyfip1 plays a crucial role for branching of actin filaments and consequently for lamellipodia formation *in vitro,* as published in *Blood* 2019.[172] By using the Cyfip1 knockout mouse model it was possible to demonstrate that lamellipodia formation is not required for the formation of a hemostatic plug or a thrombus. Moreover, Cyfip1-deficient mice maintained vascular integrity at the site of inflammation. Finally, these data suggest that megakaryocyte- and platelet-specific Cyfip1-deficient mice represent a unique mouse system to study the role of platelet lamellipodia in other platelet-dependent processes like the bundling of bacteria *in vivo*.[36] Further studies will be required to address this. Recently, another evolutionarily conserved regulator of actin-based protrusions termed CYRI (CYFIP-related Rac interactor), also known as Fam49 (Family of unknown function 49) was identified by the group of Laura Machesky.[173] Fam49 shares homology with Cyfip1 and is also able to directly interact with activated Rac1 *in vitro*. Knockdown of Fam49 by small interfering RNA (siRNA) in COS-7 cells promoted unusually large and broad lamellipodia. Fam49 was shown to regulate the duration and extent of cell protrusions. It was suggested that Fam49 could be a specific buffer for the WAVE complex-driven lamellipodia plasticity and so far, Fam49 is the only described negative regulator of the WAVE complex by competing with Cyfip1 for Rac1 binding. The analysis of Fam49 knockout mice and other proteins that are involved in the cytoskeletal composition and therefore the biophysical construction of platelets would be of high interest to understand which components are essential for platelet function, thrombus formation, maintenance of vascular integrity and the interaction with pathogens.

Understanding the mechanisms of platelet receptor trafficking

Within the five subunit-containing WASH complex, the WASH protein possesses the WCA region that mediates the activation of the Arp2/3 complex and thereby actin filament polymerization on endosomal vesicles. It was shown in melanocytes that the lack of the Strumpellin-subunit leads to a decreased protein abundance of the other WASH complex subunits.[162] Despite the Strumpellin-deficiency in those cells the WASH complex can still assemble and maintain a partial ability in activating the Arp2/3

complex.[162] It would be interesting to investigate if WASH-deficient megakaryocytes and platelets show a more pronounced decrease in αIIbβ3 expression compared to cells from Strumpellin-deficient mice used in this study. This could give further insights into the regulation of cargo sorting and receptor trafficking in platelets. Because how cells choose a specific internalization route (or routes) for different integrins is unclear and especially in platelets only poorly studied.[174] To identify specific recycling routes of integrins or other important cargos, costaining of the precise organelles with antibodies against the respective Rab GTPases or other endosomal markers like EEA1 could provide further information. Since Strumpellin overexpression studies can only be performed in megakaryocytes and not in platelets and currently no commercially available Strumpellin antibody is working specifically in immunofluorescence staining, the generation of such an antibody would be of great advantage.

Role of cytoskeletal crosslinking and interacting proteins

Although the results of this thesis show that the cytoskeletal crosslinking protein Macf1 is dispensable for thrombus formation and hemostasis, as published in *Scientific Reports* 2019,[175] it was recently published that the protein plays an important role in bone formation and osteoblast differentiation.[176] Other crosslinking proteins, besides spectraplakins, are the GAS2-like proteins which possess both actin- and microtubule-binding regions.[167] Although the expression of Gas2L1 was unaltered in Macf1-deficient platelets (Figure 6.3.1) it would be interesting to investigate if even the loss of Gas2L1 alone or of both Gas2L1 and Macf1 would affect platelet physiology. Even though Macf1 turned out to be dispensable for basic platelet function, further studies on other cytoskeletal crosslinking proteins in megakaryocytes and platelets would help to fully better understand the contribution of this group of proteins in platelet biology.

Furthermore, the role of intermediate filaments as proteins that interact with other cytoskeletal components and thereby mediate cytoskeletal crosstalk has only been poorly investigated in platelets and megakaryocytes. Intermediate filaments are composed of many related proteins that share similar structural and sequence components among each other. Based on their similarity these proteins are categorized into six types, whereas most types are cytoplasmic proteins except type V which is the nuclear laminin.[114] Despite many differences in size, structure and protein composition, the three main cytoskeletal components are in constant communication with each other.[114] Electron-microscopy studies provided the first evidence that

microtubules and intermediate filaments interact as they revealed their close association in fibroblasts. Treatment of fibroblasts with microtubule inhibitors like colchicine or nocodazole (inhibition of microtubule polymerization) leads to the reorganization of vimentin intermediate filaments.[177] The microtubule motors kinesin and dynein perform the movement of intermediate filaments along microtubules.[178] A close connection between keratin fibers and F-actin was also shown in fibroblasts. The treatment of murine epidermal keratinocytes with the actin inhibitor cytochalasin D disrupted the organization of keratin intermediate filament networks.[179] In neurons it was shown that the F-actin associated motor protein myosinVa associates with intermediate filaments and the deletion of the respective myosin Va gene results in an altered intermediate filament distribution within axons.[180]

In 1987 the vimentin-like protein, categorized as a type III intermediate filament, was detected in human and bovine platelets[181] and in 2013 immunofluorescence staining and confocal microscopy revealed that the intermediate filaments desmin and vimentin are associated with actin filaments in human platelets.[117] Vimentin is also listed in a human proteomics database (protein copy number per platelet = 2400), whereas it was not detected in a murine platelet proteomic approach.[60,61] Latest studies report that recombinant human vimentin binds to P-selectin, thereby blocking neutrophil capture and rolling on platelets and the endothelium.[182] Taken together, these publications indicate that intermediate filaments and their role in mediating the cytoskeletal crosstalk in platelets and megakaryocytes might have been underestimated until now.

8 REFERENCES

1. Machlus, K. R. & Italiano, J. E. The incredible journey: From megakaryocyte development to platelet formation. *J. Cell Biol.* **201**, 785–796 (2013).
2. Junt, T. *et al.* Dynamic Visualization of Thrombopoiesis Within Bone Marrow. *Science (80-.).* **317**, 1767–1771 (2007).
3. Italiano, J. E., Lecine, P., Shivdasani, R. A. & Hartwig, J. H. Blood platelets are assembled principally at the ends of proplatelet processes produced by differentiated megakaryocytes. *J. Cell Biol.* **147**, 1299–1312 (1999).
4. Michelson, A. D. *Platelets - Thrid Edition*. *ELSEVIER* (2013). doi:10.1017/CBO9781107415324.004.
5. Kaushansky, K. *et al.* Promotion of megakaryocyte progenitor expansion and differentiation by the c-Mpl ligand thrombopoietin. *Nature* **369**, 568–571 (1994).
6. Giaccia, A. *et al.* Thrombocytopenia in c-mpl-Deficient Mice. **265**, (1994).
7. Geddis, A. E. & Kaushansky, K. Endomitotic megakaryocytes form a midzone in anaphase but have a deficiency in cleavage furrow formation. *Cell Cycle* **5**, 538–545 (2006).
8. Machlus, K. R., Thon, J. N. & Italiano, J. E. Interpreting the developmental dance of the megakaryocyte: A review of the cellular and molecular processes mediating platelet formation. *Br. J. Haematol.* **165**, 227–236 (2014).
9. Long, M. W., Williams, N. & Ebbe, S. Immature megakaryocytes in the mouse: Physical characteristics, cell cycle status, and in vitro responsiveness to thrombopoietic stimulatry factor. *Blood* **59**, 569–576 (1982).
10. Ogawa, M. Differentiation and proliferation of hematopoietic stem cells. *Blood* **81**, 2844–2853 (1993).
11. Lefrançais, E. *et al.* The lung is a site of platelet biogenesis and a reservoir for haematopoietic progenitors. *Nature* **544**, 105–109 (2017).
12. Schulze, H. *et al.* Characterization of the megakaryocyte demarcation membrane system and its role in thrombopoiesis. *Blood* **107**, 3868–3875 (2006).
13. Antkowiak, A. *et al.* Cdc42-dependent F-actin dynamics drive structuration of the demarcation membrane system in megakaryocytes. *J. Thromb. Haemost.* **14**, 1268–1284 (2016).

14. Noetzli, L. J., French, S. L. & Machlus, K. R. New insights into the differentiation of megakaryocytes from hematopoietic progenitors. *Arterioscler. Thromb. Vasc. Biol.* **39**, 1288–1300 (2019).

15. Geue, S. *et al.* Pivotal Role of PDK1 in Megakaryocyte Cytoskeletal Dynamics and Polarization during Platelet Biogenesis. *Blood* (2019) doi:10.1182/blood.2019000185.

16. Bender, M. *et al.* ADF/n-cofilin-dependent actin turnover determines platelet formation and sizing. *Blood* **116**, 1767–75 (2010).

17. Tablin, F., Castro, M. & Leven, R. M. Blood platelet formation in vitro. The role of the cytoskeleton in megakaryocyte fragmentation. *J. Cell Sci.* **97**, 59–70 (1990).

18. Bender, M. *et al.* Microtubule sliding drives proplatelet elongation and is dependent on cytoplasmic dynein. *Blood* **125**, 860–869 (2015).

19. Aurbach, K., Spindler, M., Haining, E. J., Bender, M. & Pleines, I. Blood collection, platelet isolation and measurement of platelet count and size in mice—a practical guide. *Platelets* **30**, 698–707 (2018).

20. Schmitt, A., Guichard, J., Massé, J., Debili, N. & Cramer, E. M. Of mice and men: Comparison of the ultrastructure of megakaryocytes and platelets. *Exp. Hematol.* **29**, 1295–1302 (2001).

21. Meng, R. *et al.* Defective release of α granule and lysosome contents from platelets in mouse Hermansky-Pudlak syndrome models. *Blood* **125**, 1623–1632 (2015).

22. Flaumenhaft, R. & Sharda, A. The life cycle of platelet granules. *F1000Research* **7**, 1–12 (2018).

23. Radomski, M. W., Palmer, R. M. J. & Moncada, S. The anti-aggregating properties of vascular endothelium: interactions between prostacyclin and nitric oxide. *Br. J. Pharmacol.* **92**, 639–646 (1987).

24. Vögtle, T., Cherpokova, D., Bender, M. & Nieswandt, B. Targeting platelet receptors in thrombotic and thrombo-inflammatory disorders. *Hamostaseologie* **35**, 235–243 (2015).

25. Nieswandt, B., Pleines, I. & Bender, M. Platelet adhesion and activation mechanisms in arterial thrombosis and ischaemic stroke. *J. Thromb. Haemost.*

9, 92–104 (2011).

26. Versteeg, H. H., Heemskerk, J. W. M., Levi, M. & Reitsma, P. H. New Fundamentals in hemostasis. *Physiol. Rev.* **93**, 327–358 (2013).

27. Welsh, J. D. *et al.* A systems approach to hemostasis: 1. The interdependence of thrombus architecture and agonist movements in the gaps between platelets. *Blood* **124**, 1808–1815 (2014).

28. Stalker, T. J. *et al.* A systems approach to hemostasis: 3. Thrombus consolidation regulates intrathrombus solute transport and local thrombin activity. *Blood* **124**, 1824–1831 (2014).

29. Sakariassen, K. S., Orning, L. & Turitto, V. T. The impact of blood shear rate on arterial thrombus formation. *Futur. Sci. OA* **1**, (2015).

30. Aarts, P. A. M. M. *et al.* Blood platelets are concentrated near the wall and red blood cells, in the center in flowing blood. *Arteriosclerosis* **8**, 819–824 (1988).

31. Papaioannou, T. & Stefanadis, C. Vascular Wall Shear Stress: Basic Principles and Methods. *Hell. J Cardiol* **46**, 9–15 (2005).

32. McCarty, O. J. T. *et al.* Rac1 is essential for platelet lamellipodia formation and aggregate stability under flow. *J. Biol. Chem.* **280**, 39474–39484 (2005).

33. Pleines, I. *et al.* Rac1 is essential for phospholipase C-γ2 activation in platelets. *Pflugers Arch. Eur. J. Physiol.* **457**, 1173–1185 (2009).

34. Aslan, J. E. & McCarty, O. J. T. Rho GTPases in platelet function. *J. Thromb. Haemost.* **11**, 35–46 (2013).

35. Yusuf, M. Z. *et al.* Prostacyclin reverses platelet stress fibre formation causing platelet aggregate instability. *Sci. Rep.* **7**, 1–11 (2017).

36. Paul, D. S. *et al.* Deletion of the Arp2/3 complex in megakaryocytes leads to microthrombocytopenia in mice. *Blood Adv.* **1**, 1398–1408 (2017).

37. Gunning, P. W., Ghoshdastider, U., Whitaker, S., Popp, D. & Robinson, R. C. The evolution of compositionally and functionally distinct actin filaments. *J. Cell Sci.* **128**, 2009–2019 (2015).

38. Herman, I. M. Actin isoforms. *Curr. Opin. Cell Biol.* **5**, 48–55 (1993).

39. Hundt, N. *et al.* Molecular mechanisms of disease-related human β-actin mutations p.R183W and p.E364K. *FEBS J.* **281**, 5279–5291 (2014).

40. Pollard, T. D. & Goldman, R. D. *The Cytoskeleton*. *Cold Spring Harbor Laboratory Press* (Cold Spring Harbor Laboratory Press, 2017).

41. Mannherz, H. G. *The Actin Cytoskeleton and Bacterial Infection*. *Springer; Current Topics in Microbiology and Immunology* vol. 399 (2017).

42. Kabsch, W., Mannherz, H. G., Suck, D., Pai, E. F. & Holmes, K. C. Atomic structure of the actin: DNase I complex . *Nature* **347**, 37–44 (1990).

43. Hartwig, J. H. & DeSisto, M. The cytoskeleton of the resting human blood platelet: Structure of the membrane skeleton and its attachment to actin filaments. *J. Cell Biol.* **112**, 407–425 (1991).

44. Hartwig, J. H. Mechanisms of Actin Rearrangements Mediating Platelet Activation. *J. CellBiology* **118**, (1992).

45. Jennings, L. K., Fox, J. E. B., Edwards, H. H. & Phillips, D. R. Changes in the cytoskeletal structure of human platelets following thrombin activation. *J. Biol. Chem.* **256**, 6927–6932 (1981).

46. Rouiller, I. *et al.* The structural basis of actin filament branching by the Arp2/3 complex. *J. Cell Biol.* **180**, 887–895 (2008).

47. Kahr, W. H. A. *et al.* Loss of the Arp2/3 complex component ARPC1B causes platelet abnormalities and predisposes to inflammatory disease. *Nat. Commun.* **8**, 1–14 (2017).

48. Nurden, P. *et al.* Thrombocytopenia resulting from mutations in filamin A can be expressed as an isolated syndrome. *Blood* **118**, 5928–5937 (2011).

49. Berrou, E. *et al.* Heterogeneity of platelet functional alterations in patients with filamin a mutations. *Arterioscler. Thromb. Vasc. Biol.* **33**, 11–18 (2013).

50. Robinson, R. C. *et al.* Crystal Structure of Arp2/3 Complex. *Science (80-.).* **294**, 1679–1685 (2001).

51. Alekhina, O., Burstein, E. & Billadeau, D. D. Cellular functions of WASP family proteins at a glance. *J. Cell Sci.* **130**, 2235–2241 (2017).

52. Kurisu, S. & Takenawa, T. The WASP and WAVE family proteins. *Genome Biol.* **10**, 1–9 (2009).

53. Snapper, S. B. & Rosen, F. S. The Wiskott-Aldrich Syndrome Protein (WASP): Roles in Signaling and Cytoskeletal Organization. *Annu. Rev. Immunol.* **17**, 905–

929 (1999).

54. Rohatgi, R., Ho, H. Y. H. & Kirschner, M. W. Mechanism of N-WASP activation by CDC42 and phosphatidylinositol 4,5-bisphosphate. *J. Cell Biol.* **150**, 1299–1309 (2000).

55. Moulding, D. A., Record, J., Malinova, D. & Thrasher, A. J. Actin cytoskeletal defects in immunodeficiency. *Immunol. Rev.* **256**, 282–299 (2013).

56. Sabri, S. *et al.* Deficiency in the Wiskott-Aldrich protein induces premature proplatelet formation and platelet production in the bone marrow compartment. *Blood* **108**, 134–140 (2006).

57. Schachtner, H. *et al.* Megakaryocytes assemble podosomes that degrade matrix and protrude through basement membrane. *Blood* **121**, 2542–2552 (2013).

58. Poulter, N. S. *et al.* Platelet actin nodules are podosome-like structures dependent on Wiskott-Aldrich syndrome protein and ARP2/3 complex. *Nat. Commun.* **6**, 1–15 (2015).

59. Hao, Y. H. *et al.* Regulation of WASH-dependent actin polymerization and protein trafficking by ubiquitination. *Cell* **152**, 1051–1064 (2013).

60. Burkhart, J. M. *et al.* The first comprehensive and quantitative analysis of human platelet protein composition allows the comparative analysis of structural and functional pathways. *Blood* **120**, 73–82 (2012).

61. Zeiler, M., Moser, M. & Mann, M. Copy Number Analysis of the Murine Platelet Proteome Spanning the Complete Abundance Range. *Mol. Cell. Proteomics* **13**, 3435–3445 (2014).

62. Chen, Z. *et al.* Structure and control of the actin regulatory WAVE complex. *Nature* **468**, 533–538 (2010).

63. Campellone, K. G., Webb, N. J., Znameroski, E. A. & Welch, M. D. WHAMM Is an Arp2/3 Complex Activator That Binds Microtubules and Functions in ER to Golgi Transport. *Cell* **134**, 148–161 (2008).

64. Schlüter, K. *et al.* JMY is involved in anterograde vesicle trafficking from the trans-Golgi network. *Eur. J. Cell Biol.* **93**, 194–204 (2014).

65. Zuchero, J. B., Coutts, A. S., Quinlan, M. E., Thangue, N. B. La & Mullins, R. D. p53-cofactor JMY is a multifunctional actin nucleation factor. *Nature Cell Biology*

vol. 11 451–459 (2009).

66. Schenck, A., Bardoni, B., Moro, A., Bagni, C. & Mandel, J. L. A highly conserved protein family interacting with the fragile X mental retardation protein (FMRP) and displaying selective interactions with FMRP-related proteins FXR1P and FXR2P. *Proc. Natl. Acad. Sci. U. S. A.* **98**, 8844–9 (2001).

67. Napoli, I. *et al.* The fragile X syndrome protein represses activity-dependent translation through CYFIP1, a new 4E-BP. *Cell* **134**, 1042–54 (2008).

68. Sahoo, T. *et al.* Microarray based comparative genomic hybridization testing in deletion bearing patients with Angelman syndrome: genotype-phenotype correlations. *J. Med. Genet.* **43**, 512–6 (2006).

69. Abekhoukh, S. & Bardoni, B. CYFIP family proteins between autism and intellectual disability: links with Fragile X syndrome. *Front. Cell. Neurosci.* **8**, 1–9 (2014).

70. Sayad, A., Ranjbaran, F., Ghafouri-Fard, S., Arsang-Jang, S. & Taheri, M. Expression Analysis of CYFIP1 and CAMKK2 Genes in the Blood of Epileptic and Schizophrenic Patients. *J. Mol. Neurosci.* **65**, 336–342 (2018).

71. Silva, A. I. *et al.* Cyfip1 haploinsufficient rats show white matter changes, myelin thinning, abnormal oligodendrocytes and behavioural inflexibility. *Nat. Commun.* **10**, (2019).

72. Bozdagi, O. *et al.* Haploinsufficiency of Cyfip1 produces fragile X-like phenotypes in mice. *PLoS One* **7**, (2012).

73. Bonaccorso, C. M. *et al.* Fragile X mental retardation protein (FMRP) interacting proteins exhibit different expression patterns during development. *Int. J. Dev. Neurosci.* **42**, 15–23 (2015).

74. Derivery, E., Lombard, B., Loew, D. & Gautreau, A. The wave complex is intrinsically inactive. *Cell Motil. Cytoskeleton* **66**, 777–790 (2009).

75. Kobayashi, K. *et al.* p140Sra-1 (specifically Rac1-associated protein) is a novel specific target for Rac1 small GTPase. *J. Biol. Chem.* **273**, 291–295 (1998).

76. Gautreau, A. *et al.* Purification and architecture of the ubiquitous Wave complex. *Proc. Natl. Acad. Sci. U. S. A.* **101**, 4379–4383 (2004).

77. Blagg, S. L., Stewart, M., Sambles, C. & Insall, R. H. PIR121 Regulates

Pseudopod Dynamics and SCAR Activity in Dictyostelium. *Curr. Biol.* **13**, 1480–1487 (2003).

78. Rogers, S. L., Wiedemann, U., Stuurman, N. & Vale, R. D. Molecular requirements for actin-based lamella formation in Drosophila S2 cells. *J. Cell Biol.* **162**, 1079–1088 (2003).

79. Oda, A. *et al.* WAVE/ Scars in platelets. *HTVBiol* **105**, 3141–3149 (2004).

80. Calaminus, S. D. J. *et al.* A major role for Scar/WAVE-1 downstream of GPVI in platelets. *J. Thromb. Haemost.* **5**, 535–41 (2007).

81. Dahl, J. P. *et al.* Characterization of the WAVE1 knock-out mouse: implications for CNS development. *J. Neurosci.* **23**, 3343–52 (2003).

82. Eto, K. *et al.* The WAVE2/Abi1 complex differentially regulates megakaryocyte development and spreading: Implications for platelet biogenesis and spreading machinery. *Blood* **110**, 3637–3647 (2007).

83. Innocenti, M. *et al.* Abi1 is essential for the formation and activation of a WAVE2 signalling complex. *Nat. Cell Biol.* **6**, 319–327 (2004).

84. Steffen, A. *et al.* Sra-1 and Nap1 link Rac to actin assembly driving lamellipodia formation. *EMBO J.* **23**, 749–759 (2004).

85. Valdmanis, P. N. *et al.* Mutations in the KIAA0196 Gene at the SPG8 Locus Cause Hereditary Spastic Paraplegia. *Am. J. Hum. Genet.* **80**, 152–161 (2007).

86. De Bot, S. T. *et al.* Pure adult-onset Spastic Paraplegia caused by a novel mutation in the KIAA0196 (SPG8) gene. *J. Neurol.* **260**, 1765–1769 (2013).

87. Jahic, A. *et al.* A novel strumpellin mutation and potential pitfalls in the molecular diagnosis of hereditary spastic paraplegia type SPG8. *J. Neurol. Sci.* **347**, 372–374 (2014).

88. Schule, R. & Schols, L. Genetics of hereditary spastic paraplegias. *Semin. Neurol.* **31**, 484–493 (2011).

89. Novarino, G. *et al.* Exome sequencing links corticospinal motor neuron disease to common neurodegenerative disorders. *Science (80-.).* **343**, 506–511 (2014).

90. Clemen, C. S. *et al.* Strumpellin is a novel valosin-containing protein binding partner linking hereditary spastic paraplegia to protein aggregation diseases. *Brain* **133**, 2920–2941 (2010).

91. Gomez, T. S., Gorman, J. a., Artal-Martinez de Narvajas, A., Koenig, A. O. & Billadeau, D. D. Trafficking defects in WASH-knockout fibroblasts originate from collapsed endosomal and lysosomal networks. *Mol. Biol. Cell* **23**, 3215–3228 (2012).

92. Jahic, A. *et al.* The spectrum of KIAA0196 variants, and characterization of a murine knockout: Implications for the mutational mechanism in hereditary spastic paraplegia type SPG8. *Orphanet J. Rare Dis.* **10**, 1–10 (2015).

93. Jia, D. Da *et al.* WASH and WAVE actin regulators of the Wiskott-Aldrich syndrome protein (WASP) family are controlled by analogous structurally related complexes. *Proc. Natl. Acad. Sci.* **107**, 10442–10447 (2010).

94. Gomez, T. S. & Billadeau, D. D. A FAM21-Containing WASH Complex Regulates Retromer-Dependent Sorting. *Dev. Cell* **17**, 699–711 (2009).

95. Seaman, M. N. J. The retromer complex - endosomal protein recycling and beyond. *J. Cell Sci.* **125**, 4693–4702 (2012).

96. Gautreau, A., Oguievetskaia, K. & Ungermann, C. Function and regulation of the endosomal fusion and fission machineries. *Cold Spring Harb. Perspect. Biol.* **6**, (2014).

97. Jia, D., Gomez, T. S., Billadeau, D. D. & Rosen, M. K. Multiple repeat elements within the FAM21 tail link the WASH actin regulatory complex to the retromer. *Mol. Biol. Cell* **23**, 2352–2361 (2012).

98. Zech, T., Calaminus, S. D. J. & Machesky, L. M. Actin on trafficking: Could actin guide directed receptor transport? *Cell Adhes. Migr.* **6**, 476–481 (2012).

99. Caswell, P. & Norman, J. Endocytic transport of integrins during cell migration and invasion. *Trends in Cell Biology* vol. 18 257–263 (2008).

100. Insall, R. H. & Machesky, L. M. Actin Dynamics at the Leading Edge: From Simple Machinery to Complex Networks. *Dev. Cell* **17**, 310–322 (2009).

101. Anitei, M. & Hoflack, B. Bridging membrane and cytoskeleton dynamics in the secretory and endocytic pathways. *Nature Cell Biology* vol. 14 11–19 (2012).

102. Collins, A., Warrington, A., Taylor, K. A. & Svitkina, T. Structural organization of the actin cytoskeleton at sites of clathrin-mediated endocytosis. *Curr. Biol.* **21**, 1167–1175 (2011).

103. Ferguson, S. *et al.* Coordinated Actions of Actin and BAR Proteins Upstream of Dynamin at Endocytic Clathrin-Coated Pits. *Dev. Cell* **17**, 811–822 (2009).

104. Duleh, S. N. & Welch, M. D. WASH and the Arp2/3 complex regulate endosome shape and trafficking. *Cytoskeleton* **67**, 193–206 (2010).

105. Zech, T. *et al.* The Arp2/3 activator WASH regulates α5β1-integrin-mediated invasive migration. *J. Cell Sci.* **124**, 3753–3759 (2011).

106. Derivery, E. *et al.* The Arp2/3 Activator WASH Controls the Fission of Endosomes through a Large Multiprotein Complex. *Dev. Cell* **17**, 712–23 (2009).

107. Conde, C. & Cáceres, A. Microtubule assembly, organization and dynamics in axons and dendrites. *Nat. Rev. Neurosci.* **10**, 319–332 (2009).

108. Findeisen, P. *et al.* Six subgroups and extensive recent duplications characterize the evolution of the eukaryotic tubulin protein family. *Genome Biol. Evol.* **6**, 2274–2288 (2014).

109. Gadadhar, S., Bodakuntla, S., Natarajan, K. & Janke, C. The tubulin code at a glance. *J. Cell Sci.* **130**, 1347–1353 (2017).

110. Schwer, H. D. *et al.* A lineage-restricted and divergent β-tubulin isoform is essential for the biogenesis, structure and function of blood platelets. *Curr. Biol.* **11**, 579–586 (2001).

111. Iancu-Rubin, C. *et al.* Panobinostat (LBH589)-induced acetylation of tubulin impairs megakaryocyte maturation and platelet formation. *Exp. Hematol.* **40**, 564–574 (2012).

112. Messaoudi, K. *et al.* Critical role of the HDAC6-cortactin axis in human megakaryocyte maturation leading to a proplatelet-formation defect. *Nat. Commun.* **8**, (2017).

113. Sadoul, K. *et al.* HDAC6 controls the kinetics of platelet activation. *Blood* **120**, 4215–4218 (2012).

114. Chang, L. & Goldman, R. D. Intermediate filaments mediate cytoskeletal crosstalk. *Nat. Rev. Mol. Cell Biol.* **5**, 601–613 (2004).

115. Zimek, A., Stick, R. & Weber, K. Genes coding for intermediate filament proteins: Common features and unexpected differences in the genomes of humans and

the teleost fish Fugu rubripes. *J. Cell Sci.* **116**, 2295–2302 (2003).

116. Strelkov, S. V., Herrmann, H. & Aebi, U. Molecular architecture of intermediate filaments. *BioEssays* **25**, 243–251 (2003).

117. Cerecedo, D. *et al.* Haemostatic role of intermediate filaments in adhered platelets: Importance of the membranous system stability. *J. Cell. Biochem.* **114**, 2050–2060 (2013).

118. Dogterom, M. & Koenderink, G. H. Actin – microtubule crosstalk in cell biology. *Nat. Rev. Mol. Cell Biol.* **20**, 38–54 (2019).

119. Zuidscherwoude, M., Green, H. L. H. H. & Thomas, S. G. Formin proteins in megakaryocytes and platelets: regulation of actin and microtubule dynamics. *Platelets* **30**, 1–8 (2018).

120. Green, H. L. H., Zuidscherwoude, M. & Thomas, S. G. The FH2 domain of formin proteins is critical for platelet cytoskeletal dynamics. *bioRxiv* 589861 (2019) doi:10.1101/589861.

121. Fuchs, E. & Karakesisoglou, I. Bridging cytoskeletal intersections. *Genes Dev.* **15**, 1–14 (2001).

122. Suozzi, K. C., Wu, X. & Fuchs, E. Spectraplakins: Master orchestrators of cytoskeletal dynamics. *J. Cell Biol.* **197**, 465–475 (2012).

123. Roper, K., Röper, K., Gregory, S. L. & Brown, N. H. The `Spectraplakins': cytoskeletal giants with characteristics of both spectrin and plakin families. *J. Cell Sci.* **115**, 4215–4225 (2002).

124. Hu, L. *et al.* Isoforms, structures, and functions of versatile spectraplakin MACF1. *BMB Rep.* **49**, 37–44 (2016).

125. Chen, H. J. *et al.* The role of microtubule actin cross-linking factor 1 (MACF1) in the Wnt signaling pathway. *Genes Dev.* **1**, 1933–1945 (2006).

126. Wu, X., Kodama, A. & Fuchs, E. ACF7 Regulates Cytoskeletal-Focal Adhesion Dynamics and Migration and Has ATPase Activity. *Cell* **135**, 137–148 (2008).

127. Kodama, A., Karakesisoglou, I., Wong, E., Vaezi, A. & Fuchs, E. ACF7: An essential integrator of microtubule dynamics. *Cell* **115**, 343–354 (2003).

128. Sanchez-Soriano, N. *et al.* Mouse ACF7 and Drosophila Short stop modulate filopodia formation and microtubule organisation during neuronal growth. *J. Cell*

Sci. **122**, 2534–2542 (2009).

129. Brown, N. H. Spectraplakins: The Cytoskeleton's Swiss Army Knife. *Cell* **135**, 16–18 (2008).

130. Branehög, I., Ridell, B., Swolin, B. & Weinfeld, A. Megakaryocyte Quantifications in Relation to Thrombokinetics in Primary Thrombocythaemia and Allied Diseases. *Scand. J. Haematol.* **15**, 321–332 (1975).

131. Falet, H., Hoffmeister, K. M., Neujahr, R. & Hartwig, J. H. Normal Arp2/3 complex activation in platelets lacking WASp. *Blood* **100**, 2113–2122 (2002).

132. Tiedt, R., Schomber, T., Hao-Shen, H., Skoda, R. C. & Look, A. T. Pf4-Cre transgenic mice allow the generation of lineage-restricted gene knockouts for studying megakaryocyte and platelet function in vivo. *Blood* **109**, 1503–6 (2007).

133. Rodríguez, C. I. *et al.* High-efficiency deleter mice show that FLPe is an alternative to Cre-loxP. *Nat. Genet.* **25**, 139–140 (2000).

134. Skarnes, W. C. *et al.* A conditional knockout resource for the genome – wide study of mouse gene function. *Nature* **474**, 337–342 (2013).

135. Tucker, K. L., Wang, Y., Dausman, J. & Jaenisch, R. A transgenic mouse strain expressing four drug-selectable marker genes. *Nucleic Acids Res.* **25**, 3745–3746 (1997).

136. Brownstein, D. G. Manipulating the Mouse Embryo: A Laboratory Manual. Third Edition. By Andras Nagy, Marina Gertsenstein, Kristina Vintersten, and Richard Behringer. *Q. Rev. Biol.* **78**, 365 (2003).

137. van de Linde, S. *et al.* Direct stochastic optical reconstruction microscopy with standard fluorescent probes. *Nat. Protoc.* **6**, 991–1009 (2011).

138. Wolter, S. *et al.* rapidSTORM: accurate, fast open-source software for localization microscopy. *Nat. Methods* **9**, 1040 (2012).

139. Deppermann, C. *et al.* Platelet secretion is crucial to prevent bleeding in the ischemic brain but not in the inflamed skin or lung in mice. *Blood* **129**, 1702–1706 (2017).

140. Kawamoto, T. Use of a new adhesive film for the preparation of multi-purpose fresh-frozen sections from hard tissues, whole-animals, insects and plants. *Arch. Histol. Cytol.* **66**, 123–143 (2003).

141. Pollitt, A. Y. & Insall, R. H. WASP and SCAR/WAVE proteins: the drivers of actin assembly. *J. Cell Sci.* **122**, 2575–2578 (2009).

142. Davidson, A. J. & Insall, R. H. Actin-Based Motility : WAVE Regulatory Complex Structure Reopens Old SCARs. *Curr. Biol.* **21**, R66–R68.

143. Spindler, M. *et al.* ADAP deficiency impairs megakaryocyte polarization with ectopic proplatelet release and causes microthrombocytopenia. *Blood* **132**, 635–646 (2018).

144. Heilemann, M. *et al.* Subdiffraction-Resolution Fluorescence Imaging with Conventional Fluorescent Probes. *Angew. Chemie Int. Ed.* **47**, 6172–6176 (2008).

145. Bender, M. *et al.* Megakaryocyte-specific Profilin1-deficiency alters microtubule stability and causes a Wiskott-Aldrich syndrome-like platelet defect. *Nat. Commun.* **5**, 4746 (2014).

146. Kuijpers, M. J. E. *et al.* Key Role of Platelet Procoagulant Activity in Tissue Factor- and Collagen-Dependent Thrombus Formation in Arterioles and Venules In Vivo Differential Sensitivity to Thrombin Inhibition. *Microcirculation* **15**, 269–282 (2008).

147. Munnix, I. C. A. *et al.* The Glycoprotein VI-Phospholipase Cγ2 Signaling Pathway Controls Thrombus Formation Induced by Collagen and Tissue Factor In Vitro and In Vivo. *Arter. Thromb Vasc Biol.* 2673–2678 (2005) doi:10.1161/01.ATV.0000193568.71980.4a.

148. Syvannarath, V., Lamrani, L., Goerge, T., Nieswandt, B. & Jandrot-perrus, M. Single platelets seal neutrophil-induced vascular breaches via GPVI during immune-complex – mediated in fl ammation in mice. **126**, 1017–1027 (2015).

149. Goerge, T. *et al.* Inflammation induces hemorrhage in thrombocytopenia. *Blood* **111**, 4958–4964 (2008).

150. Harbour, M. E., Breusegem, S. Y. & Seaman, M. N. J. Recruitment of the endosomal WASH complex is mediated by the extended 'tail' of Fam21 binding to the retromer protein Vps35. *Biochem. J.* **442**, 209–220 (2012).

151. Karakesisoglou, I., Yang, Y. & Fuchs, E. An epidermal plakin that integrates actin and microtubule networks at cellular junctions. *J. Cell Biol.* **149**, 195–208 (2000).

152. Durrant, T. N., Van Den Bosch, M. T. & Hers, I. Integrin αIIbβ3 outside-in

signaling. *Blood* **130**, 1607–1619 (2017).

153. Di Buduo, C. A. *et al.* Programmable 3D silk bone marrow niche for platelet generation ex vivo and modeling of megakaryopoiesis pathologies. *Blood* **125**, 2254–2264 (2015).

154. Ito, Y. *et al.* Turbulence Activates Platelet Biogenesis to Enable Clinical Scale Ex Vivo Production. *Cell* **174**, 636-648.e18 (2018).

155. Moreau, T. *et al.* Large-scale production of megakaryocytes from human pluripotent stem cells by chemically defined forward programming. *Nat. Commun.* **7**, (2016).

156. Thon, J. N. *et al.* Platelet bioreactor-on-a-chip. *Blood* **124**, (2014).

157. Agbani, E. O. *et al.* Coordinated Membrane Ballooning and Procoagulant Spreading in Human Platelets. *Circulation* **132**, 1414–1424 (2015).

158. Krause, M. & Gautreau, A. Steering cell migration: Lamellipodium dynamics and the regulation of directional persistence. *Nat. Rev. Mol. Cell Biol.* **15**, 577–590 (2014).

159. Gaertner, F. *et al.* Migrating Platelets Are Mechano-scavengers that Collect and Bundle Bacteria. *Cell* **171**, 1368-1382.e23 (2017).

160. Léon, C. *et al.* Megakaryocyte-restricted MYH9 inactivation dramatically affects hemostasis while preserving platelet aggregation and secretion. *Blood* **110**, 3183–3191 (2007).

161. Nieswandt, B., Varga-Szabo, D. & Elvers, M. Integrins in platelet activation. *J. Thromb. Haemost.* **7**, 206–209 (2009).

162. Tyrrell, B. J. *et al.* Loss of strumpellin in the melanocytic lineage impairs the WASH Complex but does not affect coat colour. *Pigment Cell Melanoma Res.* **29**, 559–571 (2016).

163. Hodivala-Dilke, K. M. *et al.* β3-integrin-deficient mice are a model for Glanzmann thrombasthenia showing placental defects and reduced survival. *J. Clin. Invest.* **103**, 229–238 (1999).

164. Arjonen, A., Alanko, J., Veltel, S. & Ivaska, J. Distinct Recycling of Active and Inactive β1 Integrins. *Traffic* **13**, 610–625 (2012).

165. Nieswandt, B. & Watson, S. P. Platelet-collagen interaction: Is GPVI the central

receptor? *Blood* **102**, 449–461 (2003).

166. Wang, Z., Leisner, T. M. & Parise, L. V. Platelet α2β1 integrin activation: Contribution of ligand internalization and the α2-cytoplasmic domain. *Blood* **102**, 1307–1315 (2003).

167. Stroud, M. J. *et al.* GAS2-like proteins mediate communication between microtubules and actin through interactions with end-binding proteins. *J. Cell Sci.* **127**, 2672–82 (2014).

168. López, M. P. *et al.* Actin-microtubule coordination at growing microtubule ends. *Nat. Commun.* **5**, 4778 (2014).

169. Thomas, S. G., Calaminus, S. D. J., Machesky, L. M., Alberts, A. S. & Watson, S. P. G-protein coupled and ITAM receptor regulation of the formin FHOD1 through Rho kinase in platelets. *J. Thromb. Haemost.* **9**, 1648–1651 (2011).

170. Pan, J. *et al.* The formin DIAPH1 (mDia1) regulates megakaryocyte proplatelet formation by remodeling the actin and microtubule cytoskeletons. *Blood* **124**, 3967–77 (2014).

171. Stritt, S. *et al.* A gain-of-function variant in DIAPH1 causes dominant macrothrombocytopenia and hearing loss. *Blood* **127**, 2903–2914 (2016).

172. Schurr, Y. *et al.* Platelet lamellipodium formation is not required for thrombus formation and stability. *Blood* **134**, 2318–2329 (2019).

173. Batista, M., Insall, R. H. & Machesky, L. M. Fam49/CYRI interacts with Rac1 and locally suppresses protrusions. *Nat. Cell Biol.* doi:10.1038/s41556-018-0198-9.

174. Moreno-Layseca, P., Icha, J., Hamidi, H. & Ivaska, J. Integrin trafficking in cells and tissues. *Nat. Cell Biol.* **21**, 122–132 (2019).

175. Schurr, Y., Spindler, M., Hendrikje, K. & Bender, M. The cytoskeletal crosslinking protein MACF1 is dispensable for thrombus formation and hemostasis. *Sci. Rep.* **9**, 1–8 (2019).

176. Qiu, W. X. *et al.* Deficiency of Macf1 in osterix expressing cells decreases bone formation by Bmp2/Smad/Runx2 pathway. *J. Cell. Mol. Med.* **24**, 317–327 (2020).

177. Goldman, R. D. The role of three cytoplasmic fibers in BHK-21 cell motility: I. Microtubules and the effects of colchicine. *J. Cell Biol.* **51**, 752–762 (1971).

178. Kreitzer, G., Liao, G. & Gundersen, G. G. Detyrosination of tubulin regulates the interaction of intermediate filaments with microtubules in vivo via a kinesin-dependent mechanism. *Mol. Biol. Cell* **10**, 1105–1118 (1999).

179. Green, K. J., Talian, J. C. & Goldman, R. D. Relationship between intermediate filaments and microfilaments in cultured fibroblasts: Evidence for common foci during cell spreading. *Cell Motil. Cytoskeleton* **6**, 406–418 (1986).

180. Rao, M. V. *et al.* Myosin Va binding to neurofilaments is essential for correct myosin Va distribution and transport and neurofilament density. *J. Cell Biol.* **159**, 279–289 (2002).

181. Tablin, F. & Taube, D. Platelet intermediate filaments: Detection of a vimentinlike protein in human and bovine platelets. *Cell Motil. Cytoskeleton* **8**, 61–67 (1987).

182. Lam, F. W., Da, Q., Guillory, B. & Cruz, M. A. Recombinant Human Vimentin Binds to P-Selectin and Blocks Neutrophil Capture and Rolling on Platelets and Endothelium. *J. Immunol.* ji1700784 (2018) doi:10.4049/jimmunol.1700784.

9 APPENDIX

9.1 Abbreviations

ACF7	Actin cross-linking factor 7
ADF	Actin depolymerizing factor
ADP	Adenosine diphosphate
APS	Ammonium Persulfate
Arp2/3	Actin-related protein 2/3
ARPC1B/2	Actin-related protein 2/3 complex subunit 1B/2
ATP	Adenosine triphosphate
BAL	Bronchoalveolar lavage
Bpag1	Bullous pemphigoid antigen 1
BSA	Bovine serum albumin
Ca^{2+}	Calcium
CCDC53	Coiled-coil domain-containing protein 53
CD	Cluster of differentiation
Cdc42	Cell division control protein 42 homolog
CLEC-2	C-type lectin-like receptor 2
c-Mpl	Cellular myeloproliferative leukemia protein receptor
CRP	Collagen related peptide
CVX	Convulxin
CYFIP	Cytoplasmic FMRP-Interacting Protein
DAPI	4′,6-Diamidin-2-phenylindol
DMEM	Dulbecco's modified eagle medium
DMS	Demarcation membrane system (DMS)
DNA	Deoxyribonucleic acid
dNTP	Deoxynucleotide
Dst	Dystonin
dSTORM	*direct* Stochastic optical reconstruction microscopy
E	Embryonic stage
ECL	Enhanced chemiluminescence
EDTA	Ethylenediaminetetraacetic acid
EEA1	Early endosome antigen 1
EGTA	Ethylene glycol-bis(β-aminoethyl ether)-N,N,N′,N′-tetraacetic acid
ELISA	Enzyme linked immunosorbent assay
ER	Endoplasmatic reticulum
ERGIC	ER-Golgi intermediate compartment

F-actin	Filamentous actin
FAM21	Family with sequence similarity 21
FCS	Fetal calf serum
FeCl3	Ferric cloride
fI	Fluorescence intensity
FITC	Fluorescein isothiocyanate
FSC	Forward scatter
G-actin	Globular actin
GAPDH	Glyceraldehyde 3-phosphate dehydrogenase
GAR	Glycine/arginine-rich domain
GP	Glycoprotein
GPCR	G protein-coupled receptors
GTP	Guanosine-5´-triphosphate
HEPES	4-(2-hydroxyethyl)-1-piperazineethanesulfonic acid
HSCs	Hematopoietic stem cells
HSP	Hereditary spastic paraplegia
HSPC300	Hematopoietic stem/progenitor cell protein 300
5-HT	Serotonin
IF	Immunofluorescence
IgG	Immunoglobulin G
JMY	Junction-mediating regulatory protein
K+	Potassium
kDa	kilo Dalton
KO	Knockout
LIMK	LIM domain kinase
LPS	Lipopolysaccharide
M	Molar
MACF1	Microtubule-actin cross-linking factor 1
MAGE-L2	Melanoma antigen family L2 protein
MFI	Mean fluorescence intensity
Mg^{2+}	Magnesium
MVB	Multivesicular bodies
min	Minutes
MPV	Mean platelet volume
mRNA	Messenger ribonucleic acid
MYH9	Myosin, heavy chain 9
n	Number

NP-40	Nonidet P-40
NPFs	Nucleation-promotion factors
N-WASP	Neuronal-WASP
P	Postnatal week
PAK	p21 activated kinase 1
PBS	Phosphate-buffered saline
PCR	Polymerase chain reaction
PDK1	Phosphoinositide-dependent protein kinase-1
PE	Phycoerythrin
PF4	Platelet factor 4
PFA	Paraformaldehyde
PGI2	Prostacyclin
Pi	Phosphate
PI	Propidium iodide
PIP2	Phosphatidylinositol-4,5-bisphosphate
PRP	Platelet rich plasma
PS	Phosphatidyl serine
Rab	Ras-related protein Rab
Rac1	Ras-related C3 botulinum toxin substrate 1
RC	Rhodocytin
RNA	Ribonucleic acid
RNAi	RNA interference
RNase	Ribonuclease
rpA	Reverse passive Arthus
RT	Room temperature
SCEM	Super cryo embedding medium
SCF	Stem cell factor
SHRC	WASH regulatory complex
SPG	Spastic paraplegia gene loci
SWIP	Strumpellin and WASH-interacting protein
$t_{1/2}$	Half-life
TAE	Tris base, acetic acid, EDTA
Taq	Thermus aquaticus
TBS-T	Tris buffered saline with tween
TEM	Transmission electron microscopy
TEMED	Tetramethylethylenediamine
Thr	Thrombin

TPO	Thrombopoietin
TxA2	Thromboxan A2
Tβ4	Thymosin beta-4
U	Units
U46619	thromboxane analogue
VWF	Von Willebrand factor
WAS	Wiskott–Aldrich syndrome
WASH	WASP and SCAR homolog
WASP	Wiskott–Aldrich Syndrome protein
WAVE	WASP family verprolin homolog isoforms
WH2	WASP homology 2 domain
WHAMM	WASP homolog associated with actin, membranes and microtubules
WT	Wild-type

9.2 Acknowledgments

The work presented here was performed at the Department of Experimental Biomedicine I, University Hospital/ University Würzburg, in the group of Dr. Markus Bender. During the period of my PhD studies (2015 – 2020) many people supported and accompanied me on my way to whom I would like to express my sincere gratitude:

Dr. Markus Bender, for being a reliable, supportive and inspiring supervisor who never got tired of discussing problems and giving advice. Thank you for your trust in me, my opinion and my ideas. I really enjoyed my work and the spirit of science you spread.

Prof. Laura Machesky, for being a member of my thesis committee and a great collaboration partner. I am still grateful for the time I spend in your lab in Glasgow and that your research somehow led me to the studies on the cytoskeleton and platelets.

Prof. Thomas Dandekar, for being a member of my thesis committee. Thank you for the fruitful scientific discussions and your supportive and positive mentality.

The Bender lab people, for all the entertaining conversations and for being my work family. Especially *Markus Spindler* who started this PhD journey with me.

All the D16 and Schulze lab people, for the pleasant atmosphere in the lab and during lunchtime.

All the D15, Nieswandt and Stegner lab people, especially Irina, Carina, Julia, Charly, Vanessa, Inga, Sarah and all the technicians for scientific and non-scientific discussions, technical advice, support on my projects and a lot of fun.

Julia Volz, for being my partner in crime inside and outside the lab.

My close friends and family from Stuttgart, Taubenheim and Würzburg for making my life so much more fun.

Daniel, my soulmate, thank you for supporting everything. With you things never get boring! I guess, our life is like an infinite set of experiments and the biggest one named "*Vincent*" just started.

9.3 Publications

9.3.1 Original articles

Schurr Y, Sperr A, Volz J, Beck S, Reil L, Kusch C, Eiring P, Bryson S, Sauer M, Nieswandt B, Machesky L and Bender M.

Platelet lamellipodia formation is not required for thrombus formation and stability.

Blood. 2019 Oct 11. pii: blood.2019002105. doi: 10.1182/blood.2019002105.

Schurr Y, Spindler M , Kurz H, Bender M.

The cytoskeletal crosslinking protein MACF1 is dispensable for thrombus formation and hemostasis.

Sci Rep. 2019 May 22;9(1):7726. doi: 10.1038/s41598-019-44183-6.

Spindler M, van Eeuwijk JMM, Schurr Y, Nurden P, Nieswandt B, Stegner D, Reinhold A, Bender M.

ADAP deficiency impairs megakaryocyte polarization with ectopic proplatelet release and causes microthrombocytopenia.

Blood. 2018 Jun 27. pii: blood-2018-01-829259. doi: 10.1182/blood-2018-01-829259.

Wiegering A, Uthe FW, Jamieson T, Ruoss Y, Hüttenrauch M, Küspert M, Pfann C, Nixon C, Herold S, Walz S, Taranets L, Germer CT, Rosenwald A, Sansom OJ, Eilers M

Targeting Translation Initiation Bypasses Signaling Crosstalk Mechanisms That Maintain High MYC Levels in Colorectal Cancer.

Cancer Discov. 2015 Jul;5(7):768-781. doi: 10.1158/2159-8290.CD-14-1040

9.3.2 Oral presentations

“Platelet lamellipodia formation is not required for thrombus formation and stability”

- The International Society on Thrombosis and Haemostasis (ISTH) XXVIIth Congress, July 2019, Melbourne, Australia
- 63rd Meeting of the Society of Thrombosis and Haemostasis Research (GTH), February 2019, Berlin, Germany
- 2nd European Congress on Thrombosis and Haemostasis (ECTH), Oktober 2018, Marseille, France
- 13th International EUREKA Symposium GSLS, Oktober 2017, Würzburg, Germany

9.3.3 Posters

“Platelet lamellipodia formation is not required for thrombus formation and stability”

- 63rd Meeting of the Society of Thrombosis and Haemostasis Research (GTH), February 2019, Berlin, Germany

“WASH complex subunit Strumpellin selectively regulates integrin αIIbβ3 expression”

- 12th International EUREKA Symposium GSLS, Oktober 2017, Würzburg, Germany
- The International Society on Thrombosis and Haemostasis (ISTH) XXVIth Congress, July 2017, Berlin, Germany

“Construction of retroviral vectors to study cytoskeletal dynamics in megakaryocytes and platelets”

- 10th International EUREKA Symposium GSLS, Oktober 2015, Würzburg, Germany

9.3.4 Awards

Young Investigator Award

- The International Society on Thrombosis and Haemostasis (ISTH) XXVIIth Congress, July 2019, Melbourne, Australia
- 2nd European Congress on Thrombosis and Haemostasis (ECTH), Oktober 2018, Marseille, France

9.5 Affidavit

Affidavit

I hereby confirm that my thesis entitled "*Studies on the role of cytoskeletal-regulatory and -crosslinking proteins in platelet function*" is the result of my own work.

I did not receive any help or support from commercial consultants. All sources and/or materials applied are listed and specified in the thesis.

Furthermore, I confirm that this thesis has not yet been submitted as part of another examination process neither in identical nor in similar form.

Würzburg, _____

Yvonne Schurr

Eidesstattliche Erklärung

Hiermit erkläre ich an Eides statt, die Dissertation "*Studien zur Rolle von Zytoskelett-regulierenden und -vernetzenden Proteinen in der Thrombozytenfunktion*" eigenständig, d.h. insbesondere selbständig und ohne Hilfe eines kommerziellen Promotionsberaters, angefertigt und keine anderen als die von mir angegebenen Quellen und Hilfsmittel verwendet zu haben.

Ich erkläre außerdem, dass die Dissertation weder in gleicher noch in ähnlicher Form bereits in einem anderen Prüfungsverfahren vorgelegen hat.

Würzburg, _____

Yvonne Schurr